Title
Distributed Fiber Optic Sensing for Deep Foundation and Soil Vertical Strain Monitoring

Author
Yeskoo, Richard Andrew

Publication Date
2022

Peer reviewed|Thesis/dissertation

Distributed Fiber Optic Sensing for Deep Foundation and Soil Vertical Strain Monitoring

by

Richard Andrew Yeskoo

A dissertation submitted in partial satisfaction of the

requirements for the degree of

Doctor of Philosophy

in

Engineering - Civil and Environmental Engineering

in the

Graduate Division

of the

University of California, Berkeley

Committee in charge:

Professor Kenichi Soga, Chair

Professor Dimitrios Zekkos

Professor Hayden Taylor

Fall 2022

Distributed Fiber Optic Sensing for Deep Foundation and Soil Vertical Strain Monitoring

Richard Andrew Yeskoo

Abstract

Distributed Fiber Optic Sensing for Deep Foundation and Soil Vertical Strain Monitoring

by

R. Andrew Yeskoo

Doctor of Philosophy in Engineering - Civil and Environmental Engineering

University of California, Berkeley

Professor Kenichi Soga, Chair

Geotechnical engineering, more so than any other branch of engineering, relies on measurement for the design and execution of our works. The natural materials that form the basis of geotechnical engineering design cannot be specified in a factory – they were formed through geologic processes and are already in place, awaiting discovery by the engineer. To characterize their properties, the materials must be measured. The execution and performance of the design must also be measured if it is to be confirmed to conform to the quality and behavior expected by the engineering team. Since the subsurface structures cannot be directly observed, we rely on instrumentation to measure their behavior.

Distributed Fiber Optic Sensing (DFOS) refers to a range of technologies that enable the measurement of physical phenomenon along a fiber optic cable. DFOS relies upon the fiber optic cable as both the sensor as well as the data conduit. By carefully interrogating changes in light that is sent through the fiber optic cable, measurements such as strain and temperature can be taken in a continuous readout along the cable. This technology has been in development for several decades and has been adopted for applications within civil engineering, including geotechnical engineering. The unique ability to generate continuous measurement profiles offers a significant benefit over conventional point-based instrumentation, particularly in applications where the strain and temperature fields are changing in non-linear and unpredictable ways.

This research explores the use of DFOS for the monitoring of strain and temperature in deep foundations during loading and vertical soil displacements. These applications are particularly suited to the benefits that DFOS offers, specifically the continuous strain readout that is produced by fiber optic monitoring. Best practices for installation and monitoring were developed, and these advancements were applied on a series of field projects to ascertain their performance and gain insight into the behavior of the monitored assets. The applications

included monitoring of strain development in deep foundations during post grouting, monitoring of strain in deep foundations during top-down load testing, monitoring of blanket uplift on a river levee, and monitoring of vertical ground deformations during surcharge loading of a soft clay site. In each case, the author developed novel improvements for the design, installation, monitoring, and interpretation of DFOS data to provide new insight into the geomaterial and geostructure behavior.

In the application of strain measurements in deep foundations, three major improvements and new findings were explored and verified. For the installation phase, the current state of practice of pre-tensioning strain cables prior to concreting was replaced with installation with slack removed but without any additional pre-tension. The encapsulation in concrete was proved to be enough to fully transfer compressive strains within the foundation element to the fiber optic sensing cable through validation data using conventional point-based strain measurement. During the data processing, installation of 4 vertical strain cables over the standard 1 or 2 verticals in the literature allowed for identification and analysis of non-uniform strain distribution across the pile at single depths. This variation has often been ignored or discarded in favor of averaging the strain measurements across the pile, missing real non-idealized pile behavior during loading, or incorrectly discarding valid data. Finally, lab and field testing was performed to capture and quantify the effect of fiber optic analyzer architecture on the processed strain readout when the strain along the sensing fibers is not constant during the reading interval. This effect has not been identified or explored and was shown to have a quantifiable and correctable impact on the data, as well as highlighting an additional performance metric to consider when selecting a fiber optic analyzer for a particular application.

In the application of DFOS for soil vertical strain monitoring, two improvements on the state of practice were developed. The first is the detailed exploration and demonstration of the benefit of continuous strain measurements over point-based measurements in the identification and quantification of local subsurface strain. The highly local nature of these strains, as well as the judgement required in the placement of point-based measurement points, result in DFOS offering a clear advantage over the standard state of practice. The necessity for temperature compensation of subsurface DFOS strain measurements was also explored and quantified. The current state of practice is to treat the subsurface temperature as stable, however measurements show that surface temperature fluctuations can impact the soil temperature to significant depths and must be corrected prior to integration of the distributed strain profiles to calculate cumulative surface displacement.

For my family, without whose support I would not be where I am today

Table of Contents

1. Introduction

The practice of geotechnical engineering is inherently characterized by uncertainty. Unlike in other branches of civil engineering, the soil and rock properties that govern the performance of geotechnical designs are not specified – they instead must be measured through field investigation and testing. There are practical limitations on the extent of ground investigation that can be performed, and it is the responsibility of the engineer to apply their knowledge and understanding to infer the properties and behaviors in between the measurement gaps. One method to manage the uncertainty in geotechnical practice is to strategically monitor the behavior and performance of our executed designs. However, this too requires interpolation on the part of the engineer as the monitoring data is often discontinuous and limited in coverage.

The transition from point-based measurements to continuous measurements has had a dramatic impact on the level of uncertainty that must be tolerated in geotechnical projects, and in turn, reduced the amount of inference that is required in the interpretation of data sets. In the geotechnical investigation phase, this can be best illustrated by the transition from characterization of the soil by Standard Penetration Test (SPT) during drilling to the continuous Cone Penetration Test (CPT) measurement profiles. The increase in resolution and fidelity that the CPT offers as compared to the SPT, accompanied by lower cost and decreased investigation time, has allowed the uncertainty associated with subsurface characterization to decrease significantly when applied. The same scale of benefit can be realized in the monitoring of geotechnical behaviors in the transition from point-based sensing equipment to distributed monitoring systems.

Distributed Fiber Optic Sensing (DFOS) offers the ability to create a continuous profile of strain and temperature measurements along an installed sensing fiber optic cable. Unlike point-based sensors which rely on a separate sensor for measurement and cable for power and data transfer, DFOS generates a continuous measurement profile along the fiber optic cable. Distributed sensing removes the need for engineers to infer the behavior of the monitored asset between discrete measurement points, allowing for a more complete and accurate understanding of the asset's performance. This ability becomes more valuable when the field performance of materials and structures deviate from the idealized behaviors predicted by engineering methodologies. Indeed, it is sometimes only through the deployment of DFOS that the recognition of non-idealized behavior is possible.

The application of DFOS within civil and geotechnical engineering has been the topic of research and industry development for several decades. However, there remain several important questions regarding the design, installation, and performance of these monitoring systems and the specific applications under which they can provide the most benefit as compared with conventional sensing technology. DFOS is most suited in applications involving measurements over a long, linear feature. Two such applications which have been identified as being particularly suited for a transition from point- to distributed-measurement are the

monitoring of deep foundations during loading and the measurement of vertical subsurface displacement.

1.1 Research Hypotheses and Objectives

The objectives of this study include the following.

- Improvement of the current state of practice for fiber optic monitoring of strain in deep foundations
- Development of the use of vertical fiber optic sensing cables for subsurface strain measurement
- Qualitative and quantitative comparison between the interpretation of point-based measurement systems and DFOS measurements of deep foundation and soil deformation
- Recommendations for best practices for the specification and deployment of DFOS for geotechnical monitoring

Based on the research objectives, a thorough review of the pertinent literature and evaluation of the current state of practice was performed to identify gaps that could benefit from novel research and development. These areas were then framed into hypotheses which could be tested and evaluated in the laboratory and research testing of the study. The tested hypotheses are summarized as follows.

- Distributed fiber optic strain cables for deep foundations, when fully encapsulated in concrete, can be installed without the need for pretension during installation.
- Distributed fiber optic strain cables in deep foundations, when installed in a 3- or 4-vertical array, provide valuable insight into the strain variability across the pile at a single depth. This variation is important to be evaluated and is not appropriate to discard and offers a distinct advantage over a 2-vertical installation or the averaging of strain across the pile without first evaluating this variation.
- The architecture of distributed fiber optic analyzers has a direct and quantifiable effect on the processed strain output when the strain field of the measurement fiber is changing during the reading interval.
- Distributed fiber optic strain measurement offers a distinct advantage over conventional point-based monitoring for the identification and quantification of local soil strain in the subsurface.
- Temperature compensation of distributed fiber optic strain measurement is required for subsurface installations where temperature fluctuations at the ground surface affect the embedded strain cable.

1.2 Outline of the Dissertation

This dissertation is organized into six chapters as follows.

- Chapter 1 is an introduction to the dissertation, including the research objectives and the dissertation outline.
- Chapter 2 is an overview of fiber optic sensing and provides a technical background of the fiber optic sensing methods used in this research.
- Chapter 3 presents the equipment and materials used in the research, as well as the results of laboratory testing of the equipment's performance.
- Chapter 4 presents a study of the application of DFOS for measurements of deep foundation strain. The chapter is centered upon a trial project for the use of DFOS for strain monitoring of post-grouted drilled shafts in Northern California. The chapter is organized into a literature review on the use of DFOS for deep foundation measurements, the project overview and field testing, strain measurements of the piles during post grouting, strain measurements of the piles during load testing, and discussion and analysis of the monitoring results.
- Chapter 5 presents a study of the application of DFOS for measurements of vertical soil displacement. Two field projects were performed which each involved the design, installation, and analysis of a DFOS monitoring system for the measurement of vertical soil deformations. The chapter is organized into a literature review on the use of DFOS for subsurface vertical deformation measurement, a field trial applying vertical fiber optic monitoring in borehole installations for the measurement of subsurface displacement of a levee, and a field trial applying vertical fiber optic monitoring installed via CPT-direct-push for the measurement of subsurface displacement during a surcharge loading program.
- Chapter 6 provides a summary of the research conclusions and recommendations for future work in the field.

2. Overview of Fiber Optic Sensing

Over the past two decades, the use of fiber optic sensing within infrastructure monitoring has grown tremendously. The combination of advances in analyzer technology, the development of a range of fiber optic monitoring cables, and refinement of the installation techniques have opened the application breadth to a wide range of asset and behavior types. This chapter is intended to provide an introductory background to fiber optic monitoring, including a cursory introduction to the technology fundamentals, which will serve as a basis to inform the chapters to follow.

Fiber optic sensing refers to a variety of different sensing techniques which allow the interaction of light along a fiber optic cable to be used to measure various physical parameters along the cable length. The systems are broadly divided into point-based sensing systems and distributed systems (Kechavarzi et al. 2016; Soga and Luo 2018). The first category includes Extrinsic Fabry-Perot interferometers and Fiber Bragg Gratings (FBGs). These incorporate optical reflectors or etched treatments along the fiber optic cable, allowing the measurement of physical parameters at the sensing points. In the case of FBG systems, multiple sensing treatments can be installed along the same cable, allowing for a quasi-distributed sensing system. The second category of Distributed Fiber Optic Sensing (DFOS) relies on the fiber optic cable itself as a sensing instrument. When light is sent through a fiber optic cable, several types of scattering occur to a small proportion of the light's power while traveling within the fiber core. Of the scattering within the cable, a small subportion of the scattered light is reflected towards the source, a phenomenon called backscattering. By carefully recording differences in the backscattered light, measurements of physical phenomenon can be made along the cable. The types of DFOS technologies are divided by the type of scattering that they rely upon. These are divided into Raman scattering, which is proportional to temperature changes, Rayleigh scattering, which is proportional to vibration or dynamic rate-of-strain, and Brillouin scattering, which is proportional to strain and temperature changes. A diagram illustrating this phenomenon is shown in Figure 2-1.

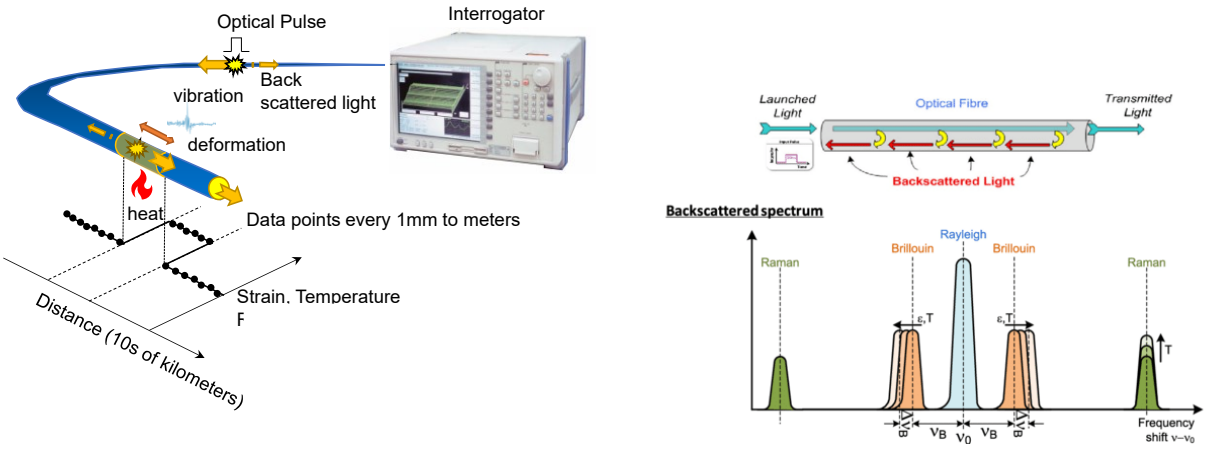

Figure 2-1: Backscattered light phenomenon (after Kechavarzi et al. 2016)

For civil engineering applications, FBG and Brillouin based sensing systems are the most common for measurements of strain and temperature. A brief overview of how these technologies function is presented below.

2.1 Fiber Bragg Grating (FBG) Sensing

Fiber Bragg Grating sensing relies on discrete sensing points created within a fiber optic cable by creating evenly spaced etchings, referred to as gratings, within the fiber optic core. The spacing of the fiber optic gratings is designed to correspond and interact with a specific wavelength of light. When a broadband light pulse is passed through the fiber optic cable, each grating will create a reflection back to the source of its signature wavelength, allowing the remainder of the light to continue propagating down the cable in the original direction of travel. This principle is illustrated in Figure 2-2.

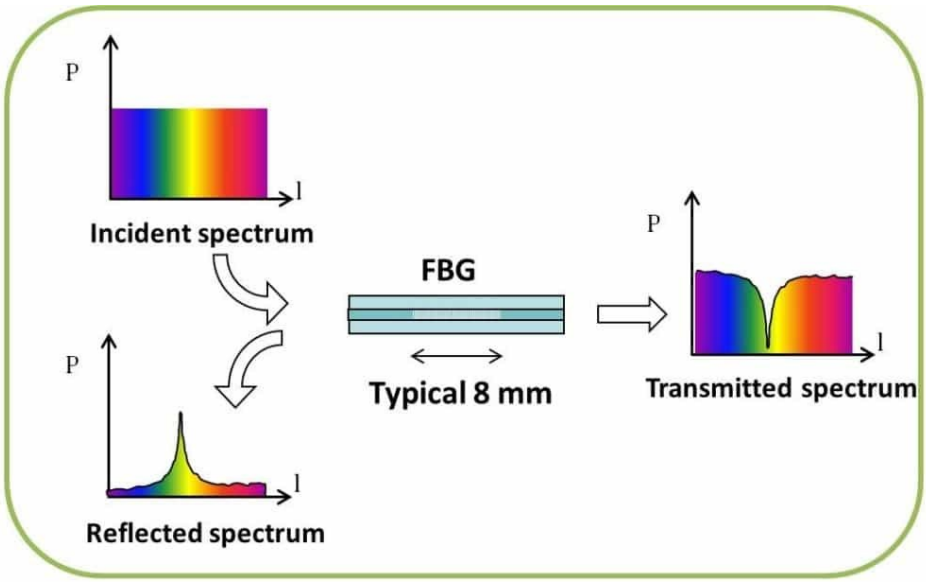

Figure 2-2: Spectral reflection and shadowing of FBG (image credit: FBGS)

Extension or contraction of the cable containing a grating results in a proportional increase or decrease in the spacing of the grates, shifting the reflected wavelength. This principle is illustrated in Figure 2-3. The shift in the wavelength is proportional to strain (either mechanically generated or thermally generated, or both).

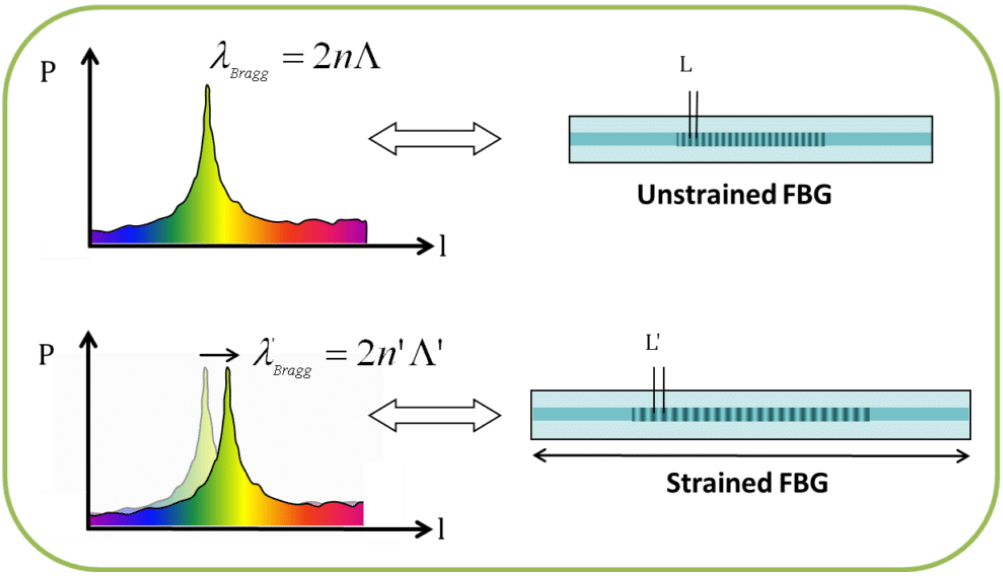

Figure 2-3: FBG central and strained wavelength (image credit: FBGS)

Multiple gratings can be included on a continuous length of fiber, so long as their central wavelengths are spaced far apart enough to allow for identification of the signal for each discrete sensor, including as they shift within their measurement range. Commercial analyzers can track the wavelength peaks along the fiber optic cable dynamically and include the ability to enter calibration factors to convert from wavelength to temperature or strain. Strain sensors along the fiber are created by allowing the surrounding strains to be transferred into the grating. Temperature sensors along the fiber take the opposite approach, physically preventing external strains from being applied to the grating and using the thermal coefficient of the fiber to convert thermal strain to temperature change. Since the strain sensors are also subjected to thermal strain, it is often prudent to co-locate a temperature sensor with each strain sensor to allow later correction for the thermal strains.

The sensing points themselves can either be etched directly onto a fiber optic cable, either at standardized or custom spacing, or can be housed within stand-alone sensor packages which are networked together using standard fiber optic cable. The sensor housings can be tailored to match the function and form of more conventional point-based sensors, such as vibrating wire strain gauges. However, they are often much more expensive than vibrating wire sensors. FBG sensors offer the benefit of being unaffected by electronic or magnetic interference, as well as functioning without any electrical current at the sensing locations.

2.2 Distributed Brillouin Strain and Temperature Sensing

Distributed Brillouin sensing relies on backscattered light signals generated along the length of a fiber optic cable. As a light pulse travels down the fiber optic cable, it interacts with minute changes in density fluctuations within the fiber core. Standard single-mode telecommunications fiber optic cable contains these fluctuations because of their manufacturing – no specialized fiber core is required for the majority of Brillouin sensing. Certain high resolution Brillion

technologies rely on specialized non-linear fibers with additional density fluctuations introduced during manufacturing. However, these fibers are not commonly deployed in long distances or common applications within civil engineering.

The density fluctuations scatter a small amount of light within the fiber, including a portion which propagates back towards the source. The Brillouin scattering phenomena results in a change in the photon energy, corresponding to a shift in the frequency of the scattered light. The frequency shift from the source light is referred to as the Brillouin frequency shift, and it is this shift that is recorded by the measurement instrument (i.e., analyzer). The shift is proportional to small changes in material density and varies linearly with applied longitudinal strain along the fiber core, either thermal or mechanical.

The Brillouin scattering effect occurs naturally within the fiber optic core at low energies, a phenomenon called spontaneous Brillouin scattering. The strength of the scattered signal can be magnified by introducing a "pump" light pulse from the opposite end of the fiber, an approach called stimulated Brillouin scattering. This increases the resolution of the measurement. The use of spontaneous or stimulated Brillouin scattering is the fundamental difference between a Brillouin Optical Time Domain Reflectometry (BOTDR) or a Brillouin Optical Time Domain Analysis (BOTDA) fiber optic sensing analyzer. BOTDR only requires connection to one end of the sensing fiber optic cable and the strain resolution (measurement repeatability) is about 20-30 με, depending on the analyzer. Because of its use of stimulated Brillouin scattering, BOTDA requires a continuous loop within the sensing cable with the benefit of an increase in frequency (strain/temperature) sensitivity. The strain resolution (measurement repeatability) is about 2-5 με, again depending on the specific analyzer.

In commercial Brillouin fiber optic analyzers, the system both generates the light pulse to send into the sensing cable as well as records the Brillouin frequency response. The reflected light is recorded periodically with time, with the arrival time of the reflection used to localize the reflection source along the fiber based on the speed of light within the core. The regularity of how often a reading point is recorded determines the readout spacing of the analyzer – that is how often along the fiber a single measurement is taken. The readout spacing of the analyzer used in this study was 0.25 m; that is, strain/temperature data is given every 0.25 m.

The pulse width, or how long a section within the fiber is occupied by the light at any given time, determines the spatial resolution of the analyzer. This can be thought of as the length over which the strain or temperature measurement is taken within the fiber, although differences in the "shape" of the pulse mean that it is often not an exact linear average along the interval. The spatial resolution of the commercial analyzer used in the majority of this research was 0.75 m. This means that each data point is a strain of 0.75 m gauge length. In other words, it is a weighted average strain of ±0.375 m from the data point.

While taking a reading, most commercial analyzer designs only record the light response within a single frequency band at a time. The way that a complete reading is taken is by "sweeping"

the recorded frequencies within a set window and a gain (scattered light power)-frequency-distance plot is produced, as shown in Figure 2-4. The figure plots the spectrum data around the frequency range where Brillouin scattering is occurring.

Figure 2-5 shows the spectrum plot of gain versus frequency at a given sensing point along the fiber. It is common to take multiple readings at each frequency interval and average the results to reduce the associated noise in the reading (this is performed automatically by the analyzer). Using this plot generated for each sensing point along the fiber, the Brillouin frequency peak for each point is identified. As described earlier, the Brillouin peak frequency is related to strain, either mechanical or thermal. The figure shows one reading in white and another reading in pink. The shift in the peaks of the two curves are related to change in strain or temperature at that sensing point on the fiber.

For a given reading, Brillouin peak frequency can be identified at each sensing point and Figure 2-6 shows a plot of Brillouin peak frequency versus distance. The output of the analyzer will be a 2D matrix with the distance from the analyzer in the first column and the peak Brillouin frequency in the second. Although a single Brillouin peak frequency value is presented in the common output of the analyzer (Figure 2-6), each point along the fiber has an entire power spectrum with amplitudes of each scanned frequency within the reading window (Figure 2-5). The combination will produce a 3D plot like the one shown in Figure 2-4.

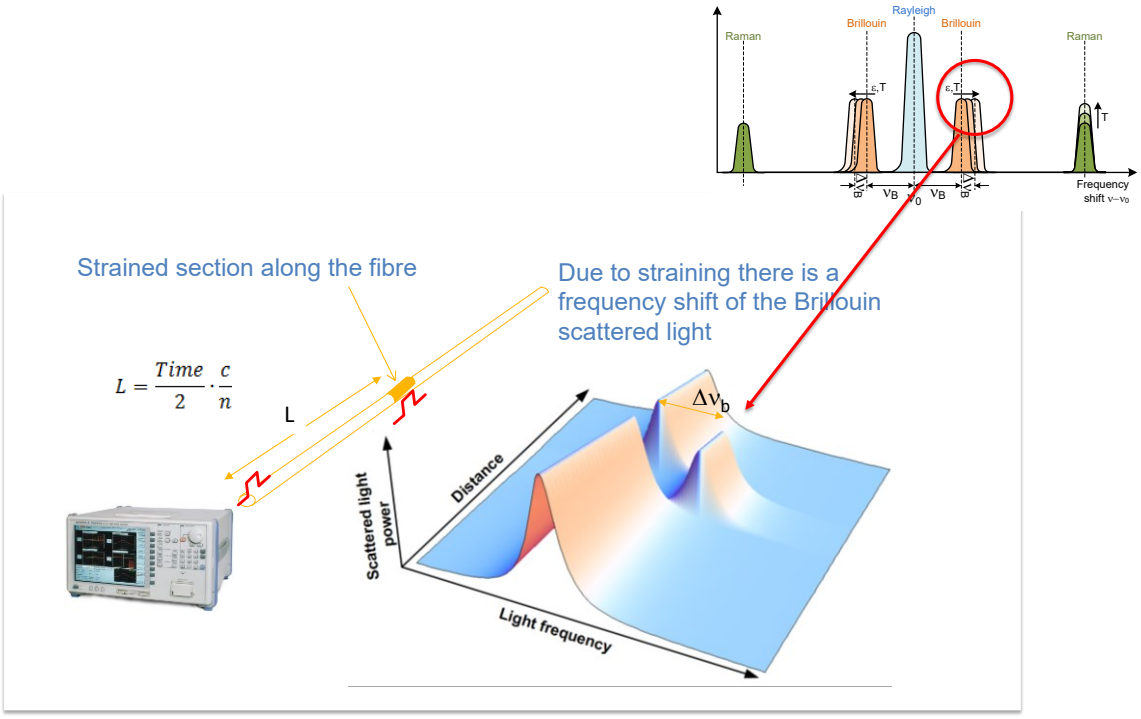

Figure 2-4: 3D power spectrum along the fiber

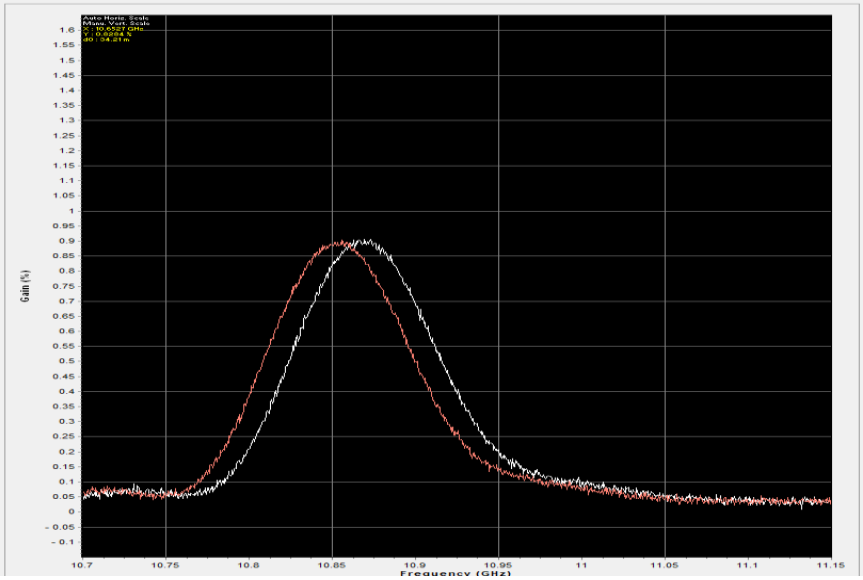

Figure 2-5: Gain (amplitude) vs. Frequency for a single reading point

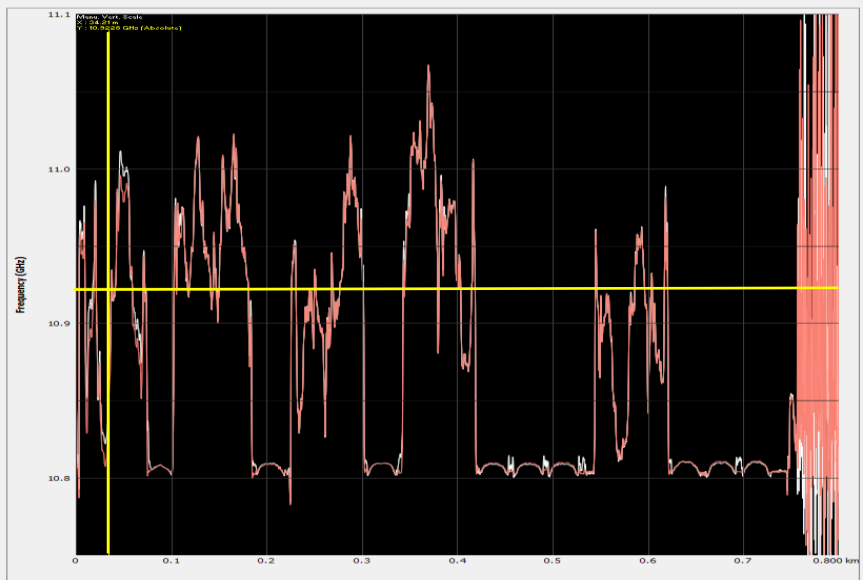

Figure 2-6: Peak Brillouin Frequency vs. Distance Along Fiber

In Figure 2-6, the peak Brillouin frequency along the length of the sensing fiber is shown for two separate readings, displayed in white and pink. The differences in frequency between the two points indicate areas along the fiber that had changes in strain or temperature between the early and later reading, with the difference in frequency linearly corresponding to a specific change in strain or temperature. The yellow crosshair on the figure is used to narrow in on a single reading point along the fiber. As described earlier, the frequency power spectrum for the two readings at this point are shown in Figure 2-5. The values for the two readings in the previous figure represent the calculated peak frequencies of the power spectrum; however, to

generate the reading the power was recorded for every frequency step within the scanning window of 10.7 GHz to 11.15 GHz. Since it can take several minutes to complete a reading for the entire frequency range, this method of Brillouin sensing can be sensitive to changes in strain or temperature during the reading interval. A detailed exploration of this effect on the final reading is presented in Chapter 3.

Since the change in Brillouin peak frequency is proportional to changes in both mechanical strain and temperature along the fiber, it is necessary to compensate for the thermal effect for monitoring projects where the temperature along the sensing fiber fluctuate during the observation period. The approach is to use specialized cable designs to either tightly bond the fiber optic core to applied external mechanical strains, or to completely debond the fiber optic core from external mechanical strains. In the first case, several specialized fiber cable designs have been developed to accommodate a wide range of applications. These include extremely thin packaging for high strain sensitivity, all the way to steel-sheathed cables designed to survive the high temperatures and pressures in downhole oil and gas applications. In all cases, the cables must be carefully designed and manufactured to reliably transfer strains from the exterior of the cable to the fiber optic core within. Any slippage or non-linearity in the strain transfer can greatly affect the fidelity of the measurements along the fiber, often to an unknown or un-correctable degree. In the second case, several standard telecommunications fiber optic cables are manufactured with a “loose-tube” design. While the specific layering and materials vary among manufacturers, this refers to a strain-decoupling layer within the cable, often either a gap or a viscous gel. Changes in the Brillouin frequency in temperature fibers can be assumed to be due only to thermal changes in the fiber; however, testing and calibration is recommended to confirm the strain decoupling of new fiber designs. Further discussion of the specific strain and temperature cables used in this research is presented in Chapter 3.

3. Research Equipment Selection and Testing

As the range of applications for fiber optic monitoring has expanded in the past decade, so has the variety of analyzer and cable technology in the marketplace to meet the new needs. A successful monitoring project requires the careful selection and operation of the specific technologies to be used. In addition, it is important to probe and understand the measurement limitations inherent in the technology, especially those that directly affect the fidelity and representation within the resultant data sets. This chapter outlines the specific fiber optic sensing cables and analyzers deployed in the research projects of this report, as well as the results from calibration and performance testing on the thermal cable and commercial Brillouin analyzer.

3.1 Fiber Optic Cables

Three types of cable were used for the fiber optic monitoring research – a distributed thermal cable, a distributed strain cable, and a point-based strain cable. The distributed cables consist of a standard telecommunications single mode fiber optic cable, prepared in either a loose-tube (thermal) or tightly-buffered (strain) cable packaging. The point-based strain cable is a fiber optic cable with optical gratings etched into the fiber at prescribed frequencies and spacing.

Thermal Cable (distributed)

The distributed temperate cable chosen for this research is an 8 mm diameter standard outdoor telecommunications cable manufactured by Belden, part number FSSC002N0. A schematic cross section of the cable is shown in Figure 3-1 and a photo of the cable is shown in Figure 3-2.

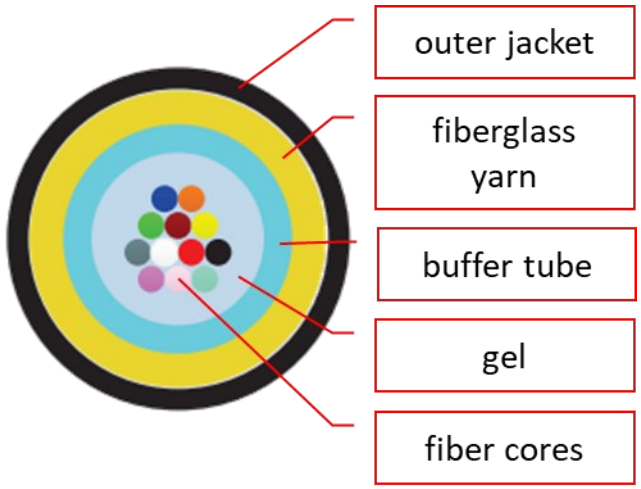

Figure 3-1: Schematic cross section of Belden 8 mm thermal cable (diagram credit: Belden Optical Fiber Catalog)

Figure 3-2: Photo of Belden 8 mm thermal cable (photo credit: Belden Optical Fiber Catalog)

The cable is a non-armored, loose tube cable with four single mode fibers in a gel-filled tube. The tube is then wrapped in a fiberglass yarn and coated with a polyethylene jacket. The gel provides a physical strain break in the cable design, preventing externally applied strains on the outer jacket from being transferred to the optical cables within. Although each cable contains four fibers, only one fiber was utilized in the temperature monitoring. The main functional parameters of the cable are listed in Table 3-1.

Table 3-1: Belden 8 mm temperature cable technical specifications

Brillouin Center Frequency (GHz)	10.84
Average Loss (dB/km)	0.3
Curvature Radius (mm)	160
Temperature Coefficient (MHz/°C)	1.100

Strain Cable (distributed)

The distributed strain cable chosen for this research is a 5 mm diameter armored cable manufactured by the NanZee Sensing Technology Co., part number NZS-DSS-C02. A schematic cross section of the cable is shown in Figure 3-3 and a photo of the cable is shown in Figure 3-4.

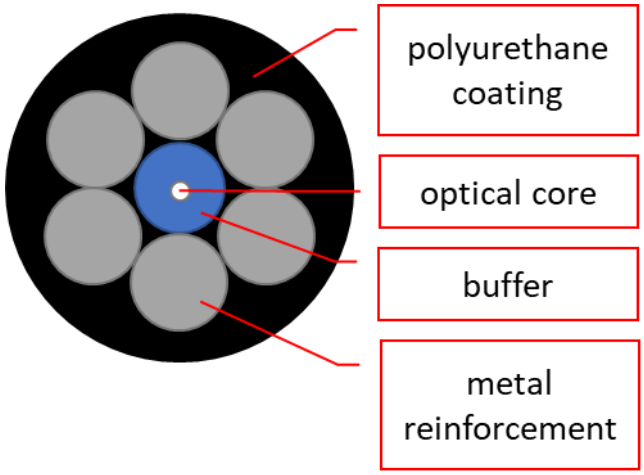

Figure 3-3: Schematic cross section of Nanzee 5 mm strain cable

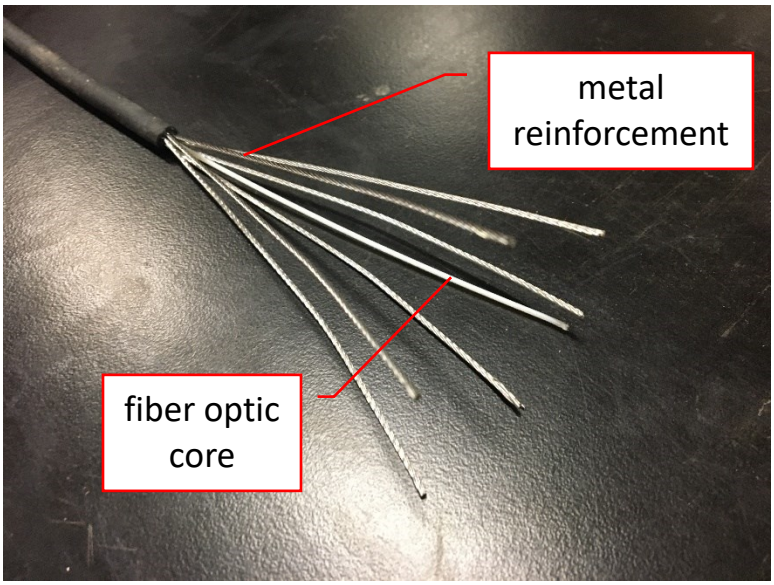

Figure 3-4: Photo of Nanzee 5 mm strain cable

This cable was chosen for its linear performance during the magnitudes of strain anticipated during the monitoring program, as well as its robustness and ease of use during installation and connection. The cable consists of a single-mode fiber optic core, tightly wound within a spiral of six braided steel cables, then wrapped in a tight polyurethane outer sheath. As opposed to thermal cable, it is necessary for strain cable to have a tightly bonded design to ensure that applied strain to the exterior sheath is transferred in a predictable and linear manner through the intermediate layers into the central fiber optic core. The main functional parameters of the cable are listed in Table 3-2.

Table 3-2: Nanzee 5 mm distributed strain cable technical specifications

Brillouin Center Frequency (GHz)	10.850
Average Loss (dB/km)	0.201
Curvature Radius (mm)	18
Strain Coefficient (MHz/με)	0.04998
Temperature Coefficient (MHz/°C)	1.775

Strain Cable (point-based)

The point-based FBG sensor cable chosen for this research is a draw tower grating produced by FBGS, part number LBL-1550. A schematic cross section of the cable is shown in Figure 3-5 and a photo of the cable is shown in Figure 3-6.

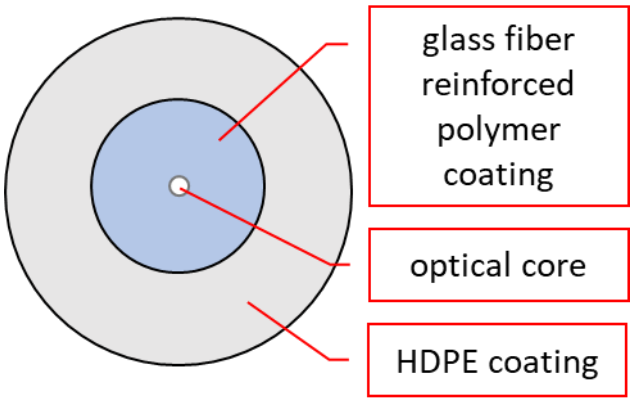

Figure 3-5: Schematic cross section of FBGS strain cable

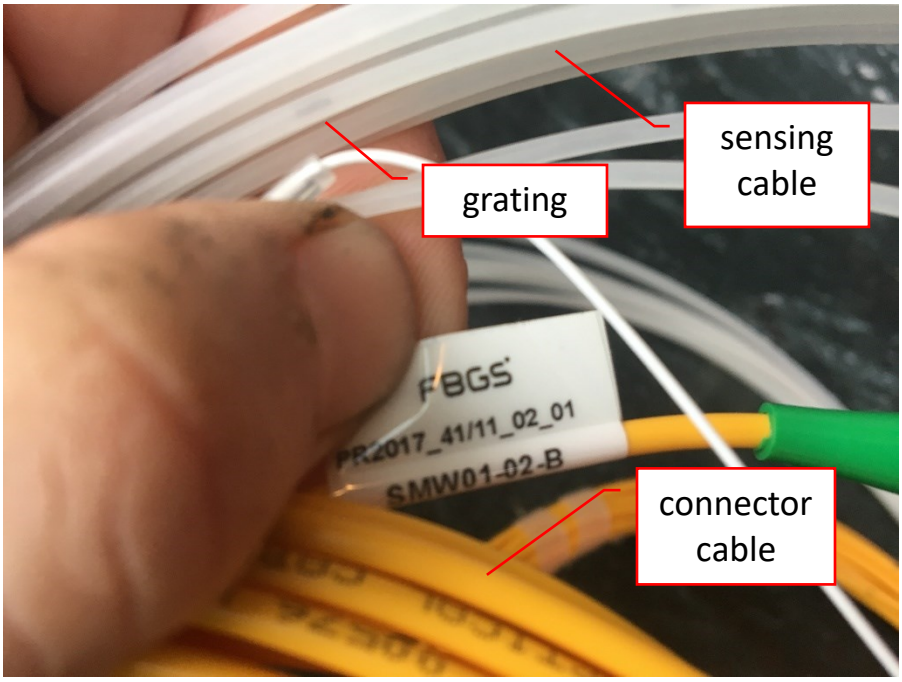

Figure 3-6: Photo of FBGS strain cable (white) and connector cable (yellow)

The fiber consists of standard 20m lengths with FBG points etched at regular one meter spacing (20 sensors for a total sensing length of 19m). Once prepared, the fiber is then drawn in 1 mm of glass fiber reinforced polymer (GFRP) coated by 2mm of HDPE. The grating frequency spacing is standardized to fit within the standard sensing wavelength window of 1510 nm to 1590 nm. This allows the product to be offered as a standard off-the-shelf item, reducing the cost by several times as compared to a bespoke FBG sensor string. For our project application, we specified one 20 m pre-manufactured string into two, 9 m sensing lengths with 10 gratings each. The main functional parameters of the cable are listed in Table 3-3.

Table 3-3: FBGS strain cable technical specifications

Center Wavelength Range (nm)	1510-1590

Absolute Wavelength Accuracy (nm)	≤ 0.5
Relative Wavelength Accuracy (nm)	≤ 0.3
Grating Length (mm)	8.0
Strain Sensitivity ($\Delta\lambda/(\lambda \cdot \Delta\varepsilon)$)	7.8 $\mu\varepsilon^{-1} \cdot 10^{-7}$
Temperature Sensitivity ($\Delta\lambda/(\lambda \cdot \Delta T)$)	6.5 $K^{-1} \cdot 10^{-6}$

3.2 Fiber Optic Analyzers

Three fiber optic analyzers were utilized in this research. Two of the analyzers were used for distributed strain and temperature readings, while the third was used for point-based strain readings. All of the fiber optic analyzers rely on a separate control laptop, running specific software for interfacing with the unit and controlling the associated readings. Power during monitoring was provided through a dedicated inverter generator with a battery surge protector and power supply to protect against power loss during monitoring.

Omnisens VISION Dual

The primary fiber optic analyzer used on the research projects was a commercial distributed strain sensing box produced by Omnisens SA of Switzerland, as shown in Figure 3-7. This analyzer is a Brillouin scatting based distributed sensing unit, capable of performing readings in both Brillouin Optical Time Domain Analysis (BOTDA) and Brillouin Optical Time Domain Reflectometer (BOTDR) modes.

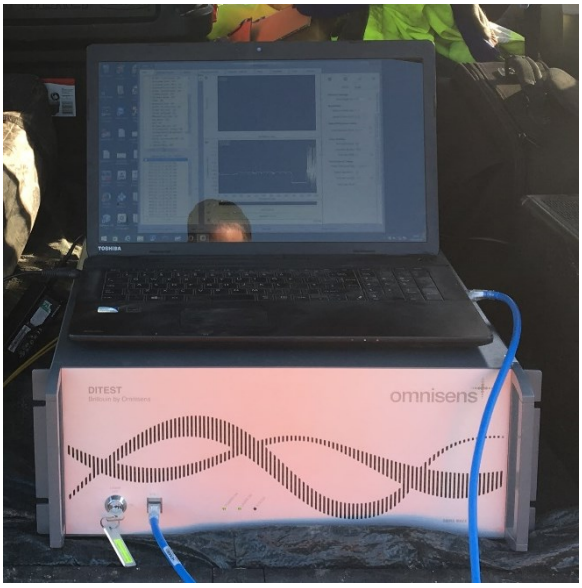

Figure 3-7: Omnisens fiber optic analyzer and control laptop during thermal readings

When operating in BOTDA mode, the analyzer is connected to both ends of the fiber optic cable, forming a continuous loop from the analyzer. A signal is sent through the sensing port into the cable, while a pump is sent from the other end to stimulate (increase) the magnitude of the Brillouin scattering in the cable. This allows the system to have a smaller spatial

resolution and a higher associated strain/temperature resolution while operating in this mode. For this project, most distributed readings were taken using the Omnisens unit operating in BOTDA mode.

BOTDR mode allows measurements to be taken using a connection to a single end of the fiber optic cable. This allows readings to be taken in the event of a breakage or damage to the cable during installation or preparation for testing. Three breakages occurred during the monitoring program which resulted in the need to switch from BOTDA to BOTDR mode. The single ended readings come with an associated increase in the spatial resolution (from 0.75 m to 1 m) and decrease in the strain/temperature resolution.

In both modes, the reading time for the chosen project settings was slightly below 5 minutes. The analyzer takes readings by sweeping in frequency within the user-defines reading window, starting at the lowest frequency, performing a series of readings, averaging the results for that frequency, and then stepping to the next higher frequency. The effect of this approach on the reading and the time-representation during non-constant strains is explored later in this chapter

The standard analyzer settings used for the Omnisens readings are presented in Table 3-4.

Table 3-4: Omnisens fiber optic analyzer reading settings

Frequency Step (MHz)	0.5
Frequency Start (GHz)	10.70
Frequency Stop (GHz)	11.15
Averaging	2000
Sampling Interval (m)	0.30
Sampling Interval (m)	0.30
Spatial Resolution, BOTDA (m)	0.75
Spatial Resolution, BOTDR (m)	1.00

ALICIA and Research Analyzers

The ALICIA fiber optic analyzer (see Figure 3-8) is a research-based analyzer, first developed in Professor Kenichi Soga's research group at the University of Cambridge in 2015. It is a single ended system; only connecting to one end of the sensing fiber optic installation. While the system approach relies on the same Brillouin scattering based distributed sensing as the Omnisens analyzer, most closely mimicking it in BOTDR mode, the unique ALICIA system architecture uses digital methods for signal processing rather than the analog frequency sweeping method of the Omnisens analyzer. This results in much faster data acquisition speed, with readings taken in 1-2 seconds as opposed to 5 minutes. The system has an effective spatial resolution of 1 m with a sampling interval of 0.02 m. Being a research-based system, the system

design requires the use of separate components in addition to a control laptop to function, rather than the integrated single box employed by the Omnisens analyzer.

Figure 3-8: ALICIA fiber optic analyzer during load test

A second generation of the research box was developed and deployed for the levee monitoring project presented in Section 5.2, incorporating several improvements into the original ALICIA design and integrating them into a single box.

Micron Optics SM130

The Micron Optics SM130 (Figure 3-9) is an FBG optical interrogator, capable of simultaneously reading up to four channels of FBG strands. Each channel is individually calibrated with the manufacturer-provided central frequency for all the FBG sensing nodes in the string. The interrogator then uses these calibration factors to calculate the frequency shift, which is then converted into differential strain. The control software tracks the peak frequency of each grating continuously during monitoring at a maximum scanning frequency of 2 KHz. For this project, data was saved at a 1 second frequency during monitoring. The wavelength accuracy of the analyzer is 1 pm, which for the strain sensitivity of the FBGS cable, corresponds to a strain resolution of 0.8 με.

Figure 3-9: Micron Optics SM130 FBG interrogator (photo credit: Micron Optics)

3.3 Thermal Cable Calibration Testing

Since the Belden cable used for distributed thermal monitoring was a standard telecommunications cable and is not marketed for sensing applications, the cable did not have published calibration or validation data from the manufacturer. As such, a laboratory test was conducted to confirm the accuracy of the fiber optic thermal measurements and compare the results with a conventional thermal wire used for pile monitoring for validation. The thermal wire is manufactured by Pile Dynamics, Inc. (PDI) and is the sensing component of their proprietary Thermal Integrity Profiler (TIP) system. The cable has temperature sensing points separated by 1 foot increments and connects to a cellular data logger for measurement.

The laboratory test employed the use of a large water bath, shown in Figure 3-10, to apply controlled temperatures to the fiber optic and TIP cable. The temperature was set at incremental set points, ranging from 77° to 176°F (25° to 80°C) in 9°F (5°C) increments. Approximately 30 ft of fiber optic cable and TIP wire were submerged within the water bath, with an additional 2 to 3 monitoring points outside the bath at room temperature.

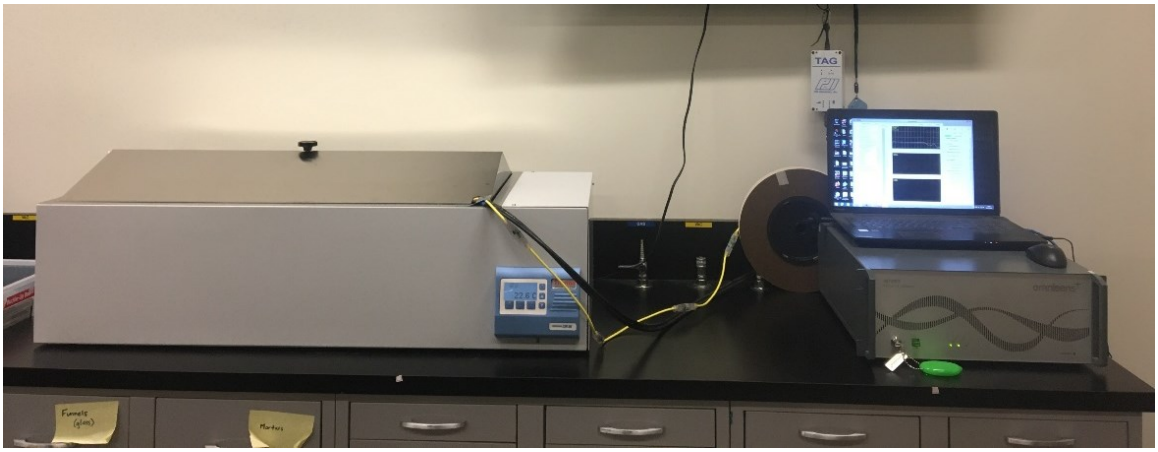

Figure 3-10: Photograph of the water bath testing setup.

Within the water bath, the two cable types were coiled in loops of approximately 10 inches in radius in the center of the bath, as shown in Figure 3-11. The cables were taped to the bottom tray of the bath to prevent flotation and keep the cables fully submerged during the test. A series of baseline readings were taken using the fiber optic analyzer to confirm that no significant bending strain was imparted on the fiber optic thermal cable. The cables exited the water bath at a small cutout in the lid, where they were routed to the respective reading systems, as shown in Figure 3-12.

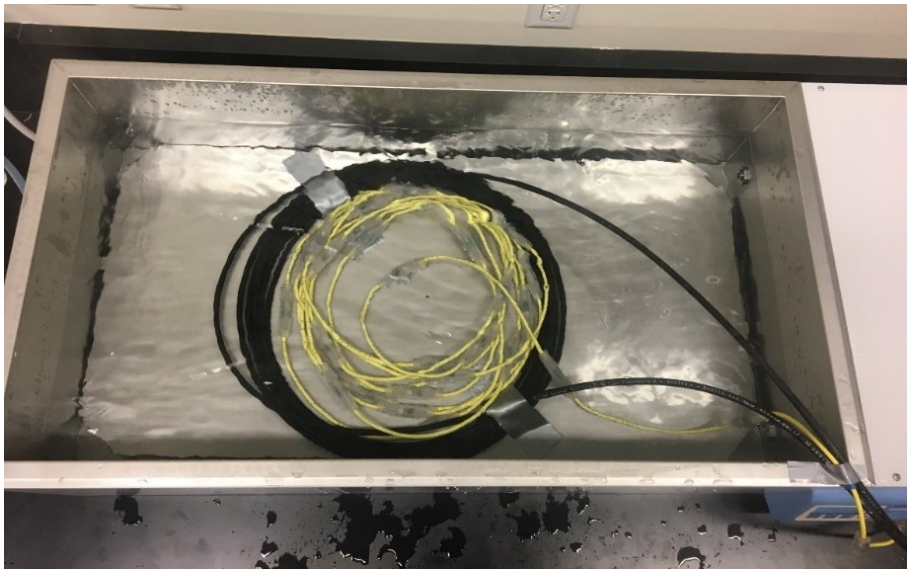

Figure 3-11: Photograph of the cable configuration within the water bath.

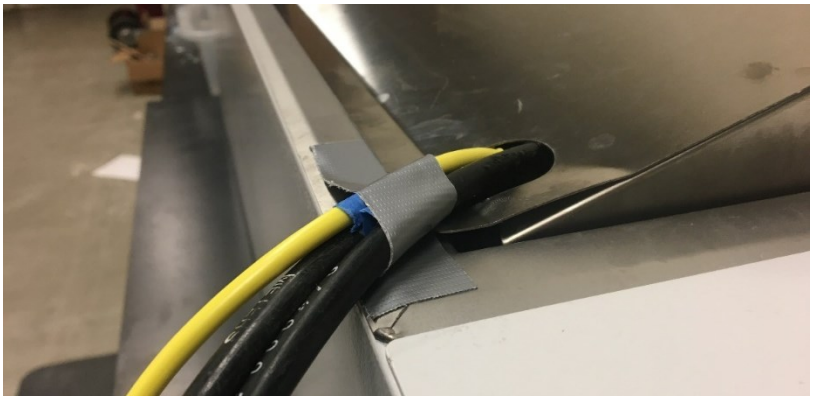

Figure 3-12: Photograph of the cable routing at the access port within the water bath lid.

The temperature set points during the test were manually recorded, with a minimum of 3 readings from the fiber optic analyzer at each set point. The TIP data logger was set to read automatically at 1-minute intervals. The holds at each temperature were a minimum of 12 minutes long to allow for 3 full thermal fiber optic readings, each taking approximately 4 minutes to complete. No fiber optic readings were taken during the transitions between temperature set points, although the TIP data logger continued to take readings during these

transitions. The ambient air temperature within the laboratory was also automatically recorded using a digital thermometer.

While the TIP data logger records in temperature Fahrenheit, the fiber optic analyzer outputs peak Brillouin frequency for each readout point along the cable, as shown in Figure 3-13. The conversion from frequency to temperature is a linear transformation. The slope is a standard value based on the coefficient of thermal expansion of the glass fiber core that falls within a narrow range for all telecommunications fiber. The slope value can be fine-tuned using laboratory testing in a water bath like this experimental setup. The offset can vary depending on the analyzer and specific cable and is best determined using a series of measurements at a known temperature. In this case, the temperature measurements on the fiber optic cable outside the water bath were compared to the measurements from the digital thermometer, and an offset was fit to minimize the difference between the two temperature records. This approach is identical to what was performed in the field testing, with the cable recorded temperatures outside of the drilled shafts fit to temperature measurements of the ambient air during readings.

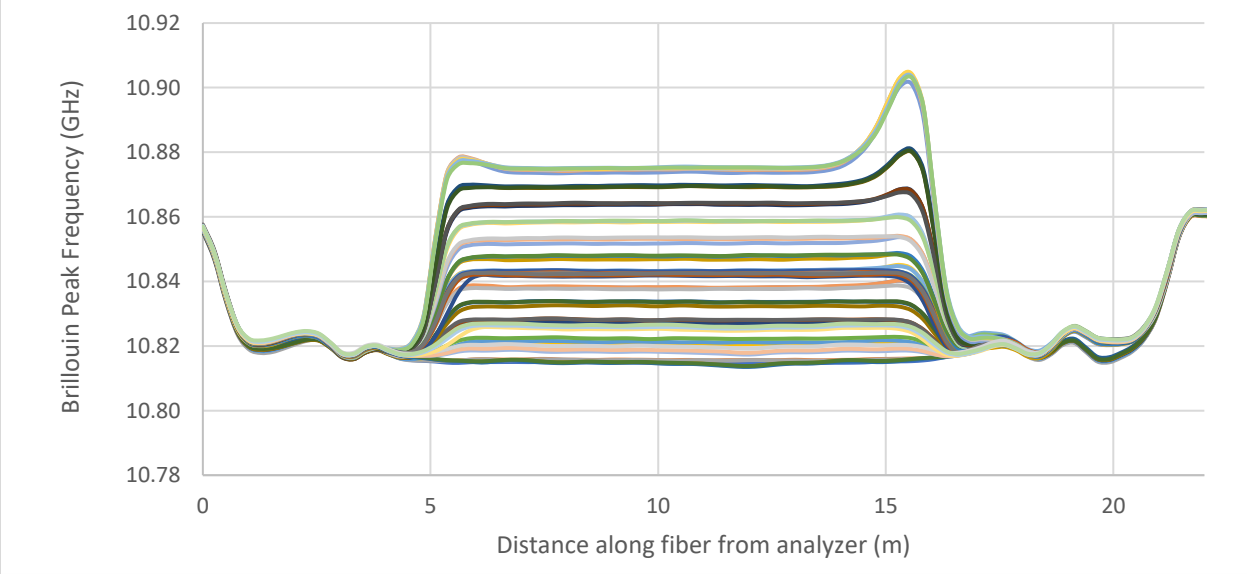

Figure 3-13: Fiber optic peak frequency during water test.

The section from approximately 6 to 16 meters in Figure 3-13 represents the 10 meters of thermal fiber optic cable within the water bath. The peak frequency within the majority of the submerged cable is horizontal and linear, indicating that the cable is experiencing uniform temperature and no external mechanical strain. The two peaks of higher frequency (and associated higher temperature) represent the points where the thermal fiber optic cable entered and exited the water bath. Upon inspection after the testing, it was noted that the cable in these areas was resting directly upon the metal tub of the water bath (Figure 3-12), which was experiencing hotter temperatures than the water itself. At the rim of the bath, one

of the thermal cables is on top of the other. The cable that was in direct contact with the tub of the bath is shown as the higher peak within the data readout.

Following the conversion of the raw fiber optic frequency data into temperature, the results between the TIP thermal wire and the distributed fiber optic system could be compared. For the purposes of the comparison, a single measurement point for each system at the center of the submerged portion was chosen for plotting. The measured temperature for the two systems is shown in Figure 3-14.

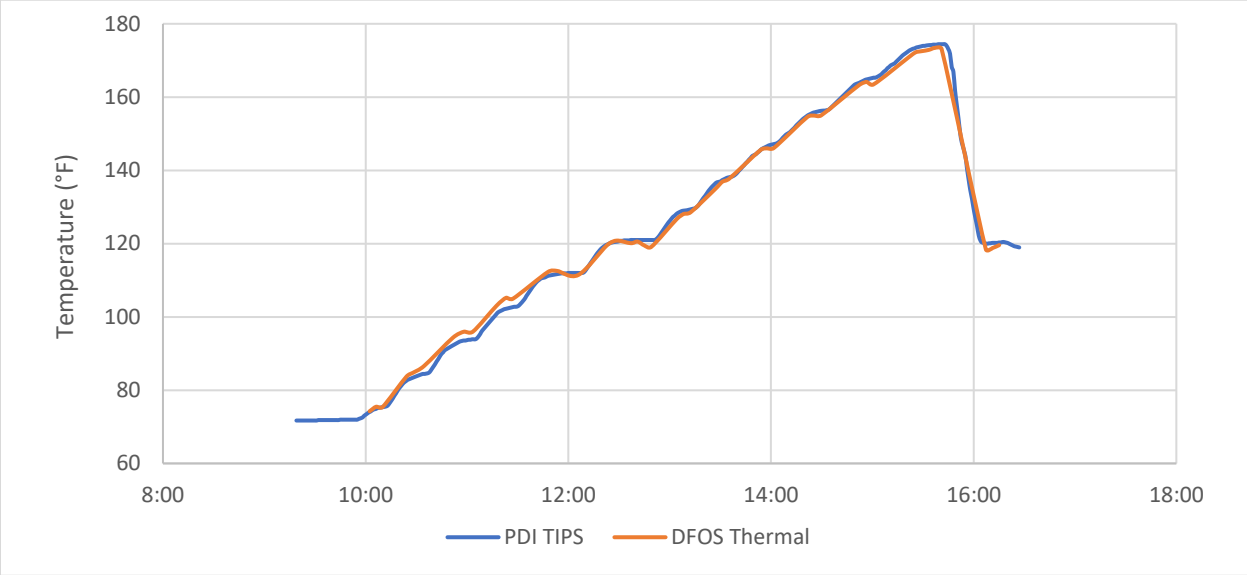

Figure 3-14: Recorded temperature during the water bath test from the two measurement systems.

As can be seen in Figure 3-14, the two systems recorded very similar temperatures. The average deviation between the two systems during temperature hold periods (excluding records during temperature transitions) was less than 0.1°F. The fiber optic cable took a longer time to equilibrate at the water bath temperature than the TIP sensors, lagging the water temperature by approximately 2-4 minutes and 2-3° F as compared to the temperature set point. This analysis was compared for all measurement points for both systems and the results were similar within the submerged portion.

One area of difference that is important to note is in sections of high thermal gradient, or a concentrated temperature change. This is most evident at the entry and exit of the water bath, although the temperature spike from the water bath tub partially conceals the true magnitude. As can be seen in the transition, the temperature readings going from the water to the ambient air extend over 1-2 meters. This is due to the spatial resolution limitation of how the fiber optic analyzer functions. For each reading, the Brillouin frequency peak represents a “sample” of the fiber optic cable. While the sample is not quite an arithmetic average, the reading output is influenced by the measured strain or temperature within this length. The spatial resolution of the analyzer was set at 0.75 m. Therefore, for a reading just at the edge of the water bath at a

high temperature, the reading is influenced by both the water temperature and the ambient air temperature. This creates a smoothing effect that can be seen in the lower temperature data. The extension of this effect at higher temperatures from the artificial peak is instead believed to be conduction within the cable, as opposed to a real artifact of the fiber optic reading method.

3.4 Commercial Analyzer Measurements During Variable Strain

Distributed fiber optics offer a near-unprecedented distribution and density of strain measurement along the installed route. However, with this dramatic increase in range and coverage comes an associated drawback of a long reading time. Rather than readings being taken over a few seconds, many commercial distributed fiber optic interrogators require minutes to complete a distributed reading. During this reading time, it is unclear from the manufacturer's product specifications how the optical system and associated algorithms deal with changing strains along the fiber length during the reading interval. A laboratory test of a popular commercial distributed fiber optic strain sensing system was conducted to examine the effect of reading time on interpreted strain data over a range of varying strain.

Test Approach and Setup

The main criteria of the test are to be able to apply a controlled, measured, and linearly variable displacement along a length of fiber optic cable with time. To maximize the benefit of the test and the applicable strain ranges, the original test plan was to include multiple fiber optic loops of varying lengths, each attached to the same linear actuator. In this design, applying a single displacement could produce multiple strain ranges, depending on the length of each fiber loop. Over a series of visits to the Pacific Earthquake Engineering Research Center (PEER) at the UC Berkeley Richmond Field Station, several potential test setups and orientations were explored with the PEER researchers. The original test design called for the fibers to be oriented vertically - offering the benefit of the self-weight of the fiber contributing to pre-tensioning the fibers. Unfortunately, no area with both adequate headroom and an easily accessible fixed point was available. The option of fixing the top cable pulley to the lab gantry crane was considered but was abandoned due to safety concerns related to access. Ultimately, it was decided to switch to a horizontal orientation of the fiber optic cables with two loops with a length ratio of roughly 1:2, as shown in Figure 3-15.

The test setup was oriented to the south face of the strong wall in building 484 at the Richmond Field Station. The pulleys were attached using threaded rods into the existing anchor holes in the strong wall blocks, while the clamping mechanism was assembled using steel members at the east end of the Single Degree of Freedom shake table. A component diagram of the test layout is shown in Figure 3-15.

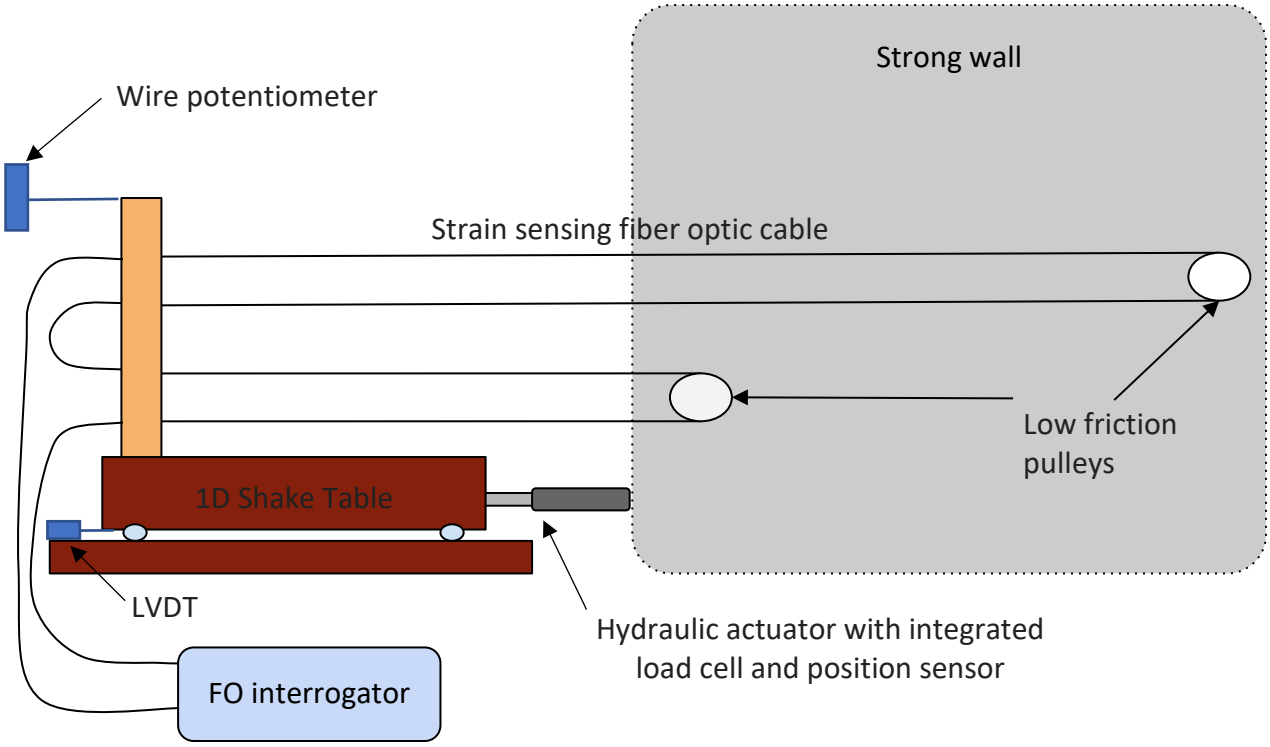

Figure 3-15: Component diagram of the test layout

The pulleys, as shown in Figure 3-16, were selected to be made of a low friction material to allow the cable to rotate around the pulley axis freely. The pulleys were 6” in diameter; chosen based on the center-to-center clamp spacing as well as ensuring a large enough curvature to prevent the risk of signal loss or breakage in the fiber optic cable during testing. The pulleys had a circular cross-section channel ~¼” deep to route the cable within. The pulleys were mounted vertically using a threaded rod in the anchor holes in the first and last blocks of the strong wall. The clamps and pulley heights were selected to have the cable arms as close to horizontal as possible. Nuts were installed on the threaded rod to prevent the pulleys from moving along the bar, although a small gap was left between the nuts and pulleys to allow free rotation of the pulley on the bar.

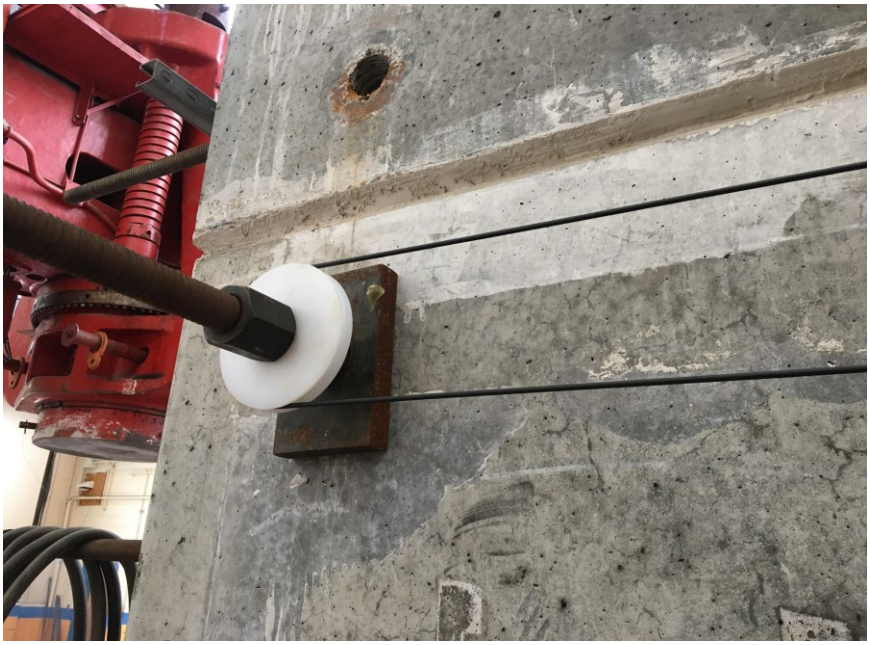

Figure 3-16: Photo of Loop 2 (long loop) pulley mounted on strong wall

Each clamping mechanism was made of two separate pieces of wood (see Figure 3-17). The first was a vertical length of 2x12 lumber, connected to a stack of cross steel members that were bolted to a horizontal extension from the shake table. This vertical board provided the clamping face for all four loops. Adhesive discs of 40-grit sandpaper were adhered to the face of the 2x12 along the four cable paths to increase the friction between the wood and the cable. Four 11.25" long wood boards (custom planed lumber 2" x 5") were then bolted to the clamping face of the lumber using 1⁄2" diameter bolts with fender washers to distribute the clamping load along the board. A triangular channel was cut into the centerline of each board using a table saw with the blade tilted at a 45° angle, then smoothing the lip using a hand plane. Various depths of the channel were tested to maximize the clamping force while avoiding crushing (and potentially damaging) the cable. A final depth of the channel of 3mm (for the 5mm diameter cable) was chosen. The clamping bolts were tightened in an alternating pattern to ensure the clamping force was applied symmetrically. During the tightening of the clamps, the fiber optic cable was pulled taught by hand to remove slack in the system and apply an initial pretension to the cable. The bolts were then tightened to 10 foot-lbs using a torque wrench to ensure an even clamping force between all four boards. Tell-tale marks were made on each cable at the front and rear of the clamp to provide a visual check of any slippage of the cable during the test.

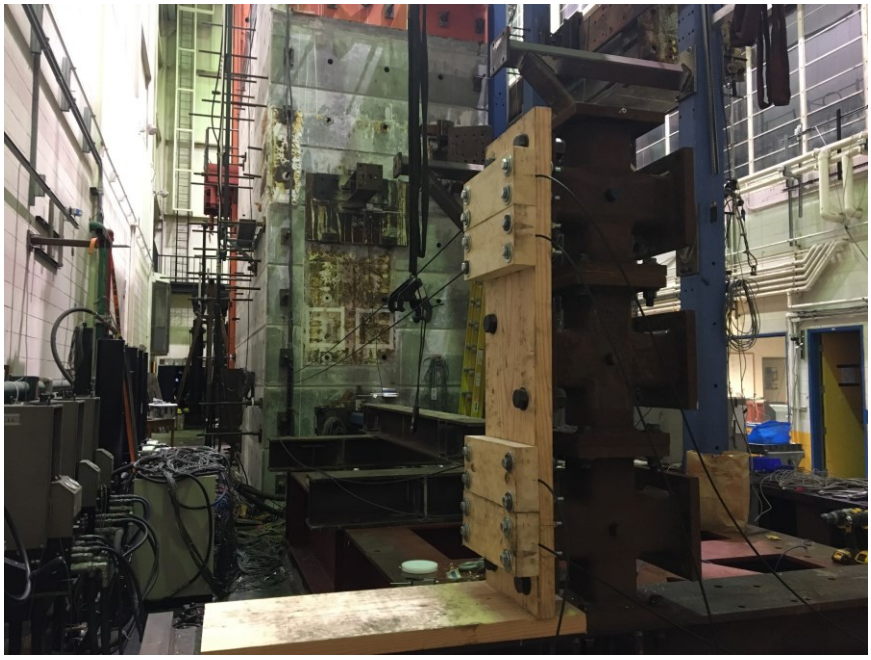

Figure 3-17: Photo of wood clamp setup at far corner of 1D shake table

In addition to the fiber optic strain measurements taken during the test, four other instruments were used to monitor the test procedure, as shown in Figure 3-15. The first pair was the displacement sensor and load cell, which were incorporated into the hydraulic piston attached to the shake table. Although these instruments were not installed specifically for our test, the data from these were recorded and used to control the movement of the shake table. The second pair of instruments were two displacement gauges attached near the clamping mechanism. The first, an LVDT, was attached at the base of the shake table to measure the linear displacement of the cable directly beneath the clamping mechanism. The second, a wire pot potentiometer, was attached at the top of the clamping mechanism to the wall via a wire to measure any differential movement between the base of the shaking table and the top of the clamp. The potential sources of the differential movement identified prior to testing were movement within the horizontal bolt connections (the holes were oversized compared to the bolts) and bending of the stack of x-connectors that the cable boards were clamped to. Prior to installation, each potentiometer was calibrated for a range of 0.3” to 1.8”, allowing a functional range of 1.5”. With the fiber optic cables slack, the table was also checked for linearity and error over the range of desired displacement rates. An achievable displacement rate of 1mm was established and was set as a lower threshold in the testing plan. The table was then centered at approximately 0.3” in the stroke of the potentiometers and the cable was tensioned by hand and clamped.

Test Program

A three-part test program consisting of three primary set points and two intermediate points was designed to explore a range of strain combinations. The baseline zero for the test was established after setting the zero setpoint of the fixed table and pre-tensioning the fiber optic

cables by hand in the clamps. From the baseline, target setpoints of 10 mm and 20 mm displacement were established. In between these setpoints, intermediate points of 5 mm and 15 mm were also established to provide an average value of the primary setpoints. The primary and intermediate setpoints, as well as the calculated associated strains, are presented in Table 3-5. A large range of strains was chosen to test (ranging from 0-2466 με) to explore the effect of different magnitudes of frequency (strain) shift during the fiber optic readings. The first phase of the test was taking steady (constant) strain readings at the 3 primary setpoints (pretension, 10 mm, 20 mm). Once the primary setpoints were taken, additional steady readings were taken at the intermediate setpoints (this step was postponed as there was concern that the actuator may not achieve precise displacements of 10 and 20 mm during testing).

Table 3-5: Proposed primary and secondary test setpoints

	Loop 1 **Installed length: 8.11m**	**Loop 2** **Installed length: 15.75m**
Displacement (mm)	Strain (microstrain)	Strain (microstrain)
0 (pretension)	0	0
5	*617*	*317*
10	1233	635
15	*1850*	*952*
20	2466	1270

The second phase of the test consisted of fiber optic strain readings taken while first ascending, then descending, between the primary setpoints over a 5 minute (300 second) constant displacement rate. The 3 ramp intervals were 0 – 10 mm, 0 - 20 mm, and 10 - 20 mm.

The third phase consisted of fiber optic strain readings taken while changing the strain rapidly (over 10 seconds) between setpoints at the 2.5-minute point in the reading. The same intervals as in the second phase testing were used. For all individual tests, as well as the holds, 3 readings using the fiber optic analyzer were taken to capture any potential scatter or variance in repeatability.

The fiber optic strain readings were taken using the commercial Ominsens DITEST fiber optic analyzer in BOTDA mode. The fiber optic analyzer settings were carefully controlled to reliably complete each reading within exactly 5 minutes, +/- 2 seconds. Since the settings directly affect the later interpretation of the fiber optic strain data, both the scanning window and frequency step of the analyzer were selected using the minimum values to provide the best achievable frequency resolution, given the reading time constraint. The fiber optic analyzer settings are presented in Table 3-6.

Table 3-6: Fiber optic analyzer read settings

Sensor length (m)	100
Spatial resolution (m)	0.75

Sampling interval (m)	0.25
Measurement step (MHz)	0.2
Start manual scan (GHz)	10.87
Stop manual scan (GHz)	11.06
Averaging (profile)	2000

Based on the above settings, the analyzer performed a scan in 951 steps, with an approximate duration of 0.315 seconds per frequency step (based on the 5-minute read time - it is unknown if a portion of the read time at the beginning or end is used for the system function outside of the reading duration). Based upon this timing, the readings for the control and the other measurement data acquisition system were taken at 10 Hz.

Deviation from Test Program

Three deviations were encountered during the test program. The first, which was expected based on preliminary testing with the 1D shake table control system, was that the actuators were not reliably reaching the input test points. This may have been due to a miscalibration within the control system, or potentially from the extra load imparted on the system by the tension from the fiber optic cables. However, the deviation from the setpoint was repeatable in a series of test cycles and was therefore considered acceptable for the purposes of this project.

The second deviation was that a linear (non-constant) difference was observed between the displacement measurements at the base of the shake table and the top of the clamping apparatus. While this was not entirely unexpected and was the motivation for including the two measurement points in the first place, it provided an unforeseen challenge in selecting which displacement to use in the subsequent analysis of the fiber optic strain data. The identified options were to use the bottom displacement, the top displacement, or a linear interpolation between the two. Given the various system design components and the fact that most of the opportunities for relative movement were low in the system, making a linear interpolation potentially inappropriate, it was decided to use the top displacement for analysis.

The final and most significant deviation involved an interruption to the proposed test program. During the initial cycle testing (0 – 10 mm), a loud noise occurred in the laboratory, and it was observed that a separate hydraulic jack unrelated to the fiber optic test had fully extended itself, significantly tilting the structural specimen that it was attached to. While the cause for this issue was unknown but suspected to be a valve leak somewhere in the hydraulic system, these concerns dictated that the fiber optic test be halted and postponed to a later date. As a result, the subsequent analysis is based on the first 3 load cycles and not the originally proposed test program.

Results and Data Analysis

A preliminary reading taken prior to the pretensioning of the fiber optic cable was made to establish the amount of pretension applied to the cable. The average applied pretension was

395 με on the short loop (loop 1) and 463 με on the long loop (loop 2). The processed strain data for the pretension is presented in Figure 3-18. The difference in the strain between the two loops is due to the variation in the manual pretension prior to clamping. The amount of tension was based on manual grip, simulating the common pretensioning practice for fiber optic cables in the field.

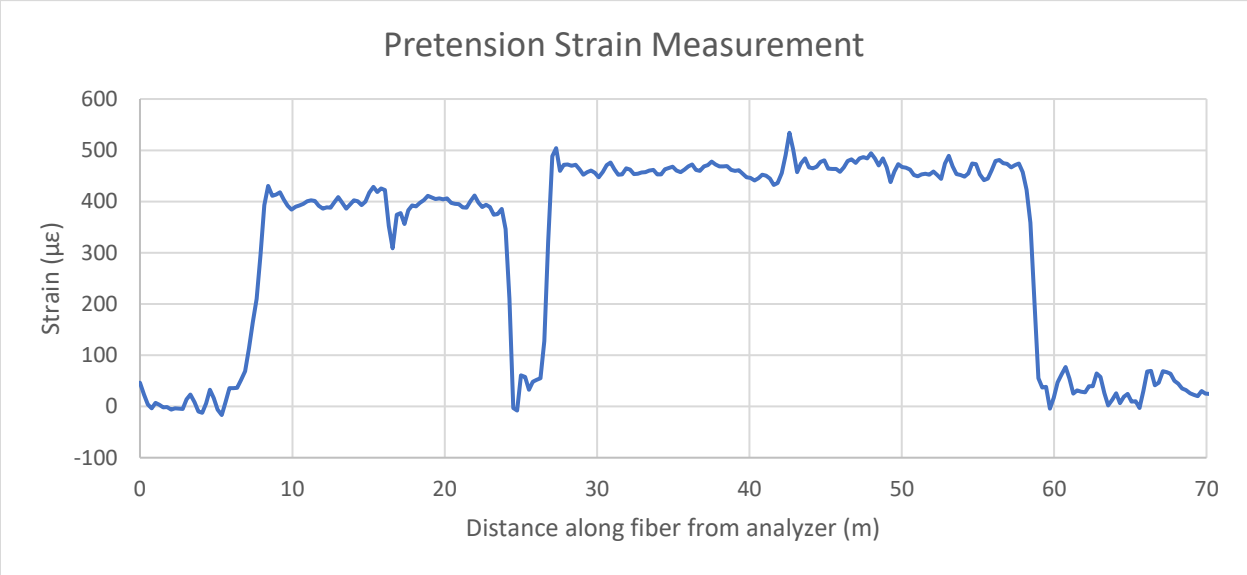

Figure 3-18: Strain measurement after initial manual pretension of fiber loops

Due to the edge effects within the spatial resolution of the analyzer, 0.5 m at each clamp was removed from subsequent processing, as well as the strain gradient around the pulley turnarounds. Loop 1 is indexed as 8.678-16.08 m (A) and 16.59-23.992 m (B) from the analyzer, while Loop 2 is indexed as 27.566-41.859 m (A) and 43.390-57.684 m (B) from the analyzer.

The first 2 load cycles were performed ramping from 0 (pretension) to 10 mm displacement. The top displacement potentiometer indicated that an actual displacement of 8.135 mm was achieved, with repeatability between the two cycles of 0.005 mm. Readings at the 10 mm setpoint (1 cm target, 8.135 mm actual) and 0 mm were taken between cycles. The associated strain measurements are presented in Figure 3-19. It is noted that the measured peak strains in Loop 1 and 2 were within 4 and 8%, respectively, of the calculated equivalent strains based on the displacement measurements.

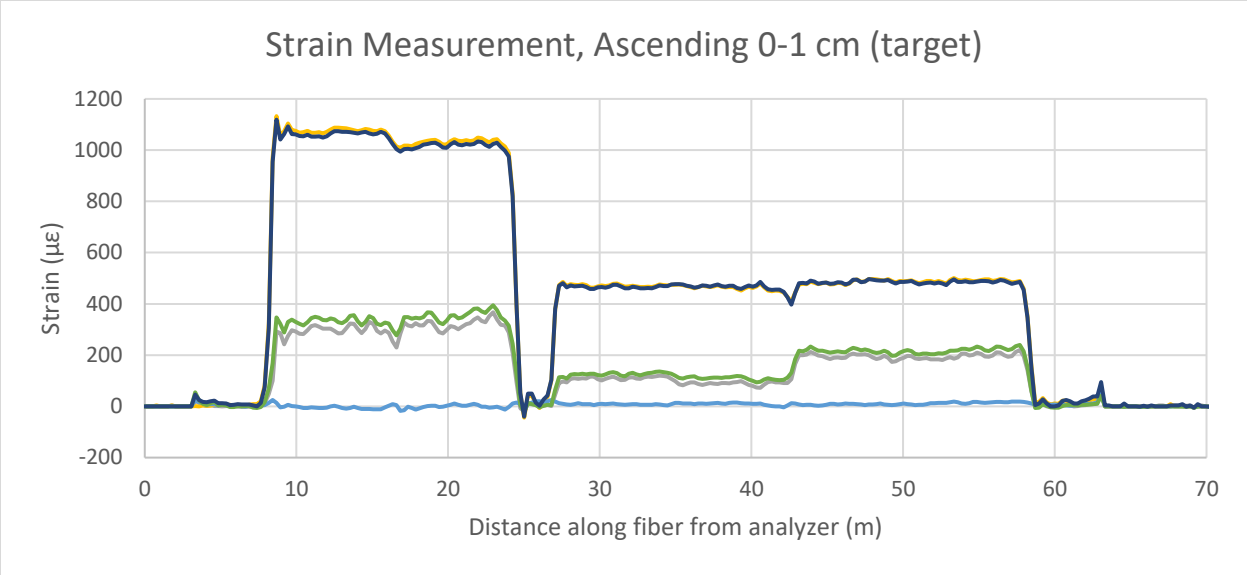

Figure 3-19: Ascending strain measurements, run 1 (grey) and 2 (green)

As shown in Figure 3-19, the higher lines represent the static strain measurements at 10 mm (target) displacement, while the intermediate lines represent the readings taken during the two ramp cycles (run 1 (grey line) and run 2 (green line) in Figure 3-19). It is clear that the intermediate strains do not represent an average (visually halfway) of the applied strains during the ramp cycle, indicating that the reported strain measurements were taken at different times during the 5 minute load. The Brillouin peak frequency values during the two ramp readings from 0 - 10 mm (target) are shown in Figure 3-20. Comparing the order of the Brillouin frequency, from smallest to largest, to the overall percentage of the total applied strain, it can be observed that an increase in the 3 starting frequencies correlate to the magnitude of the strain measurement during the transient reading. Since the strain is increasing linearly, this intuitively supports that the lower frequency portions of the fiber are being interrogated by the analyzer earlier than sections with higher frequency.

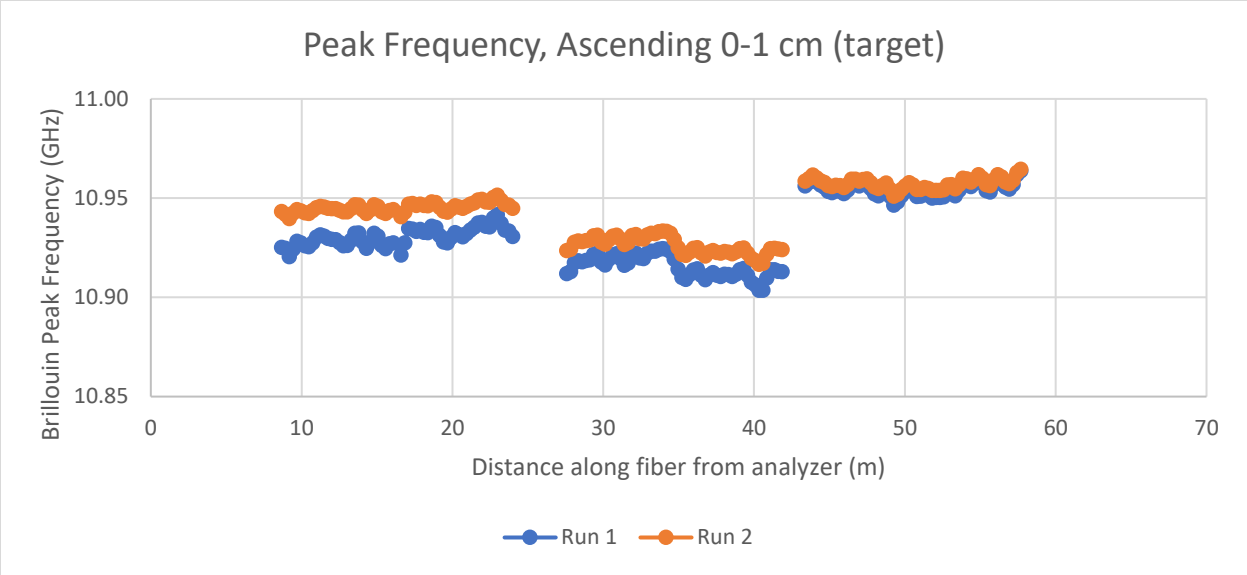

Figure 3-20: Peak frequency during two ascending strain reads

Based upon correspondence with the fiber optic analyzer manufacturer, it is understood that the analyzer sweeps from the bottom of the frequency sensing window to the top in the prescribed measurement step. This would indicate that sections along the fiber where the Brillouin backscatter is at a lower frequency would be read earlier in the read interval than those at a higher frequency. This can be represented visually by plotting the measured strain against the associated frequency, as shown in Figure 3-21, and an approximately linear trend in the data can be observed. The scatter in the data is within the system repeatability of approximately +/- 20 με. The linear trend can become even more evident if we separate the readings from the two loops and add the measured strain values at the 0 and 10 mm (target) displacements, forcing them through the minimum and maximum limits of the frequency sweep window. This is shown in Figure 3-22 for loop 1 and Figure 3-23 for loop 2. The strain readings during the ramp cycle plot linearly depending on their peak frequency between the minimum and maximum window frequency limits and the associated minimum and maximum strain (measured in static readings).

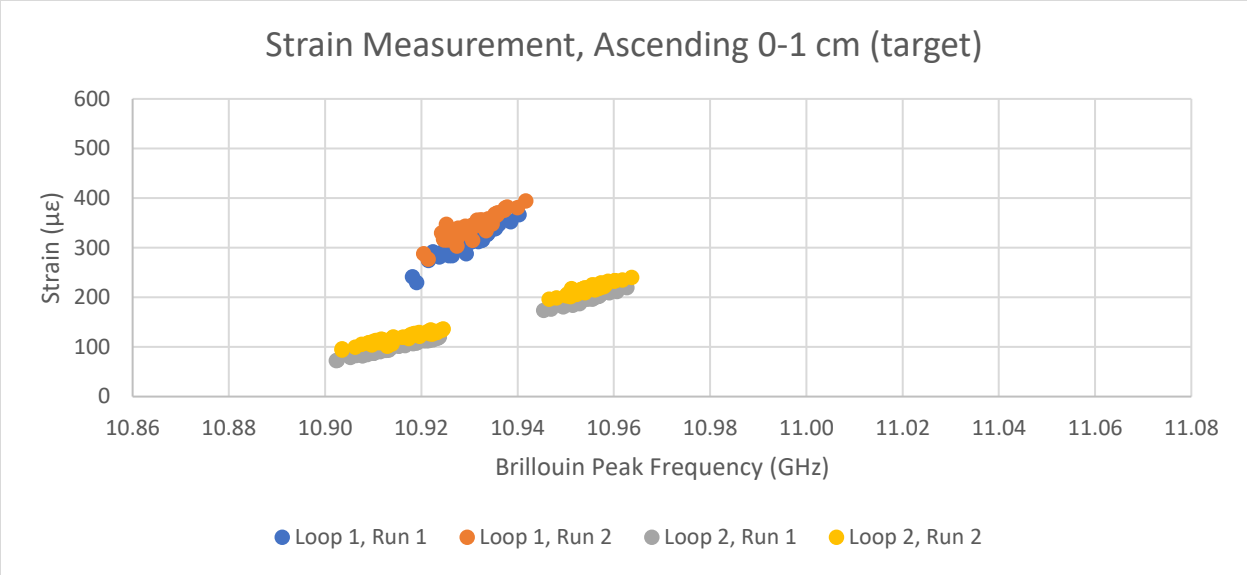

Figure 3-21: Strain vs. peak frequency during ascending read

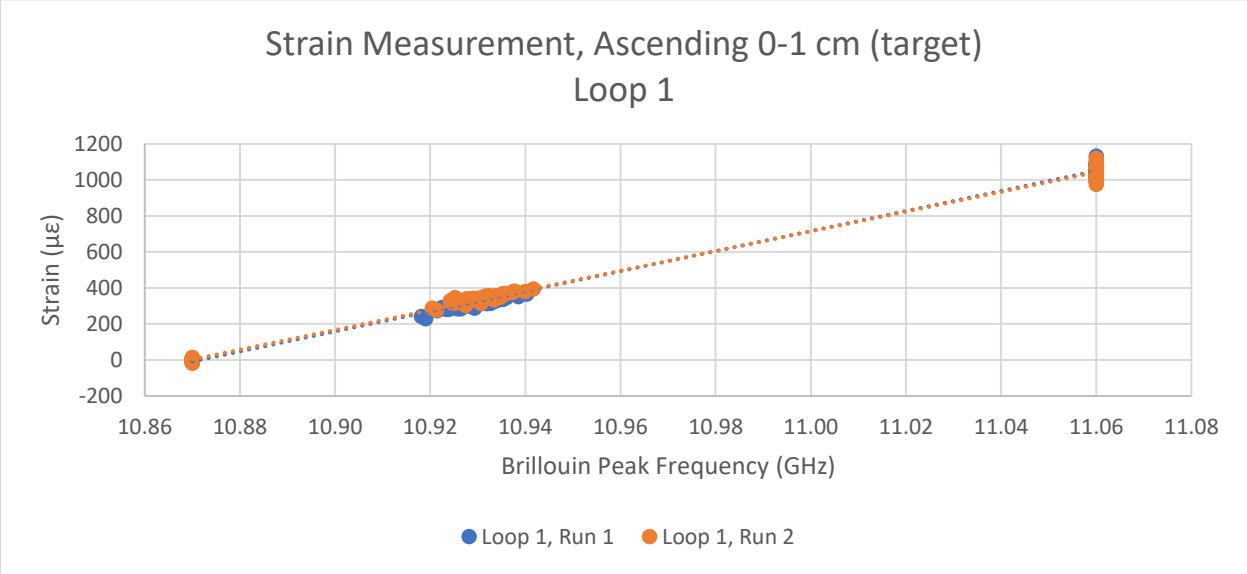

Figure 3-22: Strain vs. peak frequency during ascending reads, Loop 1

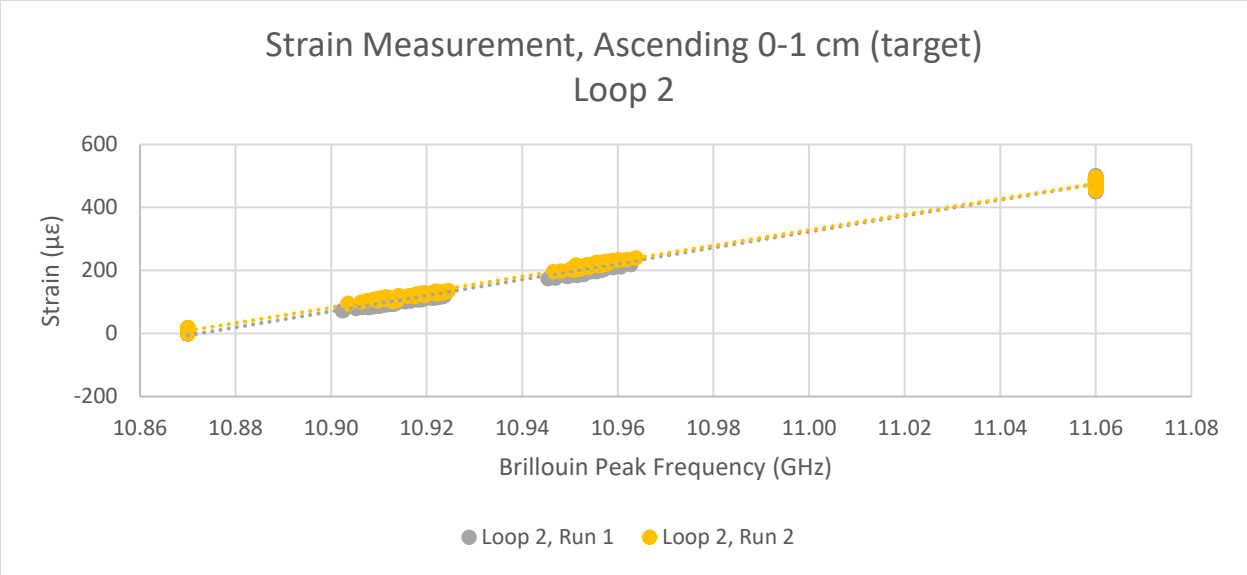

Figure 3-23: Strain vs. peak frequency during ascending reads, Loop 2

A third load cycle was performed ramping down from 10 - 0 mm. In this case, the trends observed in the two ascending load tests were reversed. Figure 3-24 shows the strain profiles at 10 mm displacement (blue line), 5 mm displacement (red line) and 0 mm displacement (grey line). It is noted that in the final descending load cycle, the fixed table overran the 0 cm setpoint, resulting in a negative strain relative to the pretension baseline. The strain vs. peak frequency plot during descending read is given in Figure 3-25 for loop 1 and Figure 3-26 for loop 2. Again, the strain readings during the ramp cycle plot linearly depending on their peak frequency between the minimum and maximum window frequency limits and the associated minimum and maximum strain (measured in static readings).

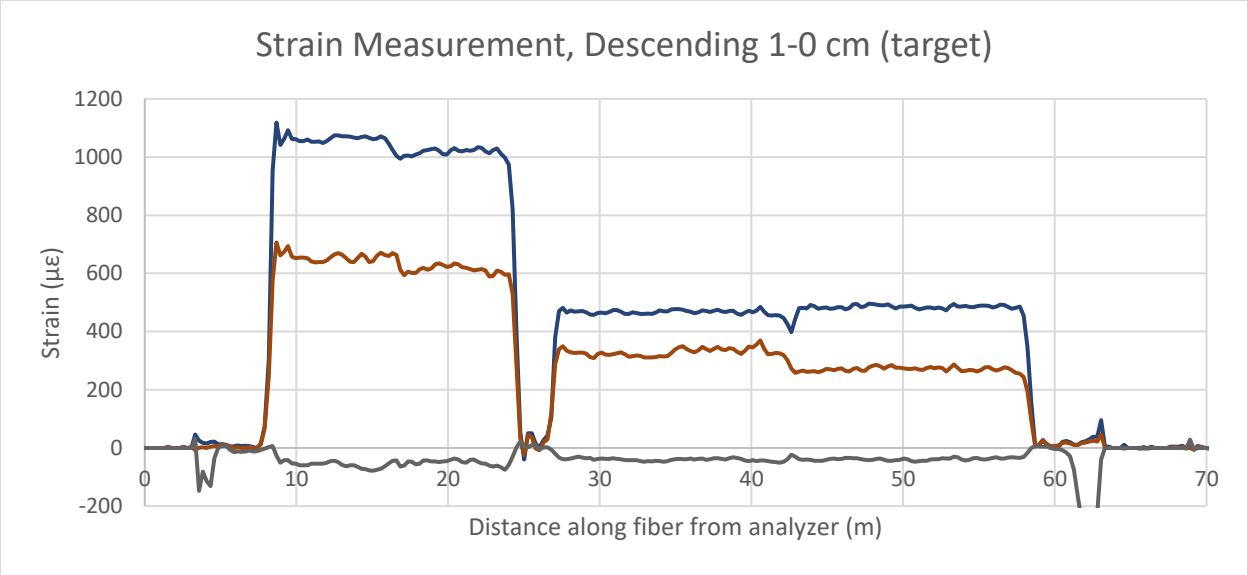

Figure 3-24: Descending strain measurements (brown)

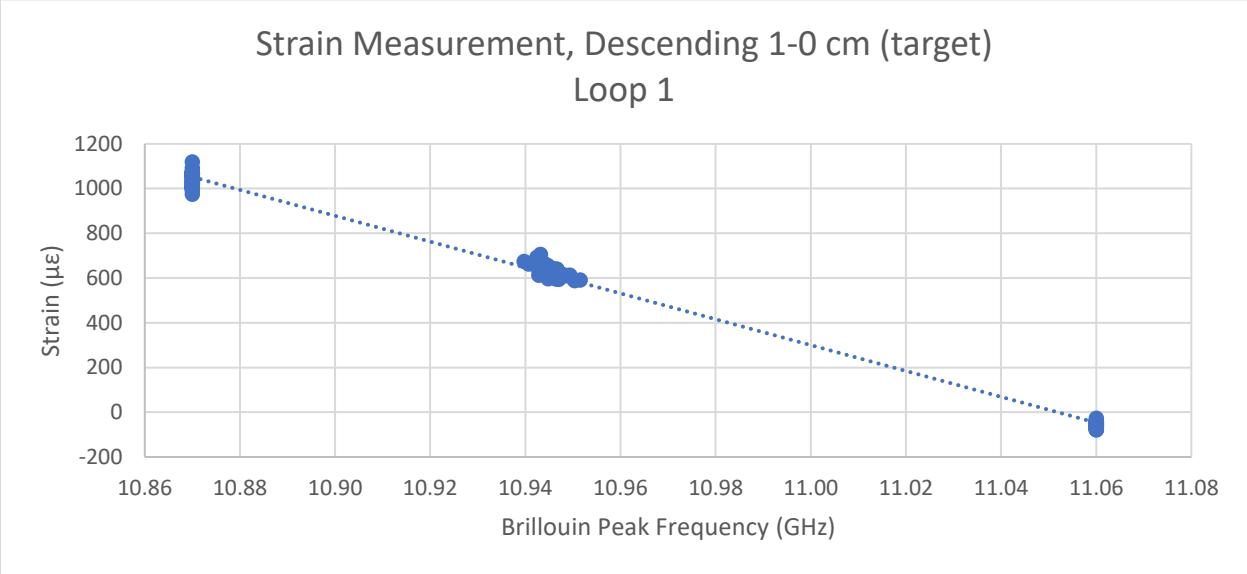

Figure 3-25 Strain vs. peak frequency during descending read, Loop 1

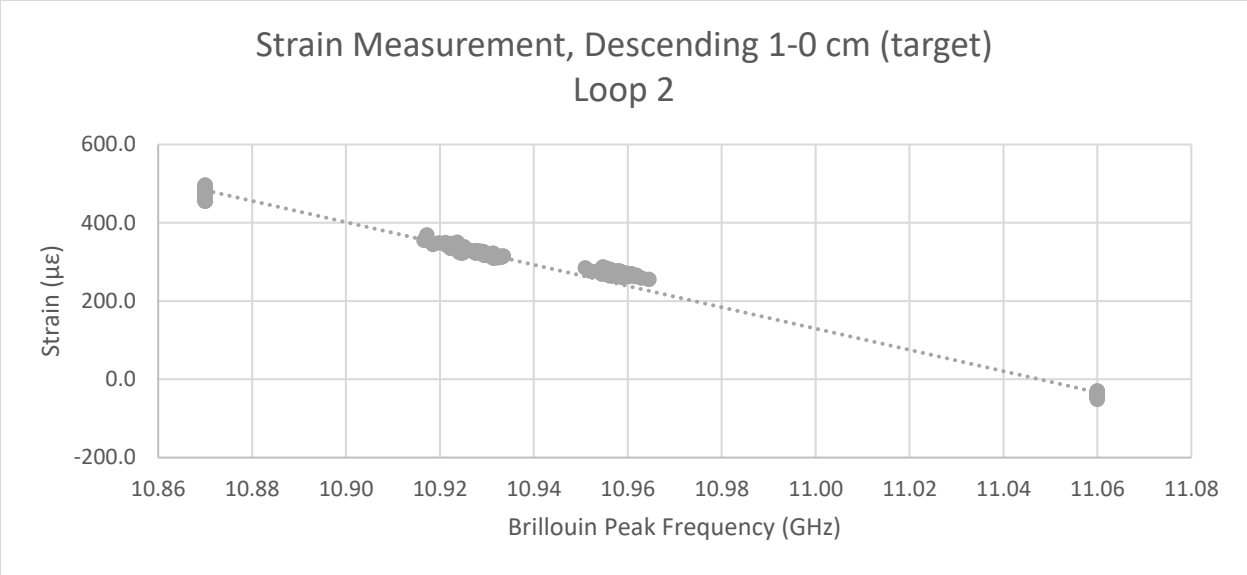

Figure 3-26: Strain vs. peak frequency during descending read, Loop 2

Discussion

As was initially suspected based on previous laboratory and field testing using the commercial fiber optic analyzer, the strain profile from a single reading taken during transient strains cannot be treated to represent the average strain along the fiber during the reading time. Instead, the resultant strain is a function of the Brillouin peak frequency, where it falls within the analyzer sweeping window, and the actual strain measurement at that time.

A preliminary literature review did not reveal any previous discussion of this limitation of the use of distributed fiber optic strain sensing during transient loading. This represents a potentially major caveat that must be incorporated in the presentation and analysis of any distributed fiber optic data during transient (or even suspected transient) loading. The correction of such data may be possible, but at this point this would rely on the assumption that the strain field is uniform along each interval of fiber (in our case, Loop 1 and Loop 2). There are several cases in which this can be true, such as suspended fiber in tension (relative displacement between two points), or uniform axial loading, such as in a vertical column. In these cases, the data can be linearized between the starting and ending frequency scans, and the approximate equivalent strain can be chosen at any time within the reading interval.

For installations of fiber optic cables in non-uniform strain fields, such as elements in bending or undergoing differential loading, the above processing technique can allow for an estimate of the time when each strain reading along the fiber was taken during the reading interval, but the strain profile cannot be collapsed to a single time since the potential range at each point is unknown.

For this challenge, three possible recommendations for potentially removing or addressing this error in the future have been identified:

- Whenever possible, hold the load constant during the fiber optic analyzer reading interval. For example, during load tests of structural elements, measure and hold the load constant rather than providing a controlled pressure (which can decrease with diminishing load).
- Reprogram the fiber optic analyzer to perform its averaging over all frequencies in the reading window, rather than at each frequency step. In this way, for a hypothetical 500 step reading sweep, all 500 frequency steps would be performed, then repeated multiple times over the averaging input. This would produce a true average over the reading interval, as well as potentially allow for statistical analysis of the distribution of the frequency peaks at each point, potentially allowing for the back calculation of the associated strain range during the reading interval (this would depend on the signal-noise ratio for each individual read which is not published).
- Select an analyzer with a faster reading time. The development of a Brillouin-based distributed fiber optic strain analyzer at Berkeley is ongoing, which can achieve sub-1 second reading intervals.

Short of implementing one of the above recommendations or development of another technique to address this potential shortfall of distributed fiber optic strain reading, it is important that practitioners recognize this behavior of fiber optic analyzers and incorporate this understanding into the presentation and analysis of distributed fiber optic strain data. While distributed fiber optic strain sensing still offers a good deal of value in many civil engineering applications where changes in strain are on time periods far in excess of the reading interval (months-years), there are several instances where strains cannot be treated as constant in the minutes-long reading intervals of fiber optic analyzers.

4. Distributed Fiber Optic Sensing for Deep Foundation Strain

Distributed fiber optic sensing is uniquely suited for monitoring strain development and distribution in deep foundation elements. The continuous strain profiles that fiber optic sensing provides can allow the project team and engineers to gain insight into the pile behavior and load shedding that would be infeasible with point-based strain sensors. Furthermore, the installation of fiber optic sensing cables is no more onerous than the data cables already required for point-based sensors. While the use of fiber optic sensing for deep foundation monitoring has been adopted abroad, both in research and production projects, its use in North America remains relatively rare.

This chapter is intended to provide a detailed description and analysis of the use of distributed fiber optic sensing for the measurement of strains in deep foundations on a trial project in California. The project was sponsored by the California Department of Transportation (Caltrans) to trial the use and performance of post grouting for deep foundation improvement. While the primary project motivation was to explore the reliability and performance of various base grouting delivery systems, a secondary goal was to provide an opportunity to deploy fiber optic sensing for measurements of strain during both grouting and the subsequent load testing. The focus of the analysis is on the unique insights into the pile performance during the two construction phases that the fiber optic monitoring systems were able to offer. The chapter is divided into the following sections:

4.1 Literature Review
4.2 Project Introduction and Test Overview
4.3 Fiber Optic Strain Measurements During Grouting
4.4 Fiber Optic Strain Measurements During Load Test
4.5 Discussion

4.1 Literature Review

Distributed fiber optic monitoring of deep foundations has been the topic of research as early as the mid-1990s (Vulliet et al. 1995). These earliest field trials used sensing technology based on careful measurements of changes in length of a pair of fiber optic cables embedded within a pile. This technology was interferometric and relied on one fiber being mechanically coupled to the concrete or rebar, while the second was isolated from mechanical movements. The resulting measurements were changes in length over the monitored zone, providing a single point-to-point distance along the length of the fiber optic cable. While the entire length of the fiber optic cable was used as the gauge length of the measurement, the differential change in length could not be localized along the fiber optic cable and indeed only a single measurement value (change in length) was provided by the measurement. This system and similar types were termed *fiber optic extensometers* and fall into a mid-point between point-based fiber optic sensing systems such as FBG sensors vs a truly distributed fiber optic sensing where multiple measurement/readout points are generated along the instrument fiber length. This trial highlighted some of the difficulties in embedding fiber optic sensors in foundation elements as

compared to above-ground concrete structures, including survivability and access during monitoring.

The first reference to the use of Brillouin-based distributed strain sensing for deep foundations was published in 2002 (Ohno et al. 2002). In this field trial, a BOTDR fiber optic analyzer was used to measure strain in two production piles in Japan: one for a bridge foundation and a second for a tunnel foundation. Each pile was instrumented with two vertical strain sensing fiber optic cable loops, each forming a loop along a single rod (down and up on the same rod) with the two loops located 180° apart in the pile. The rods were then attached to the steel reinforcement cage and lowered into the pile bore during construction. The fiber optic cable used for the experiment were nylon-coated single-mode fibers installed in a pair of opposing grooves in the steel rod. The cables were pretensioned to 0.1% strain and glued to the metal rod, after which the channel was filled with an epoxy. By this design, the cable is coupled in such a way to measure the axial strain in the metal rod. An image showing the schematic installation is shown in Figure 4-1.

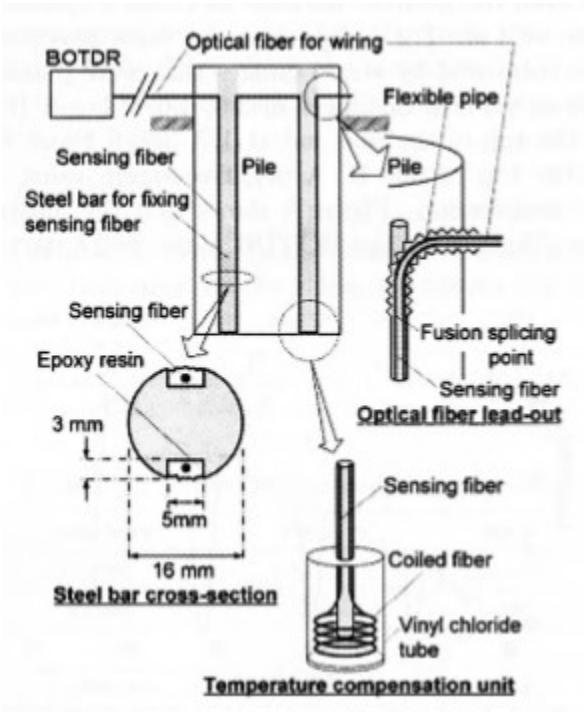

Figure 4-1: Schematic diagram of BOTDR strain measurement system (Ohno et al. 2002)

The results from strain monitoring during load tests on the two piles were positive, showing good agreement between the strain measurements from the BOTDR fiber optic system and an array of conventional point-based strain sensors. The averaged strain results from both systems at the four peak applied loads are shown in Figure 4-2.

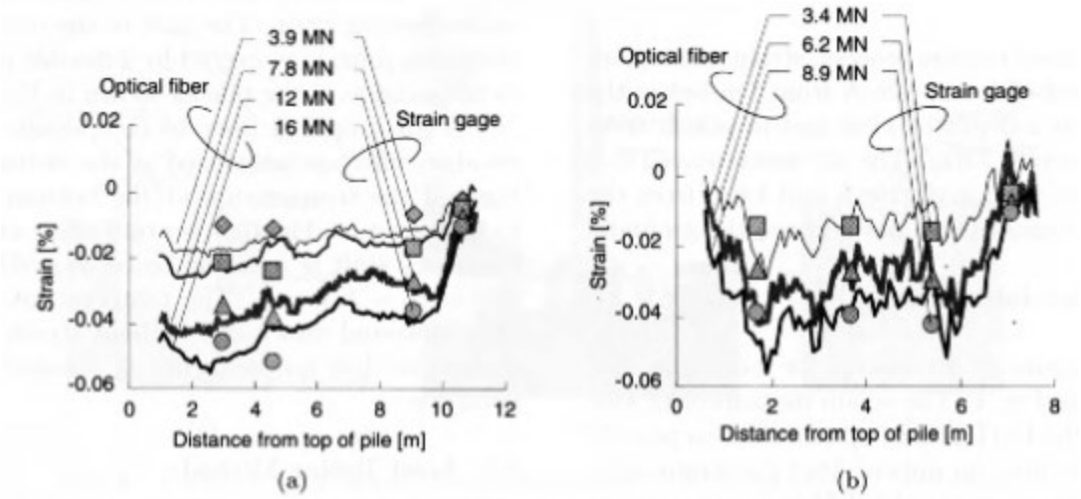

Figure 4-2: Load testing results from the two tested piles (Ohno et al. 2002)

As can be seen in the figures, particularly in the results from Pile A, the DFOS strain results match the results of the point strain gauges with relatively good agreement, both in trends with depth in the pile as well as relative strain magnitude with increasing load. The distributed strain data provided by the DFOS system has the added benefit of showing clearly how the strain distribution changes with depth, connecting the blanks between the discrete strain sensors. The authors observe but do not present that the data could be used to calculate the friction load shedding in the soil profile, observing changes in the slope of the strain correlating with stratigraphy changes at 4.6m and 9.1m in Pile A and 6.6m in Pile B.

By 2006, further research into the use of DFOS for strain measurements in deep foundations had been published based on work in the United Kingdom in collaboration between researchers at the University of Cambridge and Cementation Skanska (Bennett et al. 2006; Klar et al. 2006). There were several key differences in the installation methods employed in the UK versus the earlier presented research in Japan. Some of the more significant differences are listed below, divided by the two instrumented sites.

- Chattenden site, 14.3cm diameter minipiles
    - Unarmored, unreinforced plastic fiber optic cable used for strain sensing
    - Fiber optic cable was attached to a single vertical reinforcing bar in a loop (down and up the same bar), with the cable epoxied to the bar at 15-30 cm intervals (unclear if spacing was systematically controlled)
    - The strain cables were pretensioned with approximately 2000-3000 με prior to being epoxied to the bars
    - The strain readings along each bar were averaged to reduce random error in the readings (this approach is suspected but not stated in the Ohno research)
- Farringdon site, 1.2m diameter piles
    - Reinforced ribbon-style fiber optic cable used for strain sensing

- A single fiber optic loop was installed on the reinforcing cage, with each vertical clamped to a reinforcement bar at the bottom of the lowest cage section and the cable unreeled from spools during lowering of the multi-section cage into the pile bore
- After the cage was fully installed, the fiber optic cable was pretensioned to 2000 με and clamped at the top of the pile, prior to concrete placement
- Gel-filled conventional telecommunications cable was installed "in some piles" for temperature compensation

At the Chattendon site, conventional point-based vibrating wire strain sensors were installed which showed good agreement with the DFOS strain measurements, as shown in Figure 4-3.

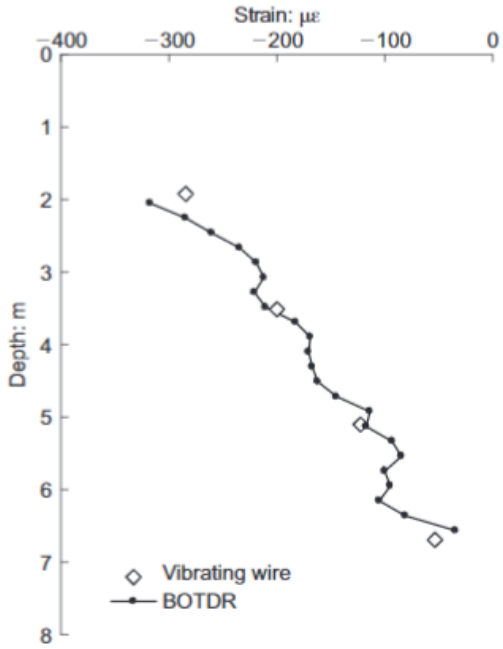

Figure 4-3: Axial strain in the Chattendon maniple with a pile group vertical load of 105t (Klar et al. 2006)

As can be seen in the strain plot, the strain measurements of the distributed fiber optic system closely followed the values and trends of the point-based measurements. While further research would often incorporate the comparison between conventional strain measurements and the distributed fiber optic systems, the comparability of the two systems at corresponding depths was well supported early in the research field. This is to be expected as the Brillouin strain sensing systems had previously been applied to conventional above-grade structural monitoring, both in the lab and field, with similar agreement and results.

The Farringdon site was the first installation where the fiber optic cables were installed loosely on the exterior of the reinforcement cage, unreeled from spools at the top of the pile bore during lowering of the cage. A photo of the installation method at Farringdon is shown in Figure 4-4.

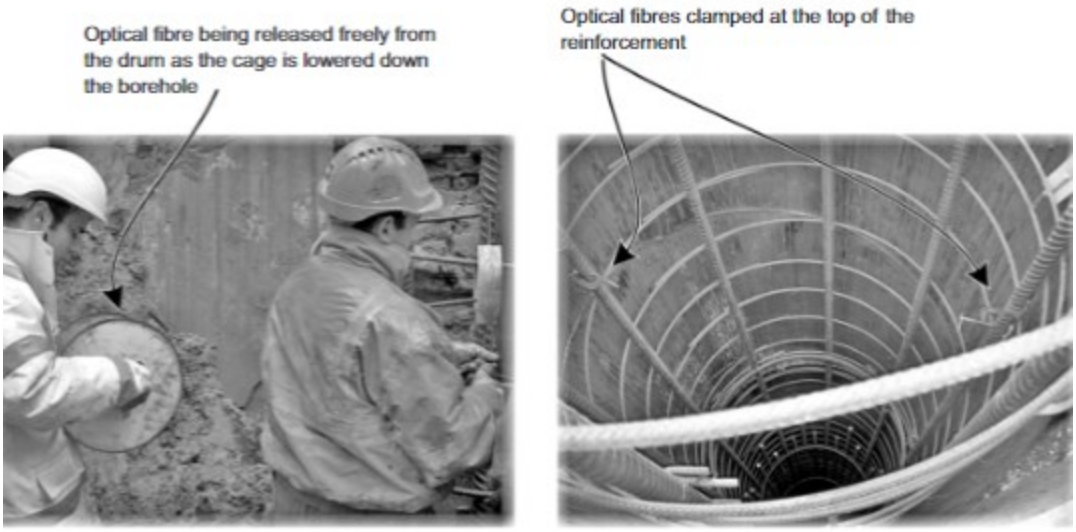

Figure 4-4: Installation of fiber optic cable via reel during lowering of reinforcement cage (Klar et al. 2006)

This advancement in installation technique offered a significant acceleration over the continuous- or periodic-epoxy method utilized in the Japanese and Chattendon field tests. This also opened the technology up to the use on piles with multiple sections of reinforcement as the splices no longer proved a barrier to the continuous vertical fiber installation.

The UK research also differentiated itself from the earlier Japanese work by including a detailed discussion of the unique insight into pile behavior under loading that distributed strain measurement could provide over point-based measurements. These include simulation of a BOTDR measurement data set in layered soil to capture differences in soil properties and behavior along the pile in different layers, as well as simulation of changes in pile capacity and induced strain due to tunneling near the foundation. While both cases were based on simulated data compared to analytical solutions, they showed the unique value that the distributed strain profiles could offer to furthering understanding of actual pile behavior in the field.

Continuing collaboration between researchers at the University of Cambridge and Cementation Skanska resulted in several field trials and associated developments in the use of Brillouin-based distributed fiber optic sensing of strain in deep foundations. Applications included monitoring of energy (thermal) piles (Ouyang et al. 2011; Soga et al. 2015), the reuse of deep foundations (Bell et al. 2013), and load test measurements performed using embedded Osterberg cells (Ouyang et al. 2015; Soga et al. 2015; L. Pelecanos et al. 2017). As the sensing technology improved and more advanced analysis techniques were developed, the analysis and insight into the geotechnical performance of the monitored foundations continued to advance. Many of the publications from this period in the UK in the 2010s were based on the same projects and captured a growing field expertise. Some of the key advancements and their first publication are captured below.

- Integration of continuous strain data to create vertical displacement plots (Bell et al. 2013): This is one of the key advantages of the continuous readout nature of the DFOS strain systems, allowing for the integration of strain to form a displacement with depth profile for each reading. Although a comparison of the integrated displacement profile verses other instrumentation (e.g., head movements via vertical survey, LVDT, extensometers, etc.), the resulting profiles provided a data set unique to distributed fiber optic strain measurement shown in Figure 4-5.

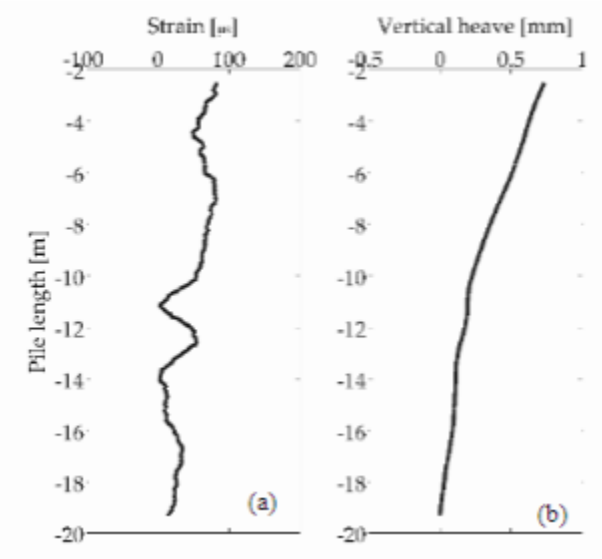

Figure 4-5: Axial strain (a) and vertical heave (b) along instrumented pile (Bell et al. 2013)

- t-z curves derived from fiber optic strain data (Soga et al. 2015): Based on the displacement with depth plots derived from the integrated strain profiles, t-z curves can be directly derived from the fiber optic data by looking at the applied force against the measured displacement. In this study, the direct-fitting was then augmented through the use of a simple 1-D finite element model to match the field results with a numerical estimation. This approach is further developed in Pelecanos and Soga 2018.
- Discussion (but not adoption) of the fact that pre-strain of the fiber optic cables may not be necessary in CIDH pile installation (Kechavarzi et al. 2016): The authors suggest that pre-strain (pre-tension) of the strain sensing fiber optic cables is only important when the cable is not fully bonded to the monitored asset and compression is anticipated. In cases such as cast-in-drilled-hole (CIDH) pile construction where the fiber optic cable is fully embedded in concrete, pre-strain is performed by the team to ease identification of the instrumented strain verticals during processing and is not necessary for compatibility between the cable and pile during compression.
- Fiber optic strain data for outlier detection and evaluation (Kechavarzi et al. 2016; Pelecanos et al. 2017): First published discussion of the use of DFOS records to evaluate and provide insight into strain peaks in piles. In the test under discussion, an outlier in

vertical strain was detected using conventional vibrating wire strain gauges. The authors propose that this data,

> *…could be considered as unrepresentative of the actual strains in the pile and therefore ignored by the design engineers. Eliminating outliers that do not conform to the expected ranges is common in data interpretation as instrument malfunctions do occur occasionally. However, in some cases the recorded data are in fact true representations that can be attributed to changes in ground conditions and construction quality.*

Upon inspection of the fiber optic records at the outlier depths, the same spike in compressive strain is observed, as shown in Figure 4-6. However, the continuous nature of the fiber optic strain profiles vs the single point of the suspected outlier supports the correct interpretation of the data's validity.

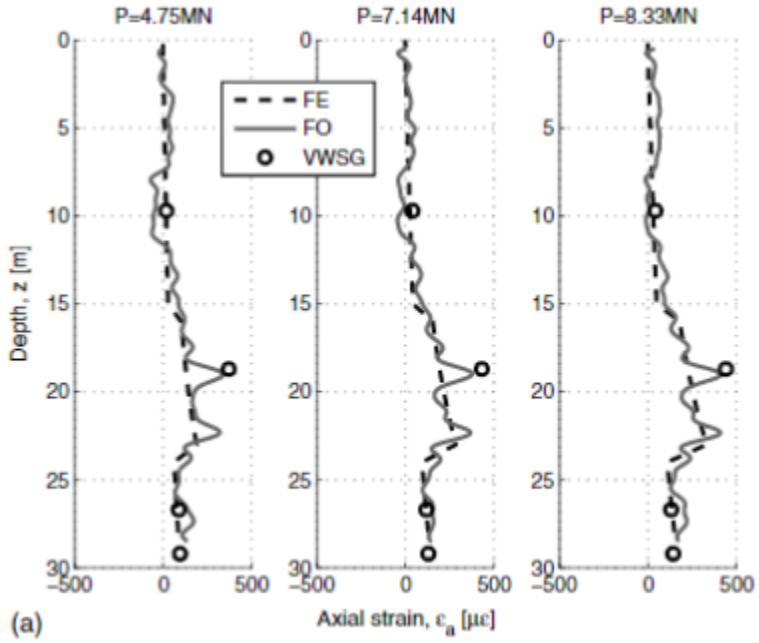

Figure 4-6: Fiber optic strain outlier at ~19m depth (Pelecanos et al. 2017)

- Installation of more than two fiber optic strain vertical cables at even spacing around circumference (de Battista et al. 2016): First published mention of installing 4 strain verticals at even 90° spacing around the circumference of the pile reinforcement. Although the strain data is still averaged with depth, as is the standard practice in all published research to date, this field trial represents the first time that a 3- or 4-point strain measurement array has been adopted in pile monitoring; an approach necessary to separate axial strain from bending strains.
- Individual presentation of fiber optic strain data and subsequent interpretation (Bersan et al. 2018): The first presentation of individual strain profile data for a pile

instrumented with 3 or more vertical cables. In this field test, 3 vertical cables were installed at 120° separation around the reinforcement circumference of a continuous flight auger (CFS) pile. All three profiles were presented individually, and a difference was noted across the pile in the top 6m which was attributed to potential load eccentricity. However, no calculation or further discussion of the difference or its potential significance is offered. The strain versus depth profile from the pile test is presented

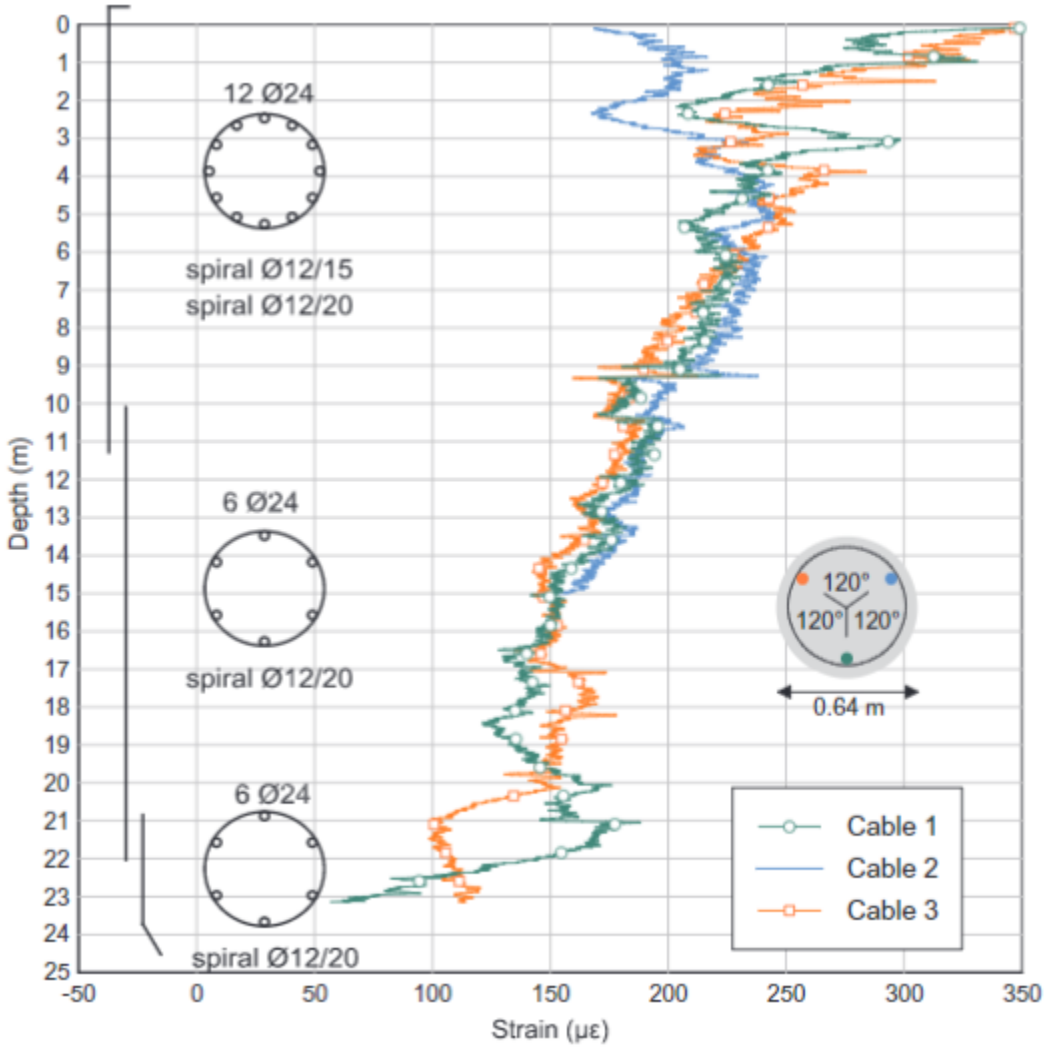

Figure 4-7: Individual fiber optic strain profile data from CFA pile test (Bersan et al. 2018)

In addition to the above listed advancements in the literature focused on the use of DFOS strain monitoring for deep foundations, complimentary research was being conducted on the use of DFOS for monitoring bending in retaining walls for excavations. Several of these trials involved the use of corresponding pairs of fiber optic vertical strain cables located on opposite sides of the retaining wall; that is, one on the retained soil side and a second on the excavation side. The earliest published reference of this technique was in 2011 (Mohamad et al. 2011), when a

pair of fiber optic strain cables were attached to the steel casing of a secant-pile wall, 180° apart and on a perpendicular line to the face of the subsequent excavation. Using the two strain profiles, the bending strain (difference), curvature (difference over diameter), gradient (single integration), and lateral displacement (double integration) of the pile with depth can be calculated. The plot of strain versus depth of one of the instrumented piles is presented in Figure 4-8.

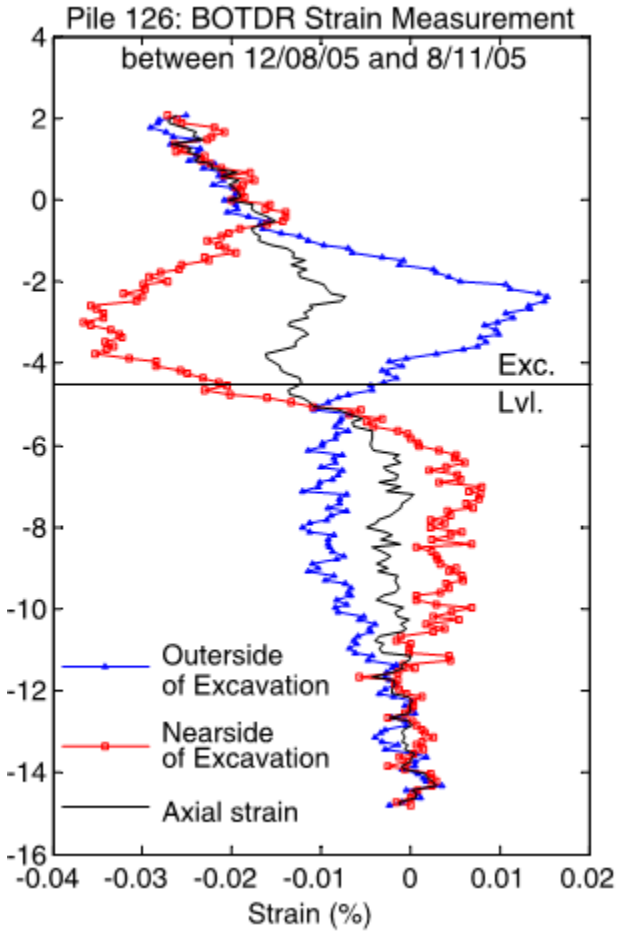

Figure 4-8: Bending and axial strains in secant pile at -4.5m of excavation (Mohamad et al. 2011)

State of Practice

The following is a presentation of the current state of practice of distributed fiber optic strain monitoring for pile foundations, taken from a recent 2021 publication based on the UK developed practice (de Battista and Kechavarzi 2021).

- Brillouin-based fiber optic sensing is used for strain and temperature monitoring, either utilizing BOTDR or BOTDA.
- Strain fiber optic cables are installed in loops, with each vertical on opposite sides of the pile and a half or more circumferential loops installed at the bottom of the pile for the turnaround.

- A complementary temperature sensing cable is installed in the pile to allow for thermal compensation of the readings, if deemed necessary.
- All fiber optic cables are preinstalled on the bottom section of reinforcement. Where multiple cage sections are installed; the fiber optic cables are then unspooled as the additional sections are lowered into the pile bore.
- Attachment to the reinforcement bars is periodic, utilizing mechanical clamps or zip-ties rather than adhesives. The cables are anchored to the cage at a minimum at the top and bottom of the pile, with intermediate attachment occasionally used.
- Pre-tensioning is often but not always applied to the fiber optic strain sensing cables.
- Comparability between the strain measurements of distributed fiber optics systems and conventional point-based sensors
- The resulting strain measurement profiles are often averaged with depth, although they have been occasionally presented as separate verticals in more recent publications since 2018 as an intermediate step in the data processing.

Literature Gaps and Proposed Research

Reviewing the body of literature surrounding the use of distributed fiber optic sensing for strain monitoring of piles, there are several gaps that can be identified which provide potential topics for further research to advance the field.

- Importance of pre-strain on accuracy of readings during compression: Although it was proposed that the pre-straining of fiber optic strain cables is not needed when the cable is fully encapsulated in concrete (Kechavarzi et al. 2016), the standard practice is still to pre-tension the fiber optic cables prior to concrete. No field trials have been located in the literature where strain cables were installed without pre-tension for evaluation of their performance.
- Averaging of strain readings with depth: In most of the literature, both within fiber optic strain sensing and in the broader practice of pile load testing, individual strain readings are averaged with depth. Variations with depth are either completely ignored, or those data that fall outside of the expected range are discarded as anomalies most often ascribed to instrument malfunction. Little to no discussion or analysis is offered for variations within the strain profile across the pile in the literature.
- Limited number of fiber optic strain verticals: The most common installation scheme in pile monitoring is a single loop (two verticals) installed at 180° across the pile. This limits the ability to reconcile non-uniform strains with depth with potential causes, such as bending moments generated within the pile.
- Behavior of fiber optic analyzers during transient strain: Fiber optic strain measurements are treated as true measurements during the reading interval. No recognition or discussion of the effect of transient strain on the output of any fiber optic analyzers was found in the literature. This ignores the potential effect of analyzer scanning and peak detection during changing strains along the sensing cable.

Based on the identified gaps, the following hypotheses can be formulated for additional research:

- Hypothesis 1: Fiber optic strain cable in piles, fully encapsulated in concrete, can be installed with slack removed but without additional pre-tension without any detrimental effect on compressive strain measurements.
- Hypothesis 2: Observed differences in measured strain across the pile at a single depth may represent real data and would therefore be inappropriate to discard. The continuous fiber optic strain profiles allow for potential outliers to be evaluated based on the surrounding data and reduce the likelihood of mistakenly discarding valid data. Furthermore, installation of 3- or 4-vertical strain fiber optic cables offers a significant advantage over a 2-vertical pair in allowing for the detection of bending strain within the pile.
- Hypothesis 3: Fiber optic analyzer architecture has a major effect on the processed output of strain when the strain along the sensor fibers is changing during the reading interval. This results in a non-uniform shift within the processed strain record, which is important to recognize, quantify, and when possible, correct.

The above hypotheses have been used to directly inform the research objectives of the pile monitoring and load test project, presented in the following sections.

4.2 Project Overview and Field Testing

Caltrans is one of the largest client-owner for the installation of deep foundations in the state of California, if not the United States. As such, the balance between reliability and performance with optimized design is a major focus of the organization, both at a project level as well as a research priority. In the past decade and a half, post grouting of deep foundations has been proposed on projects that Caltrans was either directly or indirectly involved with. Based on the interest of this approach in the engineering and construction industries, as well as the potential performance and cost benefits that it can offer the organization, Caltrans formed a research team to explore the use of base grouting of piles on future Caltrans deep foundations. The research team, under the leadership of Tom Schantz, is comprised of members from the University of Missouri (Erik Loehr and Andy Boeckmann), and members from the University of California, Berkeley (Kenichi Soga and Andrew Yeskoo). The University of Missouri team has focused its efforts on development of the design and reliability of base grouting, while the Berkeley team has focused on exploration of the use of Distributed Fiber Optic Sensing (DFOS) as a complimentary or alternative method for strain measurements during grouting and load testing.

Post Grouting of Deep Foundations

Post grouting of deep foundations generally refers to a range of methods to introduce grout under pressure to the tip of a deep foundation element. Also referred to as tip or base grouting, the technique is most commonly employed on large diameter drilled shafts with the goal to

improve the performance of the pile during loading. Post grouting has been performed on production foundation projects throughout Europe for many decades; however, it has been slow to be adopted within the United States. Continuing testing and research on the practice in the U.S. is ongoing, both in the academic and public sector, to refine the design guidelines of successful base grouting programs and improve the quality assurance / control of grout delivery during construction (FHWA et al. 2017).

There remains debate within the geotechnical community regarding contribution of the specific combination of mechanisms that contribute to the improvement, with the apportionment split between ground improvement at the tip, pre-mobilization of tip displacements, and pre-mobilization of shaft resistance (Ruiz and Pando 2009; Day et al. 2015; FHWA et al. 2017). Regardless of the mechanism, an increase in the stiffness of the foundation element's response under loading has been observed in load tests, as compared to un-grouted piles in the same stratigraphy. The performance of post grouted piles can vary widely depending on a range of factors, including the dimensions of the pile, the type of soil at the tip, the grout delivery system, and the quality and effectiveness of the grouting operation.

The injection of grout at the tip of deep foundations to improve performance under loading has been in development and use since the early 1960s (Bruce 1986; Mullins 2016), although it was not until the 1980s that the practice began to gain widespread adoption in Europe and Asia. Post grouting has historically been divided into internal and external systems, with internal systems having the grout delivery apparatus incorporated into the pile construction and external systems relying on grout delivery through drilling or other delivery methods outside of the pile itself. While both internal and external delivery systems have been proven to improve the performance of the pile under axial loads, internal systems are incorporated and deployed as part of the original foundation design. External systems are more commonly used as a post-construction intervention, generally to remediate subpar performance or to improve the foundation system to lessen the impact of future adjacent works. The focus of this review and research is on the performance of internal systems, and all subsequent discussion and reference to post grouting shall be in reference to internal delivery.

Post grouting delivery systems can be characterized as either open or closed (FHWA et al. 2017). This distinction is based on the grout containment, or lack thereof, at the delivery point at the base of the shaft. Open-type systems deliver the grout directly in contact with the surrounding ground. Closed-type systems deliver the grout into an expandable chamber at the base of the pile, keeping the grout from directly contacting the surrounding ground. The most common open-type delivery system is the sleeve-port (tube-à-manchette), comprised of one or multiple "U" grout loops from the surface extended to the pile tip, with injection holes cut into the pipes at the bottom and covered by sleeves which are ruptured at the start of grouting. Closed types are commonly comprised of either an expandable rubber membrane or a piston-style vertical expansion chamber, both of which have grout injected into the expandable cavity. Examples of the open- and closed-type delivery systems are shown in Figure 4-9.

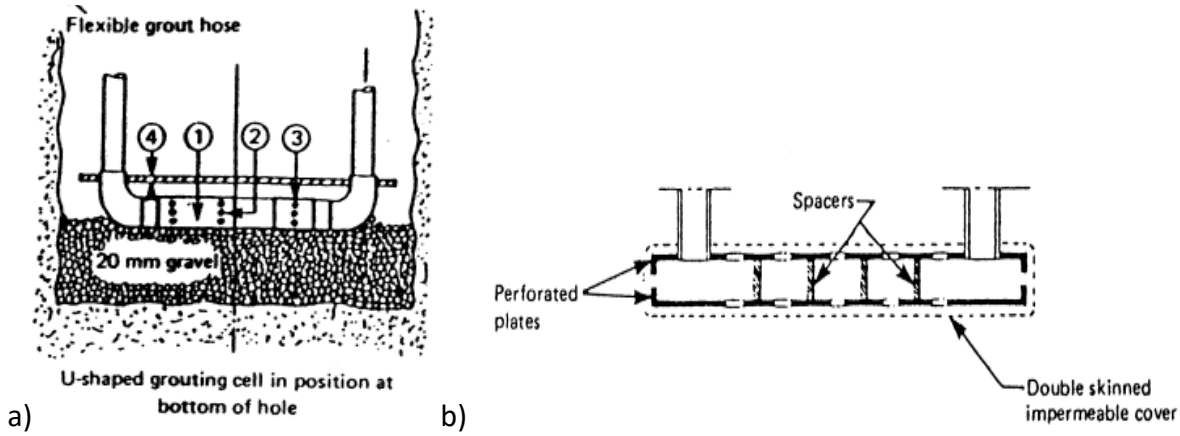

Figure 4-9: Example diagrams of a) open-type (Silwinski and Fleming 1984) *and b) closed-type* (Lizzi 1981) *base grouting apparatus*

A wide spread of performance of post grouted shafts, even those in close proximity, has been observed both in research and in production. The predictability and reliability of the improvement of post grouting has therefore been the topics of ongoing research. One of the most important aspects of ensuring consistency during a base grouting program is the quality assurance and quality control during grouting. The focus of this has typically been monitoring the grout delivery to the pile, specifically grout pressure and volume, as well as vertical movement of the pile head (DFI and Large 2016; Mullins 2016; FHWA et al. 2017).

The earliest monitoring and termination criteria during post grouting was focused on measurements of grout delivery, both volume and pressure (Bruce 1986; Mullins 2016). The acceptance pressure is commonly determined by balancing the equivalent pre-load imparted on the pile base while preventing fracturing of the soil formation. The acceptable pre-load is determined by balancing the net load of the imparted grout pressure against the total side friction capacity of the shaft, similar to the method of balancing the load in a bi-directional load test (Mullins 2016). The acceptance volume is determined by calculating the area required to cover the base of the pile, multiplied by the maximum potential expansion (if closed-type system or open-type system with gravel bed) or the theoretical cavity expansion potential (if open-type system). The target volume can vary widely depending on the soil type, and there is often both a minimum and maximum value specified in the contract documents. In practice, if the maximum volume is reached prior to the target pressure, the grouting operation may be suspended, and a second stage of grouting performed after the initial grout has had a chance to cure. For this reason, the pressure target has often been treated as the primary engineering control as it is proportional to the load/premobilization of the shaft, while the volumetric target is often a constructability and cost measure control. The ambiguity between the setting and application of the target limits is one of the major sources of uncertainty in the quality assurance and control of a post grouting operation on site.

Shaft uplift, commonly measured at the pile head, is incorporated as an additional control criterion to ensure that the grouting pressure is resulting in loading of the pile. Shaft uplift

limits also have the added purpose of ensuring that the shaft interface is not being compromised by excessive displacement through the grouting process. This could either be through the grouting pressures exceeding the reaction shaft capacity, or as is sometimes suspected, grout migration up the sides of the shaft temporarily reducing the frictional capacity of the shaft.

Together, these three criteria provide the basis for monitoring and acceptance during grouting. However, the variable nature of grout delivery at the base of the pile and the potential for blockages to develop during grouting pose the very real risk that grout pressures and flows observed at the surface are not being transmitted to the base as intended. A joint monitoring approach for all three measurements was first proposed by Winters (2014) and has been partially adopted in the US practice, with a combined approach incorporating review of all three in relationship in real-time during grouting. The template for the graphical approach is shown in Figure 4-10.

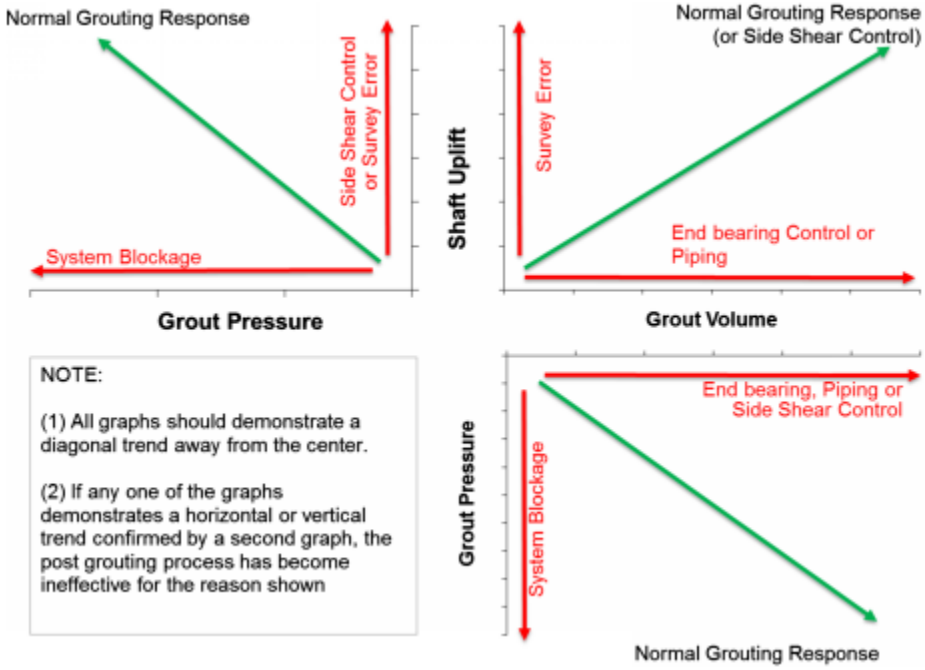

Figure 4-10: Quality assurance plots for post grouting drilled shafts (Winters 2014)

In an ideal post grouting delivery, the measurements plotted in the three graphs of Figure 4-10 should plot on the diagonal line, shown in green and labeled “Normal Grouting Response”. Deviations from this, specifically one or multiple of the graphs moving vertically or horizontally, represent a problem in the grout delivery with labels of the likely mechanism shown in red. By monitoring the response of the measured metrics in real time, the effectiveness of the grouting program can be controlled, and issues can be recognized quickly, as opposed to after the fact in a post-grouting review of the data.

While the graphical approach is largely successful in recognizing issues during grouting in the field, there are still a small number of grouting projects that have failed to reach the design performance in load testing despite the observations of grouting pressure, volume, and uplift satisfying the acceptance criteria. While the specific causes of this vary from project to project, many of the issues are concentrated on shafts where uplift of the shaft is negligible, either due to small shaft capacities on shorter piles where uplift is limited by necessity, or on very long piles with large deposits of soft overburden where pile movements do not reach the ground surface (Mullins 2016). In such cases, measurement of movements at the bottom of the shaft using tell-tales or monitoring of internal strain near the base can be used as a replacement for shaft uplift. These measurements provide confirmation of whether the grout pressure at the base is resulting in load in the shaft, as well as an indication of the uniformity of the load. However, these more advanced methods are often limited to test piles and are rarely widely used once the project has moved into production. Industry feedback has been that uncertainty in the area and composite modulus of the pile makes calculation of load from strain measurements unreliable. It is therefore suggested that strain be treated as a qualitative rather than quantitative measure of the grouting program's performance. Further uncertainty related to the load shedding below the level of point-based strain sensors, as well as the variable stress regime in the pile during grouting, have made deployment and interpretation of strain measurements during grouting an ongoing topic of refinement.

Distributed fiber optic sensing of strain within the pile can offer a relatively inexpensive method to incorporate distributed strain measurements within test and production piles as another means to monitor the performance of the pile during base grouting. This is particularly useful in cases where uplift cannot be relied upon as a measure of the grouting's effectiveness in transferring load into the pile. The distributed nature of DFOS can address some of the issues in previous strain monitoring of post grouting, including the ability to create a continuous profile of the increase and decrease in strain with distance from the base of the pile and the uniformity of strain around the pile area. The relative simplicity of installation of DFOS sensing cable can prove a cost-effective way to incorporate strain measurements into base grouting to provide an additional measurement check where uplift measurements alone are unable to satisfactorily confirm the success of the post grouting. Even without converting the strain into load, the measurements can provide a qualitative indicator of the distribution and extent of the load transfer into the pile.

Field Test Overview

The primary phase of the research testing was a field trial consisting of the installation of thirteen drilled shafts, each approximately 35-feet deep below ground surface. The piles were divided into four three-foot-diameter test piles and nine five-foot-diameter reaction piles. The nine reaction piles were installed in a 3x3 grid, 28-feet on center, with the smaller test piles located in the center of each quadrant of four reaction piles. The test site was located approximately 18 miles north of Sacramento, California, within the Caltrans right-of-way at the junction of CA State Routes 99 and 77. A satellite image of the test site from Google Earth,

taken August 28, 2019, is shown in Figure 4-11. The grid of the nine reaction piles can faintly be seen within the satellite image and are marked with a red box in the figure.

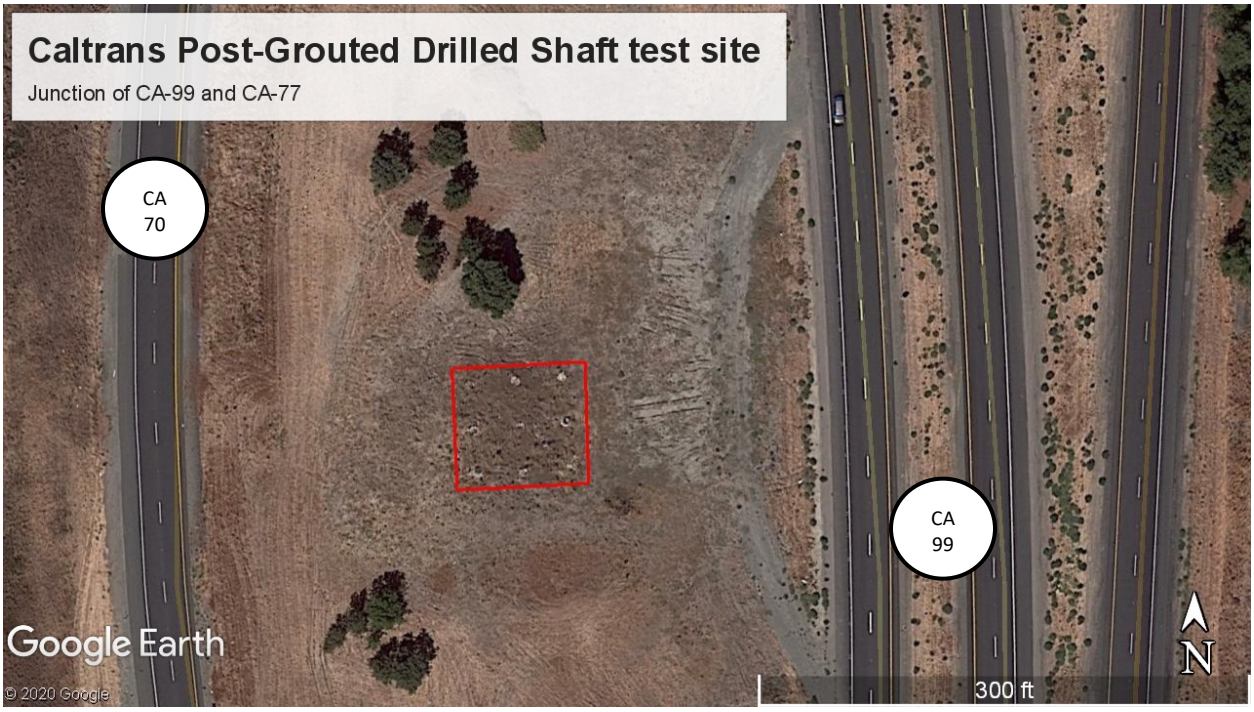

Figure 4-11: Satellite image of the field test site in August 2019 (Google Earth)

Several types of measurements and observations were taken during the construction of the piles, including scans of the drilling fluid-filled borehole wall, measurements of the base hardness of the drilled borehole, and measurements of the integrity of the pile concrete after pour. The integrity methods used on the project included thermal monitoring during curing using both distributed fiber optics and a commercial monitoring system, cross-hole sonic logging (CSL), and Gamma-Gamma logging (GGL).

Following construction of the piles, twelve of the piles were base grouted including all of the reaction piles and three of the four test piles. Three base grouting delivery methods were used on the project. These include an open-type system (tube-à-manchette), a closed-type system (rubber bladder), and a proprietary expansion cell system (RIM-Cell by Loadtest). The delivery grout pressure and volume were recorded by an in-line data logger between the grout plant and the pile. Movements of the pile were measured using a combination of dial gauges and survey methods of points at the top of the pile and tell-tales extending to the bottom of the pile. Mechanical strains within the pile were measured using vibrating wire strain gauges as well as distributed fiber optic strain cable. Temperatures within the pile were also measured using distributed fiber optic thermal monitoring. A photo showing the typical site setup of the various monitoring systems during base grouting is shown in Figure 4-12.

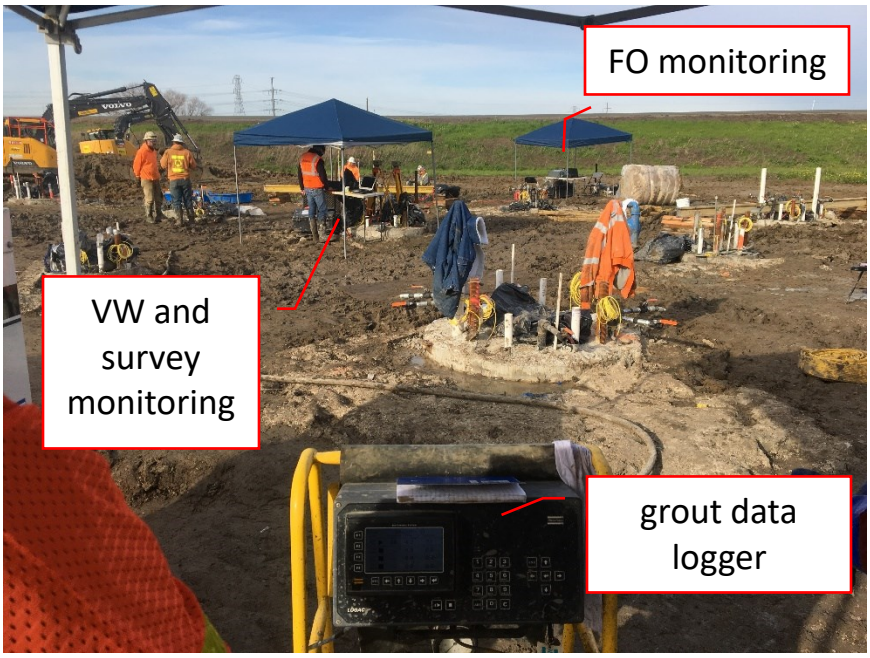

Figure 4-12: Monitoring systems during base grouting

After the base grouting was complete, the four test shafts were load tested. The axial loads were imposed on the test pile using four hydraulic jacks, connected to the four surrounding reaction piles through a steel load frame. A photo of the load test frame is shown in Figure 4-13.

Figure 4-13: Load test frame

Displacement and strain measurements were taken in the manner as described above for base grouting, with additional measurements taken of top displacements of the pile using LVDTs and the hydraulic jack pressure and associated load on the pile were taken during the load test.

Overview of Monitoring Program

The fiber optic monitoring portion of the larger drilled shaft instrumentation program consists of thermal and strain monitoring in all thirteen of the installed drilled shafts. The thermal monitoring was performed using distributed fiber optic sensing, while the strain monitoring was performed predominantly using distributed fiber optic sensing with one additional shaft instrumented with point-based fiber optic sensors. The distributed fiber optic sensing was performed using Brillouin optical time domain analysis (BOTDA) and Brillouin optical time domain reflectometry (BOTDR). The point-based fiber optic sensing was performed using Fiber Bragg Grating (FBG) sensors. All the distributed cables were installed in loops; both a necessity for BOTDA interrogation as well as for redundancy in the case of a cable breakage during installation. The FBG strings were installed in individual vertical strings.

The thermal monitoring was divided by breadth. Five shafts (reaction shafts R1, R2, R3, R7, R9) were instrumented with three temperature loops to facilitate thermal monitoring during concrete curing. The remaining eight shafts were instrumented with a single temperature loop to allow for later correction to the fiber optic strain data, if determined necessary.

The strain monitoring consisted of two tightly-buffered strain loops installed in each of the thirteen shafts. In addition, test shaft T2 had two point-based FBG fiber optic strings installed to measure strain. Strain measurements were taken during the grouting phase, as well as during the four load tests.

A summary of the pile types and dates of installation, grouting and load testing is shown in Table 4-1.

Table 4-1: Post grouted research project pile summary

Pile	Diameter	Grout System	Date Installed	Date Grouted	Date Load Tested
R1	5’	RIM Cell	Dec. 19, 2018	Feb. 6, 2019	-
R2	5’	Open-type	Jan. 10, 2019	Feb. 7, 2019	-
R3	5’	Closed-type	Jan. 10, 2019	Feb. 4, 2019	-
R4	5’	Open-type	Dec. 21, 2018	Feb. 6, 2019	-
R5	5’	Closed-type	Jan. 9, 2019	Feb. 5, 2019	-
R6	5’	Open-type	Jan. 10, 2019	Feb. 8, 2019	-
R7	5’	Closed-type	Jan. 2, 2019	Feb. 5, 2019	-
R8	5’	Open-type	Jan. 3, 2019	Feb. 7, 2019	-
T1	3’	None	Jan. 4, 2019	-	Feb. 23, 2019
T2	3’	RIM Cell	Jan. 9. 2019	Feb. 6, 2019	Feb. 28, 2019
T3	3’	Open-type	Jan. 8, 2019	Feb. 7, 2019	Mar. 4, 2019
T4	3’	Closed-type	Jan. 4, 2019	Feb. 5, 2019	Feb. 21, 2019

Cable Installation

a) Preparation

All the fiber optic monitoring cables were precut to length prior to pile installation. For the distributed thermal and strain cables, a minimum of an extra 8 m beyond the pile length was included in each run to allow for splicing and connection at the pile head. Each pile was instrumented with a minimum of one thermal loop and two strain loops. A summary of the installed fiber optic instrumentation is presented in Table 4-2.

Table 4-2: Fiber optic sensing cable by pile

Pile Designation	Temperature Cable	Strain Cable
T1, T3, T4, R4, R5, R6, R8	1 distributed loop	2 distributed loops
R1, R2, R3, R7, R9	3 distributed loops	2 distributed loops
T2	1 distributed loop	2 distributed loops, 2 FBG verticals

The fiber optic cable was installed on site by attaching it to the reinforcement cage. The decision was made to install the cable after delivery to the field, rather than at the yard, to reduce the chance of a breakage of the fiber during picking, transportation, and placement on cribbage.

b) Distributed fiber optic cable installation

Prior to cable installation, within every pile each vertical reinforcement bar was assigned a designation based on its type and location. A primary hollow bar (HB1) was spray painted for reference, with all subsequent bars numbered sequentially clockwise looking down on the cage from the top. For the reaction piles which had solid bars (SB) in addition to hollow bars, the numbering followed the same convention with the first solid bar clockwise of HB1 given the primary solid bar designation SB1. A schematic diagram of the vertical reinforcement bar numbering is shown in Figure 4-14.

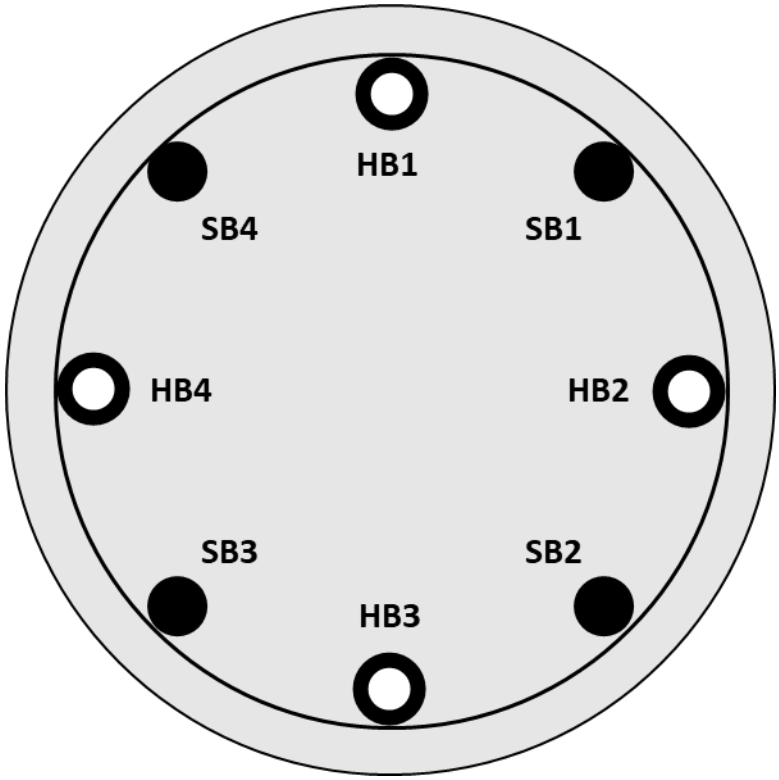

Figure 4-14: Schematic diagram of vertical reinforcement bar labeling convention, looking down from the top of the pile

For the distributed sensing cables (both strain and temperature), each pile was instrumented with a continuous cable run, measured to accommodate the number of loops planned for the specific pile. A diagram of a typical cable installation is shown in Figure 4-15 (reinforcement spacing and number of horizontals are not to scale). While each pile had several fiber optic loops, for simplicity the figure shows the routing of just a single loop (down, 1.5 circumferential loops, up).

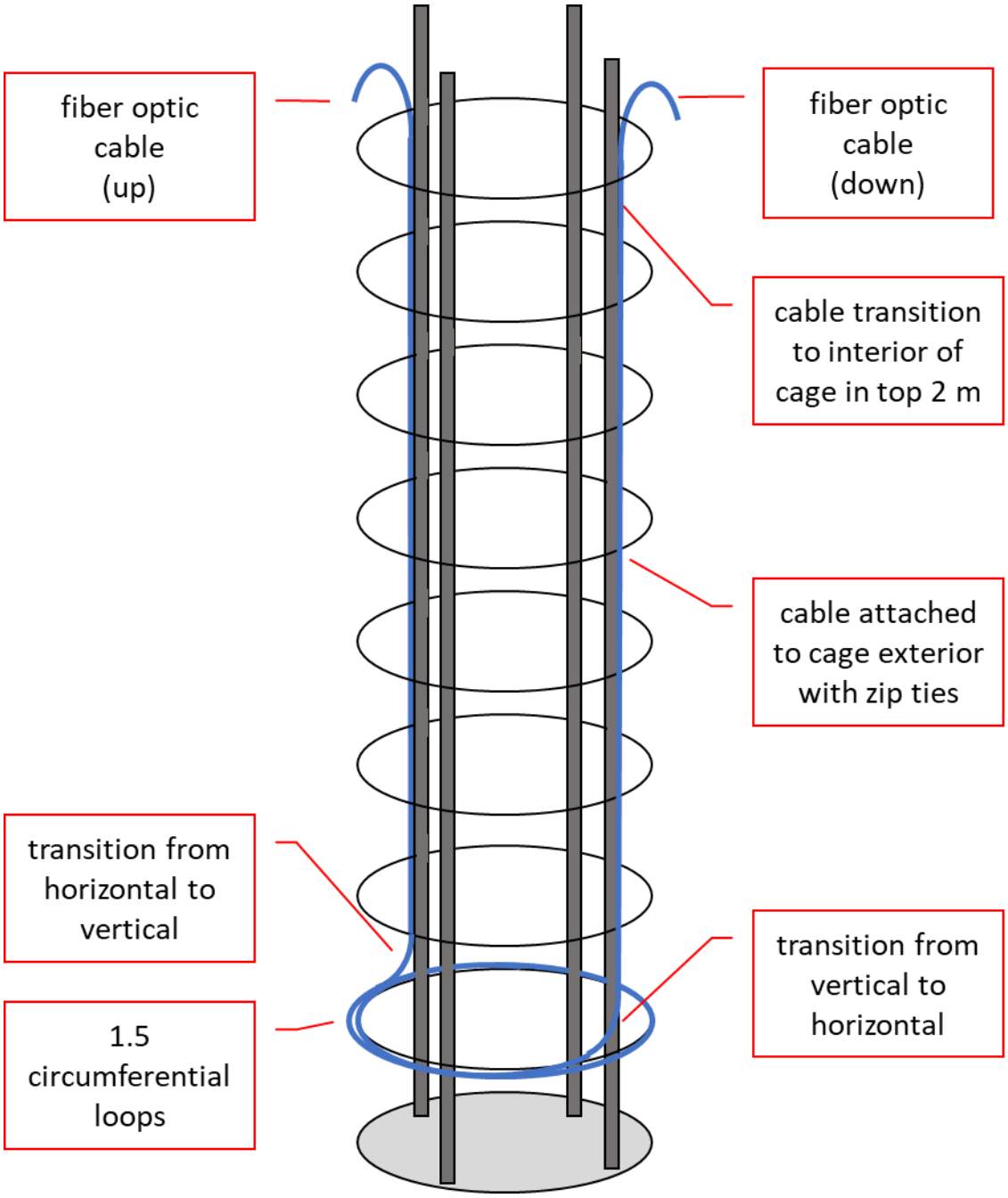

Figure 4-15: Fiber optic cable routing for a single loop

At the beginning of each cable, 4 m of cable was left coiled at the pile head to allow for connection to the cable during monitoring. The first vertical of the cable was then unreeled along a vertical bar from the top to the bottom of the cage. The cable was routed inside of the cage for the top 2 m to prevent damage to the cable from the rigging during the final hoist of the cage prior to installation in the borehole. After the top 2m, the cable was routed through the horizontal reinforcement and continued along the vertical bar on the outside of the cage, attached every three feet to the crossing horizontal loop using industrial zip ties. Care was

taken to ensure that all slack was pulled out of the cable as it was installed, as well as to make sure that the cable rested flat on the exterior of the cage without any kinks or sharp bends which could break the cable during hoisting or installation.

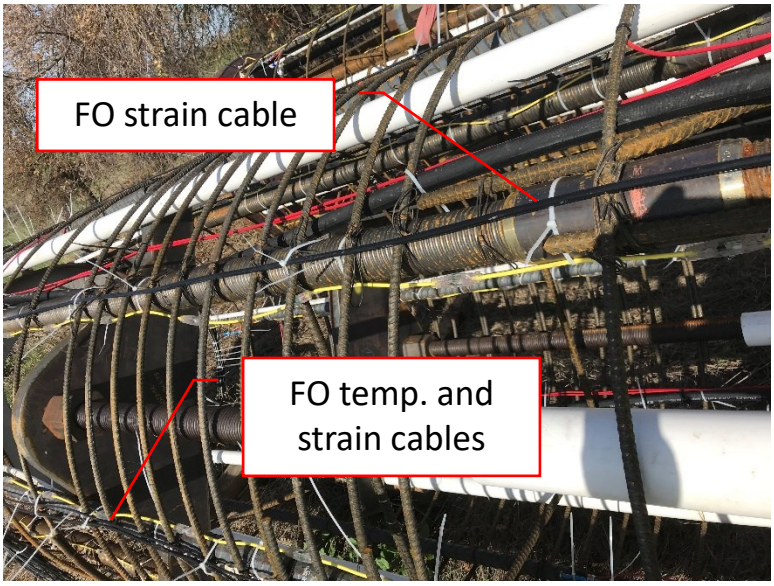

Figure 4-16: Instrumentation installed on reinforcement cage

At the bottom of the cage, each distributed fiber optic cable was routed from the vertical bar to the bottom or second to bottom horizontal reinforcement, as shown in Figure 4-15 (the schematic diagram introduced earlier). Zip ties were placed just above and below the bend to control the radius of the cable throughout the bend. The cable was then routed in 1.5 circumferential loops, circling the pile counterclockwise, before being routed back up the vertical bar opposite the first. Figure 4-17 shows the transition of a strain fiber optic cable from a vertical bar to the horizontal circumferential loops, as well as several previously installed fiber optic cables encircling the bottom.

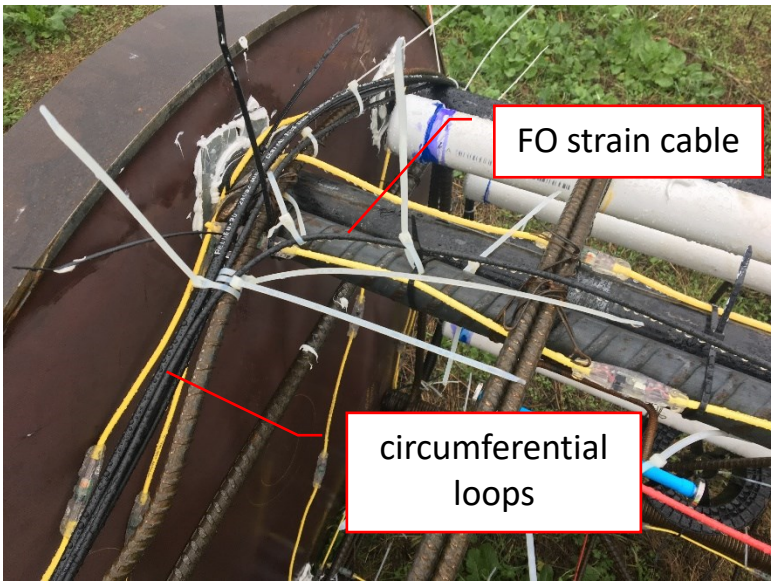

Figure 4-17: Fiber optic strain cable transitioning to circumferential loop at the bottom of the reinforcement cage

At the top of the pile, the cable was once again routed inside the cage 2 m below the top horizontal bar. This setup – the vertical "down", 1.5 circumferential loops, and a vertical "up" – constitutes a single loop, as shown in Figure 4-15. For piles with multiple loops of the same type, 7 m of cable was left between each loop to allow for reconnection in the event of a fiber break within the pile. The installation of all the fiber optic cable on the cage took approximately 2-3 hours after delivery to site with 2 researchers. Figure 4-18 shows the top of a reinforcement cage prepared for lifting into the pile bore with all cabling coiled and secured to the top bars. The fiber optic cable bundles are black, while the red cable are the conventional strain gauges and the yellow cables are the conventional thermal wire.

Figure 4-18: All instrumentation wiring installed and coiled; cage prepared for final pick

c) FBG cable installation

On pile T2, two FBG strands were installed in addition to the distributed thermal and strain fiber optic cables, following the vertical routing of two previously installed distributed strain cables. Since the FBG strands are single ended, no circumferential loops were included at the bottom of the pile. Due to the fragility of the glass polymer reinforcement on the exterior of the cable, the FBG cable was routed on the interior of the cage and attached using zip ties. One of the cables was kinked on the reinforcement during installation, causing the fiber to break and rendering that string inoperable for monitoring.

d) Instrumented cage installation and concreting

In every cage, there would be 1-2 fiber verticals, which were inaccessible due to the way the cage was supported on the cribbing. In these cases, the excess cable was coiled and attached to the side of the cage at the end of the last circumferential loop, as shown in Figure 4-19.

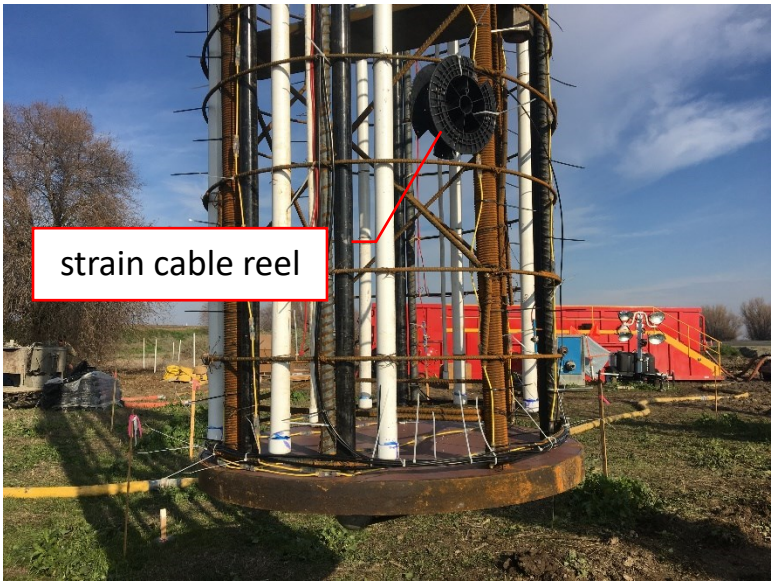

Figure 4-19: Cable reel attached to the bottom of the cage on vertical inaccessible when cage was on the ground

After the cage was lifted vertical and oriented over the pile bore, the coil was detached, and the cable was installed with zip ties along the appropriate vertical bar as the cage was lowered into the bore, as shown in Figure 4-20. This method is the same as how fiber optic cables would be installed on subsequent cages for multi-section piles.

Figure 4-20: Installation of final fiber optic cable vertical during lowering of reinforcement cage

Following the lowering of the cage, all fiber optic and conventional sensor cables were routed out of two PVC pipes to protect the cables from bending or damage during later pile work. The cable was then bundled and placed into heavy duty plastic bags to protect them during concreting.

At the completion of the pile concreting, the temperature and strain cables were spliced together and FC connectors were connected to the remaining 2 free ends. A photo of the field setup for splicing the fiber optic cables after the piles were installed is shown in Figure 4-21. The field setup was laid out on a portable folding table. Disinfecting wipes were used to carefully clean the cable ends of mud and dirt, as well as wipe down the table. The tools on the left of the table were used to remove the outer layers of the fiber optic cables include a pipe cutter, cable snips, wide and needle nose pliers, a matte knife, and wire strippers. The yellow-handled tools in the upper center part of the table were used to prepare the fiber core – stripping any protective coating and buffer to expose the core. The core was cleaned with a sterile wipe wetted with alcohol (center top, left). The core was cleaved (center bottom, left), then installed in the holder within the splicer (center, right). The process was repeated for the other section of fiber which was being spliced.

Figure 4-21: Photo of the field setup and tools used for splicing fiber optic cables from the piles

A close-up of the strain cable being prepared for splicing with a protection tube is shown in Figure 4-22. The FC connectors allowed the fiber optic cables to be connected to the analyzer channels or to each other using double-ended connectors.

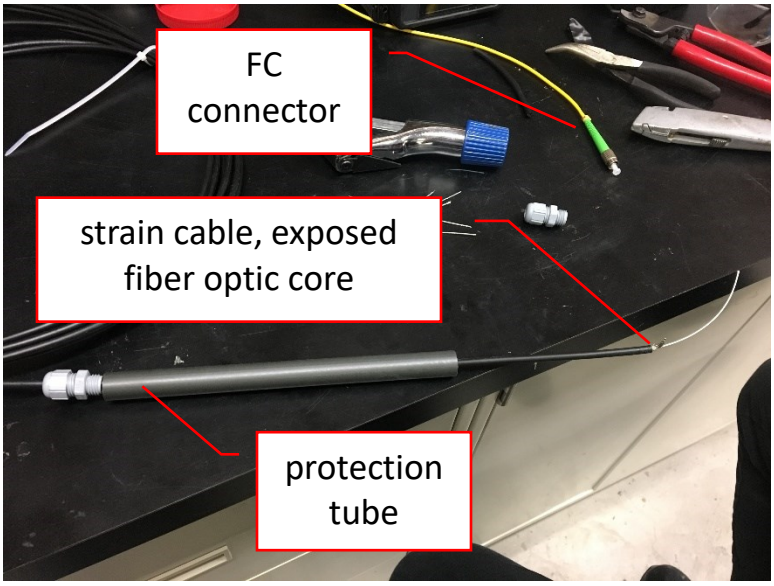

Figure 4-22: Nanzee 5mm strain cable prepared for splicing with plastic protection tube and FC connector

The splicing process entails carefully removing the protective sheathing around the fiber optic strand, cleaving the end of the fiber optic cable to a 90° face, splicing the two cable cores together using a fiber optic fusion splicer, and securing a protective sheath around the completed splice. A photo of a splice between the strain cable and an FC connector patch cable is shown in Figure 4-23. This photo was taken of a splice performed in the lab between the Nanzee 5 mm cable and an FC connector patch cable. The image on the screen shows a close-

up view of the two fiber optic cores which are aligned and measured for squareness of the cut. Any incompatibility of the angle of the two cuts will result in an error from the splicer and the fiber would have to be recut.

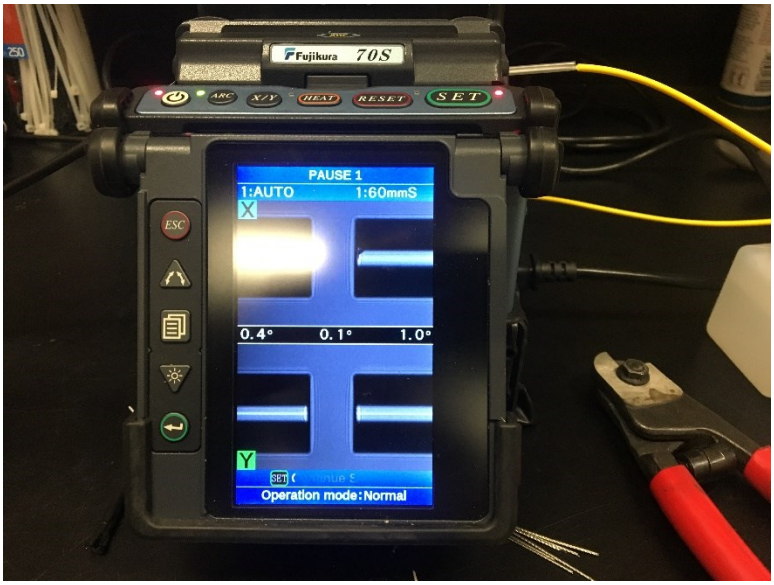

Figure 4-23: Fujikura fusion splicer, joining strain cable (left) and FC patch cable (right)

The maximum optical loss for each splice was set at 0.1 dB – any splice over this value would be cut and repeated. A photo of the same cable shown in Figure 4-23 after the splice is completed is shown in Figure 4-20.

Figure 4-24: Photo of completed splice between strain cable (left) and FC patch cable (right)

Following the completion of the splice, continuity was confirmed through all connections using an Optical Time Domain Reflectometer (OTDR) testing device. This allows for testing of both the

continuity of the splice as well as checking for any breaks or sharp bends in the fiber optic cable in the pile. A photo of the OTDR readout of the previous splice is shown in Figure 4-25. The readout shows the reflectance of the splice, as well as the loss along the cable length. This cable has a large reflectance at the end since it is a bare cut (no splice or termination), causing the reading to fail in this scan. Attaching another splice to the other end greatly diminishes the reflection at the opposite end.

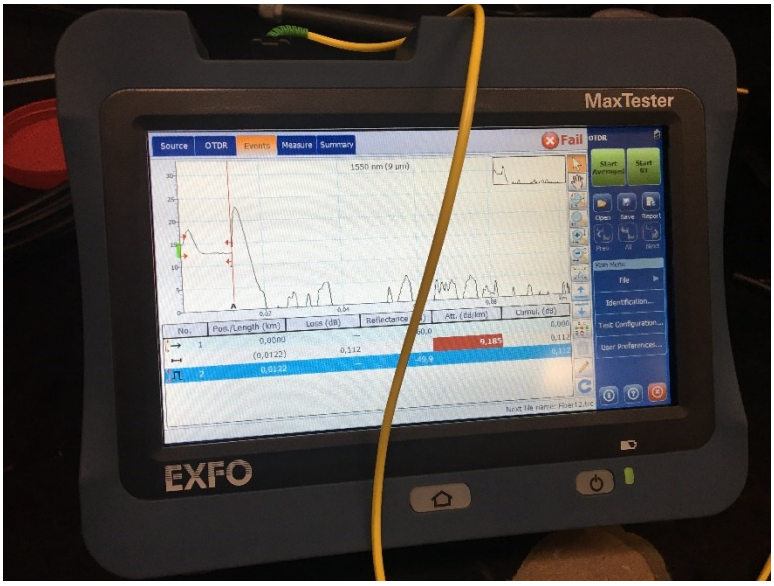

Figure 4-25: OTDR readout of a fiber optic splice and length of cable

None of the installed distributed fibers were broken during installation, including a section of temperature cable that was pinched between the reinforcement and cribbing during handling of the cage prior to picking. A photo of the kink in the cable is shown in Figure 4-26. After the cage was repositioned, an integrity test was performed on the cable using the OTDR which showed no breakage or loss at the pinch point.

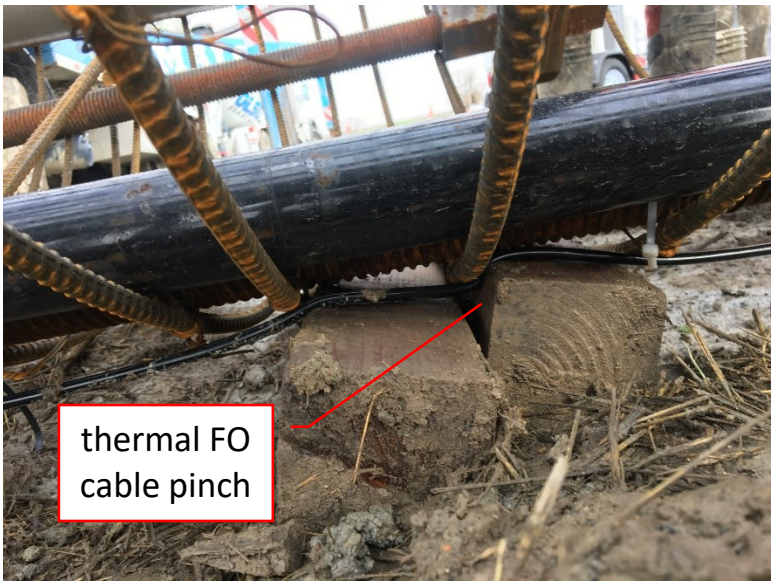

Figure 4-26: Thermal fiber optic cable pinched under reinforcement during handling prior to installation

The only breakage of a cable occurred during the load test of test pile T3. During the penultimate unload cycle, the load frame, which had previously lifted off its cribbing due to the high reaction force from the applied load, settled onto a section of thermal cable which had shifted slightly during the test. The cable was caught on a sharp edge between the two steel pieces, severing the fiber optic core. A close-up of the break is shown in Figure 4-27.

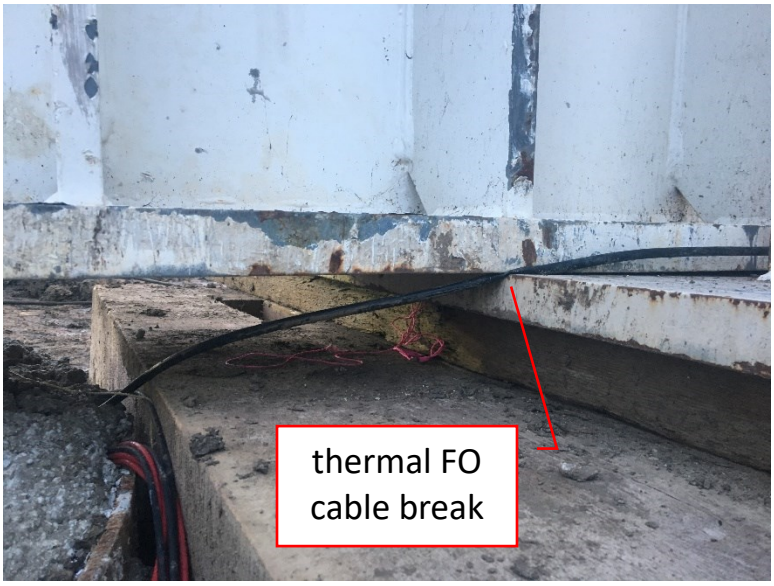

Figure 4-27: Thermal fiber optic cable severed by load frame

The splice and protection system used to join cable loops and attach FC connectors proved to be robust. Of the 39 splices installed for the monitoring program, only 2 splices experienced failures. In both cases, this was due to a strong pull being exerted on the fiber optic cable, for instance someone tripping on the cable and jerking the splice apart as they stumbled.

4.3 Fiber Optic Strain Measurements During Grouting

Overview

Following the installation of the thirteen drilled shafts, twelve of the shafts were base grouted using three different grout delivery methods (RIM Cell, Open-type and Close-type). Distributed fiber optic measurements of strain and temperature were taken during the grouting process. A summary of the base grouting program is shown in Table 4-3.

Table 4-3: Pile base grouting program summary

Pile	Diameter	Grout System	Date Grouted
R1	5’	RIM Cell	Feb. 6, 2019
R2	5’	Open-type	Feb. 7, 2019
R3	5’	Closed-type	Feb. 4, 2019
R4	5’	Open-type	Feb. 6, 2019
R5	5’	Closed-type	Feb. 5, 2019
R6	5’	Open-type	Feb. 8, 2019
R7	5’	Closed-type	Feb. 5, 2019
R8	5’	Open-type	Feb. 7, 2019
R9	5’	Closed-type	Feb. 4, 2019
T2	3’	RIM Cell	Feb. 6, 2019
T3	3’	Open-type	Feb. 7, 2019
T4	3’	Closed-type	Feb. 5, 2019

Grouting

Each pile was grouted progressively, clearing each delivery circuit with water before switching to grout and cycling through the different circuits, as necessary. The grout pressure was measured by an automated data logger immediately downstream of the grout plant, as well as at a manually read dial gauge placed on the feed line at the final connection at the pile head. Separate readings of grout volume and pile head and base displacements were read using a combination of automated and manual systems. This report focuses on the strain measured by the distributed fiber optic sensors installed within the piles. A separate report by the University of Missouri team provides an in-depth discussion into the grouting design, methodology, and analysis for the project.

Fiber Optic Measurements

Measurements

For the distributed fiber optic monitoring, the strain and temperature fiber optic loops in each shaft were interrogated during the base grouting. Prior to the start of grouting, the strain and temperature loops were spliced together to form a continuous fiber line for each pile. In all cases, the sensing side of the analyzer was connected to the strain side of the fiber optic line. The readings were taken using the commercial Omnisens analyzer. All the readings were taken in the loop BOTDA mode with the exception of those for pile R5 which had a broken splice,

necessitating using the single-ended BOTDR mode for the readings. A minimum of three readings were taken prior to the commencement of grouting to serve as a baseline. Readings during grouting were taken based on the progression of the grout progress, with the grout line dial pressure gauge at the top of the pile noted at the start of each reading. Each reading took approximately five minutes to perform, with the grout pressure fluctuating during the interrogation time. A minimum of three readings were taken after the conclusion of grouting to observe the strain decay in the pile after the supply pressure was released.

Data analysis

The raw output of each fiber optic reading is a series of frequency values at increasing distances away from the sensing side of the analyzer. The first step necessary to process the raw data into engineering units is to "index" the 1-dimensional data set to specific locations within the pile; both radially (by reinforcement bar) and depth in the pile (measured as depth below the top of casing, TOC). The data set is first divided by a set of estimated cuts based on recorded lengths of fiber installed for each fiber optic loop, including the 1.5 circumference at the base of each pile. The frequency record is then converted into either strain or temperature using a linear transformation by the strain or temperature coefficient to create a preliminary record with depth. Further fine tuning of the vertical position of each loop is then performed by comparing the records to each other over the monitoring period, identifying strain and temperature gradients that can be used to refine the assigned depth of each individual monitoring point.

Temperature change effect

Prior to final processing of the strain profiles, the temperature changes as measured by the thermal fiber optic lines were evaluated to determine if thermal compensation of the strain measurements was necessary. Changes in excess of 1-3 MHz from the baseline were observed in the thermal fiber optic cables, corresponding to a thermal fluctuation of 0.9-2.7° C. Converting into strain using the thermal coefficients of the strain cable, this corresponds to an associated range of thermally-induced strains of 32-96 με. For illustration, the temperature readings taken during the base grouting of shaft R2 (open-type system) are shown in Figure 4-28

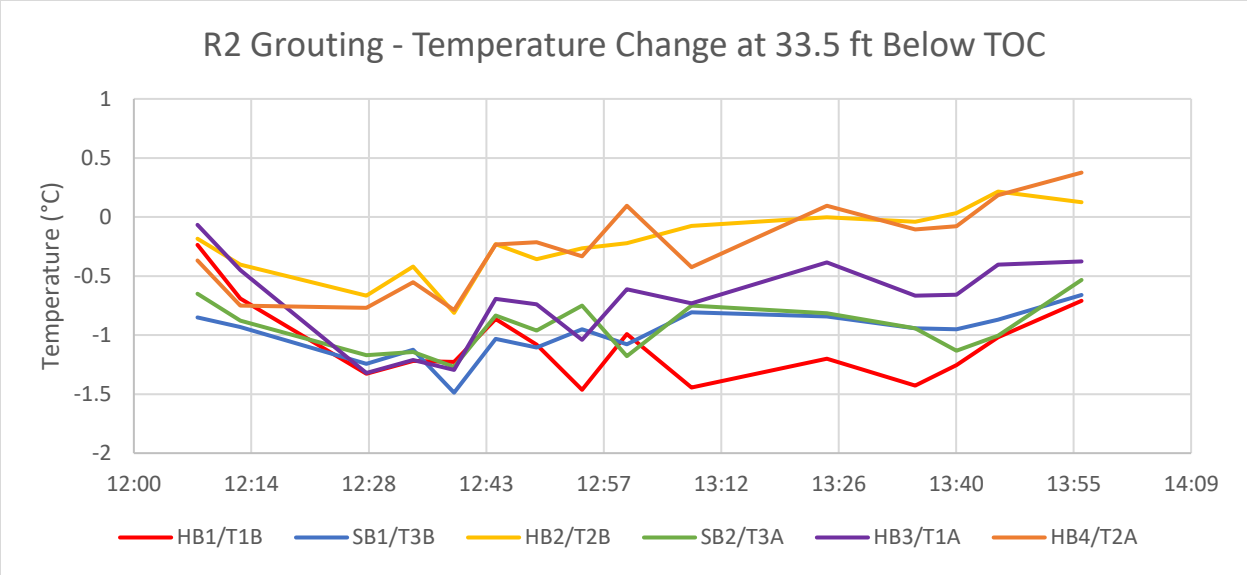

Figure 4-28: Temperature change in shaft R2 during grouting

As can be seen in the figure, temperatures in the shaft dropped by up to 1.5° C within the first half hour of monitoring. The recorded thermal changes were not uniform across the pile and were likely due to circulation of the water and grout in the vertical delivery tubes, with the largest variations recorded in the fibers closest to the active tubes. The grout delivery system for the open-type in 5' piles consisted of 3 separate loops – one roughly in the center of the shaft and 2 on either side. The lowest recorded temperature readings on hollow bars 2 and 4 were on the axis of the shaft perpendicular to the loops, making them the bars farthest from the flowing water and grout. The initial drop observed on hollow bars 2 and 4 corresponds to the time when water and grout were circulating in the middle grout circuit – the temperature rebound back to 0 is after the return valve was closed.

Based on the high observed temperature variation, thermal compensation was performed on all strain readings taken during grouting. For strain fibers with a co-located temperature fiber, the temperature compensation was performed directly using the readings from the associated fibers. For strain fibers without a directly corresponding temperature fiber, the average of the two closest temperature fibers were used to calculate the compensation value.

Results

The presentation of the strain measurements during grouting for each shaft are divided by grouting system.

RIM Cell

a) Reaction Shaft R1

Reaction Shaft R1 was grouted on February 6, 2019. The grout data logger record of pressure and volume at the grout plant is presented in Figure 4-29. After some problems with the grout plant, including a pressure spike at 9:46, grouting of the pile began at 9:51. The pressure was

initially attempted to be held at 200 psi at 9:52, after which subsequent holds were attempted at 600 psi at 10:08 and 800 psi at 10:16. At 800 psi, a vent cap at the top of the pile burst off and a stream of water was released, dropping the pressure in the line to 250 psi and pumping was stopped. The measured volumes are not adjusted for the initial flush or grout in the lines and therefore represent an upper bound of the volumes placed at the pile base.

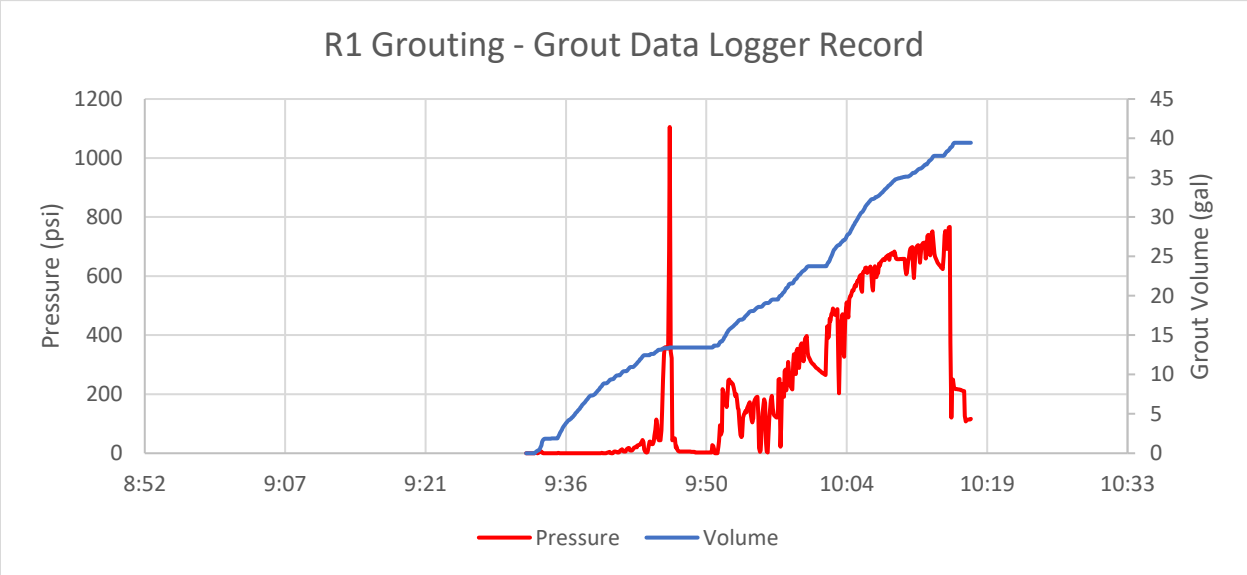

Figure 4-29: R1 grouting, grout data logger record

The fiber optic record for shaft R1 is divided into 4 strain verticals and 6 temperature verticals. The raw frequency and segment divisions are shown in Figure 4-30.

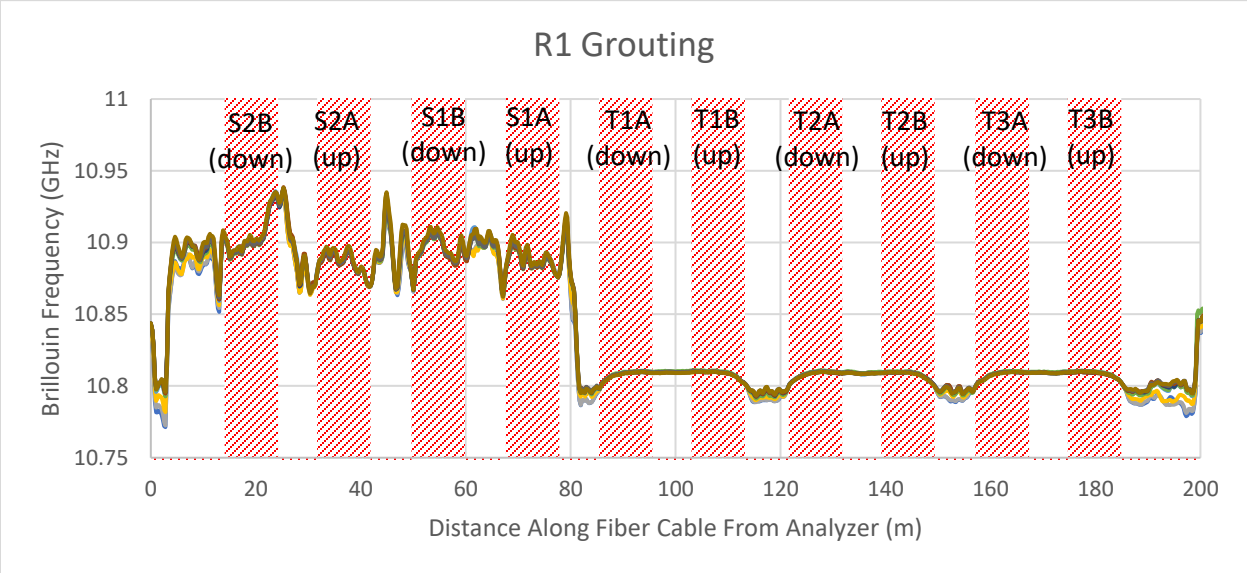

Figure 4-30: R1 grouting, raw Brillouin frequency

The measured vertical strains with time at a depth of 33.5 feet below the top of casing (TOC), approximately 1 pile diameter (5 feet) above the base, are presented in Figure 4-31. This figure shows an initial peak in vertical strain of 40 to 60 με at 9:58, when the associated grouting pressure was fluctuating around 300 psi. The strains across the pile then decreased to under 20 με, despite increasing grout pressure, until they fell dramatically after the vent cap burst. The final reading after the release of pressure shows tension developed in the pile from 0 to 60 με.

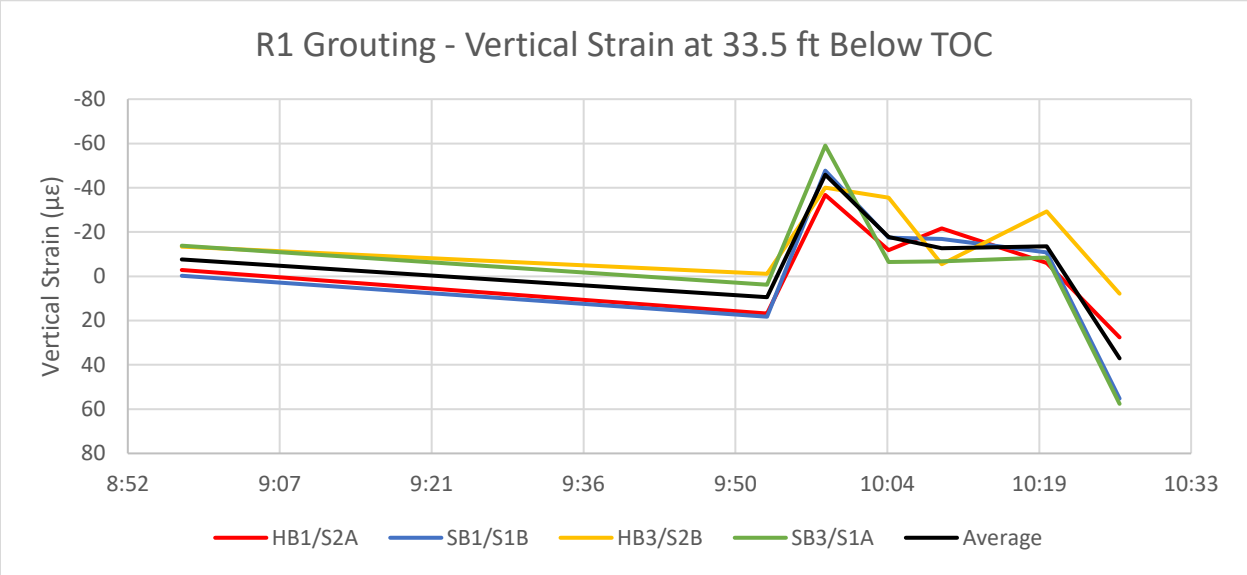

Figure 4-31: R1 grouting, vertical strains at 33.5 feet below TOC

Figure 4-32 through Figure 4-34 show the vertical strains with depth in the pile at 9:58 (~300 psi), 10:09 (~600 psi), and 10:18 (after pressure release). Figure 4-32 shows that the initial vertical strain peak around 9:58 averaged 50 με in compression and extended through most of the length of the pile before beginning to drop off at 10 feet below TOC. Looking at the 10:09 plot, the average vertical strain in the pile has decreased to below 25 με in compression, with tension developing in SB1. After the grout pressure is released, the entire pile is put into tension with average strains of just below 50 με measured through a depth of 15 feet below TOC. The measured average strain profiles are more or less uniform with depth, indicating limited shaft friction development. The change in strain indicates that the pile was in compression at 300 psi grout pressure. However, the pile experienced a decrease in stress with time even though the grouting pressure increased. When the grout pressure was released, the pile was experiencing tension, suggesting that the RIM cell was pulling the pile downwards. This indicates that the expansion of the RIM cell was generating downward displacements in excess of the upward displacements of the shaft.

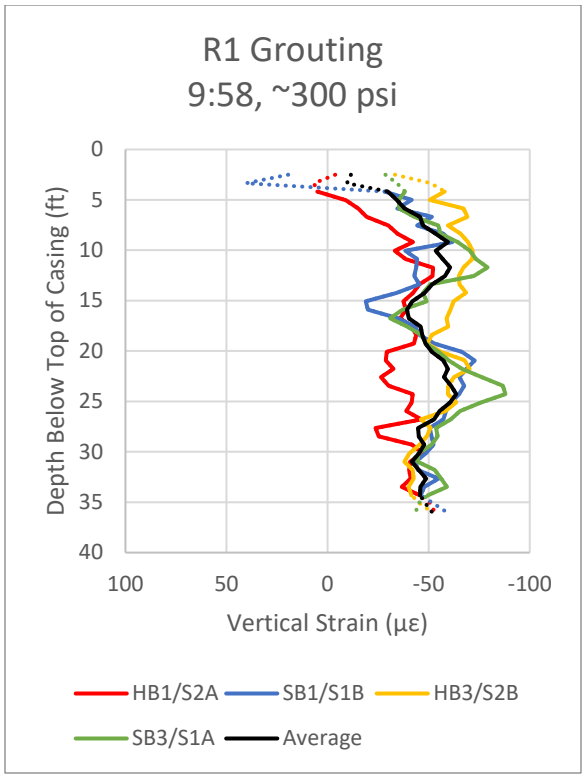

Figure 4-32: Vertical strain profile at 9:58 (~300 psi)

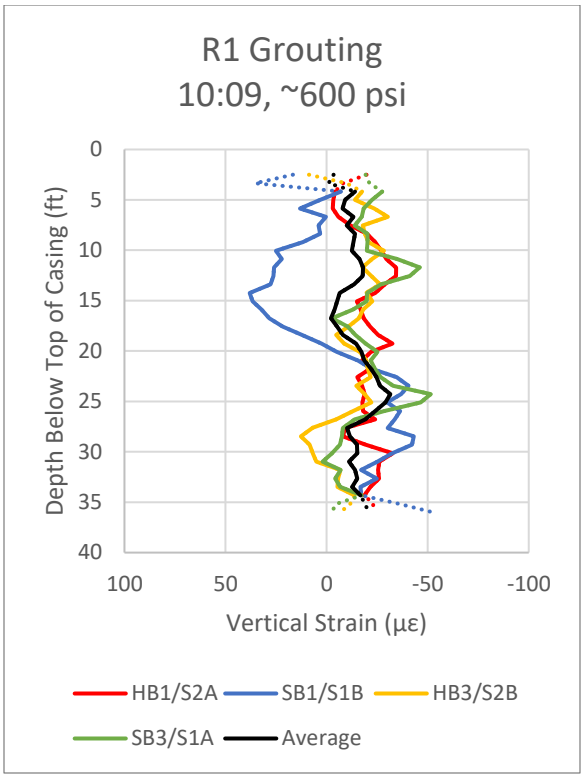

Figure 4-33: Vertical strain profile at 10:09 (~600 psi)

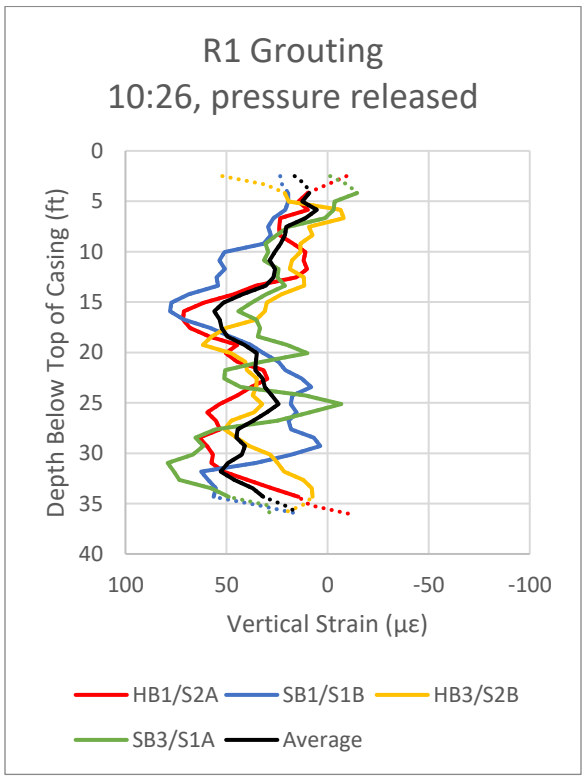

Figure 4-34: Vertical strain profile at 10:26 (after pressure release)

b) Test Shaft T2

Test Shaft T2 was grouted on February 6, 2019. The grout data logger record of pressure and volume at the grout plant is presented in Figure 4-35. Grouting of the pile with all return valves commenced at 12:08. An initial pressure hold was performed at 400 psi at 12:11. A second hold at 600 psi at 12:14 was performed with pressures fluctuating widely between 500 and 700 psi. A peak pressure of 965 psi was observed at 12:24 prior to a vent cap burst at 12:27 at which point the pressure dropped to 0 psi and pumping was stopped. The measured volumes are not adjusted for the initial flush or grout in the lines and therefore represent an upper bound of the volumes placed at the pile base.

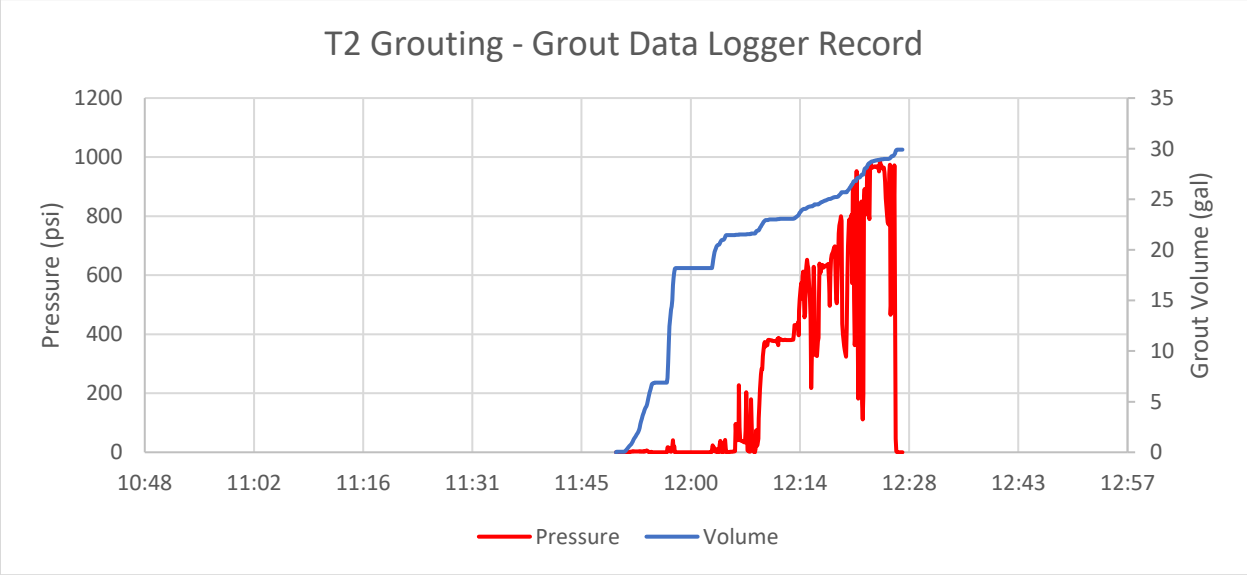

Figure 4-35: T2 grouting, grout data logger record

The fiber optic record for shaft T2 is divided into 4 strain verticals and 2 temperature verticals. The raw frequency and segment divisions are shown in Figure 4-36.

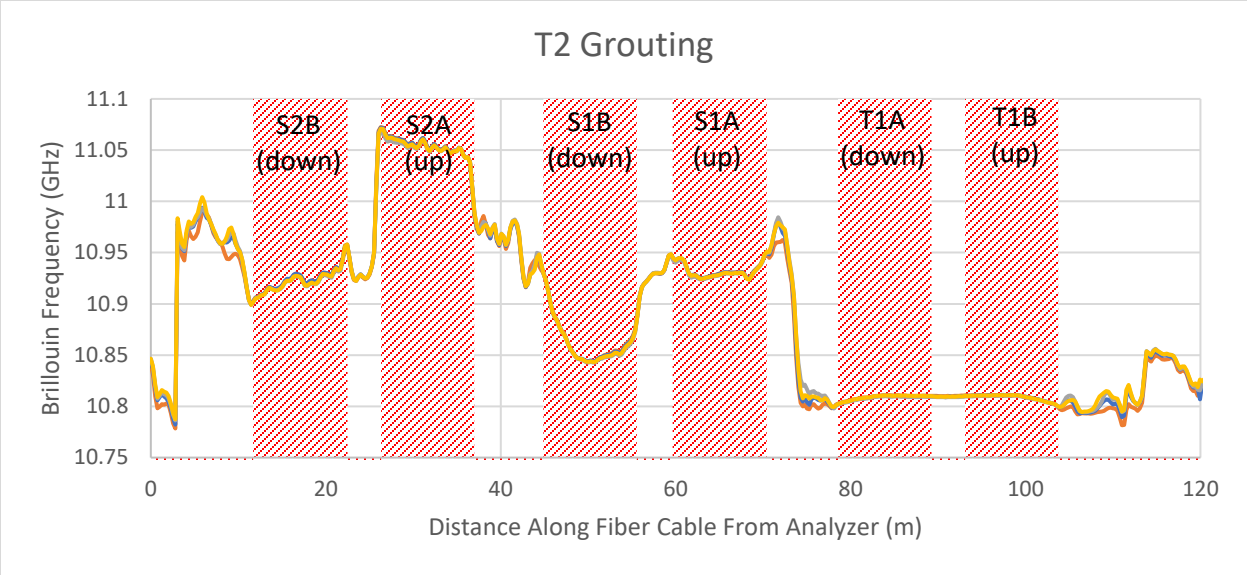

Figure 4-36: T2 grouting, raw Brillouin frequency

The measured vertical strains with time at a depth of 34.4 feet below the top of casing (TOC) are presented in Figure 4-37. This figure shows a peak vertical strain of 100 με in compression at 12:25, when the associated grouting pressure was approximately 965 psi before the vent cap burst. The peak strain on the other verticals were lower in magnitude and occurred at lower pressure, indicating a shifting strain distribution within the pile during grouting. After release of the vent cap, the strains returned to an average value just below 20 με.

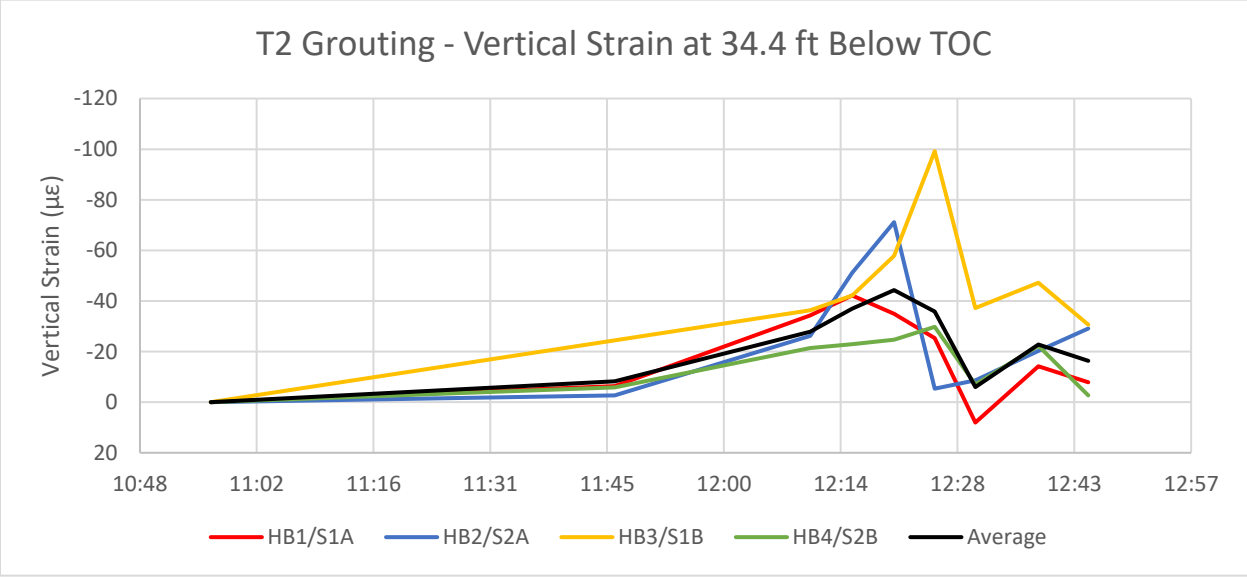

Figure 4-37: T2 grouting, vertical strains at 34.4 feet below TOC

Figure 4-38 through Figure 4-40 show the vertical strains with depth in the pile at 12:15 (~600 psi), 12:25 (~965 psi), and 12:44 (after pressure release). Figure 4-38 shows a compressive strain increase in all the verticals extending approximately 20 feet from the base of the pile. The

reading at 12:25 (Figure 5-12), the final reading prior to the vent cap bursting, shows a significant strain concentration on one quadrant of the pile with strains on all sides extending to within 5 feet of the TOC. Following the release of pressure, Figure 4-40 shows average residual strains centered just above 0 με, with variation of on the order of 30-50 με throughout the pile. In Figure 4-38, the strain profiles are increasing with depth, indicating some negative friction development during grouting. By Figure 5-12, the strain has become non-uniform, indicating a significant load concentration on the side of HB3. This could potentially be due to a variation in the loading being applied by the RIM cell, or potentially a difference in the friction resistance along one side of the shaft. In Figure 4-40, the compressive strains at the bottom of the pile have been released; however there appears to still be approximately 20 με of compressive strain in the center of the pile, potentially indicating a locked-in negative friction.

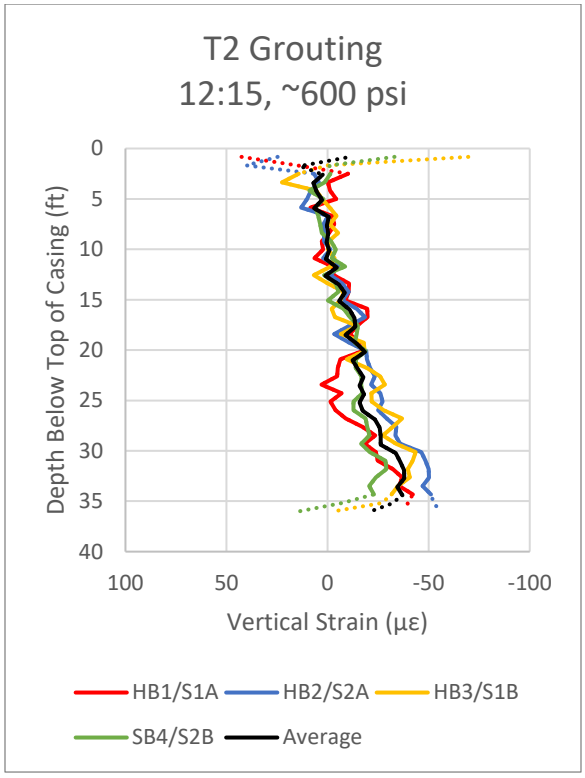

Figure 4-38: Vertical strain profile at 12:15 (~600 psi)

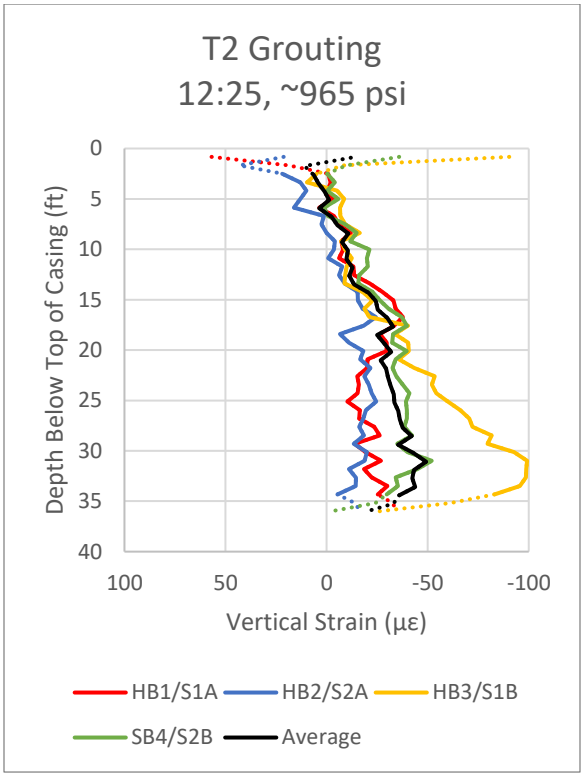

Figure 4-39: Vertical strain profile at 12:25 (~965 psi)

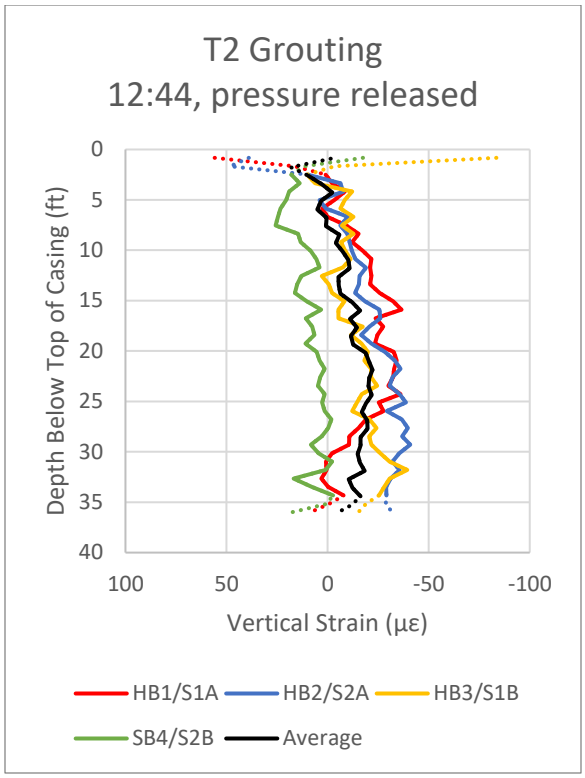

Figure 4-40: Vertical strain profile at 12:44 (after pressure release)

Open-Type (tube-à-manchette)

c) Reaction Shaft R2

Reaction Shaft R2 was grouted on February 7, 2019. The grout data logger record of pressure and volume at the grout plant is presented in Figure 4-41. Grouting was performed on three circuits, with the center circuit primed and grouted first. Grouting on the center circuit with the return valve closed began at 12:10 and continued to 13:08, at which time grouting was switched to the south circuit. The south circuit was grouted for approximately 4 minutes from 13:23 to 13:27. At 13:27, grouting was switched to the north circuit. The north circuit was grouted from 13:33 to 13:47, at which time grouting was halted. The measured volumes are not adjusted for the initial flush or grout in the lines and therefore represent an upper bound of the volumes placed at the pile base.

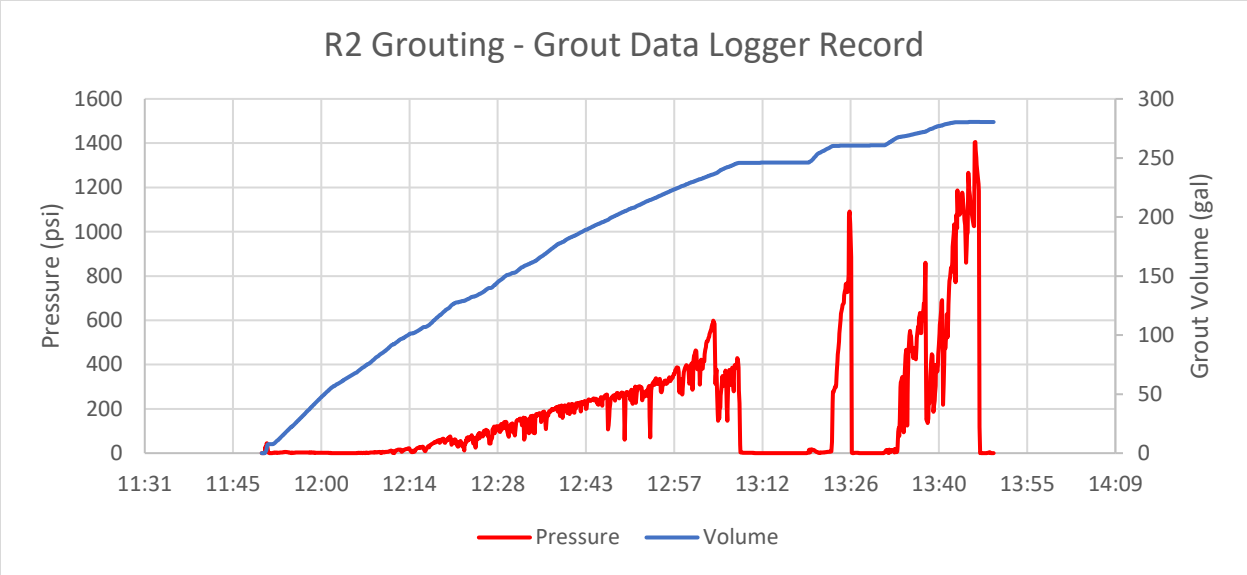

Figure 4-41: R2 grouting, grout data logger record

The fiber optic record for shaft R2 is divided into 4 strain verticals and 6 temperature verticals. The raw frequency and segment divisions are shown in Figure 4-42.

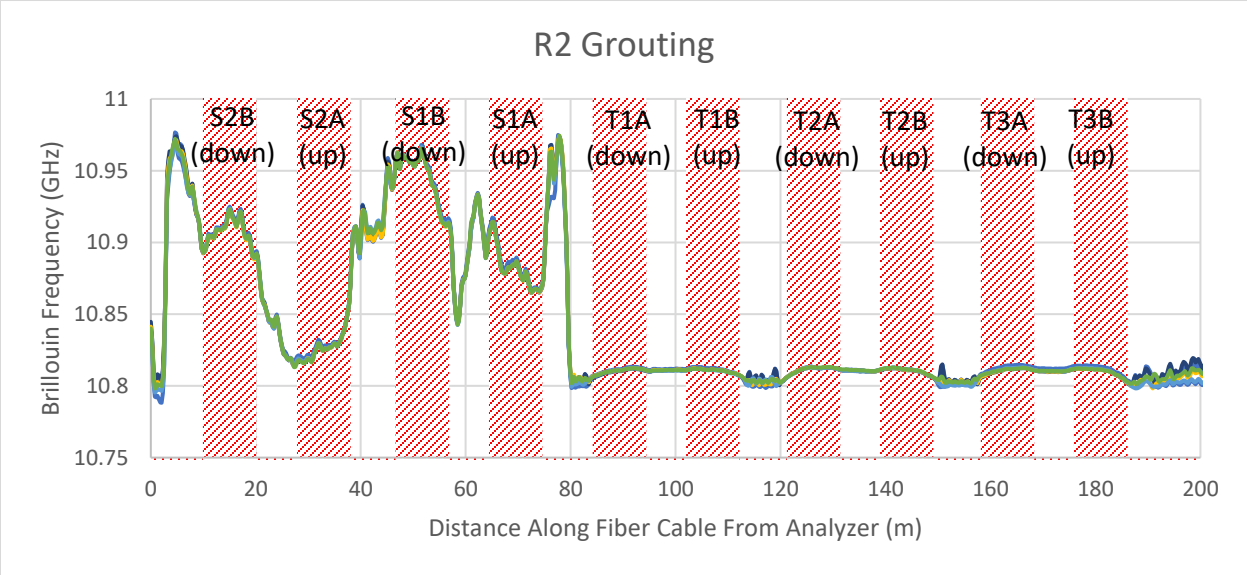

Figure 4-42: R2 grouting, raw Brillouin frequency

The measured vertical strains with time at a depth of 33.5 feet below the top of casing (TOC), approximately 1 pile diameter (5 feet) above the base, are presented in Figure 4-43. This figure shows a peak in vertical strain of approximately 45 με in compression on SB4 between 12:44 and 13:00, when the associated grouting pressure was rising between 200 and 350 psi. Once grouting was halted on the center circuit at 13:08, the average strain remained between 10 and 25 με. The strains on SB1, which were shown as approximately 35 με in tension shortly after the start of the water and grout flush, showed an increase of 25 με in compression during the final

grouting on the north circuit, potentially indicating that the grout injection at this point was still having an effect at the base of the pile. The final readings after the pressure was released show little immediate decay of the prior strains.

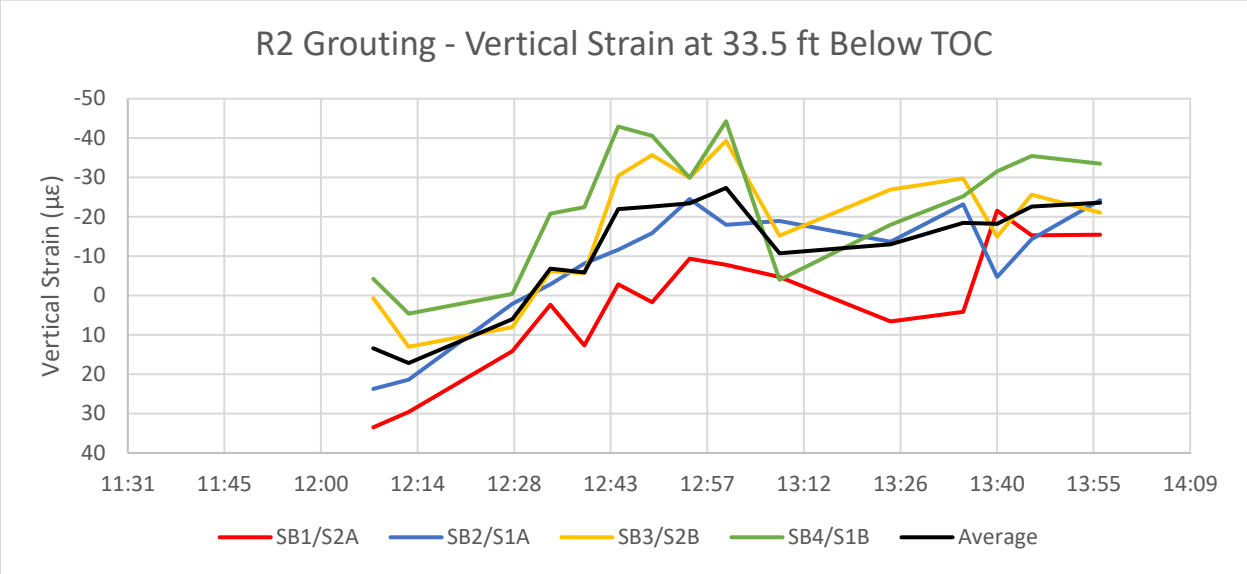

Figure 4-43: R2 grouting, vertical strains at 33.5 feet below TOC

Figure 4-44 through Figure 4-46 show the vertical strains with depth in the pile at 13:00 (~350 psi on center circuit), 13:40 (~350 psi on north circuit), and 13:56 (after pressure release). Figure 4-44 shows that the vertical strain at the bottom peak around 13:00 averaged 30 με and extended up to 20 feet below TOC, except for SB3 which had 15 με through to the TOC. Looking at the 13:00 plot of Figure 5-18, the average vertical strain in the pile has decreased to below 20 με, with the spike on SB1 mentioned above extending less than 10 feet above the base of the pile. In Figure 4-46, 10 minutes after the grout pressure was released, the pile has a linear average strain with a peak value of approximately 25 με, reducing to 0 by 5 feet below TOC. In all three figures, the strain profiles increase with depth, indicating the development of some negative friction during grouting. However, the strains reach their highest value early in the grouting on the first injection circuit, with lower strain values after switching to the other circuits and after pressure release, indicating that the additional injections are not generating a proportional increase in load at the base of the pile. This is likely due to blockage of the subsequent ports, resulting in negligible additional load being imparted to the pile during the injection on the second two circuits.

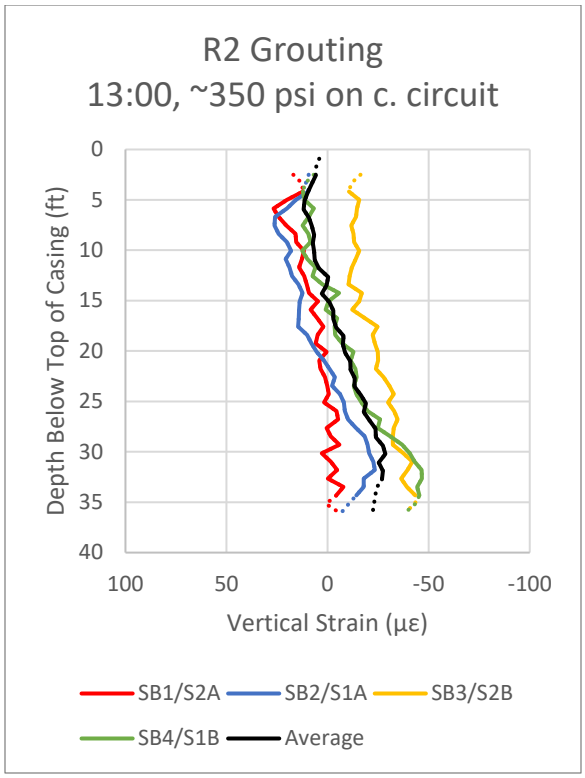

Figure 4-44: Vertical strain profile at 13:00 (~350 psi)

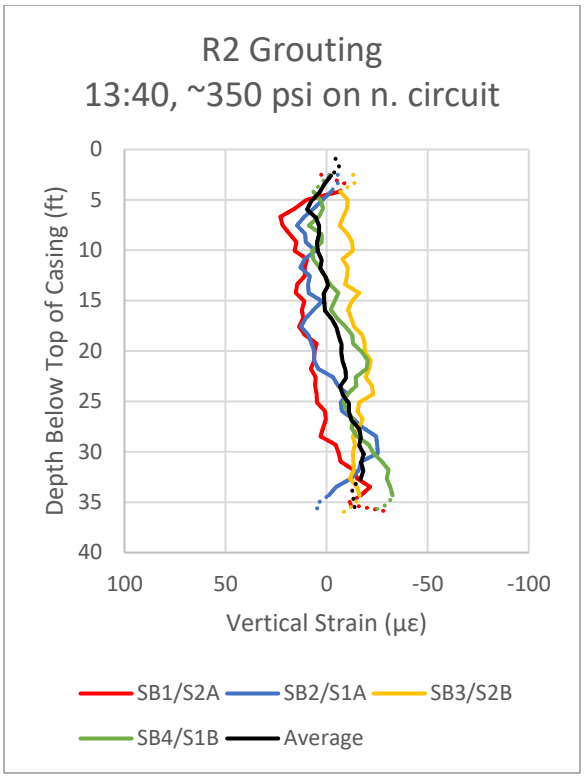

Figure 4-45: Vertical strain profile at 13:40 (~350 psi)

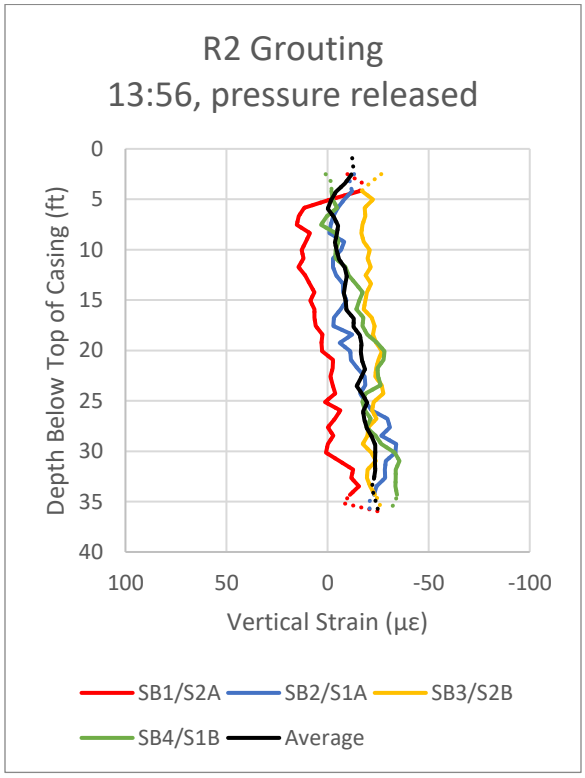

Figure 4-46: Vertical strain profile at 13:56 (after pressure release)

d) Reaction Shaft R4

Reaction Shaft R4 was grouted on February 6, 2019. Grouting was performed on three circuits, with the center circuit primed and grouted first. The grout data logger record of pressure and volume at the grout plant is presented in Figure 4-47. Grouting on the center circuit began at 14:05, with multiple starts and stops as leaks developed and pressure spikes were observed at the grout plant. The grout line was switched to the south circuit at 15:03 and continued until 15:42 with multiple pressure spikes at or above 1000 psi, at which point the grout line was switched to the north circuit. Grouting on the north circuit was performed from 15:56 to 16:09, at which point grouting was halted on the pile. The measured volumes are not adjusted for the initial flush or grout in the lines and therefore represent an upper bound of the volumes placed at the pile base.

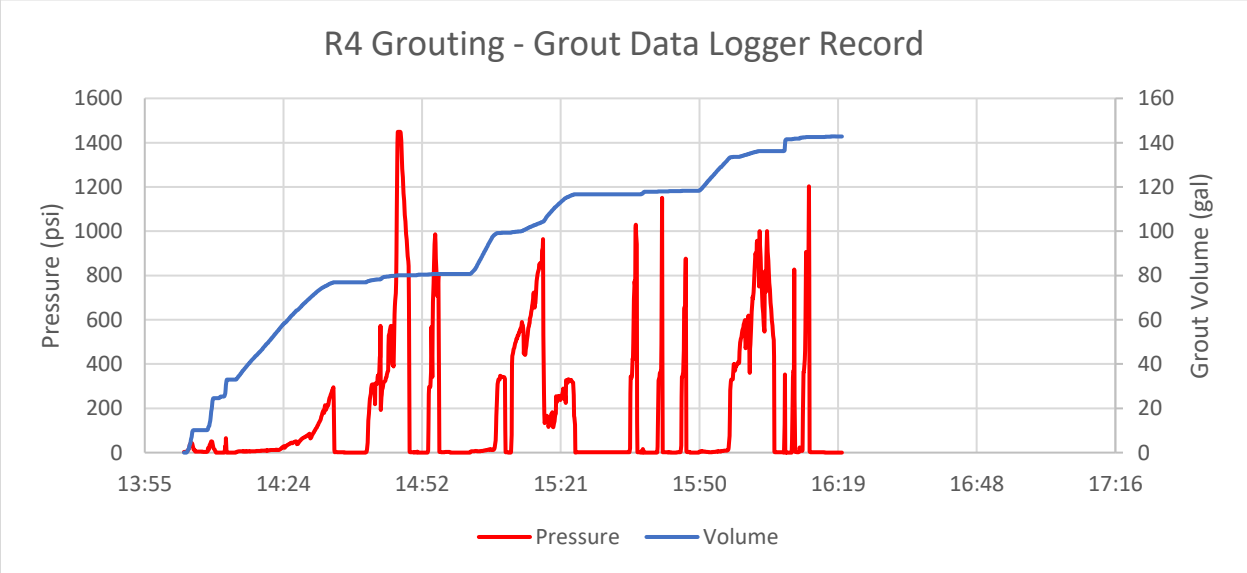

Figure 4-47: R4 grouting, grout data logger record

The fiber optic record for shaft R4 is divided into 4 strain verticals and 2 temperature verticals. The raw frequency and segment divisions are shown in Figure 4-48.

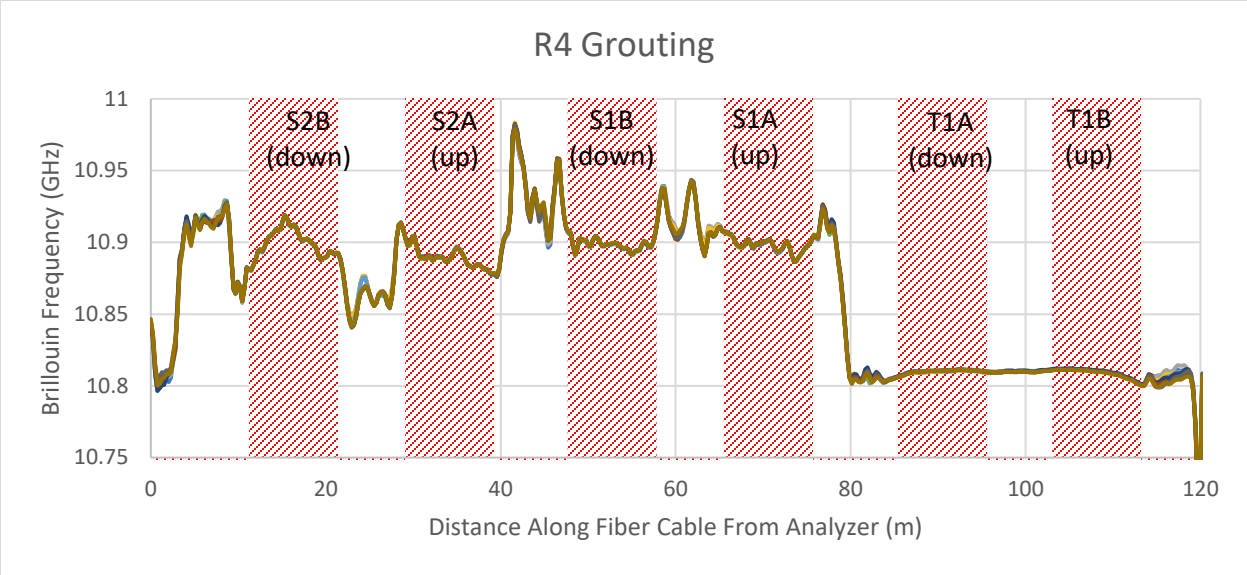

Figure 4-48: R4 grouting, raw Brillouin frequency

The measured vertical strains with time at a depth of 33.5 feet below the top of casing (TOC), approximately 1 pile diameter (5 feet) above the base, are presented in Figure 4-49. The figure shows an initial increase in average vertical strain of approximately 20 με in compression at 14:31 and 14:43, when the associated grouting pressure was approximately 295 psi. The next major strain spike is observed at 15:23, after pumping had switched to the south circuit with a pressure dropping sharply from 900 psi to 150 psi. At this time water was noted returning from HB2 (not connected to any of the grout circuits). Although this spike was observed on all strain verticals, SB2 and SB3 were observed to be in slight tension while SB 1 and SB4 were observed in compression, implying that there was non-uniform loading at the base of the pile. The strains roughly plateaued during pumping on the north circuit. However, they showed a sharp increase of an average of 22 με in compression approximately 30 minutes after the stop of pumping. It is unclear to what this rise in strain is attributed to.

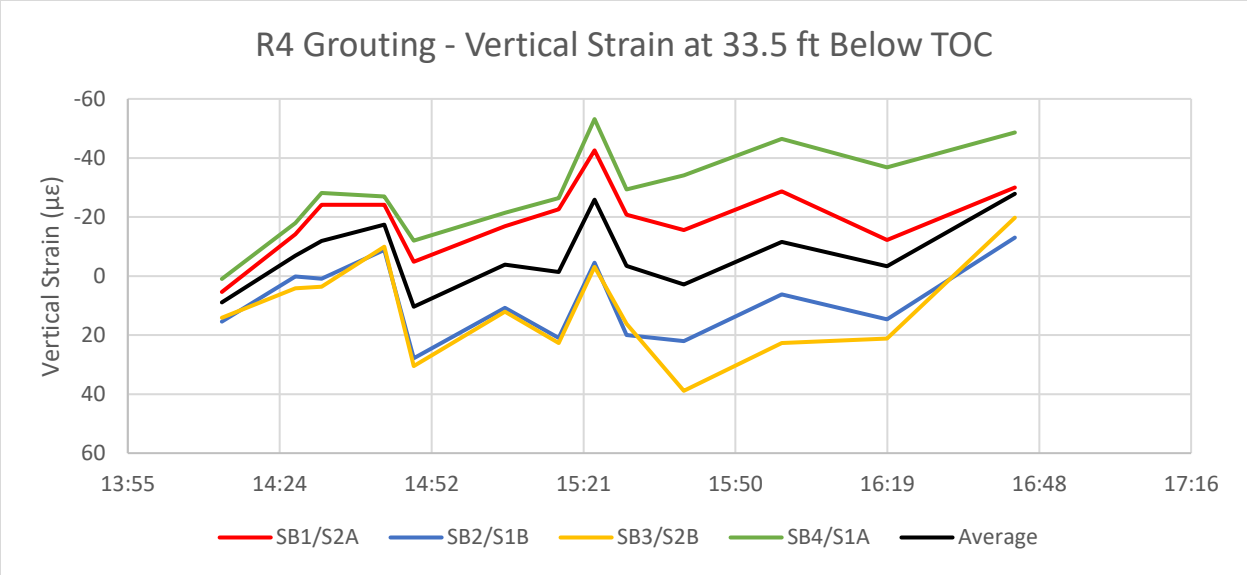

Figure 4-49: R4 grouting, vertical strains at 33.5 feet below TOC

Figure 4-50 through Figure 4-52 show the vertical strains with depth in the pile at 14:31 (~120 psi on center circuit), 15:23 (~150 psi on south circuit), and 16:43 (after pressure release). Figure 4-50 shows that there was moderate vertical strain development during pumping on the center circuit, with average strains of less than 20 με and peaks on SB1 not exceeding 30 με. In Figure 4-49, after the large pressure drop on the south circuit, large strains exceeding 50 με have developed between 10 and 20 feet below TOC on SB1. Looking closer at the data, the strain increase in this area was roughly linear during pumping, implying that the grouting is affecting this zone within the pile. In Figure 4-50, after grouting has ceased, the residual strains in the bottom portion of the pile are below 50 με with the shallow compression on SB1 in excess of 70 με.

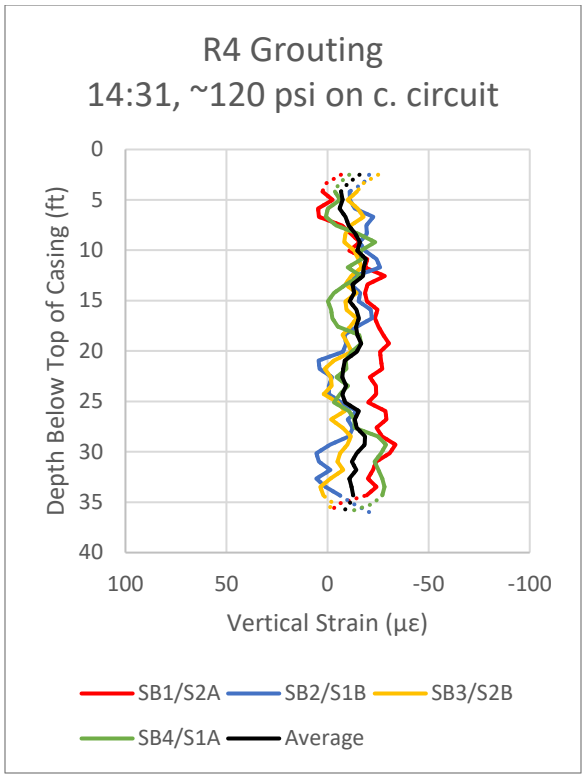

Figure 4-50: Vertical strain profile at 14:31 (~120 psi)

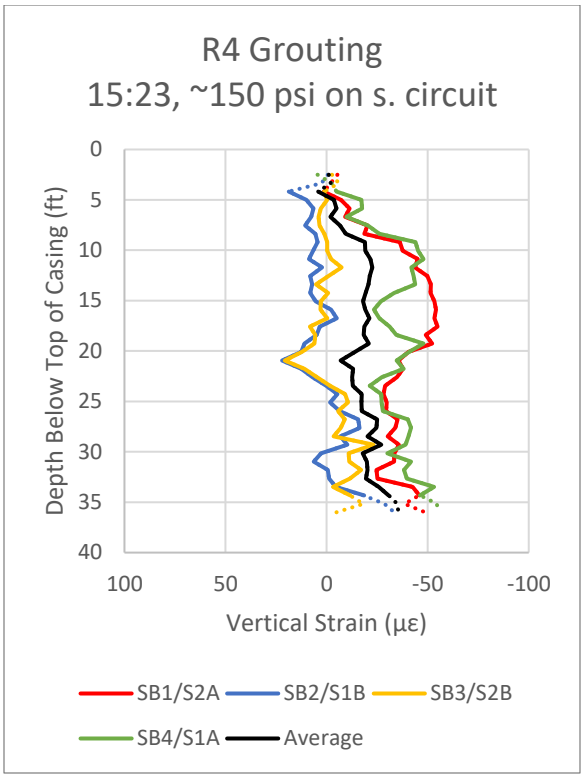

Figure 4-51: Vertical strain profile at 15:23 (~150 psi)

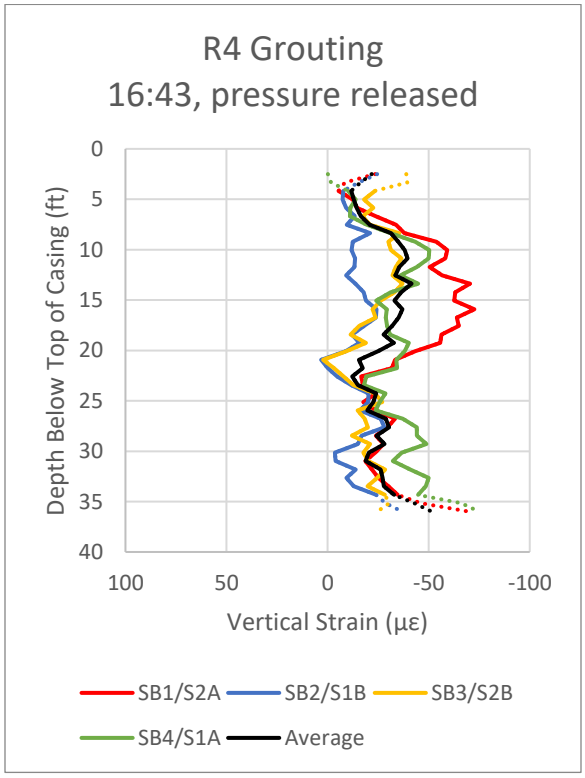

Figure 4-52: Vertical strain profile at 16:43 (after pressure release)

e) Reaction Shaft R6

Reaction Shaft R6 was grouted on February 8, 2019. The grout data logger record of pressure and volume at the grout plant is presented in Figure 4-53. Grouting was performed on three circuits, with the center circuit primed and grouted first. Grouting on the center circuit began at 9:01 and continued through 9:59. At approximately 9:30, the grout mix was thickened from a w/c ratio of 0.8 to 0.7 with an associated observed increase in pressure. The grout line was switched to the south circuit at 9:59 and continued until 10:35, at which point the grout line was switched to the north circuit. Grouting on the north circuit was performed from 10:46 to 10:51, at which point grouting was halted on the pile. The measured volumes are not adjusted for the initial flush or grout in the lines and therefore represent an upper bound of the volumes placed at the pile base.

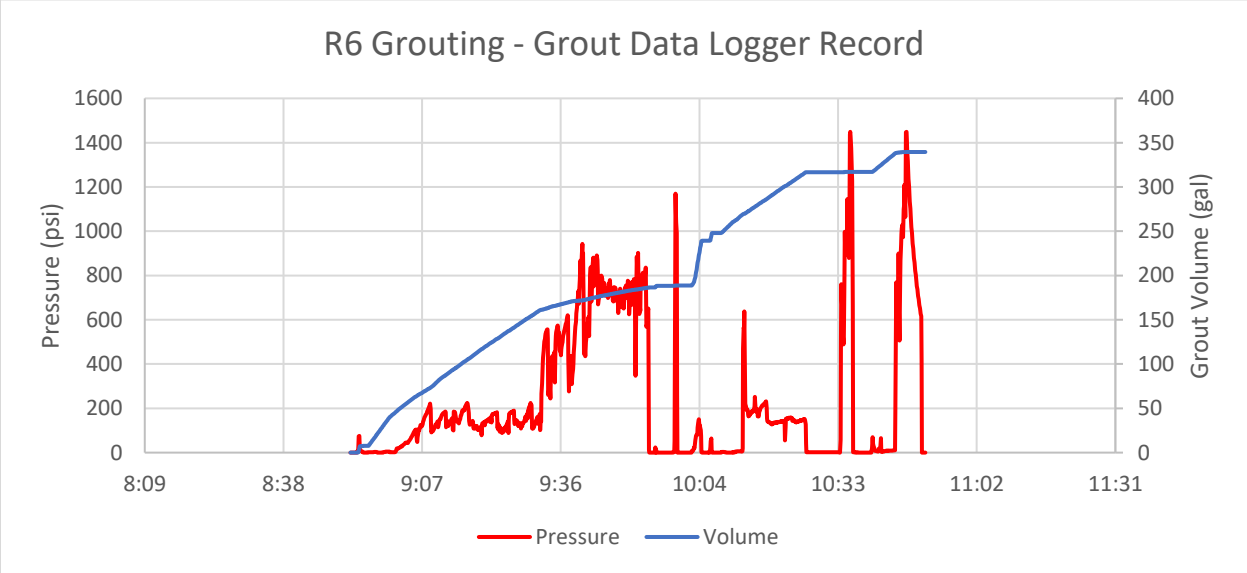

Figure 4-53: R6 grouting, grout data logger record

The fiber optic record for shaft R6 is divided into 4 strain verticals and 2 temperature verticals. The raw frequency and segment divisions are shown in Figure 4-54.

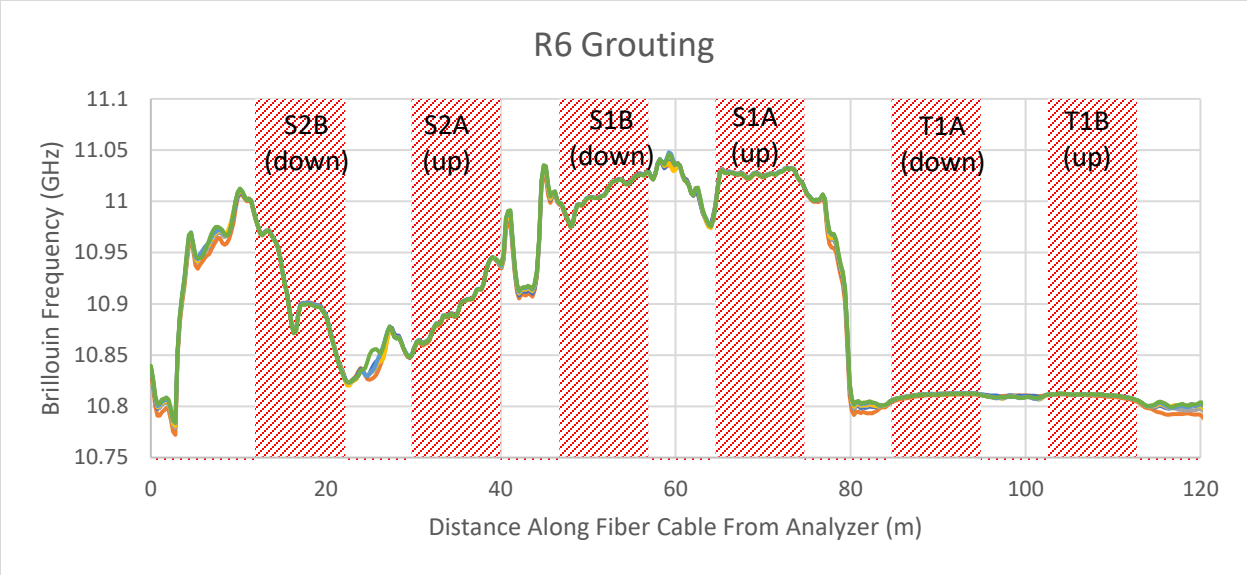

Figure 4-54: R6 grouting, raw Brillouin frequency

The measured vertical strains with time at a depth of 33.5 feet below the top of casing (TOC), approximately 1 pile diameter (5 feet) above the base, are presented in Figure 4-55. This figure shows an initial increase in the vertical strain to approximately 50 με in compression at 9:35 on SB4, when the associated grouting pressure was approximately 475 psi. Compressive strains on SB4 increased again at 10:15, immediately after pumping had switched to the south circuit. Strains in SB1 and SB3 were generally consistent with those on SB4 during this time, with strains on SB2 remaining at or just below 0 με. A major drop in compressive strain was observed at 11:00 on all 4 verticals immediately following the venting of all circuit valves on the pile after the conclusion of grouting. These strains rebounded somewhat in further readings, with a final measured average strain in the pile of 20 με, +/- 20 με at 11:22.

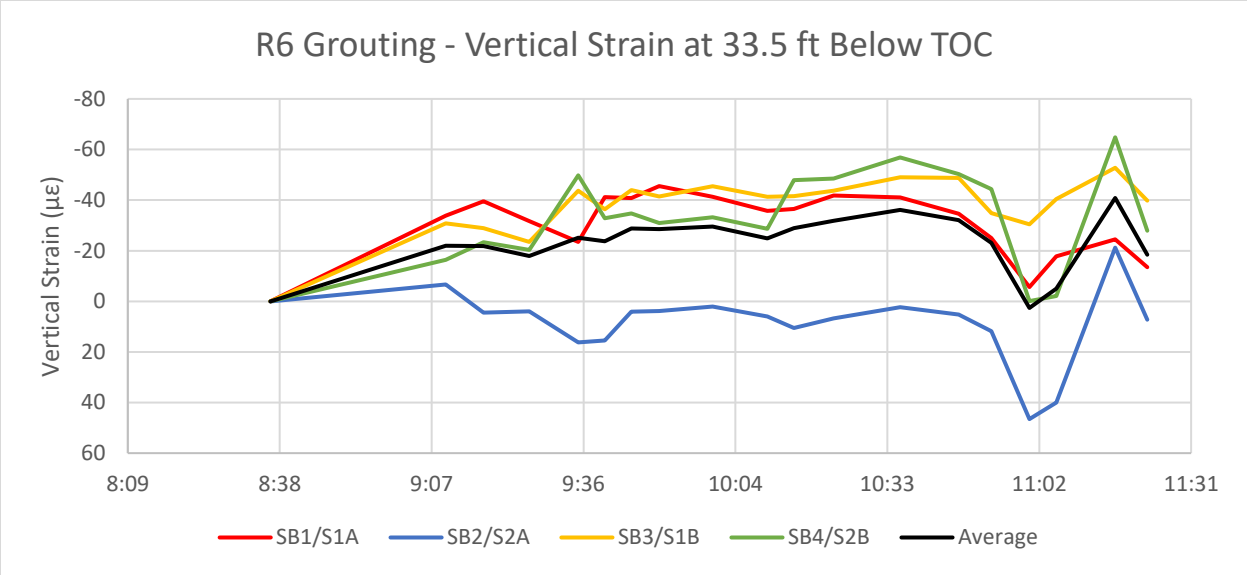

Figure 4-55: R6 grouting, vertical strains at 33.5 feet below TOC

Figure 4-56 through Figure 4-58 show the vertical strains with depth in the pile at 9:35 (~475 psi on center circuit), 10:36 (~1200 psi on south circuit), and 11:22 (after pressure release). Figure 4-56 shows vertical strain development on SB4 during pumping on the center circuit, with compressive strain of 50 με above the base of the pile roughly constant to 18 feet below TOC. SB3 showed approximately half the corresponding strain, with SB1 and SB2 showing approximately 0 strain. In Figure 5-30, by 10:36, the compressive strain on SB4 remains just above 50 με above the base with strains increasing on all other verticals with the exception of SB2. In Figure 4-58, after grouting was halted and the pressure in the circuits was released, SB3 and SB4 maintained approximately 37 με above the base with compressive strains extending upward into the pile to a depth of 20 feet below TOC. The wide variation in compressive strains suggests that the grouting pressures at the base may have been uneven, resulting in bending development in the lower 20 feet of the pile. After the pressure release, the strain differential decreases to a spread of less than 45 με, as compared to a previous peak differential of approximately 75 με during grouting.

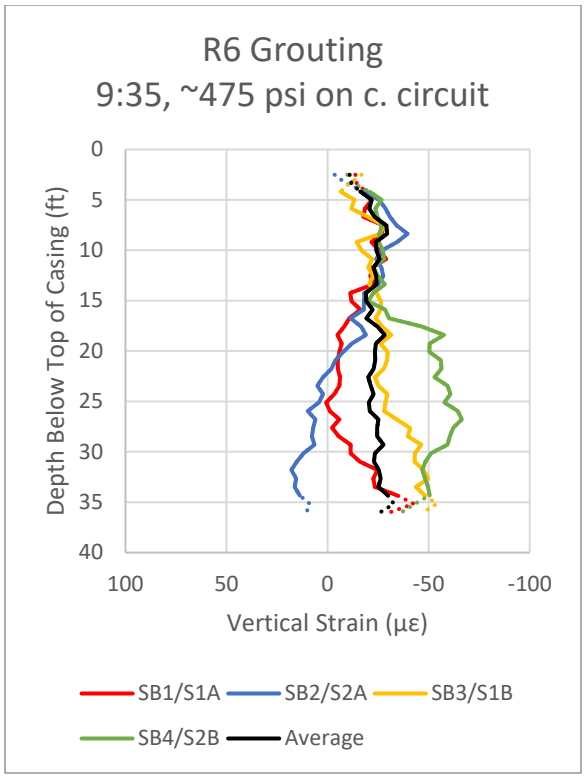

Figure 4-56: Vertical strain profile at 9:35 (~475 psi)

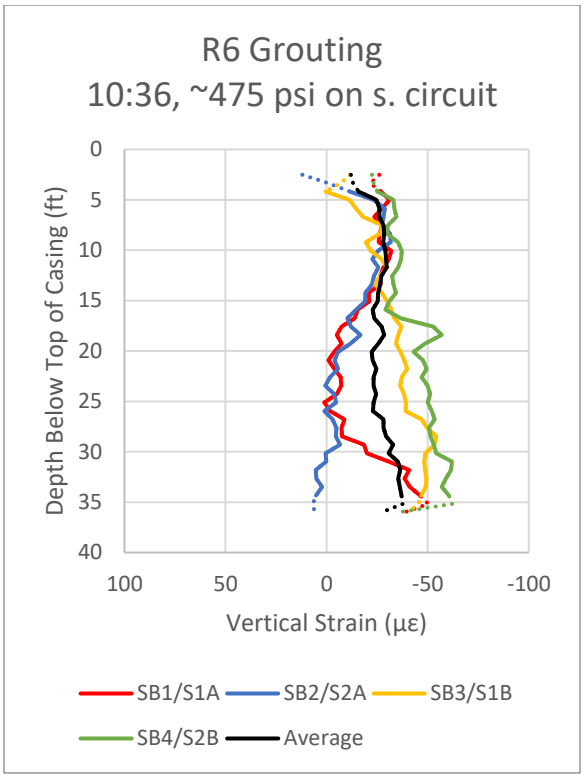

Figure 4-57: Vertical strain profile at 10:36 (~475 psi)

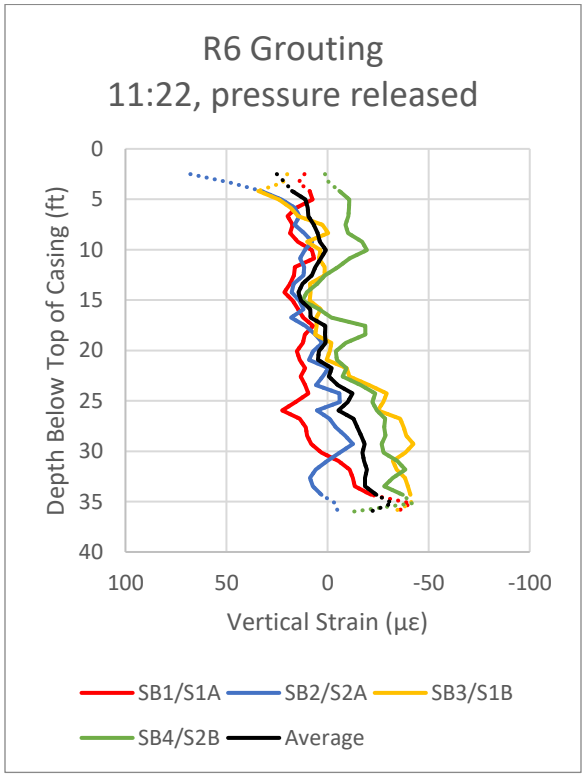

Figure 4-58: Vertical strain profile at 11:22 (after pressure release)

f) Reaction Shaft R8

Reaction Shaft R8 was grouted on February 7, 2019. The grout data logger record of pressure and volume at the grout plant is presented in Figure 4-59. Grouting was performed on three circuits, with the center circuit primed and grouted first. Grouting on the center circuit with the return valve closed was performed from 9:21 to 10:05. The grout line was switched to the south circuit and was grouted from 10:17 through 10:28. The grout line was then switched to the north circuit, which was grouted from 10:43 to 10:49, after which grouting was concluded. The measured volumes are not adjusted for the initial flush or grout in the lines and therefore represent an upper bound of the volumes placed at the pile base.

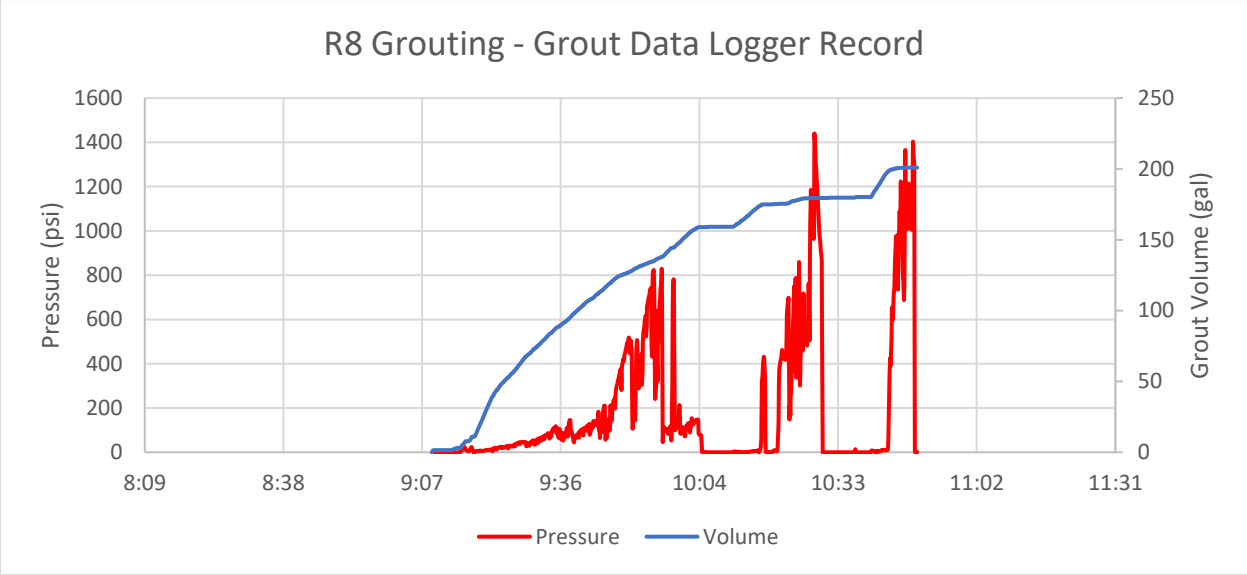

Figure 4-59: R8 grouting, grout data logger record

The fiber optic record for shaft R8 is divided into 4 strain verticals and 2 temperature verticals. The raw frequency and segment divisions are shown in Figure 4-60.

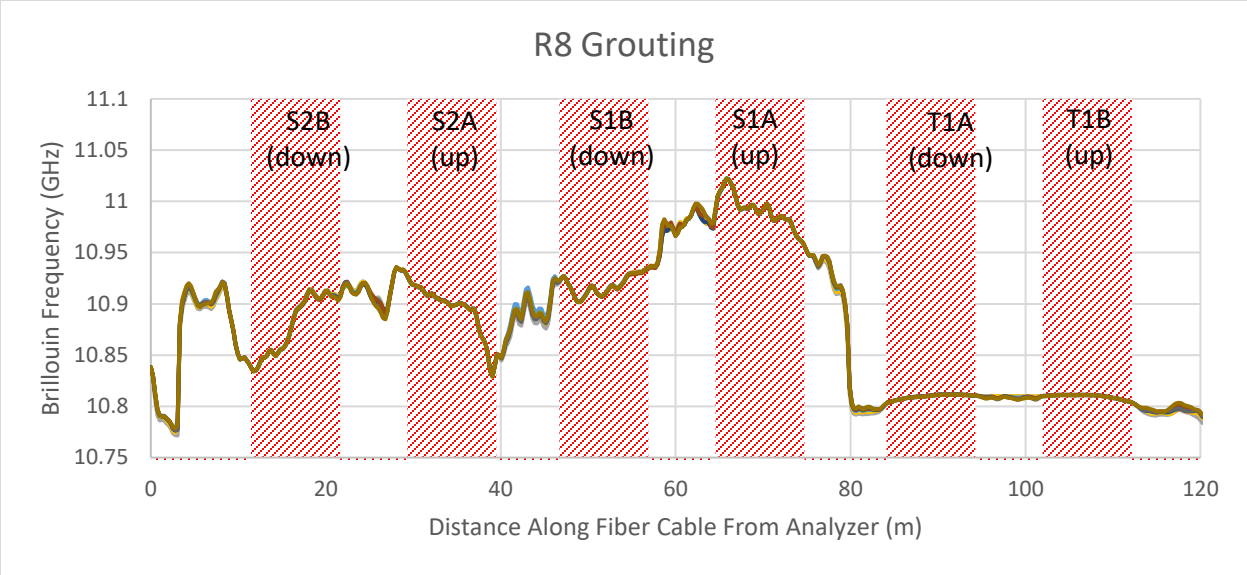

Figure 4-60: R8 grouting, raw Brillouin frequency

The measured vertical strains with time at a depth of 33.5 feet below the top of casing (TOC), approximately 1 pile diameter (5 feet) above the base, are presented in Figure 4-61. The figure shows an initial peak in vertical compressive strain of approximately 60 με at 9:54 on SB3, when the associated grouting pressure had dropped from 750 psi to 300 psi on the center circuit. Strains on SB3 continued to be the highest of the four verticals, peaking at 65 με at 10:26 with a pressure of 750 psi on the south circuit, just prior to switching to the north circuit. The strains in the other three verticals remained relatively constant through grouting with variations within +/- 20 με of 0.

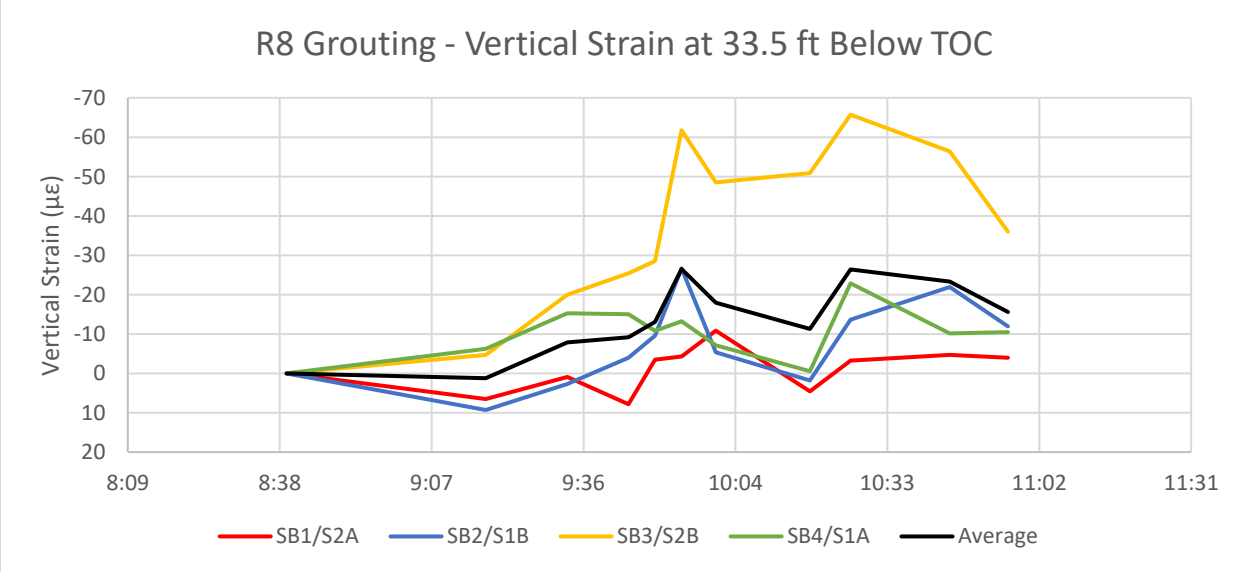

Figure 4-61: R8 grouting, vertical strains at 33.5 feet below TOC

Figure 4-62 through Figure 4-64 show the vertical strains with depth in the pile at 9:54 (~300 psi on center circuit), 10:26 (~750 psi on south circuit), and 10:56 (after pressure release). Figure 4-62 shows an "s" curve of compressive strain developing in SB3, with compressive strain of 70 με above the base of the pile decreasing to 30 με at 30 feet below TOC before increasing again to just below 50 με at 20 feet below TOC. The next Figure 5-36 shows the compressive strain in SB3 above the bottom of the pile further increasing to 84 με, with the strains in the other three verticals remaining below 25 με. In Figure 4-64, by the final reading at 10:26, much of the strain in the bottom of the pile had been lost; however, a strong strain differential of approximately +/- 40 με had developed in the top 15 feet of the pile. It is not clear from site observations what introduced this wide differential at the conclusion of grouting. The initial linear strain along the pile in Figure 4-62 implies that some negative skin friction was developed early in the pile grouting. However, this trend did not clearly persist through the end of grouting and pressure release.

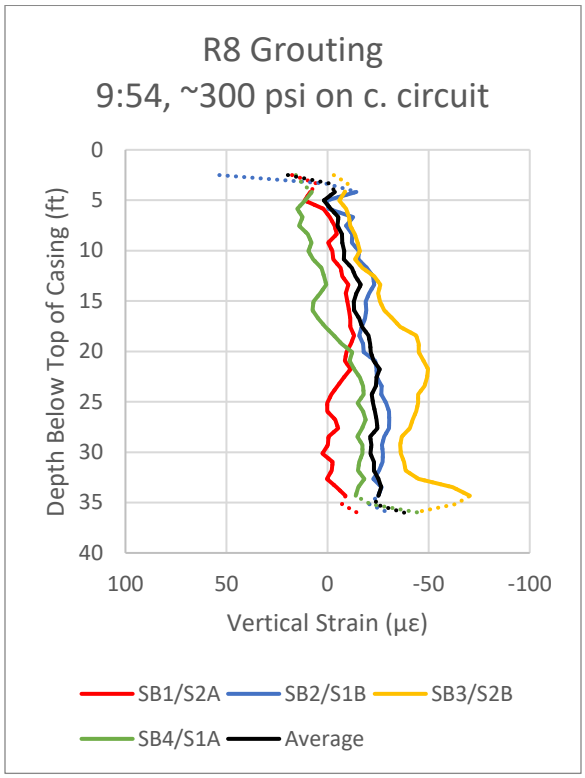

Figure 4-62: Vertical strain profile at 9:54 (~300 psi)

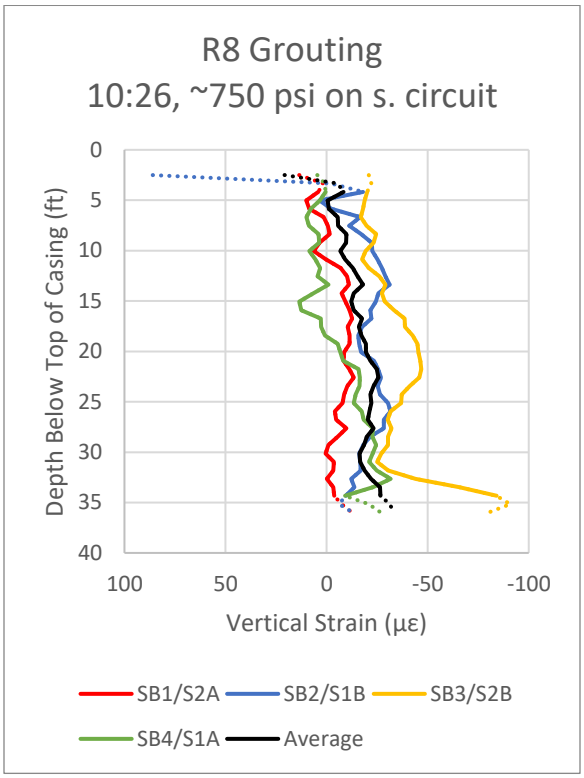

Figure 4-63: Vertical strain profile at 10:26 (~750 psi)

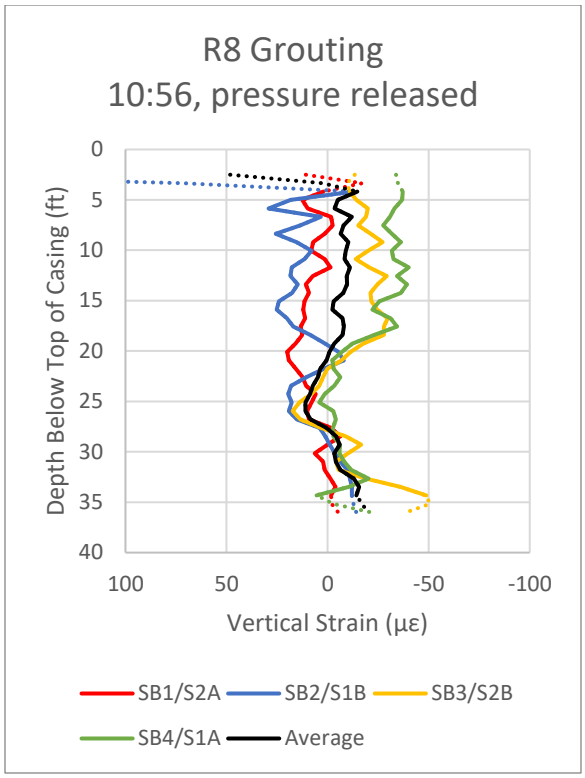

Figure 4-64: Vertical strain profile at 10:56 (after pressure release)

g) Test Shaft T3

Test Shaft T3 was grouted on February 7, 2019. The grout data logger record of pressure and volume at the grout plant is presented in Figure 4-65. Grouting was performed on two circuits, with the east circuit primed and grouted first. Grouting on the east circuit with the return valve closed was performed from 15:09 to 15:30. The grout line was switched to the northwest circuit and was grouted from 15:45 through 15:51, at which point grouting was halted. The measured volumes are not adjusted for the initial flush or grout in the lines and therefore represent an upper bound of the volumes placed at the pile base.

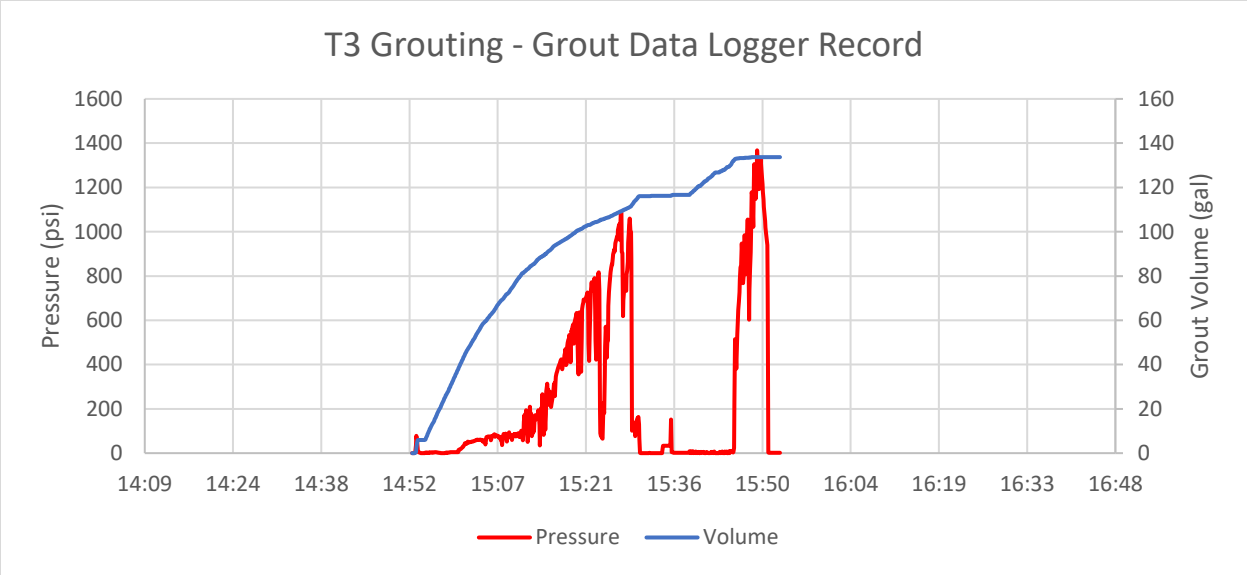

Figure 4-65:: T3 grouting, grout data logger record

The fiber optic record for shaft R3 is divided into 4 strain verticals and 2 temperature verticals. The raw frequency and segment divisions are shown in Figure 4-66.

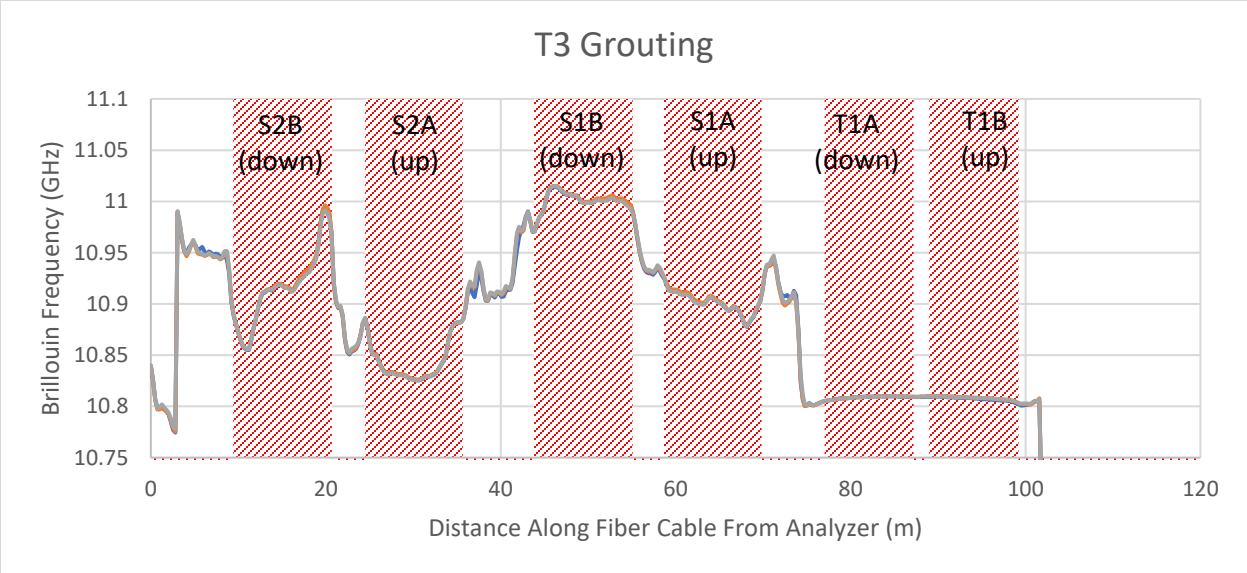

Figure 4-66: T3 grouting, raw Brillouin frequency

The measured vertical strains with time at a depth of 34.4 feet below the top of casing (TOC) are presented in Figure 4-67. The figure shows an initial peak in compressive vertical strain of approximately 87 με at 15:21 on HB1, when the associated grouting pressure was 600 psi on the east circuit. Strains on HB3 rose to 50 με at 15:47 with a pressure of 900-100 psi on the northwest circuit, just prior to halting grouting. The strains in all four verticals dropped immediately after the pressure release at 15:53, rebounding sharply before settling at an average of just below 30 με in compression at 16:27.

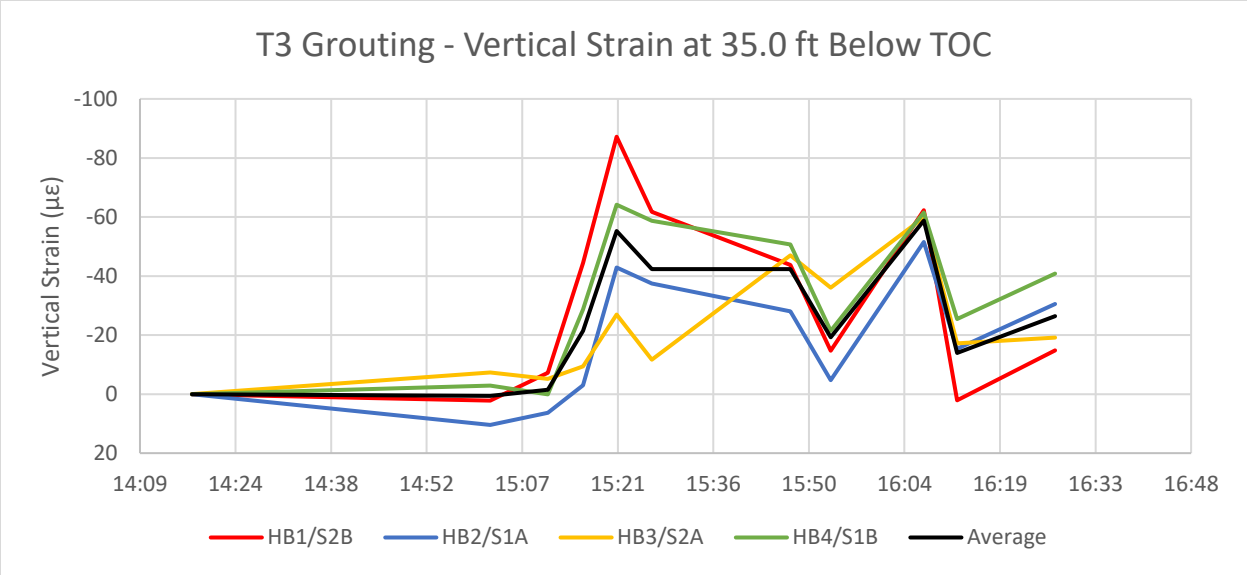

Figure 4-67: T3 grouting, vertical strains at 35.0 feet below TOC

Figure 4-68 through Figure 4-70 show the vertical strains with depth in the pile at 15:21 (~600 psi on east circuit), 15:47 (~950 psi on northwest circuit), and 16:27 (after pressure release). Figure 4-68 shows a high peak of compressive strain on HB1, with compressive strain of 114 με above the base of the pile decreasing to 0 με at 10 feet below. The other three verticals all show strains centered around 50 με. In Figure 5-42, by the time grouting had switched to the northwest circuit at 15:47, the strains at the base of the pile had decreased to at or below 50 με. In Figure 5-43, after the pressure in the grouting circuits was released, an average strain of 26 με remained above the base, extending at a constant to approximately 25 feet below TOC before fading linearly to 5 feet below TOC. In all three figures, the strain profiles increase with depth, indicating the development of some negative friction during grouting. As with earlier piles, the compressive strains at the base of the pile develop their highest values early in the grouting process and drop as grouting continues and pressure is ultimately released, indicated that injection on later circuits were not effective in generating load at the base of the pile.

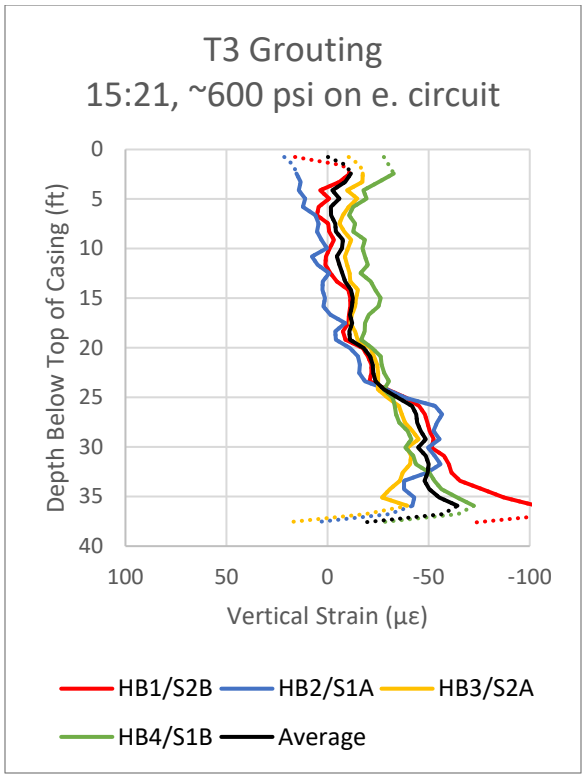

Figure 4-68: Vertical strain profile at 15:21 (~600 psi)

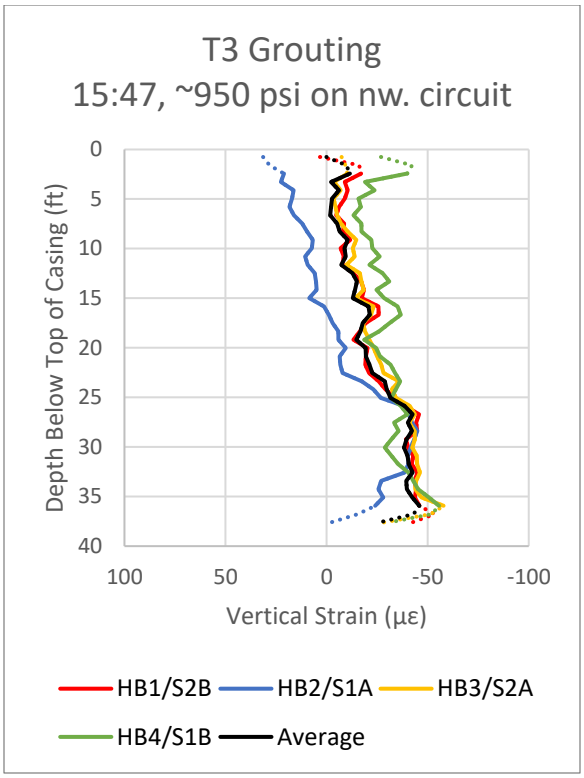

Figure 4-69: Vertical strain profile at 15:47 (~950 psi)

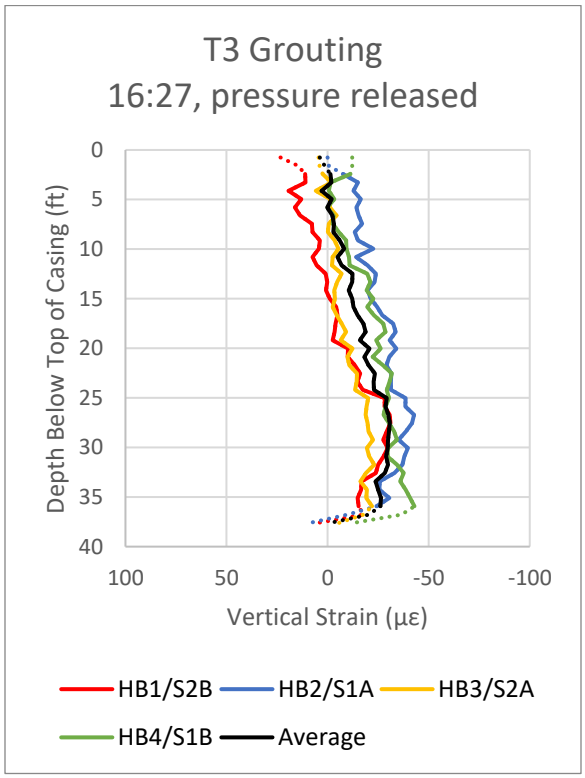

Figure 4-70: Vertical strain profile at 16:27 (after pressure release)

Closed-Type (bladder)

h) Reaction Shaft R3

Reaction Shaft R3 was grouted on February 4, 2019. The grout data logger record of pressure and volume at the grout plant is presented in Figure 4-71. All grouting was performed through a single line (of four). Connectivity between all lines was established prior to priming the system with grout. After closing the three remaining valves, grouting of the pile began at 13:44. Grouting continued until 14:15 with a peak pressure of 410 psi, after which grouting was concluded and the valve was closed. The measured volumes are not adjusted for the initial flush or grout in the lines and therefore represent an upper bound of the volumes placed at the pile base.

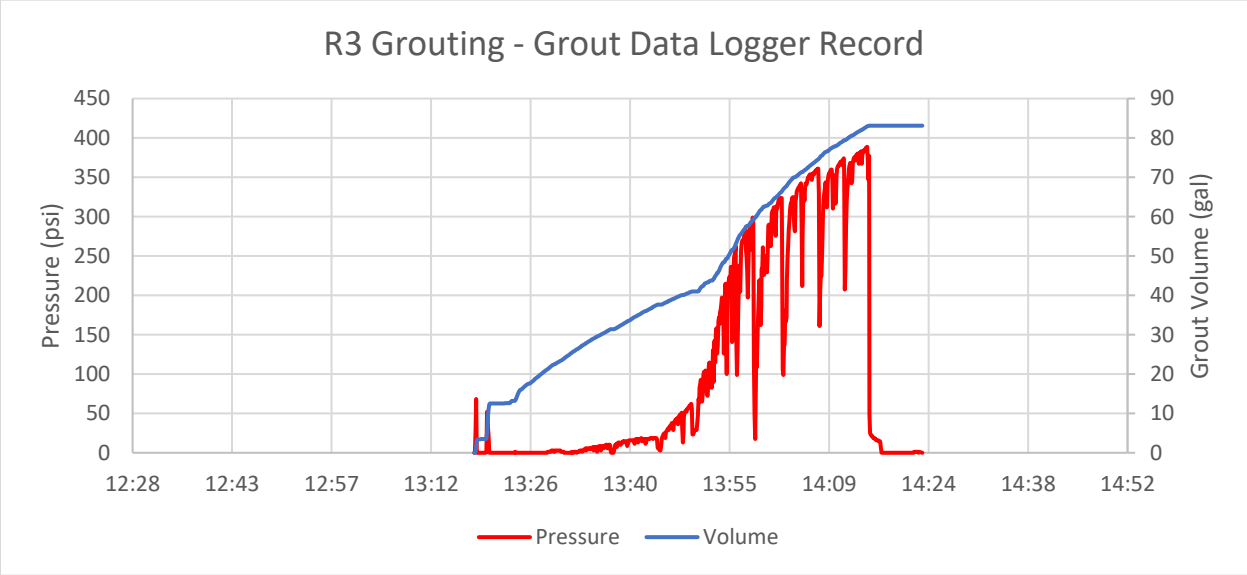

Figure 4-71: R3 grouting, grout data logger record

The fiber optic record for shaft R3 is divided into 4 strain verticals and 6 temperature verticals. The raw frequency and segment divisions are shown in Figure 4-72.

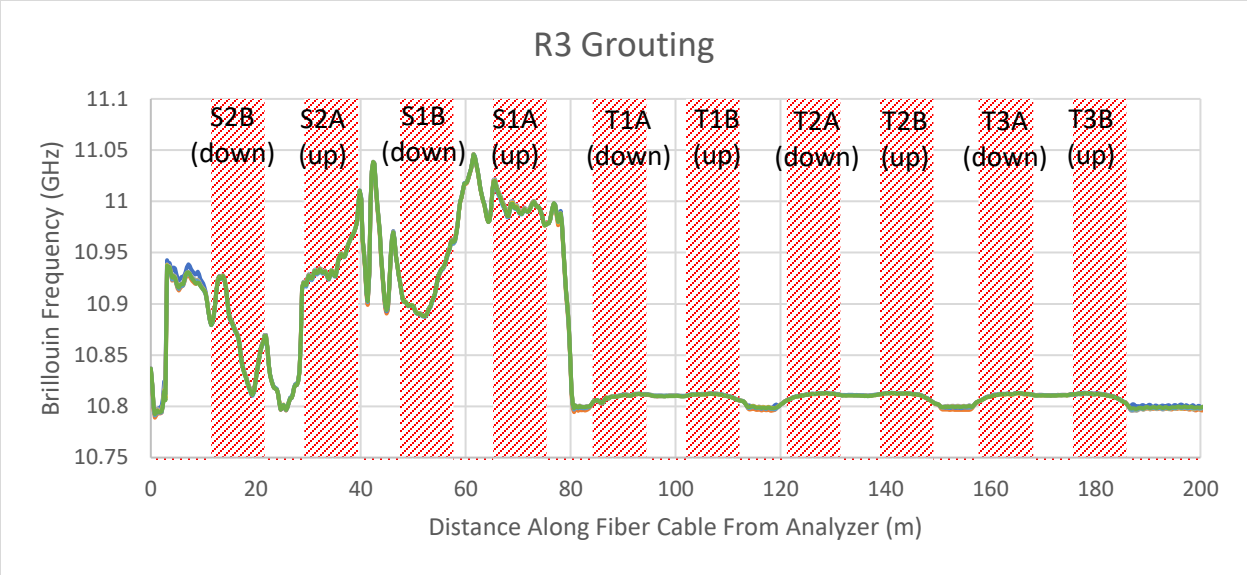

Figure 4-72: R3 grouting, raw Brillouin frequency

The measured vertical strains with time at a depth of 33.5 feet below the top of casing (TOC), approximately 1 pile diameter (5 feet) above the base, are presented in Figure 4-73. This figure shows a steady increase in vertical strain on all four verticals from the start of circuit priming at 13:22 through the highest pressure of 410 psi at 14:11. A peak strain of 63 με was recorded on SB1. Once grouting was halted at 14:15, all four verticals show a strain drop of 20-30 με, with the final measured compressive strains at 14:33 between 30 and 40 με. The strain behavior of the four verticals were similar throughout the monitoring period, indicating that the strains during grouting were roughly evenly distributed across the base of the pile.

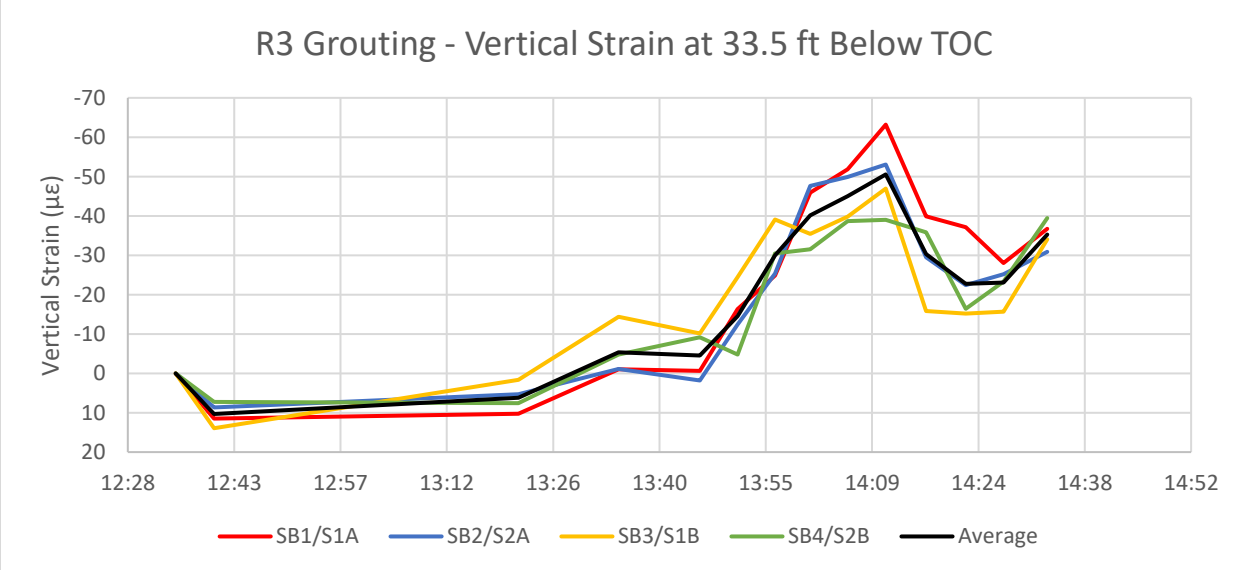

Figure 4-73: R3 grouting, vertical strains at 33.5 feet below TOC

Figure 4-74 through Figure 4-76 show the vertical strains with depth in the pile at 13:51 (~60 psi), 14:11 (~410 psi), and 14:33 (after pressure release). Figure 4-74 shows strain building on SB3 almost immediately after the start of grouting with a peak of 30 με in compression at 30 feet below TOC. In Figure 5-48, at the fiber optic reading with the highest pressure at 14:11, SB1 has a peak strain of 69 με at 30 feet below TOC. The other three verticals have peak compressive strains of approximately 50 με, with all 4 verticals having strain linearly decaying through the top of the pile. In Figure 4-76, after the pressure has been released, all of the verticals fall to below 50 με. SB2 shows the most dramatic drop in compression, dropping to 0 strain at 25 feet below TOC with the top 15 feet in slight tension. The remaining three verticals maintain a roughly linear strain distribution from 0 at the top of the pile to 35-45 με just above the bottom of the pile. This indicates that a portion of negative skin friction developed during grouting is still present after the release of pressure.

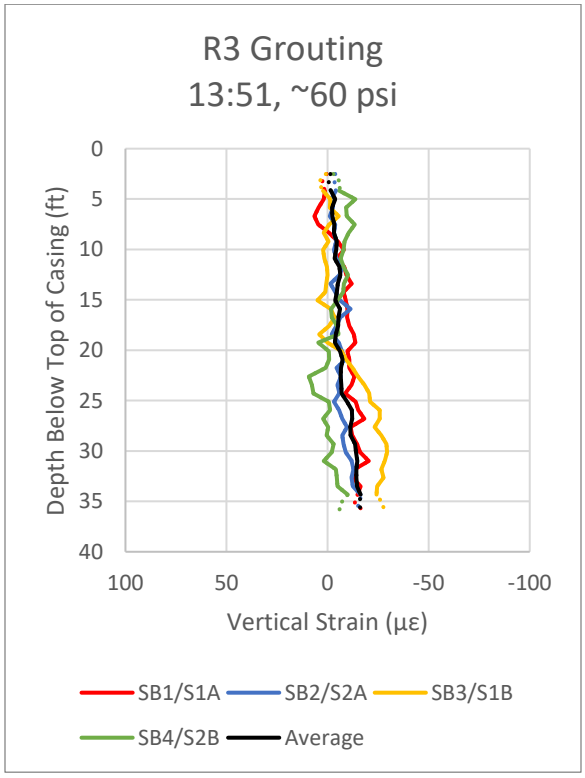

Figure 4-74: Vertical strain profile at 13:51 (~60 psi)

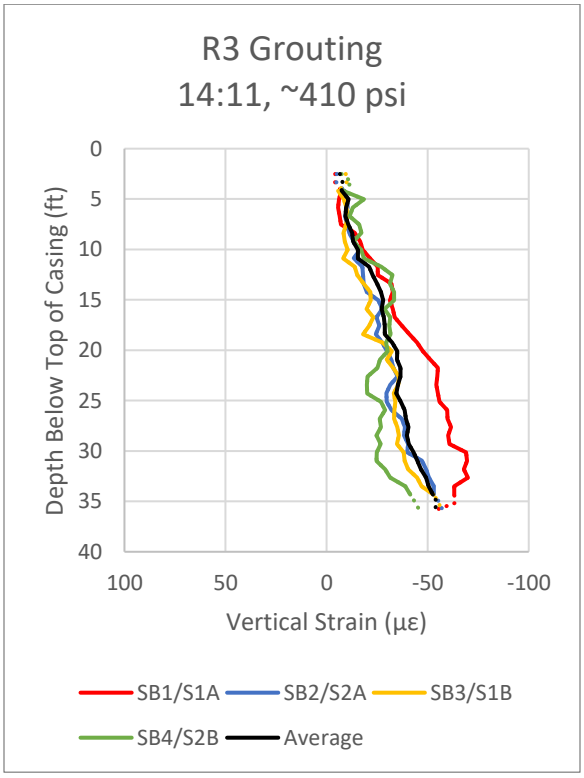

Figure 4-75: Vertical strain profile at 14:11 (~410 psi)

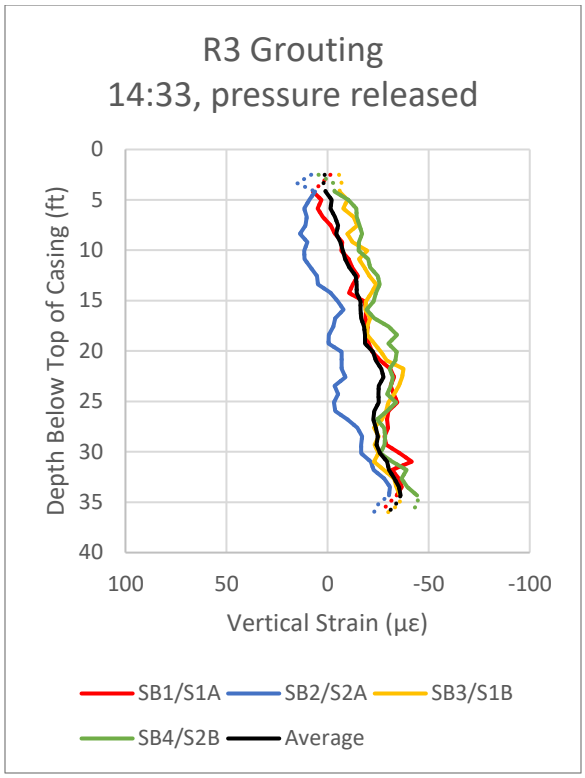

Figure 4-76: Vertical strain profile at 14:33 (after pressure release)

i) Reaction Shaft R5

Reaction Shaft R5 was grouted on February 5, 2019. The grout data logger record of pressure and volume at the grout plant is presented in Figure 4-77. All grouting was performed through a single line (of 4). Once grout return was established at the surface, all return valves were closed at 9:45 and grouting of the pile began. Grouting continued until 10:42 with an associated pressure of 410 psi, at which point the grout line was locked off and grouting was concluded. The measured volumes are not adjusted for the initial flush or grout in the lines and therefore represent an upper bound of the volumes placed at the pile base.

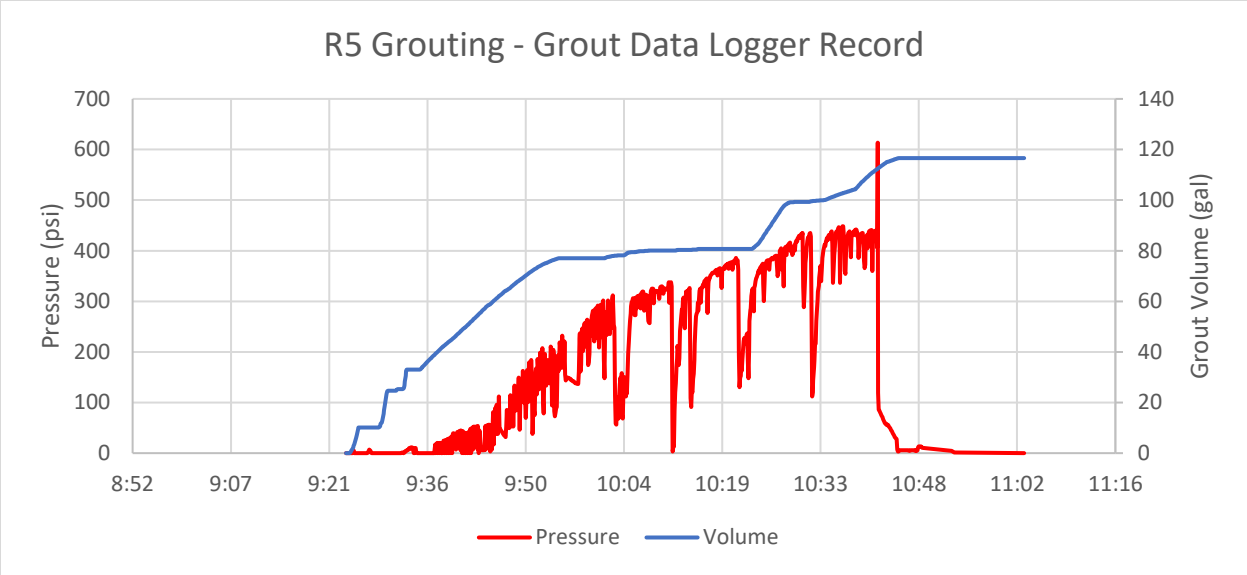

Figure 4-77: R5 grouting, grout data logger record

The fiber optic record for shaft R5 is divided into 4 strain verticals and 2 temperature verticals. The raw frequency and segment divisions are shown in Figure 4-78.

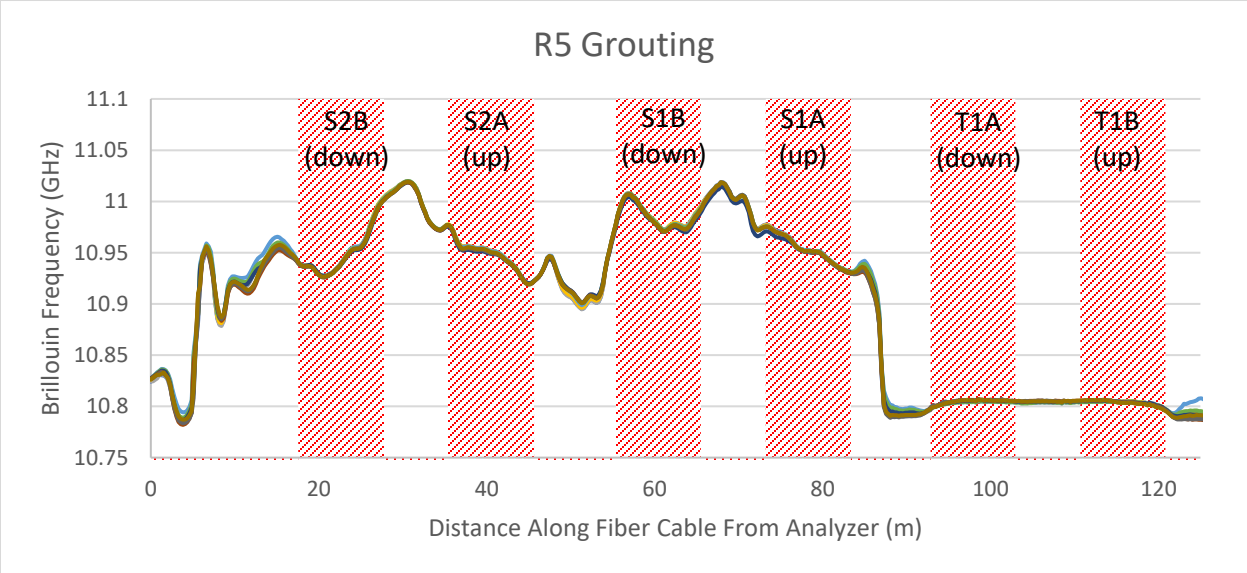

Figure 4-78: R5 grouting, raw Brillouin frequency

The measured vertical strains with time at a depth of 33.5 feet below the top of casing (TOC), approximately 1 pile diameter (5 feet) above the base, are presented in Figure 4-79. The figure shows a large increase in vertical compressive strain between 9:51 and 9:56, the second and third readings after the start of grouting at 9:45 with an associated pressure of 50 to 100 psi. After this initial rise, the strains drop to an average just above 60 με and stay roughly constant through the end of grouting at 10:42. At 10:53, just after the grout line was disconnected, all four verticals show a jump in strain of approximately 20 με. For the final read at 10:58, SB2 and

SB4 show a strain decrease while SB1 and SB3 show a small strain increase with a final average strain of 80 με.

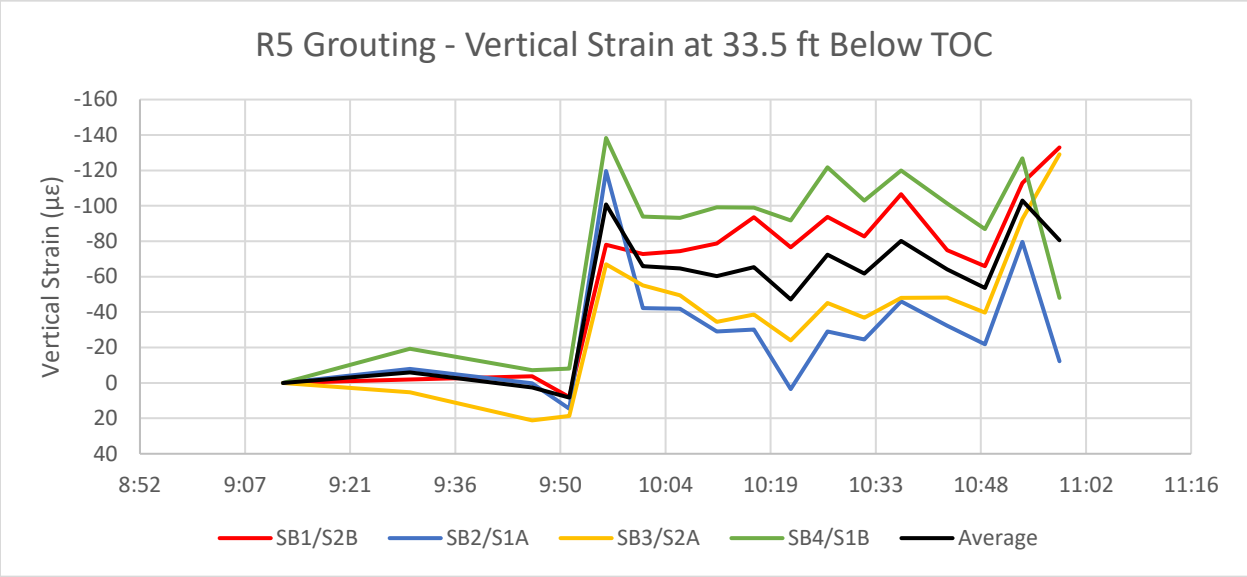

Figure 4-79: R5 grouting, vertical strains at 33.5 feet below TOC

Figure 4-80 through Figure 4-82 show the vertical strains with depth in the pile at 9:56 (~100 psi), 10:37 (~410 psi), and 10:58 (after pressure release). Figure 4-80 shows a large increase in strain very early in the grouting process, with a peak strain on SB4 of 154 με at an associated grouting pressure of 100 psi. A large compressive strain of 71 με was also observed on SB4 from the top of the pile to 10 feet below TOC. It is not clear from site observations what the cause of this shallow strain was. The remaining three verticals show a liner strain distribution from a peak value at or just below 100 με to 0 at a depth of approximately 15 feet below TOC. In the last reading before the conclusion of grouting shown in Figure 5-54, the vertical strains on SB4 at both the top and base had fallen. The average strain in the pile was roughly 93 με at a depth of 30 feet below TOC, decreasing linearly to a depth of just above 20 feet below TOC. In Figure 4-82 showing the final fiber optic reading after the pressure had been released, the strains in SB1 have increased to over 200 με at 30 feet below TOC, with strains decreasing in SB3, SB4, and SB2. The potential cause of the large spike in strain on SB1 is not apparent from the grouting records.

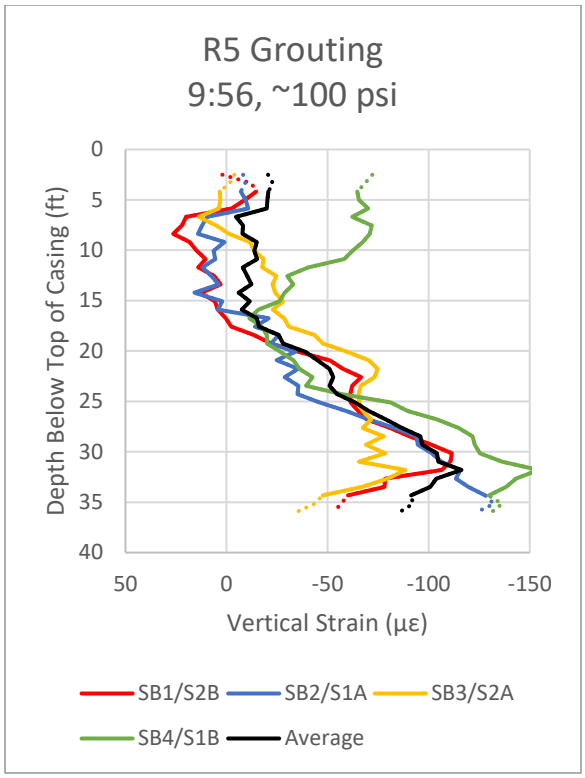

Figure 4-80: Vertical strain profile at 9:56 (~100 psi)

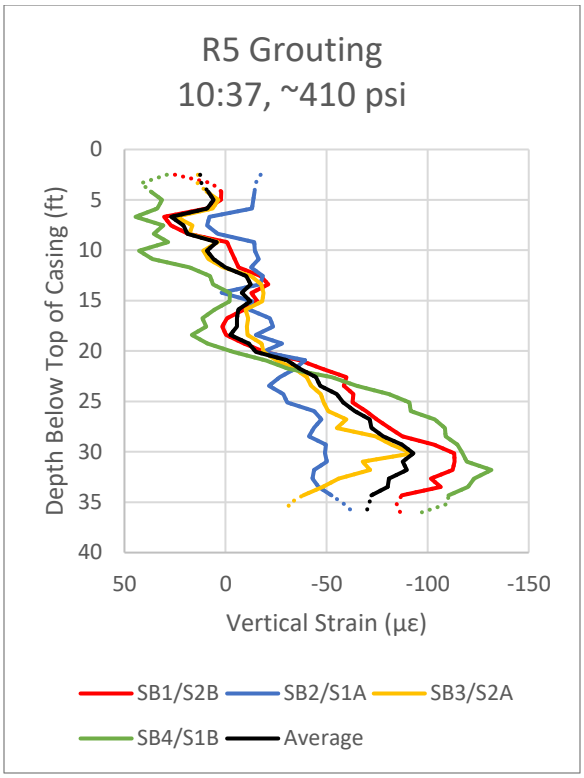

Figure 4-81: Vertical strain profile at 10:37 (~410 psi)

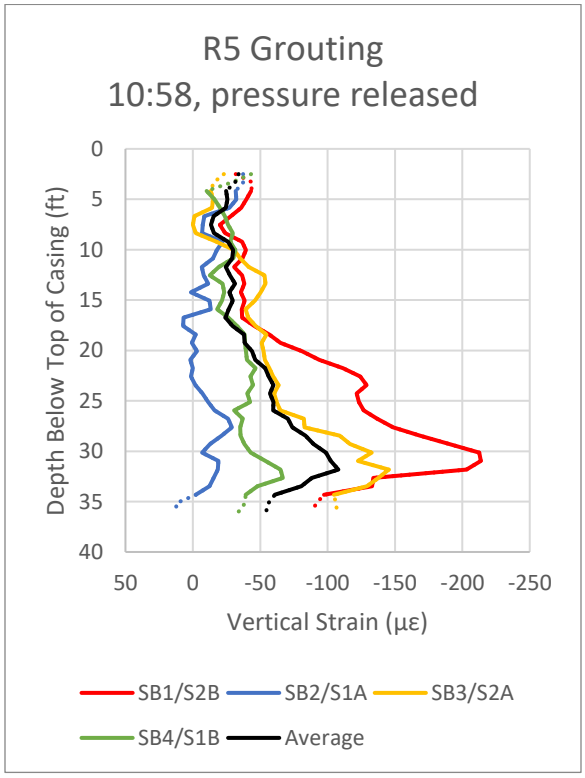

Figure 4-82: Vertical strain profile at 10:58 (after pressure release)

j) Reaction Shaft R7

Reaction Shaft R7 was grouted on February 5, 2019. The grout data logger record of pressure and volume at the grout plant is presented in Figure 4-83. All grouting was performed through a single line (of 4). Once grout return was established at the surface, all return valves were closed at 12:18 and grouting of the pile began. Grouting continued until 13:33 with an associated pressure of 520 psi, at which point the grout line was locked off and grouting was concluded. The measured volumes are not adjusted for the initial flush or grout in the lines and therefore represent an upper bound of the volumes placed at the pile base.

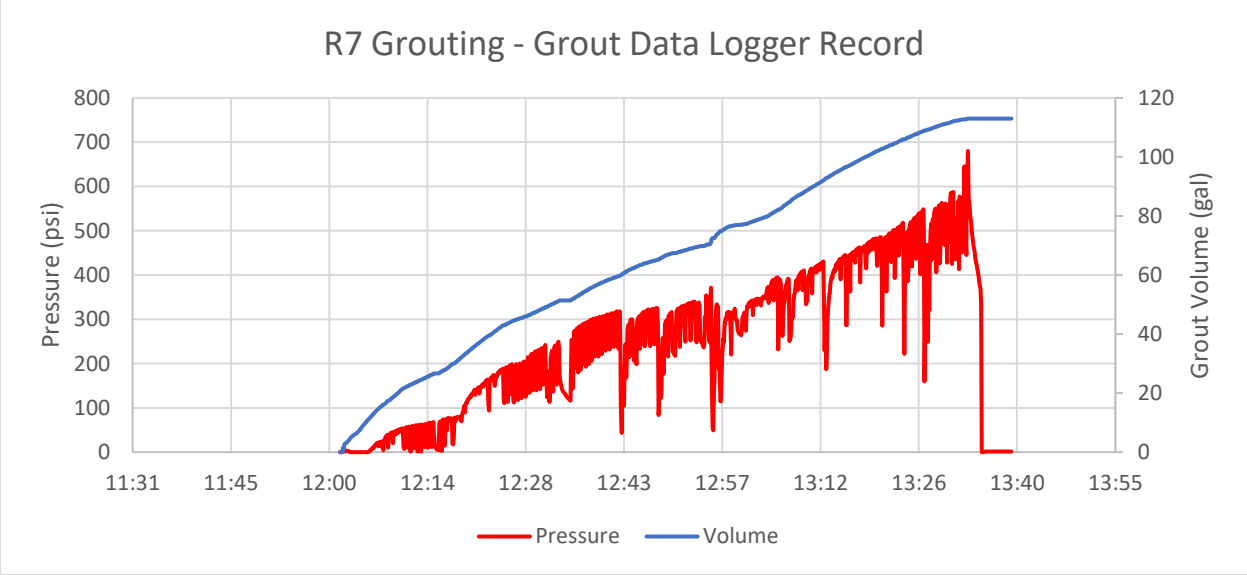

Figure 4-83: R7 grouting, grout data logger record

The fiber optic record for shaft R7 is divided into 4 strain verticals and 6 temperature verticals. The raw frequency and segment divisions are shown in Figure 4-84.

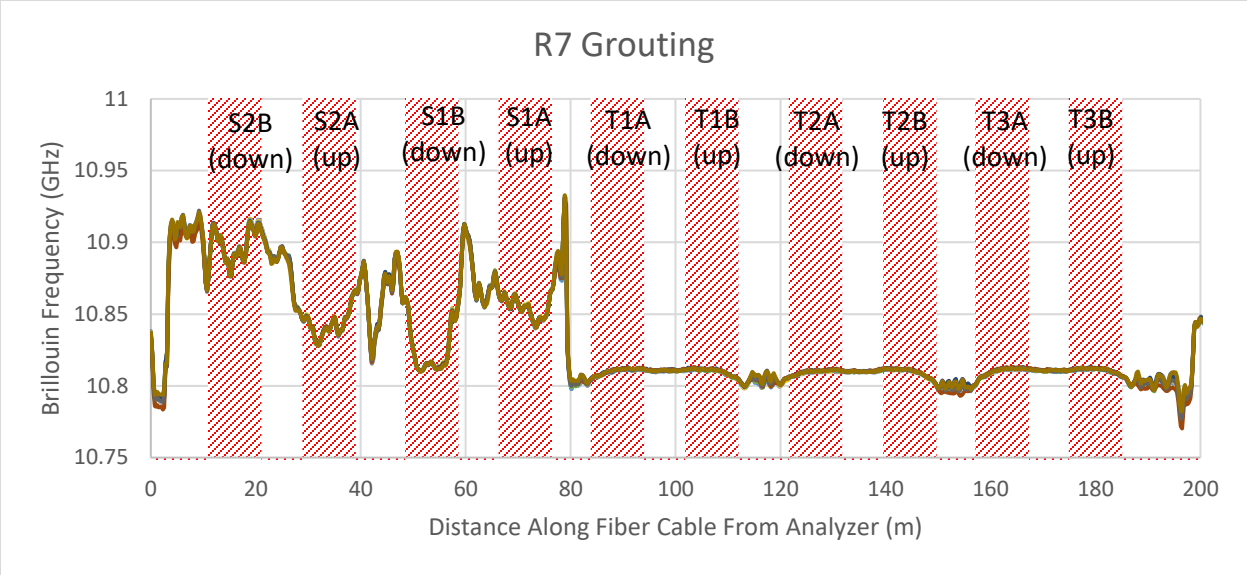

Figure 4-84: R7 grouting, raw Brillouin frequency

Preliminary analysis of the frequency data for R7 showed that the amplitude of the fiber optic signal was several times lower than that of a typical reading. While this loss was not apparent during the field readings, it resulted in the processed data being much noisier than a normal reading set. An example of this noise is shown in Figure 4-85 which displays the vertical strains with depth at 12:03, taken 13 minutes after the last baseline reading during the initial water flush of the grout circuits.

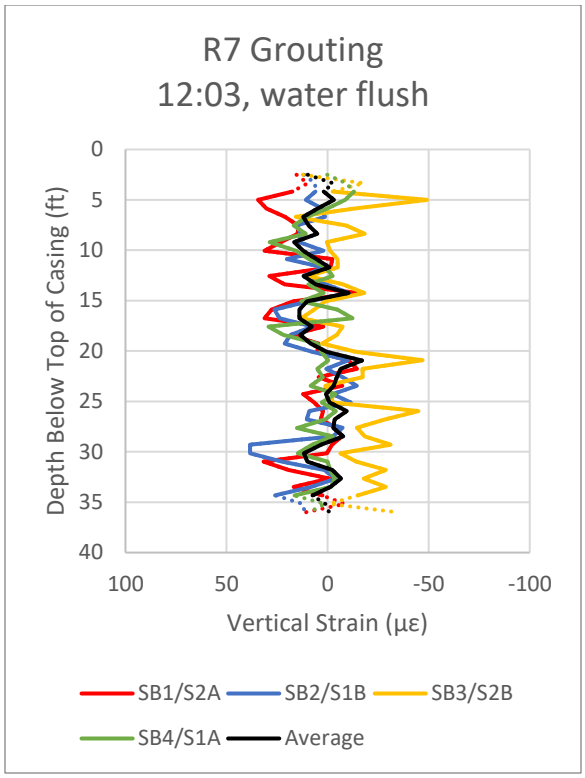

Figure 4-85: R7 grouting, strain variation during water flush due to unknown power loss in reading set

While the specific source of this power loss is unknown, it is likely that a poor connection was made either at the analyzer or the patch to the pile sensing cable. The following analysis and figures are presented with the caveat that the data contains noise of an unknown magnitude but estimated at approximately +/- 25 με. Even with this noise, the underlying trends of strain development and dissipation during and after grouting still appear to be reasonable and consistent with the observations on other piles.

The measured vertical strains with time at a depth of 33.5 feet below the top of casing (TOC), approximately 1 pile diameter (5 feet) above the base, are presented in Figure 4-86. This figure shows a general increase in strain in all four verticals throughout grouting, with the largest strains registered on SB3 with a peak value approaching 100 με. The largest single strain increase was observed from 12:25 to 12:31 with an associated grout pressure of 60 psi rising to 140 psi. Focusing on the average strain for the pile, the strain gradually increased during grouting, stayed level after the grout line was locked off at 13:33, and dropped by approximately 30 με after the pressure in the lines was released. This drop is observed on all four verticals.

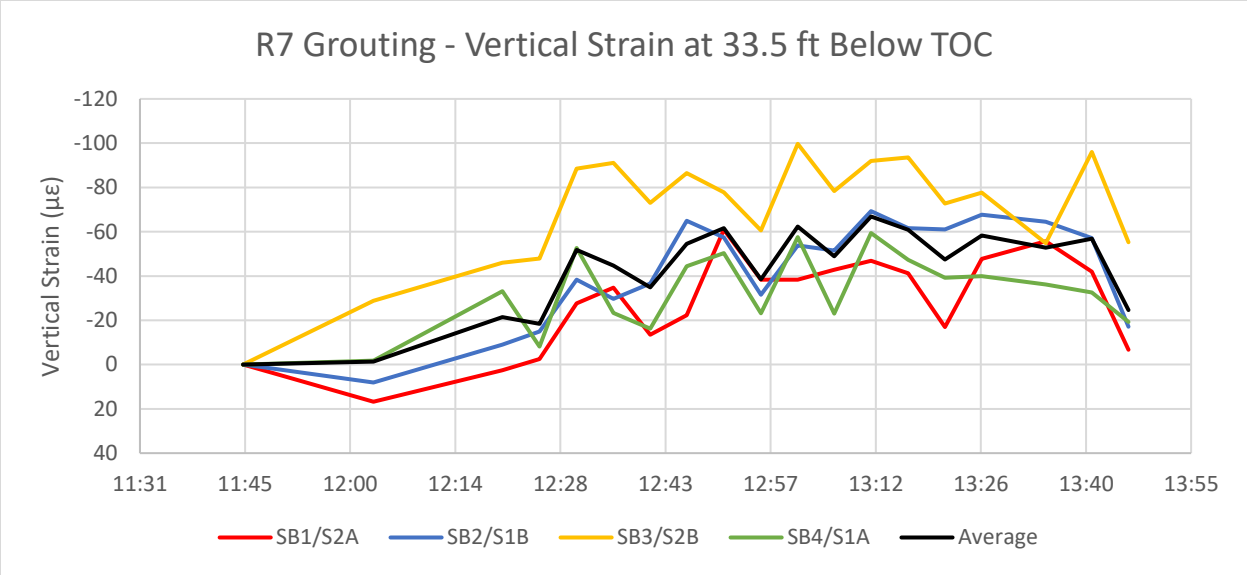

Figure 4-86: R7 grouting, vertical strains at 33.5 feet below TOC

Figure 4-87 through Figure 4-89 show the vertical strains with depth in the pile at 12:31 (~140 psi), 13:26 (~505 psi), and 13:46 (after pressure release). The high noise in the data makes direct interpretation of the strain values with depth difficult and subject to error. However, looking at the average of the four individual verticals, a trend of increasing strains over grouting can be observed. In Figure 4-87, the average strain has a peak value of just above 60 με, decreasing linearly with depth to 15 feet below TOC before staying constant at approximately 25 με. In the final reading at 13:26 just prior to the end of grouting shown in Figure 5-61, the average strain profile is similar to that observed at 12:31; implying that little additional strain has been added into the pile. In the final reading after the pressure in the pile has been released shown in Figure 4-89, the average strain just above the base of the pile has decreased to 32 με, decreasing linearly with depth before reaching 0 at approximately 20 feet below TOC. This implies that while some negative skin friction was developed during grouting, much of the associated compressive strains were released except at the deepest portion of the pile.

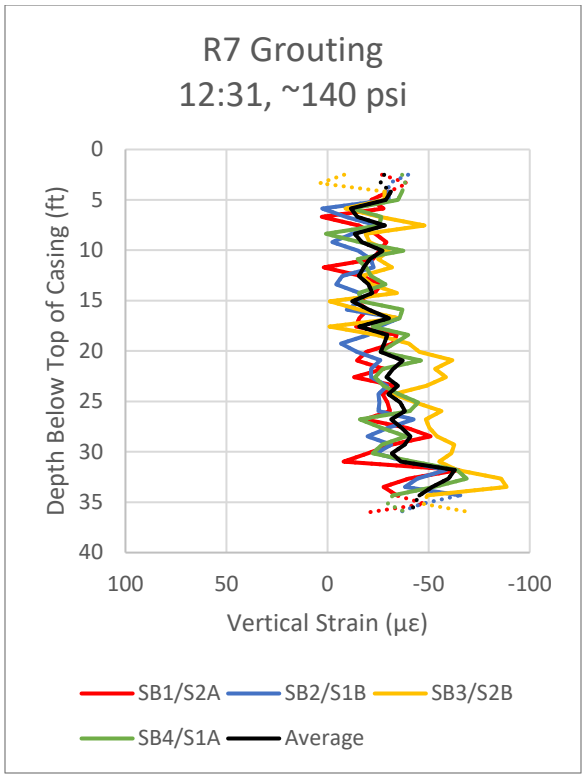

Figure 4-87: Vertical strain profile at 12:31 (~140 psi)

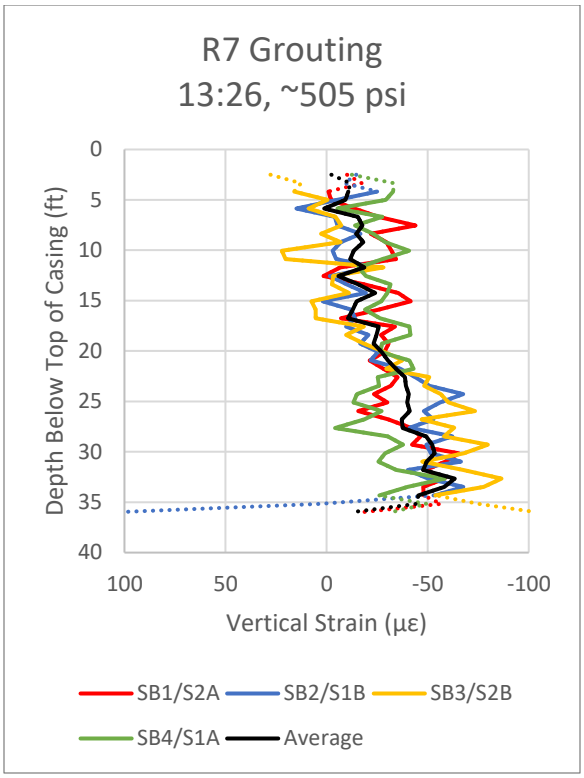

Figure 4-88: Vertical strain profile at 13:26 (~505 psi)

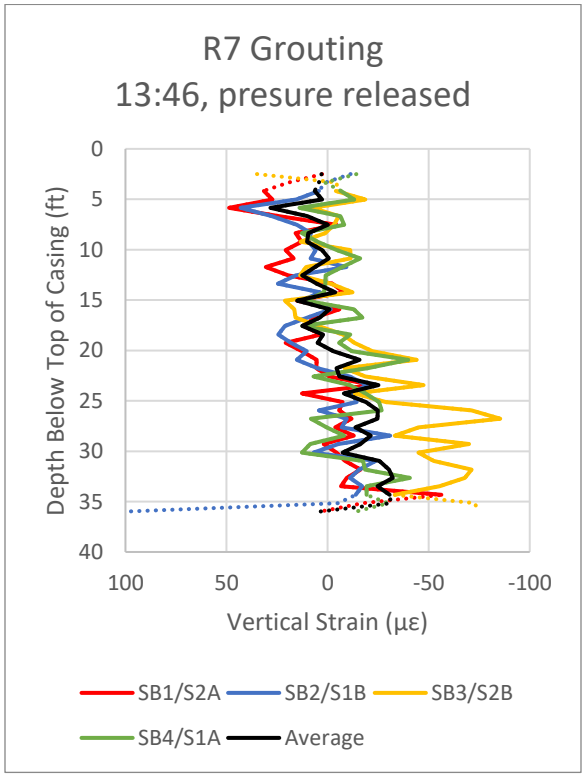

Figure 4-89: Vertical strain profile at 13:46 (after pressure release)

k) Reaction Shaft R9

Reaction Shaft R9 was grouted on February 4, 2019. The grout data logger record of pressure and volume at the grout plant is presented in Figure 4-90. All grouting was performed through a single line (of 4). Once grout return was established at the surface, all return valves were closed at 15:34 and grouting of the pile began. Grouting continued until 16:24 with an associated pressure of 500 psi, at which point the grout line was locked off and grouting was concluded. The measured volumes are not adjusted for the initial flush or grout in the lines and therefore represent an upper bound of the volumes placed at the pile base.

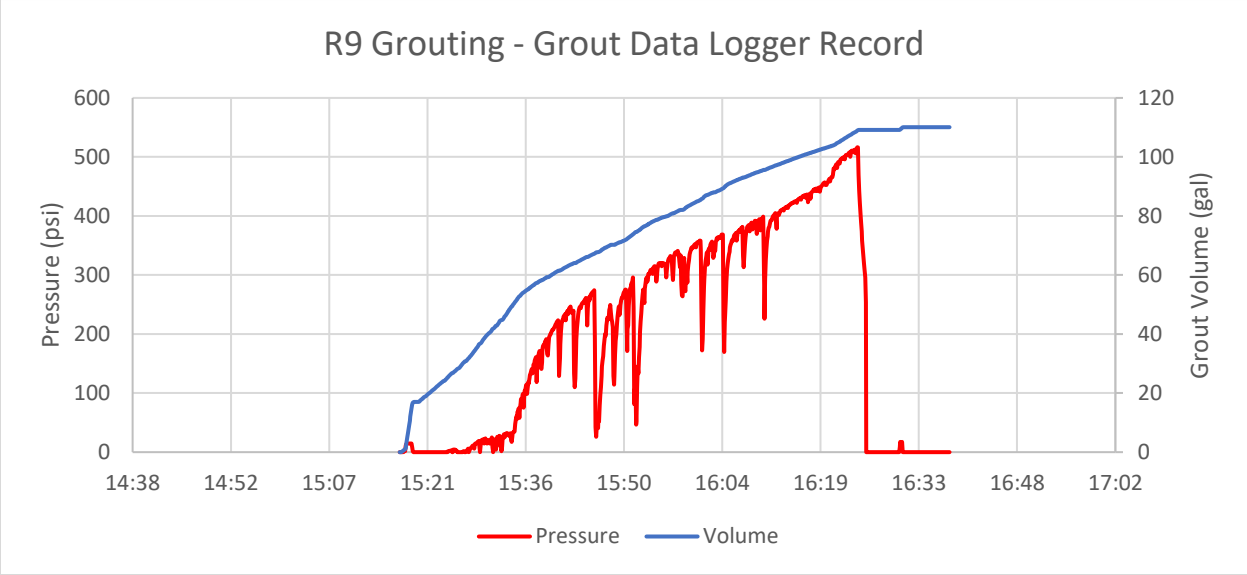

Figure 4-90: R9 grouting, grout data logger record

The fiber optic record for shaft R9 is divided into 4 strain verticals and 6 temperature verticals. The raw frequency and segment divisions are shown in Figure 4-91.

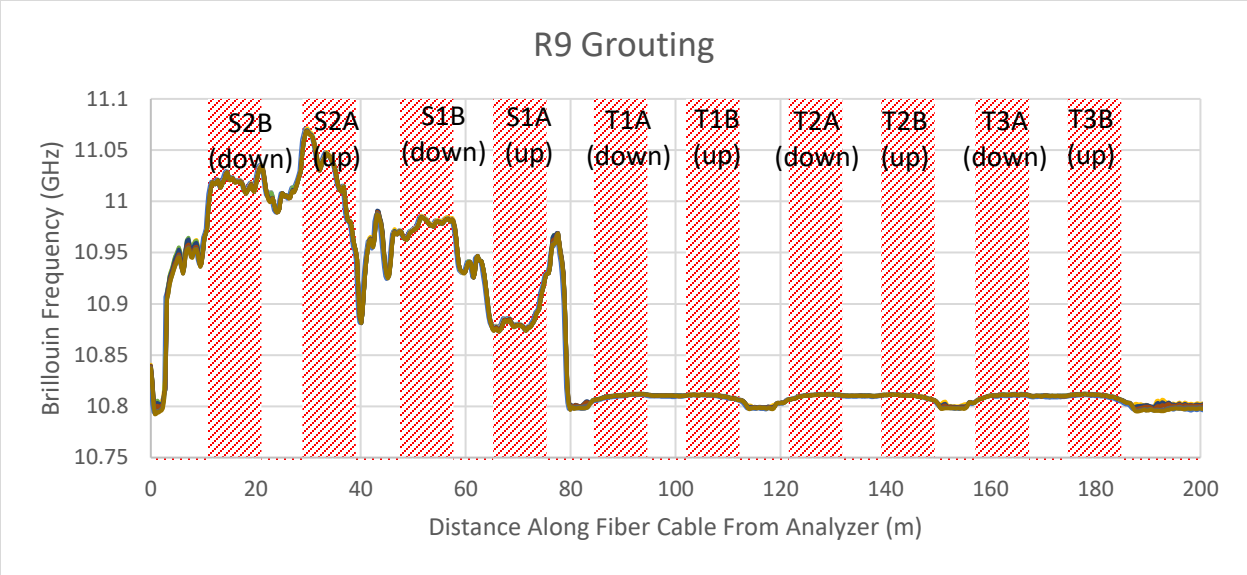

Figure 4-91: R9 grouting, raw Brillouin frequency

The measured vertical strains with time at a depth of 33.5 feet below the top of casing (TOC), approximately 1 pile diameter (5 feet) above the base, are presented in Figure 4-86. This figure shows an initial increase in strain at 15:36, corresponding with the first reading after the start of grouting. SB1, SB3 and SB4 show similar strains over the duration of grouting, with a peak value on SB4 of 66 με at 16:15 with a corresponding pressure of 420 psi. Although the pressure increased for one more reading cycle to 450 psi, the strain on all verticals dropped on the next reading, then dropped further after the end of grouting. A slight rebound was observed in the final reading at 16:53 with an average final strain of 29 με.

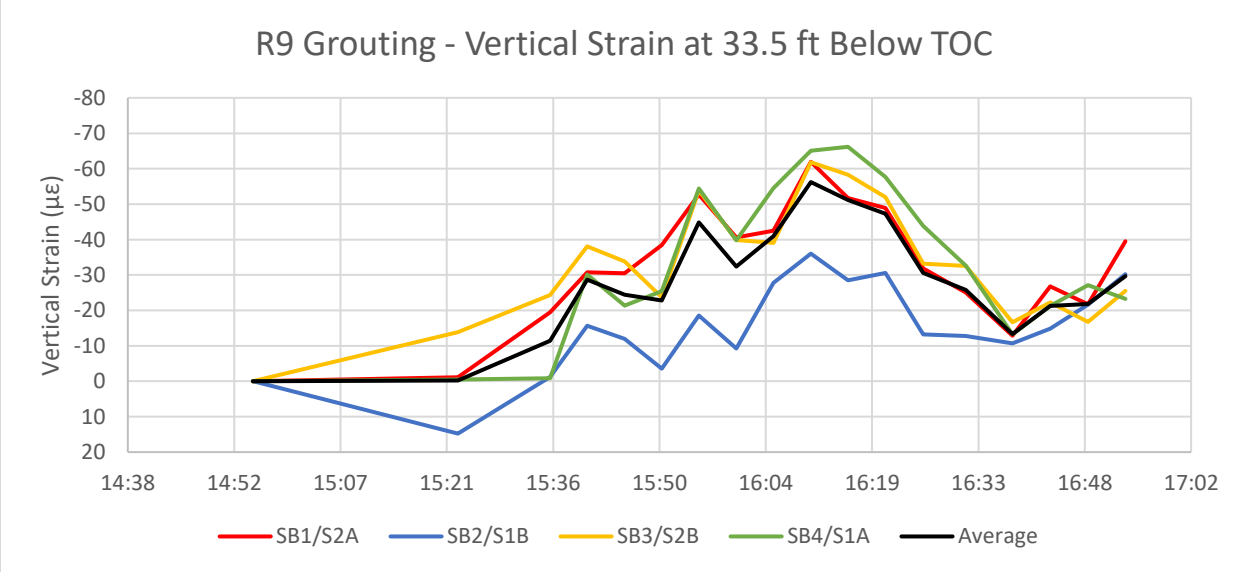

Figure 4-92: R9 grouting, vertical strains at 33.5 feet below TOC

Figure 4-93 through Figure 4-95 show the vertical strains with depth in the pile at 15:55 (~315 psi), 16:15 (~420 psi), and 16:53 (after pressure release). Figure 4-93 shows a linear increase in strain with depth, with an average compressive strain of 46 με at the base of the pile. In Figure 5-67, the average strain continues to increase to 52 με at the peak grouting pressure of 420 psi. After the grouting pressure is released, in Figure 4-95, the average peak compressive strain has fallen to approximately 30 με. The shape of the strain curve has also changed, remaining constant from the base of the pile to 15 feet below TOC, after which it decreases linearly to the top of the pile. The shape of the strain profiles observed in these three figures show a development of negative skin friction during grouting. However, a portion of the peak value in the lower portion of the pile is released once grouted is completed.

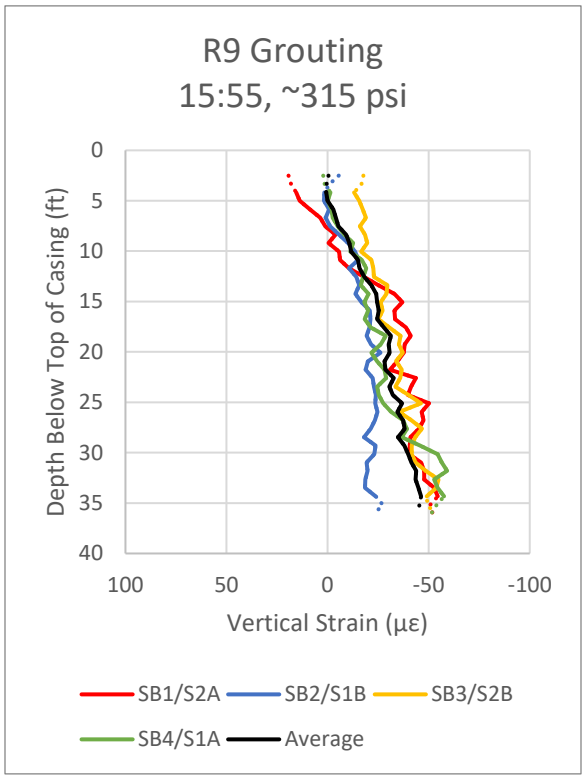

Figure 4-93: Vertical strain profile at 15:55 (~315 psi)

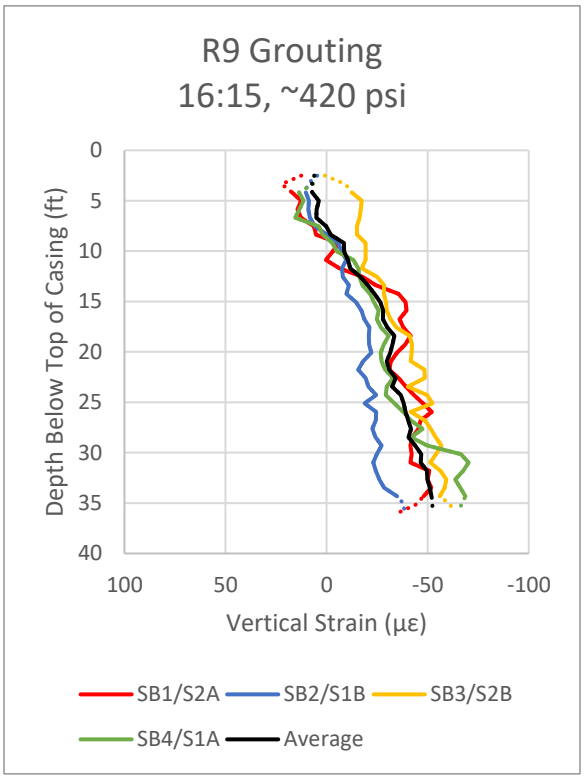

Figure 4-94: Vertical strain profile at 16:15 (~420 psi)

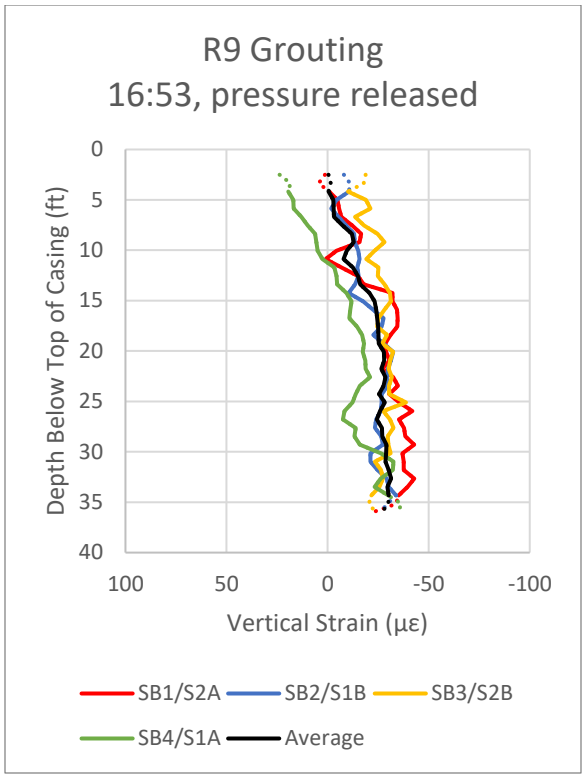

Figure 4-95: Vertical strain profile at 16:53 (after pressure release)

l) Test Shaft T4

Test Shaft T4 was grouted on February 5, 2019. The grout data logger record of pressure and volume at the grout plant is presented in Figure 4-96. All grouting was performed through a single line. Once grout return was established at the surface, all return valves were closed at 15:14 and grouting of the pile began. Grouting continued until 15:45 with an associated pressure of 600 psi, at which point the grout line was locked off and grouting was concluded. The measured volumes are not adjusted for the initial flush or grout in the lines and therefore represent an upper bound of the volumes placed at the pile base.

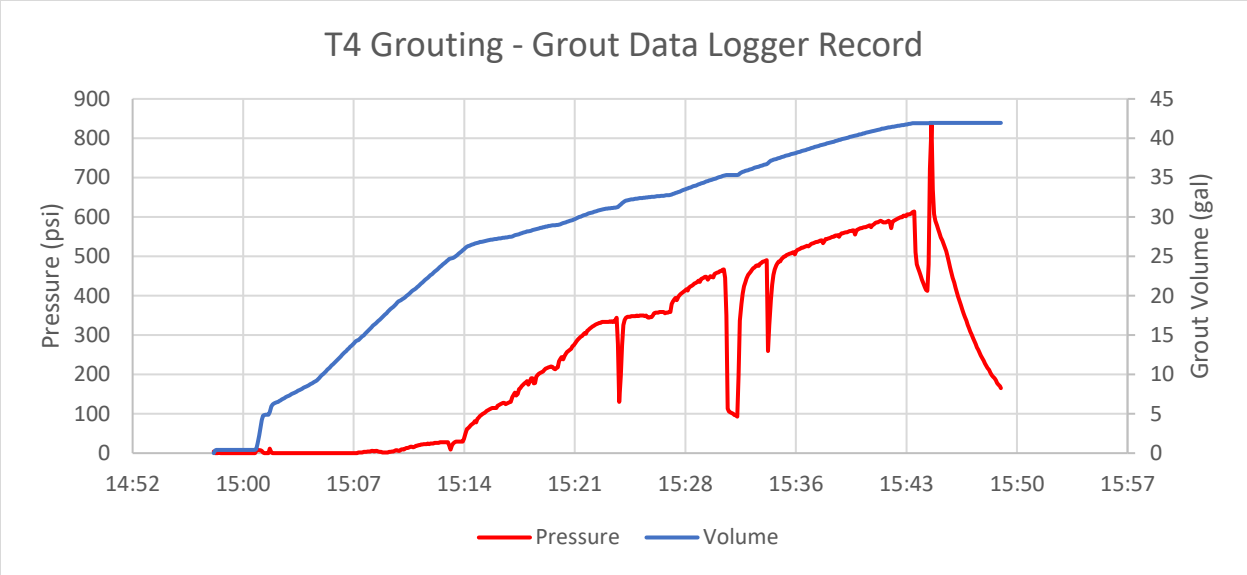

Figure 4-96: T2 grouting, grout data logger record

The fiber optic record for shaft T4 is divided into 4 strain verticals and 2 temperature verticals. The raw frequency and segment divisions are shown in Figure 4-97.

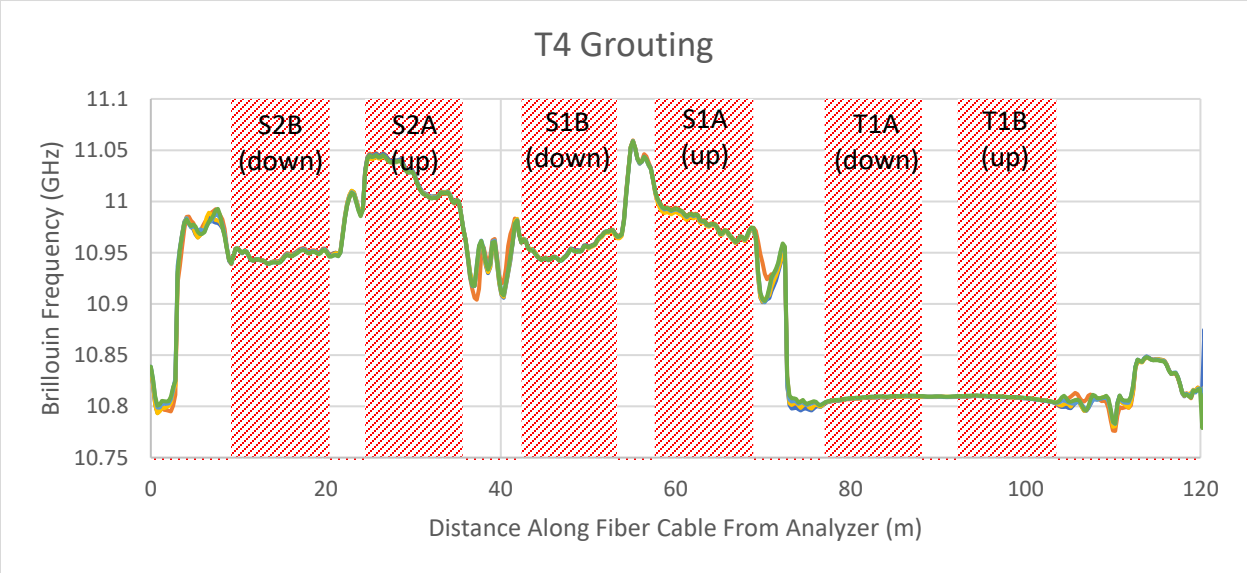

Figure 4-97: T2 grouting, raw Brillouin frequency

The measured vertical strains with time at a depth of 35.1 feet below the top of casing (TOC) are presented in Figure 4-98Figure 4-98: T2 grouting, vertical strains at 35.1 feet below TOC. This figure shows an initial increase in compressive strain on all four verticals at 15:29, followed by a large jump in strain at 13:34-13:38. The peak strain was measured at 13:38 on HB1 with 107 με in compression. At the peak, there was a wide variation in measured values across the piles with a maximum differential of over 80 με. There is a drop in strain on all verticals following the lock off of the grout lines and release of pressure at 15:46. The compressive

strains continue to gradually fall until a final rise is observed prior to the final reading at 16:12 with an average compressive strain of 36 με.

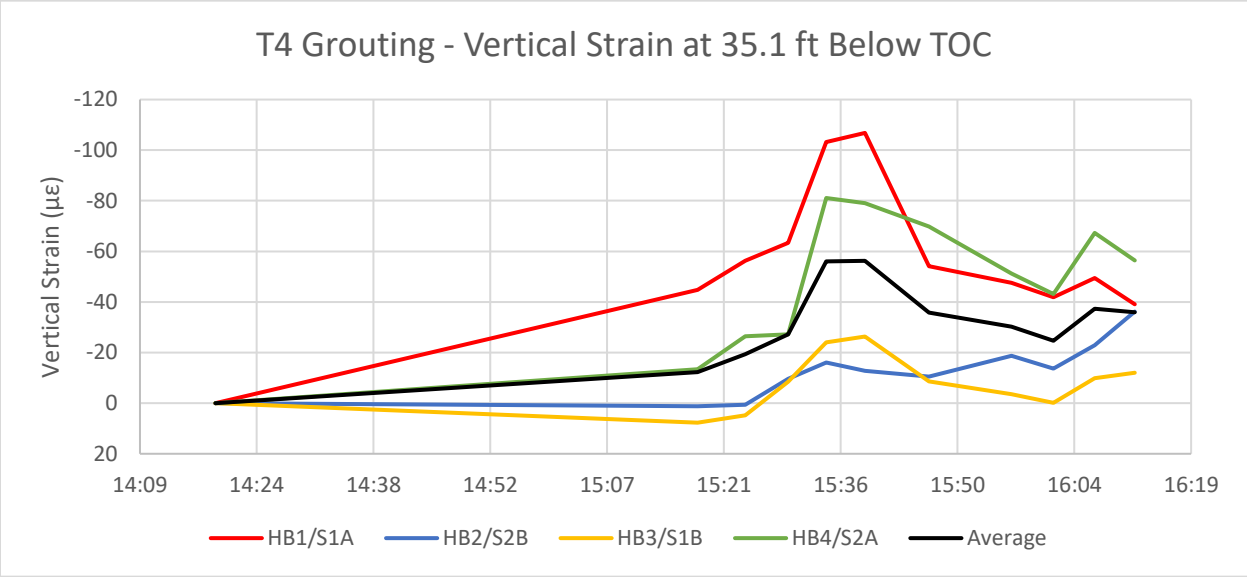

Figure 4-98: T2 grouting, vertical strains at 35.1 feet below TOC

Figure 4-99 through Figure 4-101 show the vertical strains with depth in the pile at 15:29 (~414 psi), 15:38 (~540 psi), and 16:12 (after pressure release). Figure 4-99 shows a high concentration of compressive strain on HB1, with a peak strain of 63 με decreasing linearly with depth to the top of the pile will a small deviation at 23 feet below TOC. The other three verticals register slight tension in the upper 20-25 feet of the pile and show a maximum compressive strain of less than 25 με at the base. In Figure 5-73, at the peak strain at 15:38, the strains in HB1 at the base have increased to 107 με with a rough linear decrease down to zero at the top of the pile. The strains in the other three verticals in the lower 15 feet of the pile are more evenly distributed than earlier in the grouting process, with HB4 also showing higher strains than average and HB2 and HB3 showing lower strains than average. After the pressure is released in Figure 4-101, the average strain at the base of the pile decreases to 32 με with a linear trend to 0 at the top of the pile, implying that an increment of negative skin friction remains in the pile. The deviation at 20-25 feet in HB1 has increased, however the other verticals are more closely centered around the average. It is unclear what the cause of this deviation is, but it suggests an inhomogeneity in the shaft friction at this location.

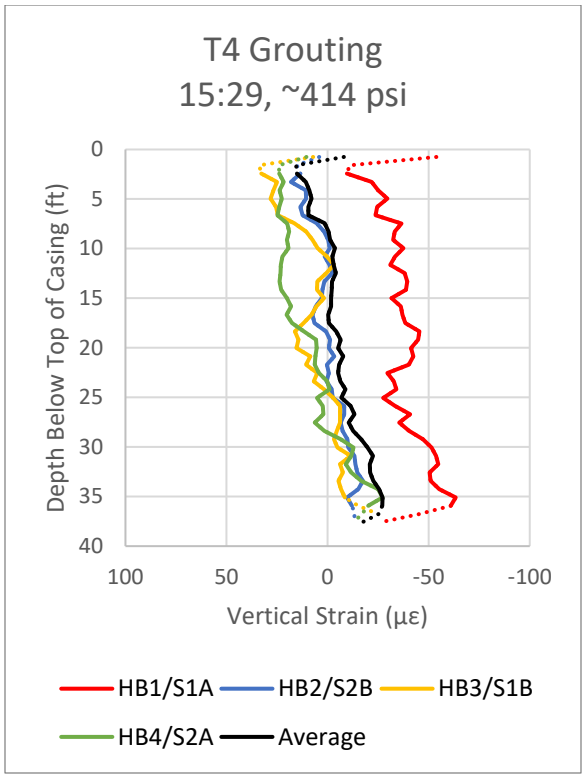

Figure 4-99: Vertical strain profile at 15:29 (~414 psi)

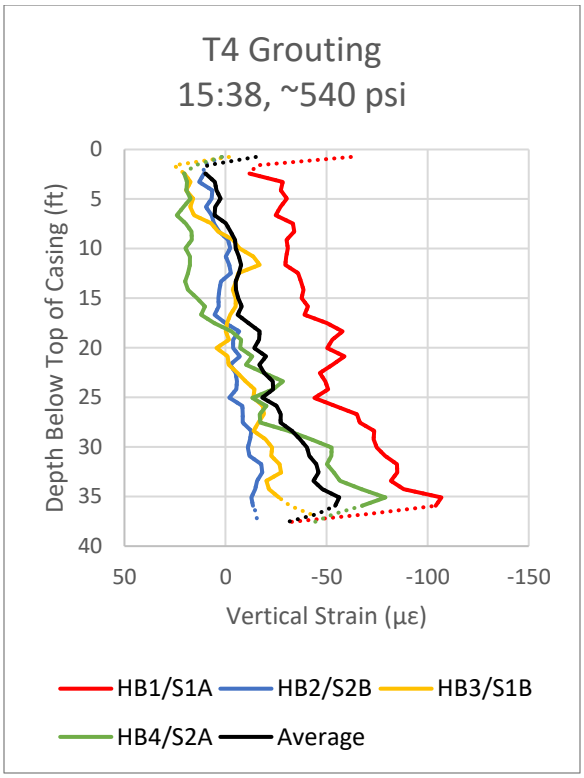

Figure 4-100: Vertical strain profile at 15:38 (~540 psi)

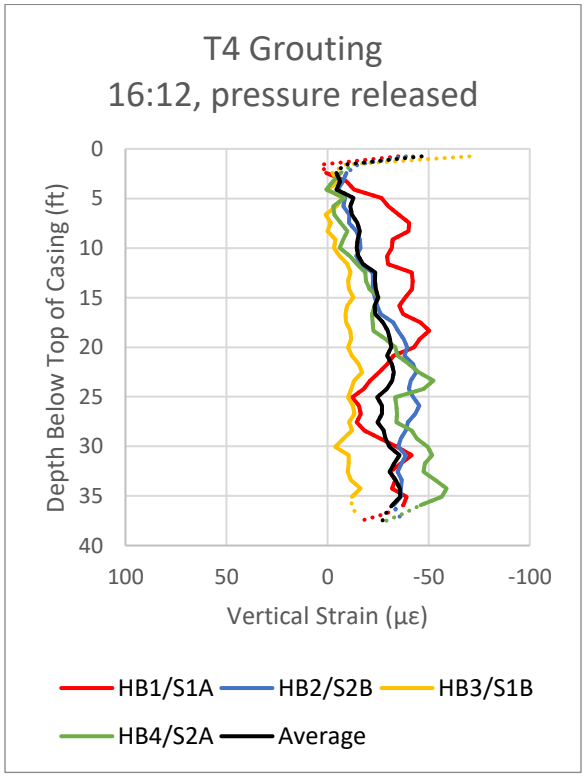

Figure 4-101: Vertical strain profile at 16:12 (after pressure release)

Summary

After reviewing the strain and temperature measurements taken during base grouting, some additional observations can be made.

- The pressure and volumes recorded at the grout plant were not directly correlated to the strains (and therefore loads) that were being applied to the pile at the base. This was the most evident for the open-type grouting system, where dramatic increases in measured grout pressure would not yield associated increases in strain within the pile.
- The strains in the pile would often reach a peak relatively early in the grouting process, with an associated low pressure. Continued grouting at increasing pressures would often not result in a proportional increase in strain.
- System blockages were the limiting factor during post grouting for the open-type systems, while shaft capacity was the more common limiting factor for the closed-type systems.
- The strains measured across the pile were often non-uniform, suggesting that the load from the grout injection was not distributed evenly across the pile base.
- Of the tested systems, the closed-type grouting system yielded the most uniform distribution of pile strains, both across the pile area as well as reaching upwards into the pile with depth.
- For strain measurements, temperature variations during grouting were significant and needed to be accounted for in processing of the data.
- Strains in the pile decreased after the pressure was released; although several of the piles displayed continuing fluctuations in the measured strain for some time after the grouting was completed.

4.4 Fiber Optic Strain Measurements During Load Testing

Overview

Following the conclusion of the base grouting, all four of the test piles (T1-T4) were load tested to determine their performance under axial loading. As with the base grouting, the test piles were monitored using a mix of conventional instrumentation and fiber optic sensors.

For the distributed fiber optic monitoring, the strain and temperature fiber optic loops in the test pile were connected in series with the fiber optic cables in the four reaction shafts as shown in Figure 4-102. For test piles T2-T4, all five piles (one test pile and four reaction shafts) were interrogated during each reading. Test pile T1 had the connection between the test shaft and first reaction shaft severed immediately prior to the load test and hence we were only able to interrogate the test shaft during the load test.

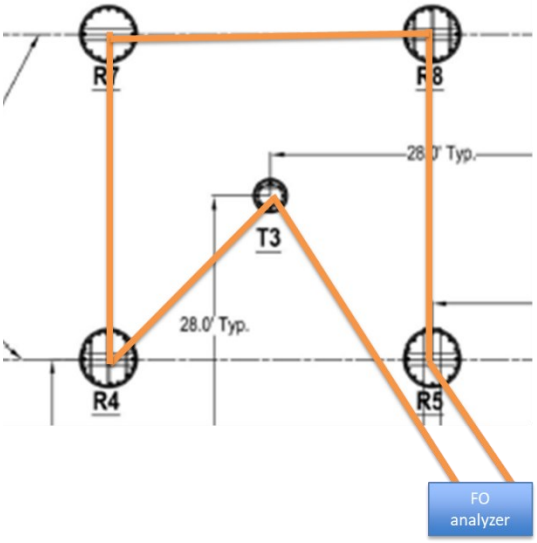

Figure 4-102: Diagram of the distributed fiber optic networking of piles during load test monitoring

Load test schedule

The load test schedule was performed in four cycles which can generally be described as follows. The first cycle was stepped up in 50 kip increments to 200 kips, then unloaded to 0 kips in 3 steps. The second cycle was stepped up back to 200 kips in 3 steps, then up to an intermediate load in 50 kip steps based on the observed displacements of the pile of approximately a half inch, followed by unloaded to 0 kips in 3 steps. The third cycle was stepped back up to the previous maximum load in 3 steps, then up to a maximum load in 50 kip steps. The maximum load was determined collaboratively by the group based on observed displacements, loads, and the stroke capacity of the hydraulic pistons. After the maximum load was reached, the pile was unloaded to 0 kips in 3 steps. The final cycle consisted of reloaded to or just below the previous maximum load in 4-5 steps, then unloading directly to 0 kips.

The loading system was manually controlled using a hydraulic pump feeding pressure to a set of four pistons. To transition from one load to the next, the operator would increase or decrease the pressure using a manual controller, carefully timing when to stop as to end with a final load close to the nominal target as measured by the load cells. Once the operator was satisfied with the pressure, the system was held for 5 minutes. During this time, the load was observed to gradually decay over the hold time. The load decay within each 5-minute hold increased in magnitude as the total applied load increased towards the maximum load value. No additional pressure was applied during the hold times.

Fiber optic measurements

Measurements

Prior to the start of each load test, a minimum of 3 fiber optic readings were taken to serve as a baseline to compare the subsequent strain measurements to. For test piles T1, T3, and T4, a single fiber optic reading was taken during each 5-minute hold. As with the presentation of the measurements taken during grouting, the following reported data for the strain measurements during the load tests represent the readings taken over the 5-minute hold and do not represent either the average strain or the strain at a single discrete point in time. For test pile T2, the ALICIA fiber optic analyzer was used, and its readings represent discrete (near) instantaneous strain measurements of a second or less.

Data analysis

As with the results during the thermal monitoring during curing and the strain and thermal monitoring during grouting, each reading output had to be translated from a series of raw frequency data into a variation in strain and temperature at specific locations in the monitored piles. The indexing values used in the grouting data were able to be reused for the load test data processing, with the caveat that several piles were networked together during monitoring which required the pile intervals to be shifted by a distance offset based on the cable length prior to the connection.

Temperature change effect

Prior to processing of the strain profiles, the temperature changes as measured by the thermal fiber optic lines was evaluated to determine if thermal compensation of the strain measurements was necessary. During the load test monitoring, the average spread in the thermal fiber optic cables away from the top of the pile was approximately +/- 0.3 MHz from the baseline, corresponding to a thermal fluctuation of +/- 0.27° C. Converting into strain using the coefficients for the strain cable, this corresponds to an average thermal strain of 9.7 με over the load test. This value is below the accuracy of the distributed fiber optic analyzers and cannot be differentiated from the noise floor; therefore, no thermal compensation of the strain values was performed on the measurements during the load tests. This is consistent with the understanding that the pile at depth (away from the ground surface) will be thermally stable during the relatively short duration of the test and is consistent with the approach taken with the conventional vibrating wire strain gauges which also did not have thermal correction applied.

The temperature variation in Test Pile T3 during the load test monitoring at the central 20 feet of the pile (10 – 30 feet below top of casing) is shown in Figure 4-103.

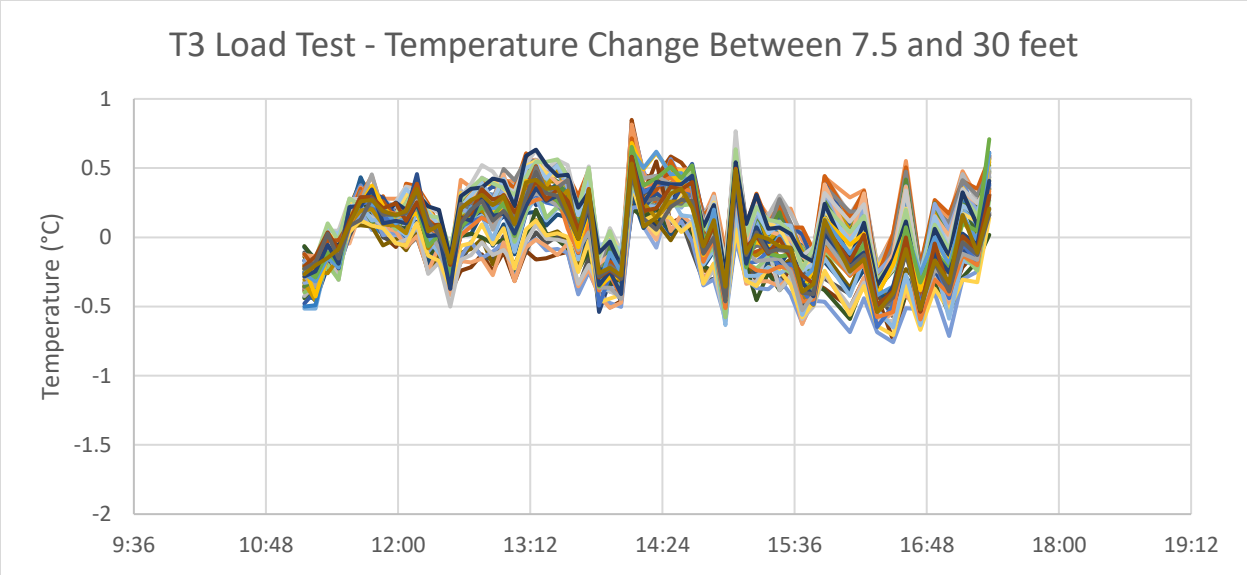

Figure 4-103: Recorded temperature variation in Test Pile T3 during load test

The average thermal fluctuation in the data is +/- 0.11° C, corresponding to an average thermal strain of 4.0 με. The maximum deviation was 0.81° C, with most readings during the load test falling within +/- 0.5° C of the baseline. While most of the readings are spread within a range approximately within the frequency (temperature) accuracy of the analyzer, the drop in temperature in all depths observed at 14:01 coincides with the unload cycle from ~1150 kips. This correlation suggests that the temperature cable may not be fully decoupled from the mechanical strains in the pile, with an approximate strain transfer of approximately 10 με, depending on how much of the observed temperature change is attributed to a transfer of strain. This trend is not observed elsewhere in the temperature data during the load cycle – it is possible that the rapid reversal of the loading direction resulted in the temporary transfer of strain through the thermal cable strain break.

Results

The presentation of the strain measurements during load testing are divided by the individual piles.

a) Test Pile T1, Control (no base grout)

Test pile T1, in which no base grouting was conducted, was load tested on February 23, 2019. Four load cycles were completed in just under 7 hours. The recorded load time history for the 4 load cells is shown in Figure 4-104. The maximum load peaks of the individual cycles were 200, 900, 1750, and 1600 kips.

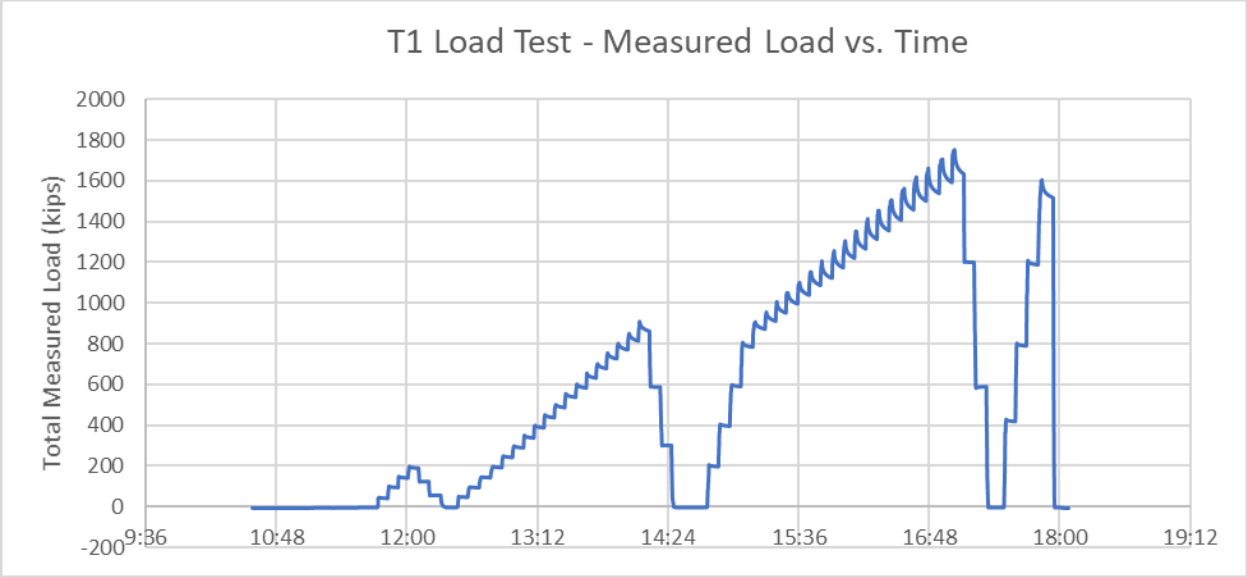

Figure 4-104: T1 load test, total load (sum of 4 individual load cells) over time

As noted earlier in the report, immediately prior to the load test, one of the test personnel tripped on the fiber optic cable connecting T1 to R1, breaking the splice and severing the connection to the four reaction shafts for the test. For this reason, the fiber optic measurements for T1 during the load test were taken using the BOTDR (single ended) mode on the Omnisens analyzer. A total of 65 distributed fiber optic readings were taken prior to, during, and after the load test. Each reading interrogated both the strain and temperature loops of the test pile. The raw frequency and segment divisions are shown in Figure 4-105.

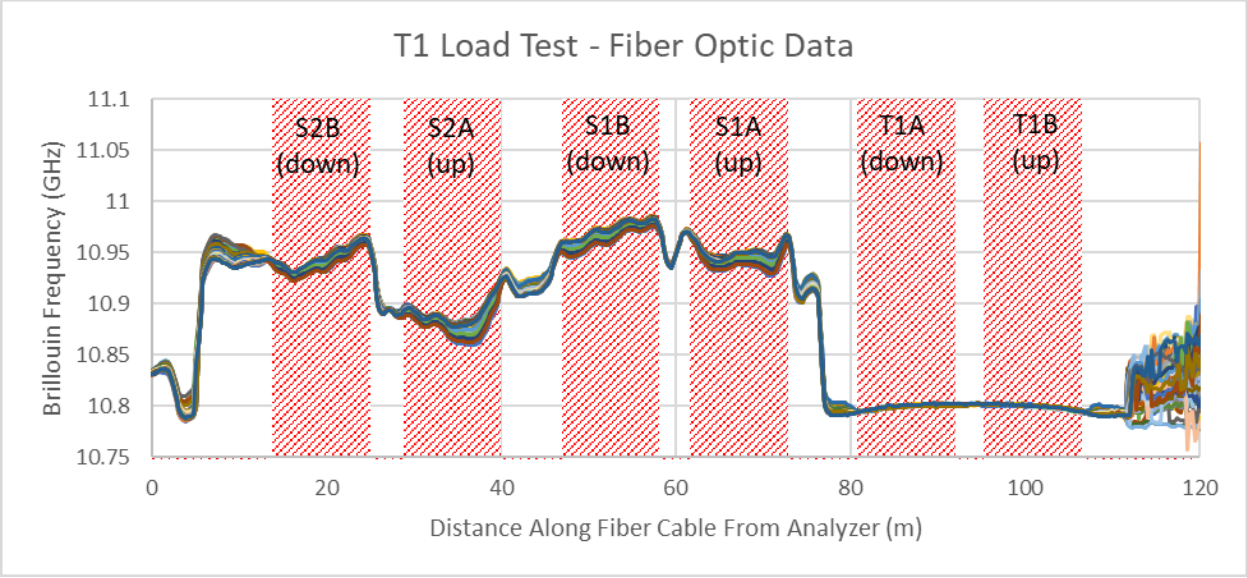

Figure 4-105: T1 load test, raw Brillouin frequency

Converting the change in frequency along the strain cable to vertical strain, the strain development within the pile at 7.5 feet below the top of casing is presented in Figure 4-106.

Each data set is divided into the individual vertical portions of the cable length, designated by both the bar that they are attached to (e.g., Hollow Bar 1) as well as the strand designation (e.g., Strain 2A). The average of all 4 strain verticals is also presented. A strong difference in the strain between the sides of the pile can be observed from the spread in the strain data. HB1 experienced the highest strain during the load test, while HB3 opposite it experienced the lowest. On the perpendicular axis, HB2 and HB4 were centered close to the average, indicating that the direction of the asymmetry was close to the HB1-HB3 line.

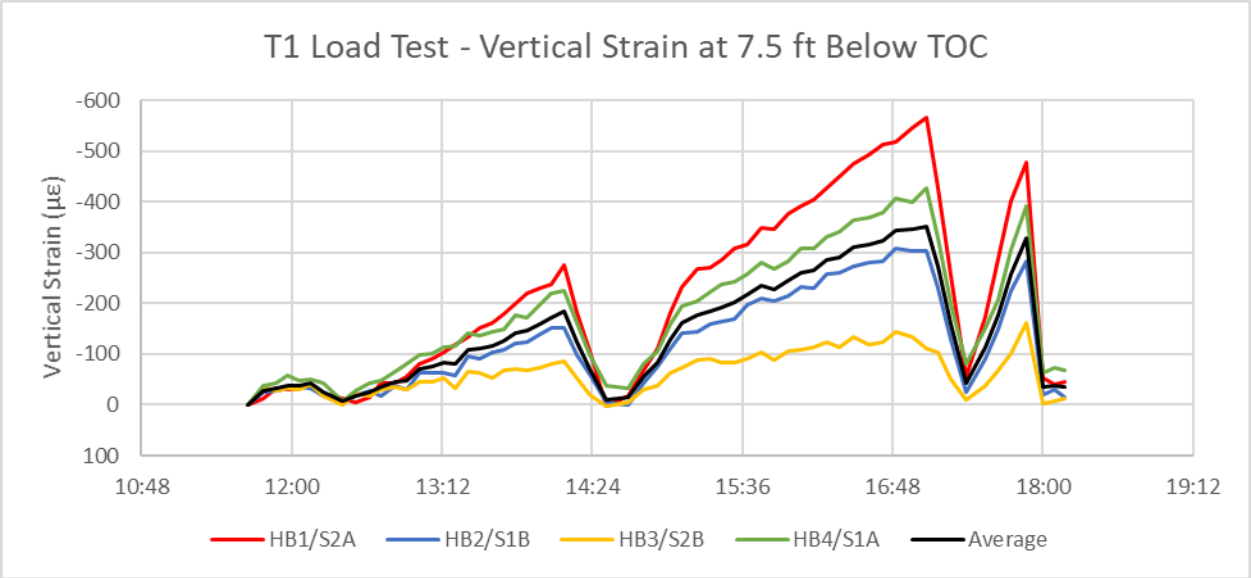

Figure 4-106: T1 vertical strain at 7.5 ft below top of casing over time

The development of strain within the pile over 6 loading increments (500 kips, 900 kips, 900 kips reload, 1500 kips, 1750 kips, and the final unload) are presented in Figure 4-107 through Figure 4-112. It is important to note that in all cases the presented load is approximate. This is due to the fact that the measured load from the load cells always had a slight deviation from the "target" load for each step, as well that the load was not constant during the approximate 5-minute hold period.

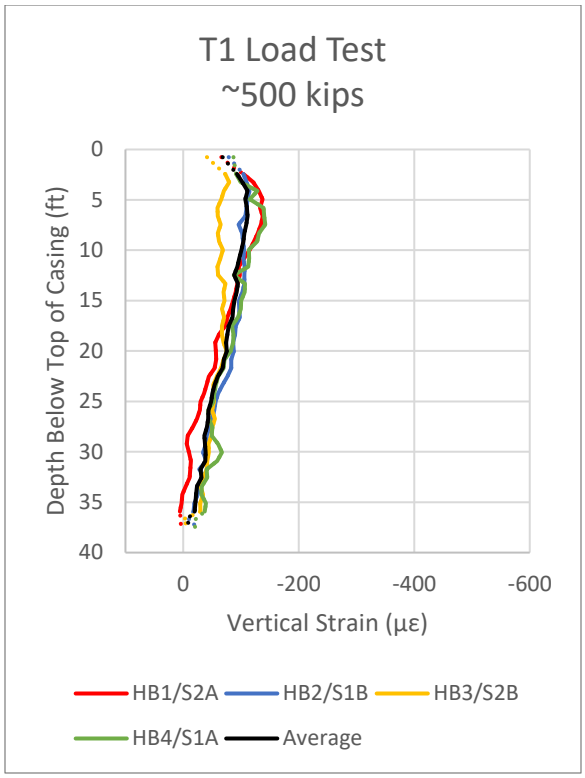

Figure 4-107: Vertical strain profile at ~500 kips load

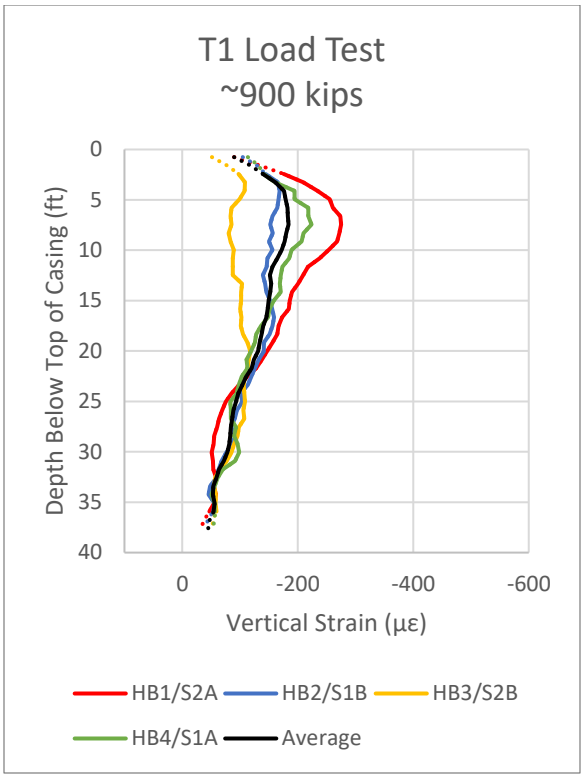

Figure 4-108: Vertical strain profile at ~900 kips load

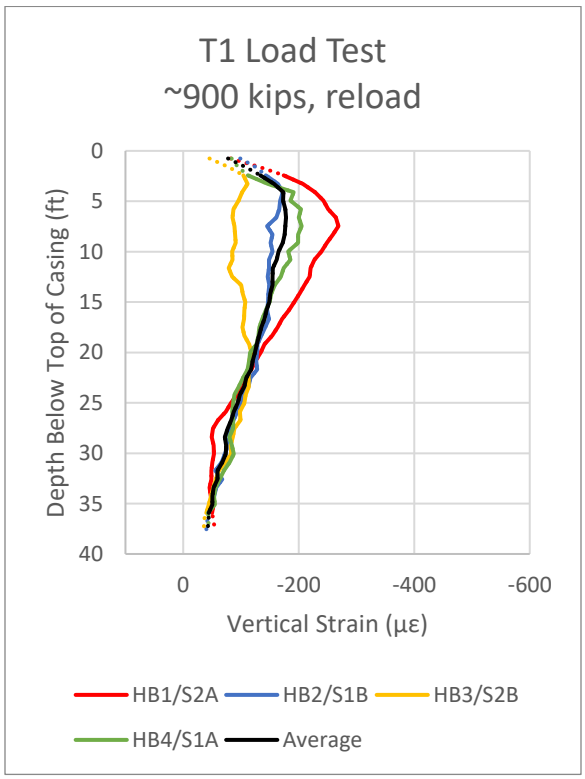

Figure 4-109: Vertical strain profile at ~900 kips reload

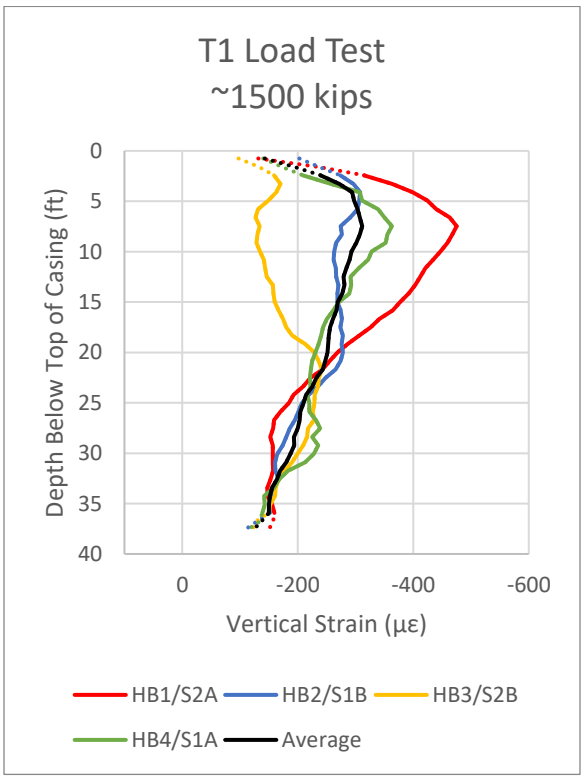

Figure 4-110: Vertical strain profile at ~1500 kips load

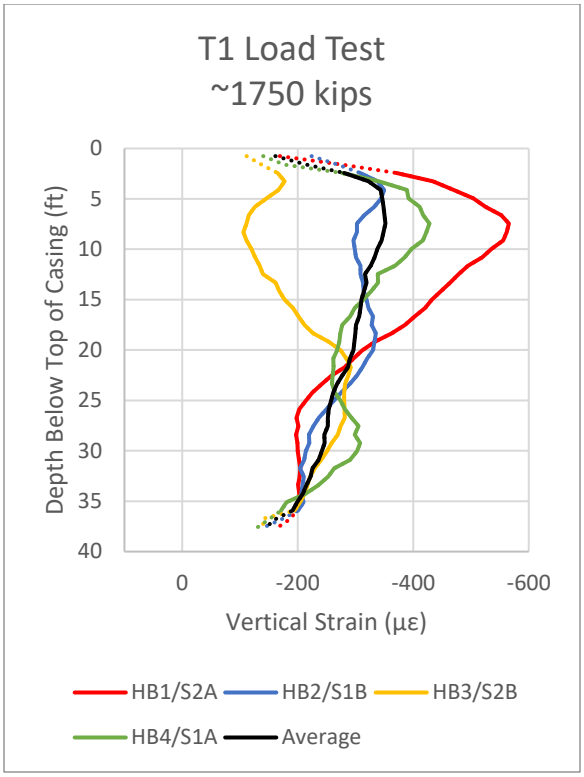

Figure 4-111: Vertical strain profile at ~1750 kips load

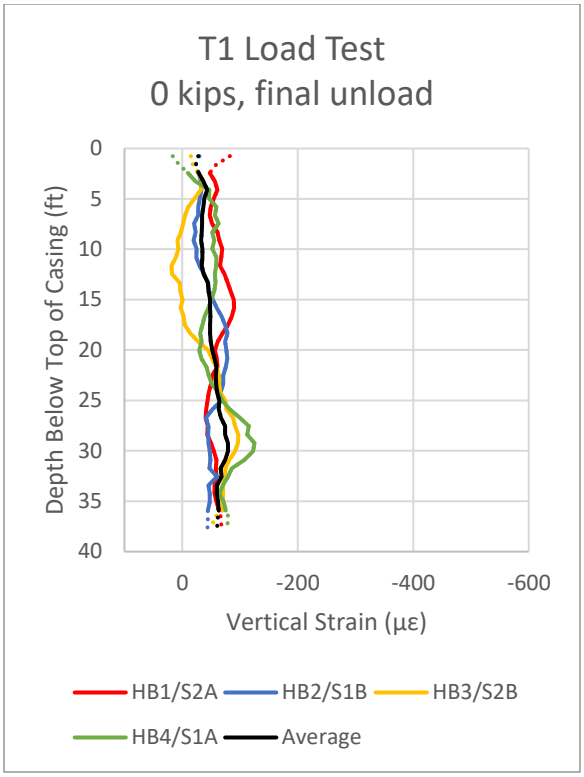

Figure 4-112: Vertical strain profile at 0 kips unload

Beginning in Figure 4-107 at the 500 kip interval, a developing separation in the strain between HB1 and HB3 can be observed in the top 20 feet of the pile. This separation continues to grow in magnitude through the maximum load interval of 1750 kips in Figure 4-111. The strains in HB1 show a positive curvature, developing to a maximum strain of 562 με at 8.3 feet below the top of casing. At the same time, the strains in HB3 show a negative curvature, with a minimum strain at depth of 106 με at 8.3 feet below the top of casing. These values compare to an average strain within the pile at the same depth of 348 με. The corresponding depths, with a peak at 8.3 feet and crossover at 20 feet below top of casing, and the approximate symmetry of the curvature around the average, imply that the pile is experiencing bending in the top 20 feet during the load test. This could be due to the applied load not being perfectly concentric with the center of the pile or being applied at an angle deviating from vertical during the load test. A third potential cause could be a deviation from vertical in the pile orientation itself, however this is less likely given the relative shallow depth of the pile. After removal of the load, the strains in Figure 4-112 show a small residual strain measured in the pile with an average value of approximately 50 με.

b) Test Pile T2, RIM Cell

Test Pile T2 was load tested on February 28, 2019. The pile was based grouted using a rim cell. Four load cycles were completed in just over 6 hours. The recorded load time history for the 4 load cells is shown in Figure 4-113. The maximum load peaks of the individual cycles were 200, 1000, 1950, and 1600 kips.

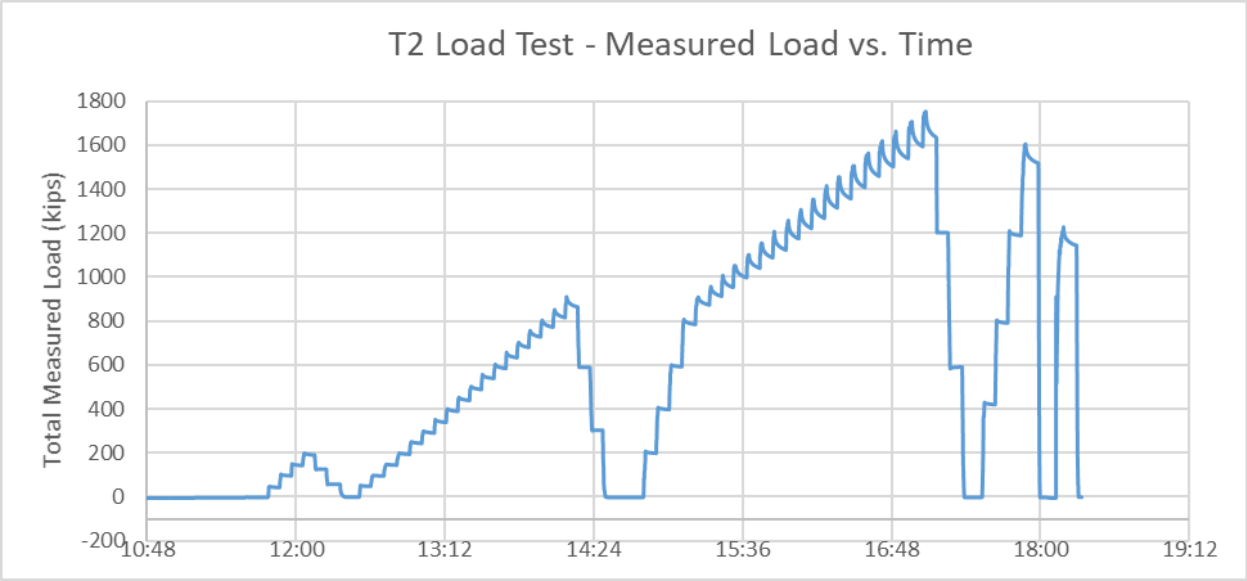

Figure 4-113: T2 load test, total load (sum of 4 individual load cells) over time

The fiber optic readings during the load test were taken with the Berkeley research analyzer, ALICIA. A total of 129 distributed fiber optic readings were taken prior to, during, and after the load test. Each reading interrogated both the strain and temperature loops of the test pile, as well as the four connected reaction piles (in order: T2, R6, R5, R2, R3). The raw frequency plot is presented in Figure 4-114. Focusing on the test pile, the fiber optic record was divided into the vertical strain and temperature loops as shown in Figure 4-115.

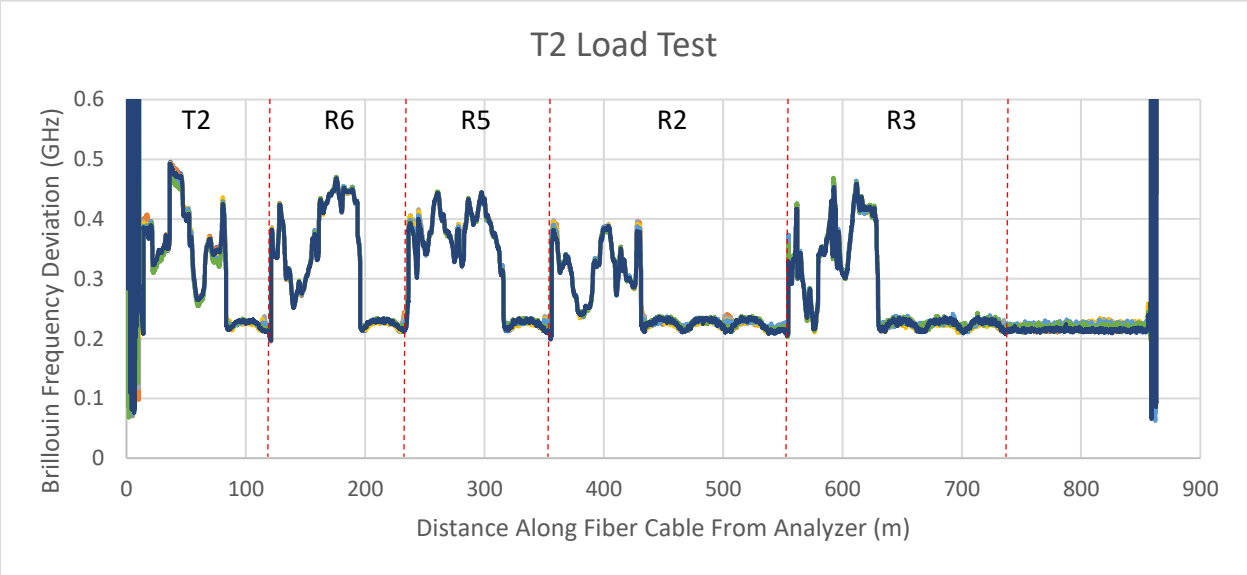

Figure 4-114: T2 load test, raw Brillouin frequency over all piles

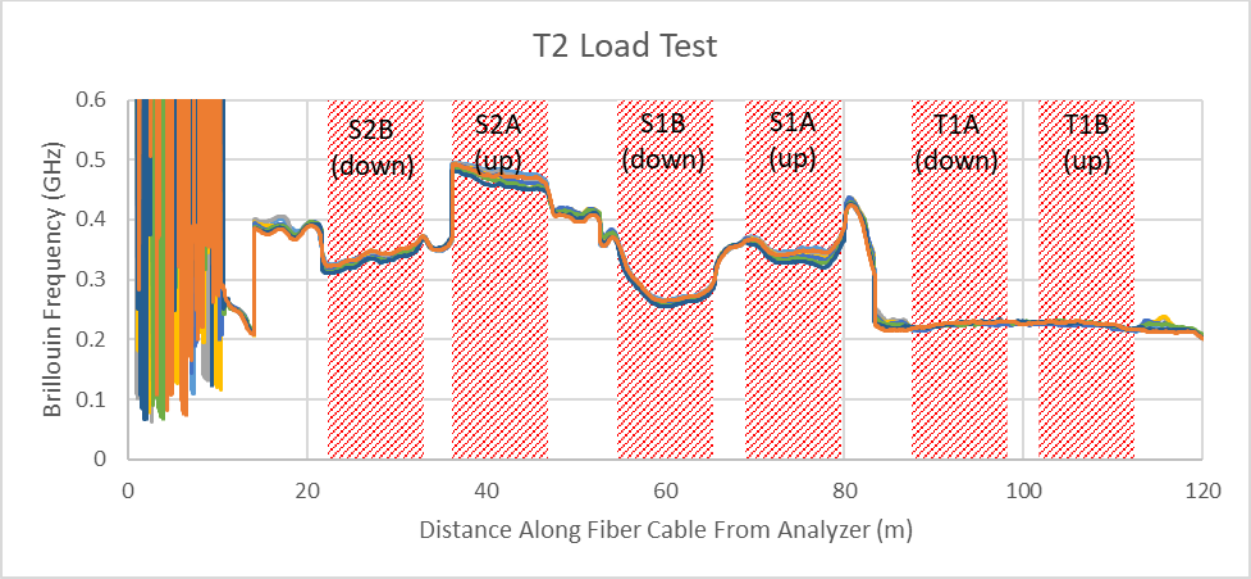

Figure 4-115: T2 load test, raw Brillouin frequency within pile T2

The development of strain over time at 7.5 feet below the top of casing in all four verticals, as well as the average strain, are shown in Figure 4-116. A difference in the strain between the sides of the pile can be observed from the spread in the strain data. HB1 and HB2 experienced the highest strain during the load test, while HB3 and HB4 on the opposite side experienced the lowest. The magnitudes of the two pairs of bars were relatively close to each other, indicating that the axis of asymmetry was approximately between HB1/2 and HB3/4, passing between each of the adjacent bar pairs. It can also be observed from the data that the linear trends during the increasing and decreasing loads displayed more noise than the corresponding reads on the other test piles using the Omnisens analyzer. This noise is likely attributed to the performance of the ALICIA analyzer in terms of its frequency resolution and repeatability, with the errors for any individual reading being higher than the more expensive Omnisens analyzer. The data is centered approximately +/- 20 με from a linear fit of the data for each strand, indicating that the repeatability is banded roughly within this magnitude. This is supported by the known optical limitations of the ALICIA analyzer and can be improved or relaxed by changing the selected optical components within its construction, depending on if higher or lower strain resolution is needed for monitoring applications.

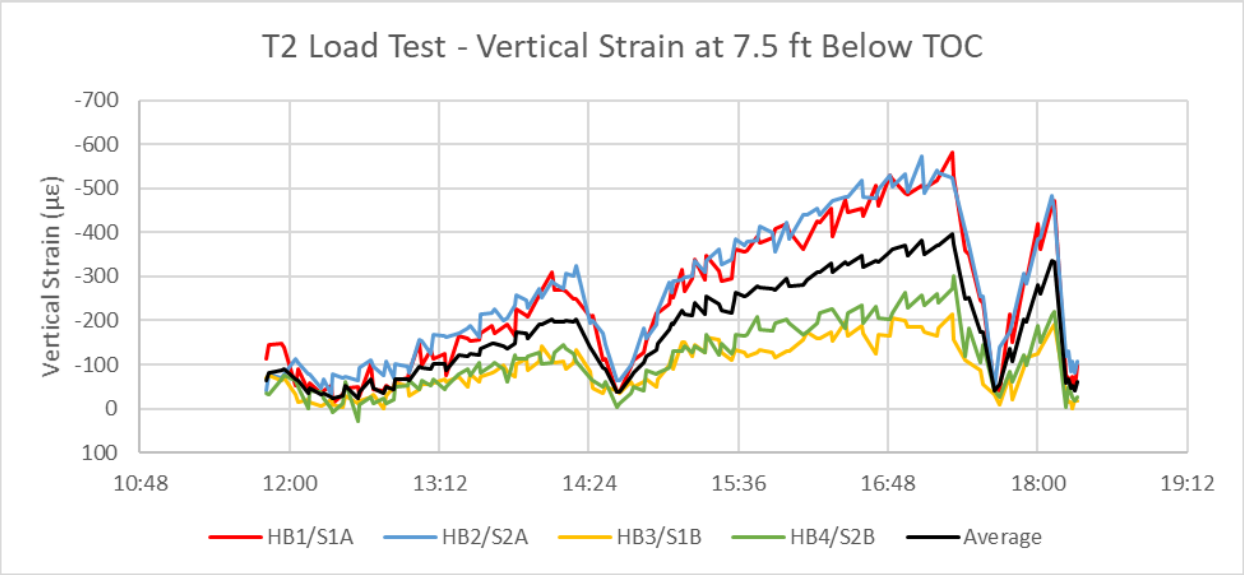

Figure 4-116: T2 vertical strain at 7.5 ft below top of casing over time

The development of strain within the pile over 6 loading increments (500 kips, 1000 kips, 1000 kips reload, 1500 kips, 1950 kips, and the final unload) are presented in *Figure 4-117* through Figure 4-122. The plotted strain represents the fiber optic readings taken just after the target load stabilized at each increment (additional load was no longer being added). The load is presented as approximate due to the deviation of the actual measured load versus the target.

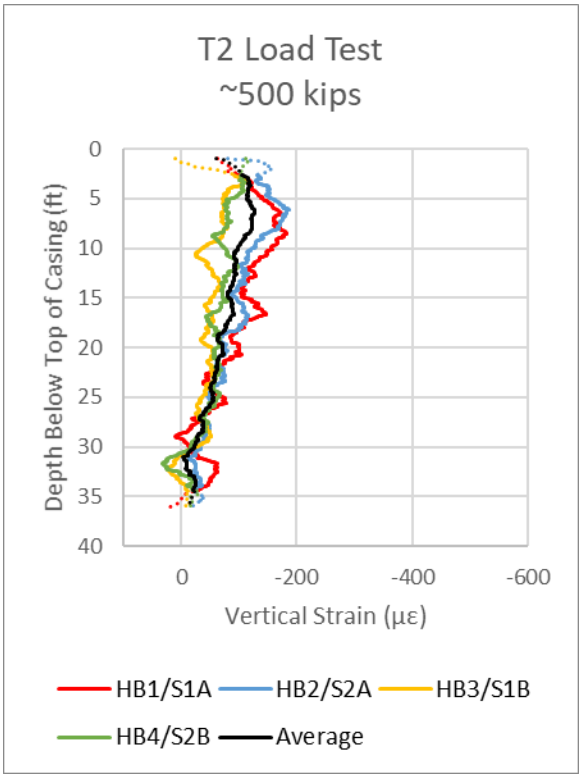

Figure 4-117: Vertical strain profile at ~500 kips load

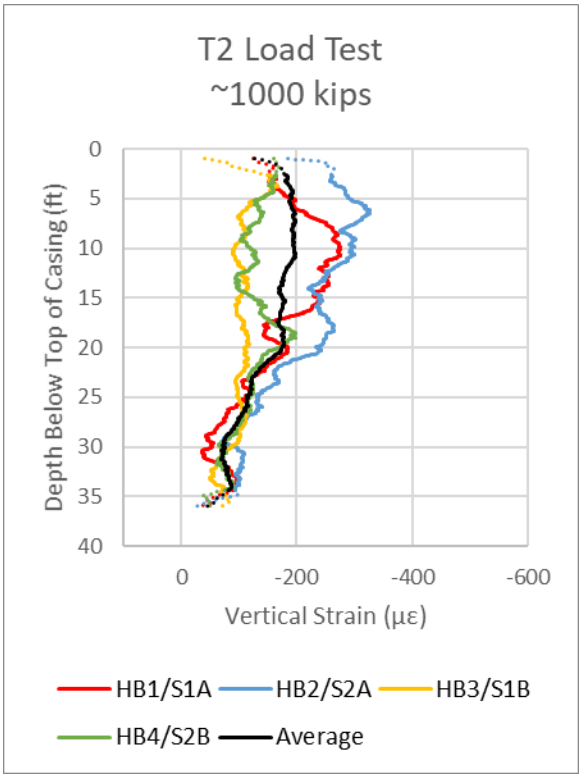

Figure 4-118: Vertical strain profile at ~1000 kips load

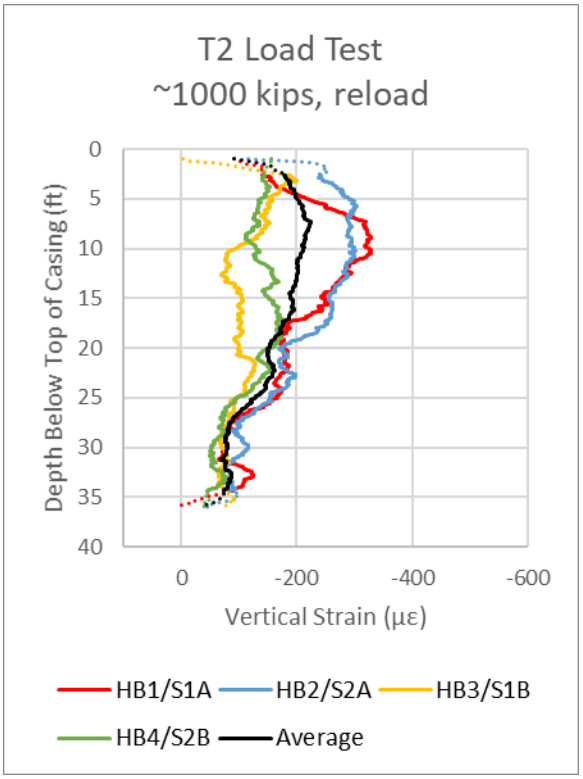

Figure 4-119: Vertical strain profile at ~1000 kips reload

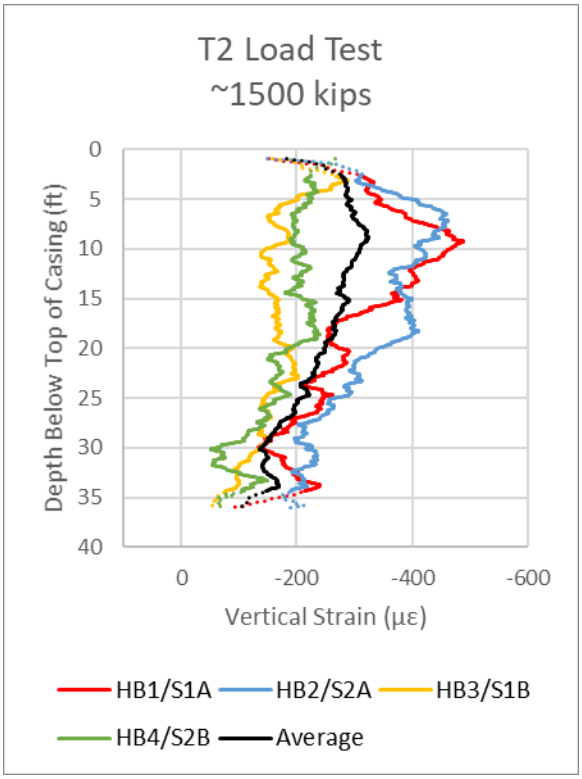

Figure 4-120: Vertical strain profile at ~1500 kips load

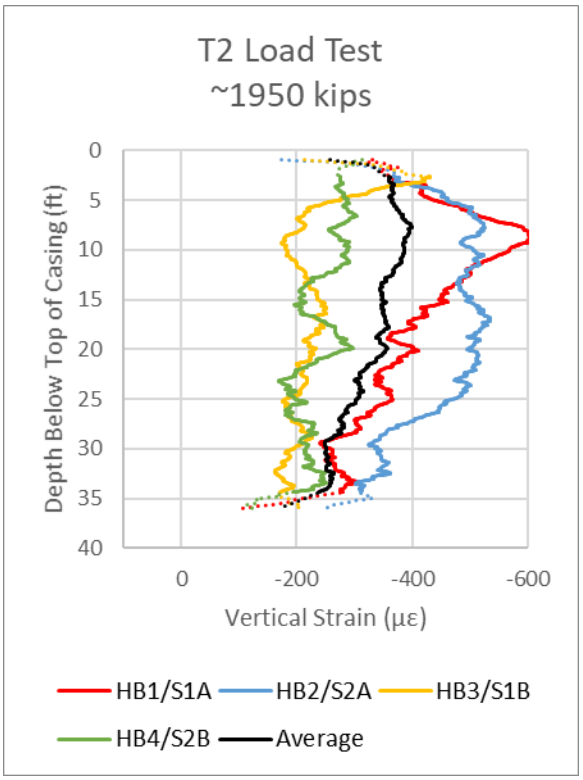

Figure 4-121: Vertical strain profile at ~1950 kips load

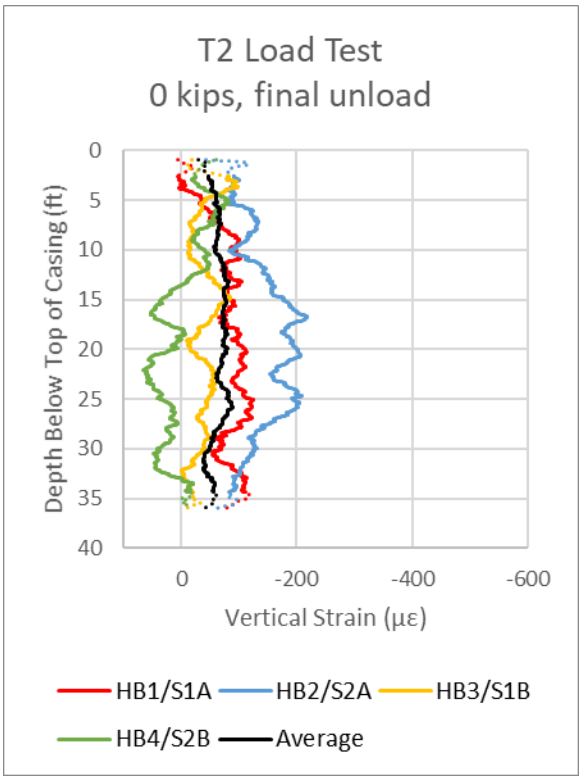

Figure 4-122: Vertical strain profile at 0 kips unload

Beginning in *Figure 4-117* at the 500-kip interval, a developing separation in the strain between HB1/2 and HB3/4 can be observed in the top 15 feet of the pile. This separation continues to grow in magnitude and also extend in depth through the maximum load interval of 1950 kips in Figure 4-121. The shape and magnitude of the HB1 and HB2 strain curves are similar through the maximum load, at which point HB1 displays a much sharper peak and strain decay with depth while HB2 shows a more gradual but rounded strain curve above the average. Likewise, the shape and magnitude of HB3 and HB4 are also similar through the maximum load, at which point HB3 develops a mild peak as compared to HB4. As with the strain profiles in Test Pile T1, the curvatures roughly mirror each other, with HB1/2 displaying positive curvature with a peak strain on HB1 of 600 με at a depth of 9.2 feet below the top of casing. HB3/4 display negative curvature in the same area with a local minimum strain of 178 με at a depth of 9.2 feet below the top of casing. The cause of the difference in strain between the sides of the pile are likely due to bending within the pile introduced during the load test. Looking at the residual strains in Figure 4-122 after the load on the pile has been removed, there is still a significant spread in the strains within the pile, with HB2 displaying strains of approximately 200 με between 15 and 25 feet below top of casing.

In addition to the distributed fiber optic strain measurements, strain measurements were also taken on the point-based FBG sensor string installed on HB3. The strain development over time of the 10 discrete measurement points is shown below. The sensor labels count up with depth from top to bottom, with FBG11 at 6.3 feet below the top of casing and FBG20 at the base of the pile at approximately 35.8 ft below the top of casing. Figure 4-123 shows the changes in FBG strains with time.

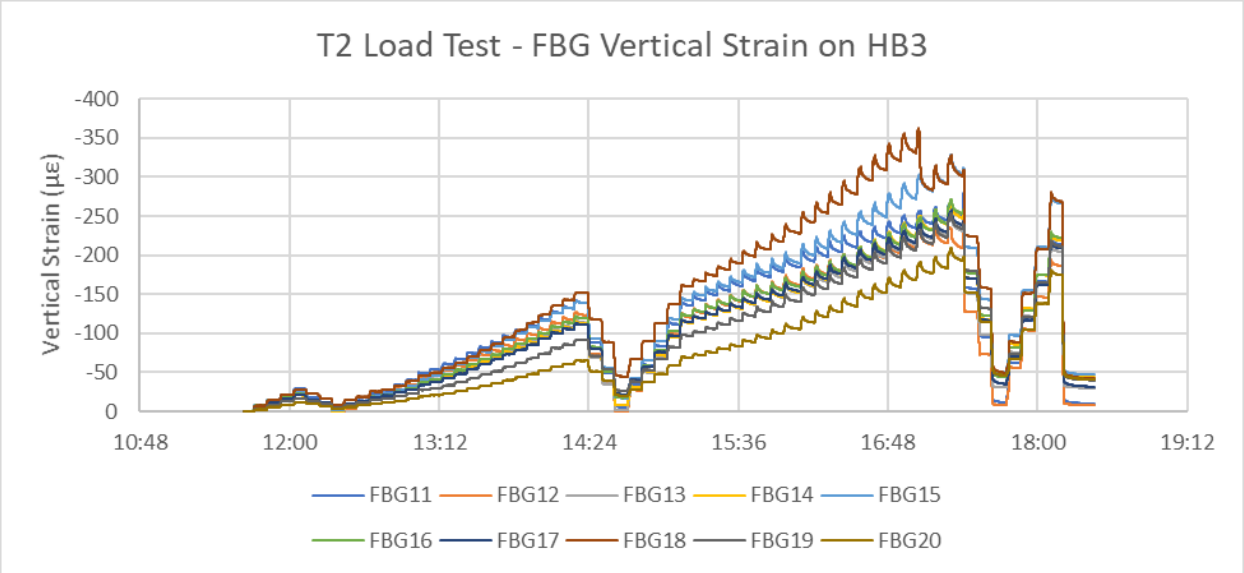

Figure 4-123: T2 load test FBG fiber optic strain readings over time

For comparison, the development of strain in the FBG sensor at approximately 9.5 feet below the top of casing is shown with the corresponding measurement from the distributed fiber

optic reading at the same point, as shown in Figure 4-124. The distributed vertical strain is from the individual cable section installed on the same HB3 bar as the FBG sensor string.

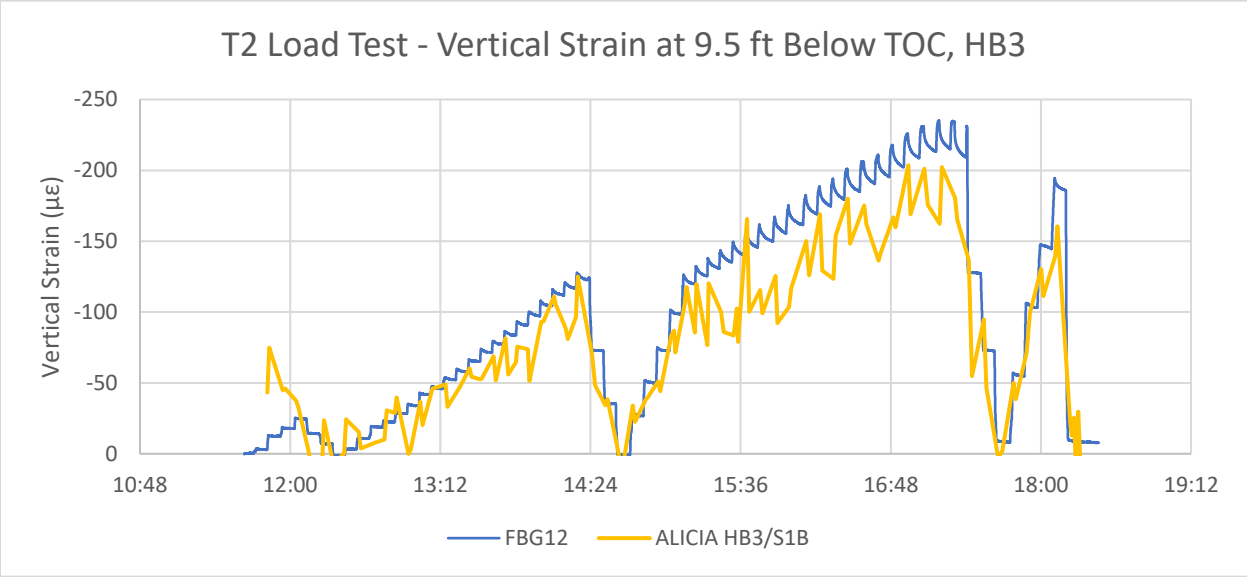

Figure 4-124: Point and distributed T2 vertical strain at 9.5 ft below top of casing over time

The FBG data shows much finer time and strain sensitivity. The Micron Optics analyzer was sampling at a 1 second interval, with a strain resolution of under 1 με. This allows the individual peak and decay within each load interval to clearly be seen in the shape of the plotted data, with the peak and decay becoming more pronounced at the higher load intervals. The distributed fiber optic data follows the same trend, but the noise previously discussed within the linear portions of the data causes the data to fluctuate above and below the likely "true" strain value at the same reading times. In general, the distributed fiber optic readings closely followed the FBG strain readings, with a slight deviation observed in the final load cycle of approximately 20-30 με. The strain readings with depth for the FBG string and the corresponding distributed readings at the maximum load interval are presented in Figure 4-125.

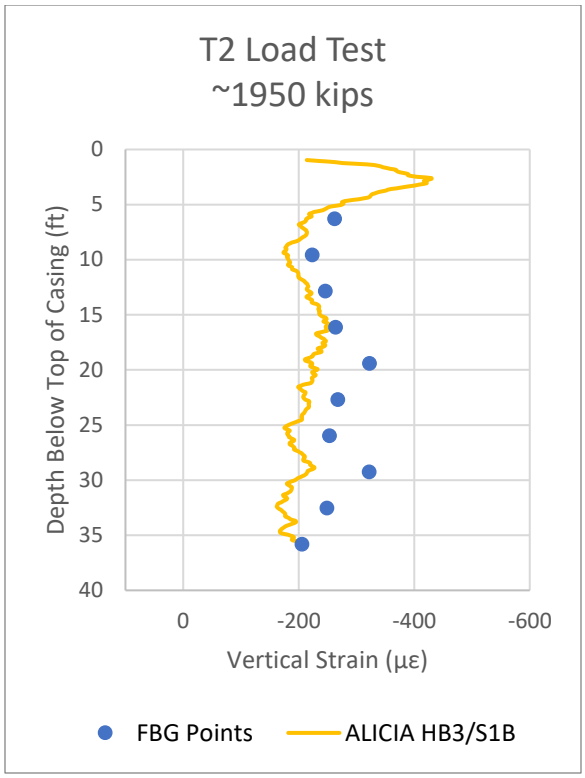

Figure 4-125: Point and distributed T2 vertical strain with depth at 1950 kips

As with the time-series plot of the comparable strains at 9.5 feet in Figure 4-124, the strains in Figure 4-125 show a similar strain shape between the FBG and distributed readings, with the FBG strains generally having a larger magnitude than the distributed readings from ALICIA at the same depth.

c) Pile T3, Open-Type (tube-à-manchette)

Pile T3 was load tested on March 4, 2019. The pile was base grouted using tube-à-manchette. Four load cycles were completed in approximately 8.5 hours. The recorded load time history for Pile T3 is shown in Figure 4-126. The maximum load peaks of the individual cycles were 200, 1150, 2027, and 1600 kips.

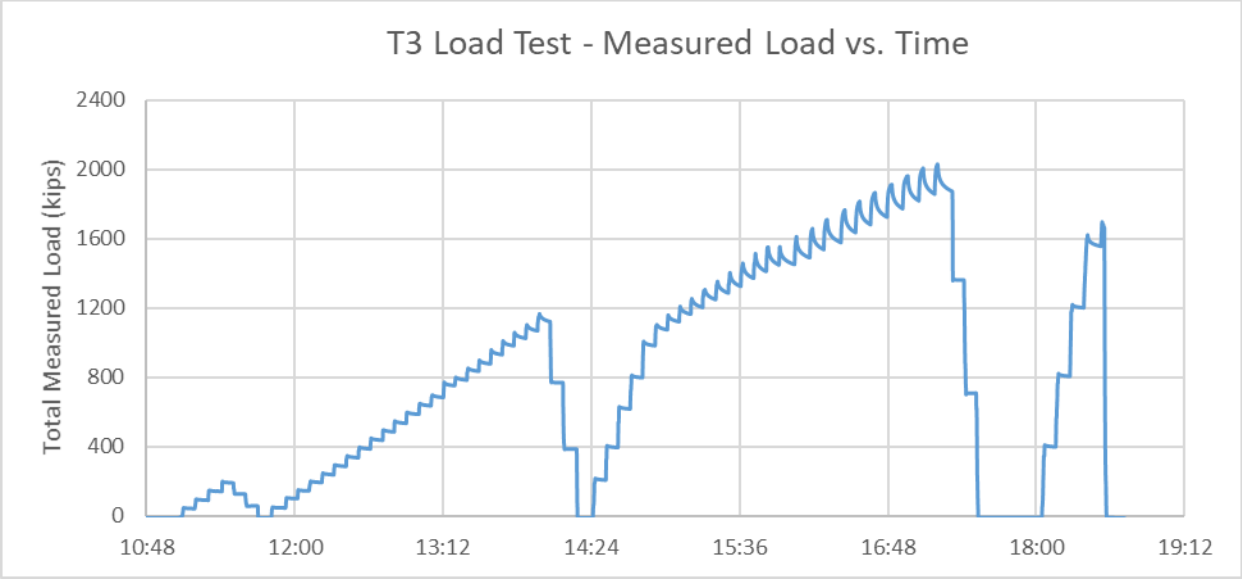

Figure 4-126: T3 load test, total load (sum of 4 individual load cells) over time

The fiber optic readings during the load test were taken in BOTDA mode (full loop) using the Omnisens analyzer. A total of 60 distributed fiber optic readings were taken prior to, during, and after the load test. Each reading interrogated both the strain and temperature loops of the test pile, as well as the four connected reaction piles (in order: T3, R5, R8, R9, R2). The raw frequency plot is presented in Figure 4-127. Focusing on the test pile, the fiber optic record was divided into the vertical strain and temperature loops, as shown in Figure 4-128.

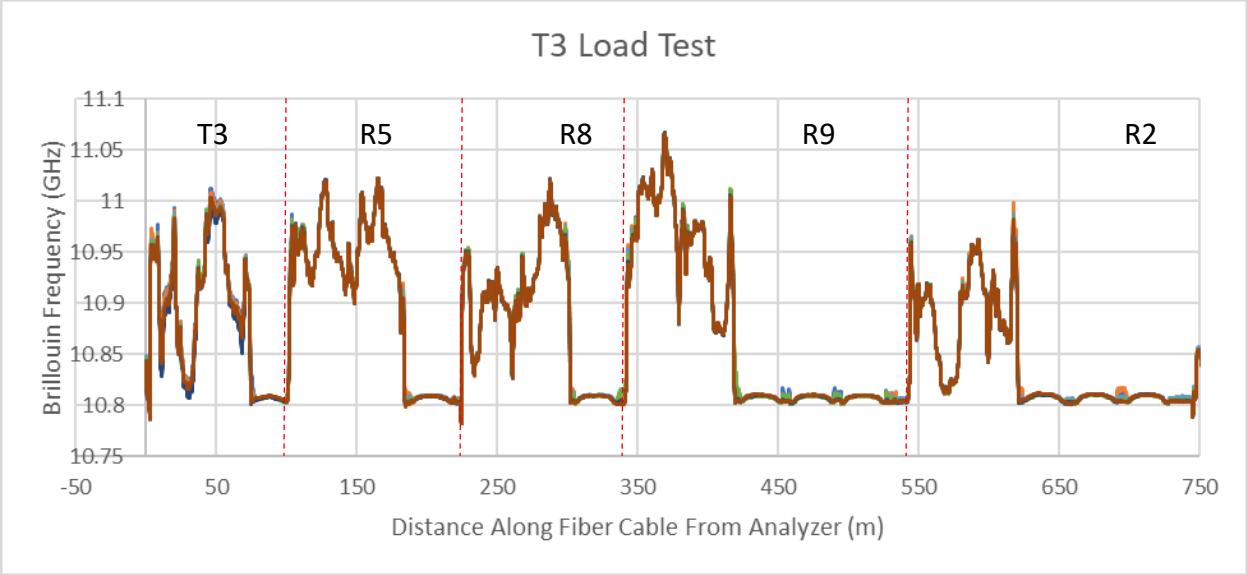

Figure 4-127: T3 load test, raw Brillouin frequency over all piles

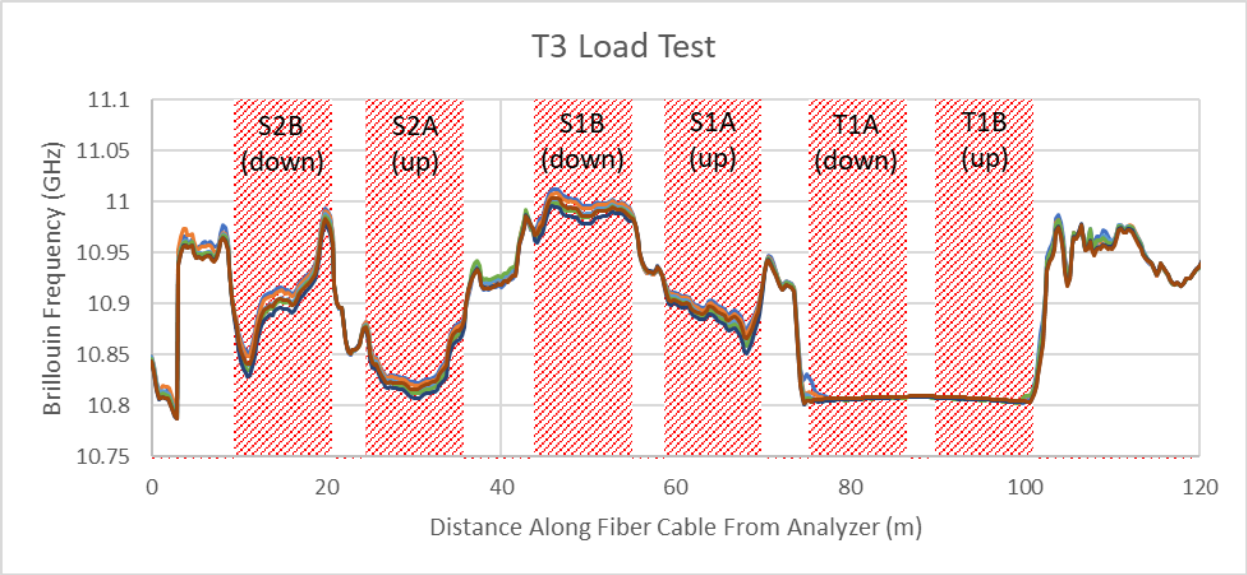

Figure 4-128: T3 load test, raw Brillouin frequency within pile T3

The development of strain over time at 7.5 feet below the top of casing in all four verticals, as well as the average strain, are shown in Figure 4-129. The distributed fiber optic record stops just prior to the penultimate unload. This is due to the fiber optic cable between R5 and R8 being severed as the reaction frame settled back to the ground as the load was released. Since no BOTDR (single-ended) baseline was taken prior to the load test, further readings in the final reload were taken but cannot be directly compared to the earlier record. Comparing the BOTDA record up to the point of the fiber optic cable break, the results are generally comparable to the BOTDR readings taken on T1 using the Omnisens analyzer and are less noisy than the BOTDR readings taken on T2 using the ALICIA analyzer.

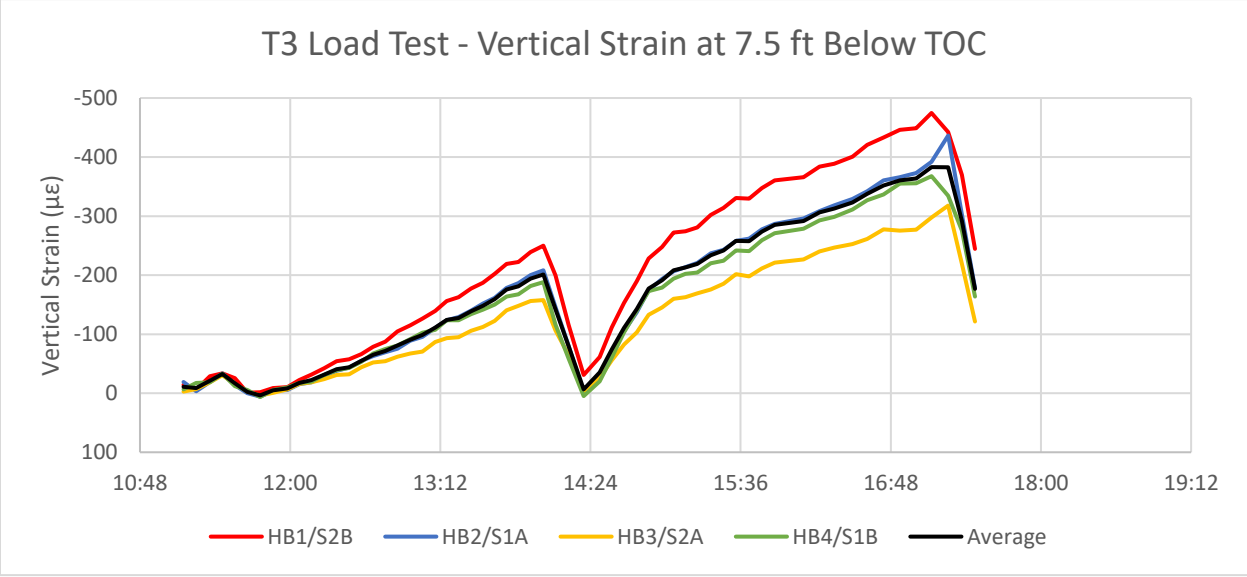

Figure 4-129: T3 vertical strain at 7.5 ft below top of casing over time

A difference between the strain in the sides of the piles can be observed in the spread in the strain data in Figure 4-129. HB1 experienced the highest strain during the load test, while HB3 opposite it experienced the lowest. On the perpendicular axis, HB2 and HB4 were centered close to the average, indicating that the direction of the asymmetry was close to the HB1-HB3 line.

The development of strain within the pile over 6 loading increments (500 kips, 1150 kips, 1150 kips reload, 1500 kips, 2027 kips, and the final reading before the cable breakage at 700 kips) are presented in Figure 4-130 through Figure 4-135. As with the readings in T1, the presented load is approximate due to the deviation in the applied load from the "target" load and the variable load decay during the 5-minute fiber optic reading.

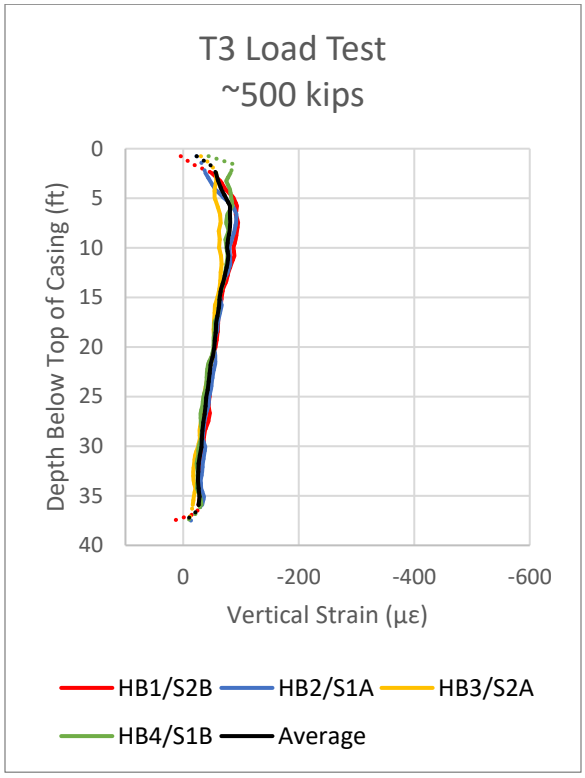

Figure 4-130: Vertical strain profile at ~500 kips load

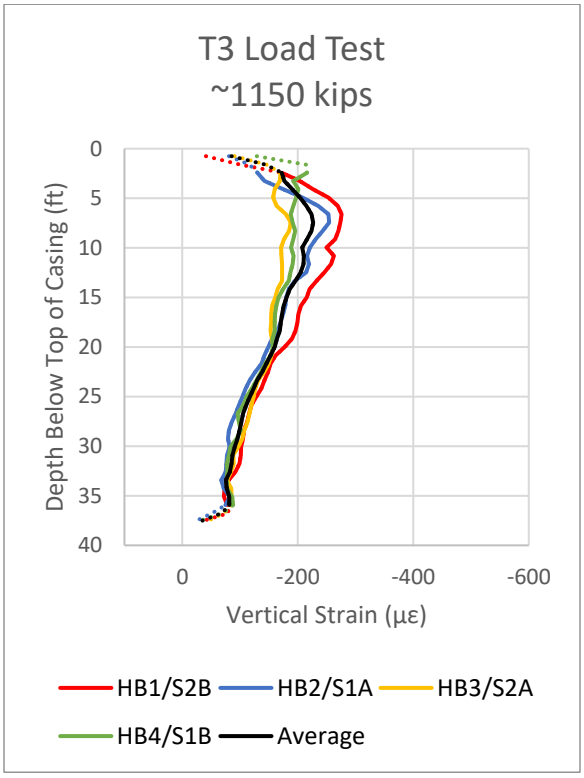

Figure 4-131: Vertical strain profile at ~1150 kips load

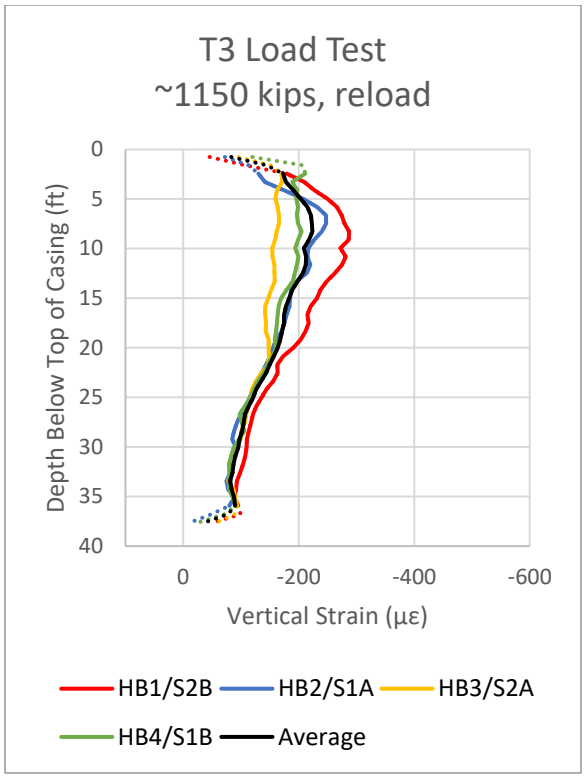

Figure 4-132: Vertical strain profile at ~1150 kips reload

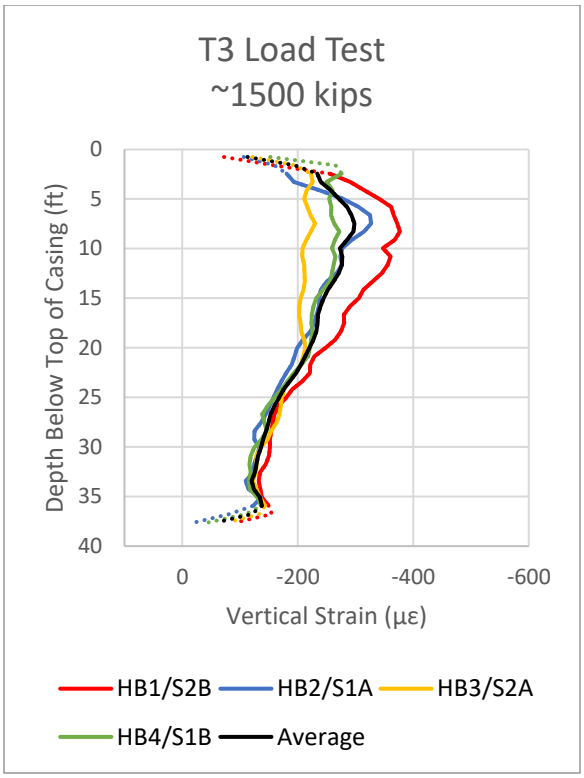

Figure 4-133: Vertical strain profile at ~1500 kips load

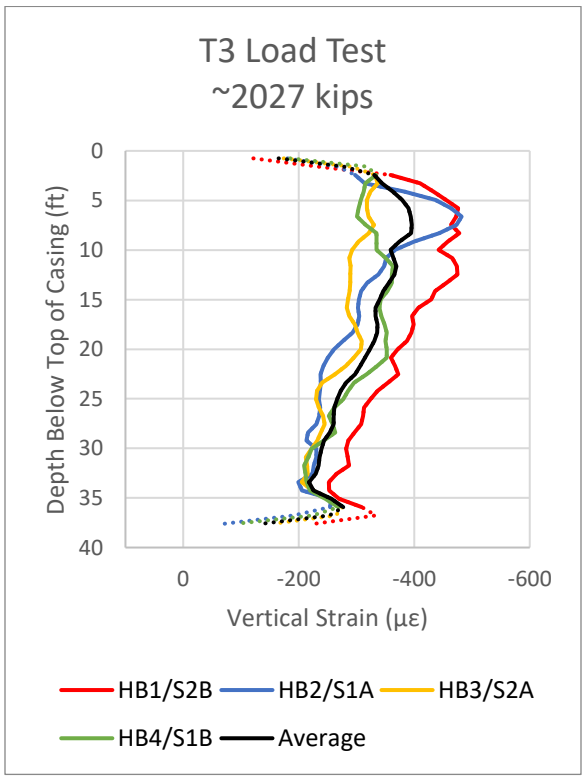

Figure 4-134: Vertical strain profile at ~2027 kips load

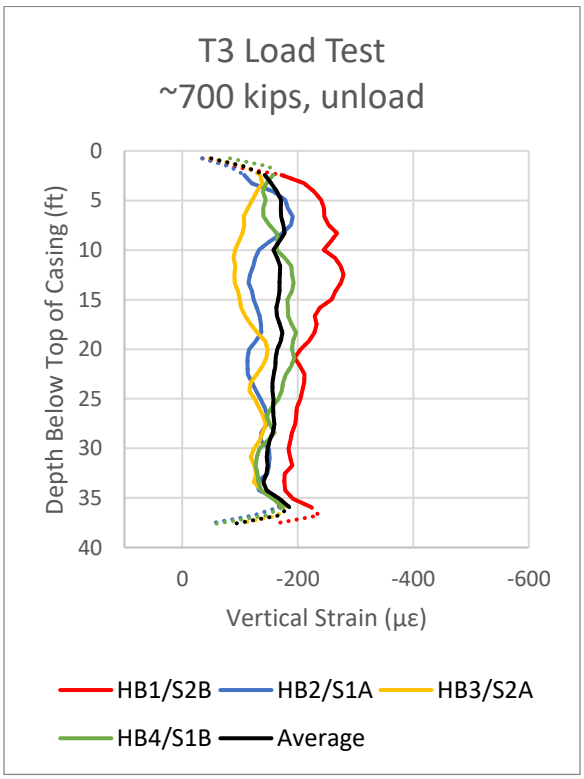

Figure 4-135: Vertical strain profile at ~700 kips unload

In comparison to the strain profiles in piles T1 and T2, the strain differential across the pile in T3 is of a much lower magnitude. The separation in strain is not apparent in Figure 4-130 at the 500-kip interval. The separation begins to appear in Figure 4-131 at 1150 kips, although the magnitude is relatively low compared to the results from the other test piles. The separation grows slightly in magnitude in the subsequent figures to the maximum load interval of 2027 kips in Figure 4-134. The strains in HB1 show a positive curvature, developing to a maximum strain of 474 με at 7.4 feet below the top of casing. The strains in HB3 do not display a clear negative curvature in the same depth, slowly decreasing in compressive strain linearly from 330 με at 7.5 feet to 297 με at 17.5 feet below the top of casing. The relatively small spread between the maximum and minimum strains and the lack of clear curvature symmetry implies that the bending in T3 during the load test was of a lower magnitude than that observed in piles T1 and T2.

d) Pile T4, Closed-Type (bladder)

Pile T4 was load tested on February 21, 2019. The pile was base grouted using the bladder system. Four load cycles were completed in just over 7 hours. The recorded load time history for total load (sum of 4 individual load cells) is shown in Figure 4-136. The maximum load peaks of the individual cycles were 200, 1050, 1750, and 1600 kips.

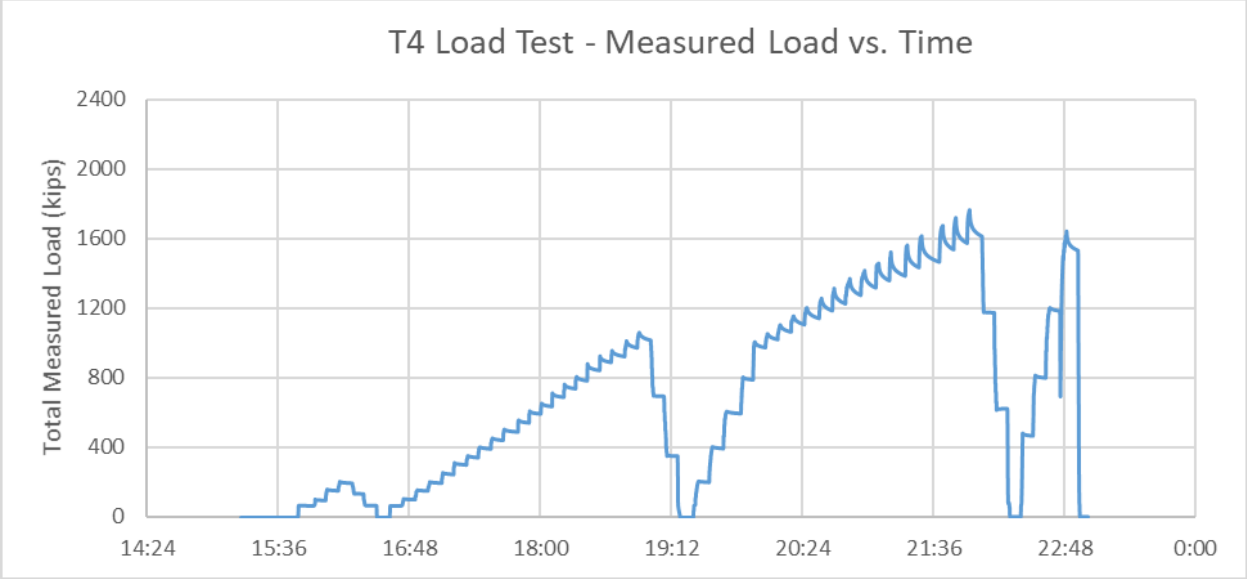

Figure 4-136: T4 load test, total load (sum of 4 individual load cells) over time

The fiber optic readings during the load test were taken in BOTDA mode (full loop) using the Omnisens analyzer. A total of 62 distributed fiber optic readings were taken prior to, during, and after the load test. Each reading interrogated both the strain and temperature loops of the test pile, as well as the four connected reaction piles (in order: T4, R4, R7, R8, R6). The raw frequency plot is presented in Figure 4-137. Focusing on the test pile, the fiber optic record was divided into the vertical strain and temperature loops, as shown in Figure 4-138.

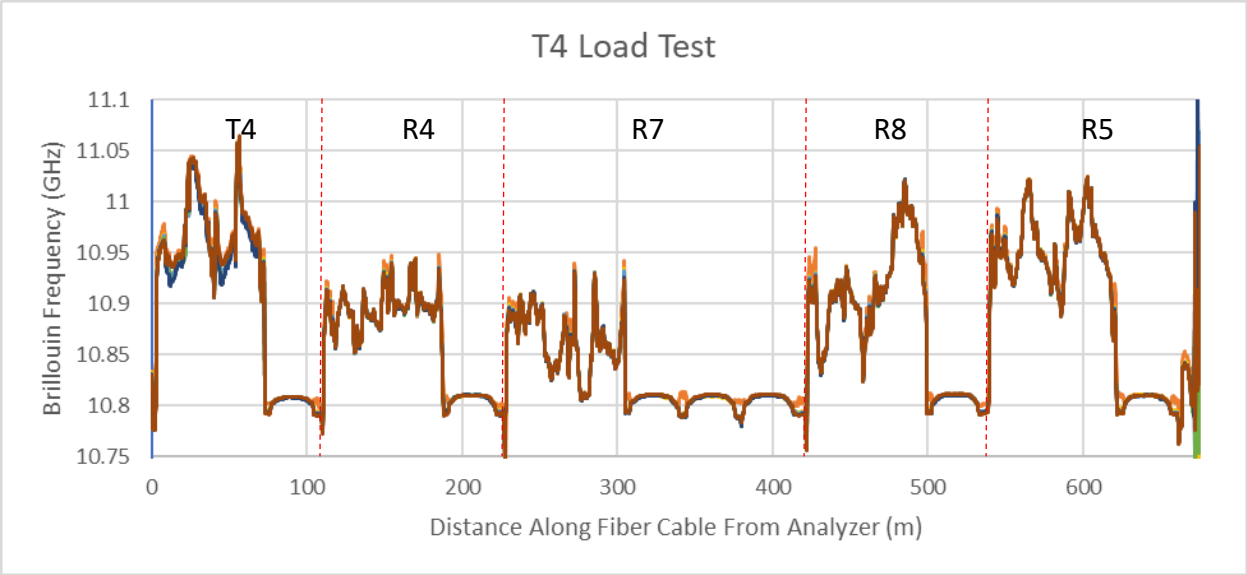

Figure 4-137: T4 load test, raw Brillouin frequency over all piles

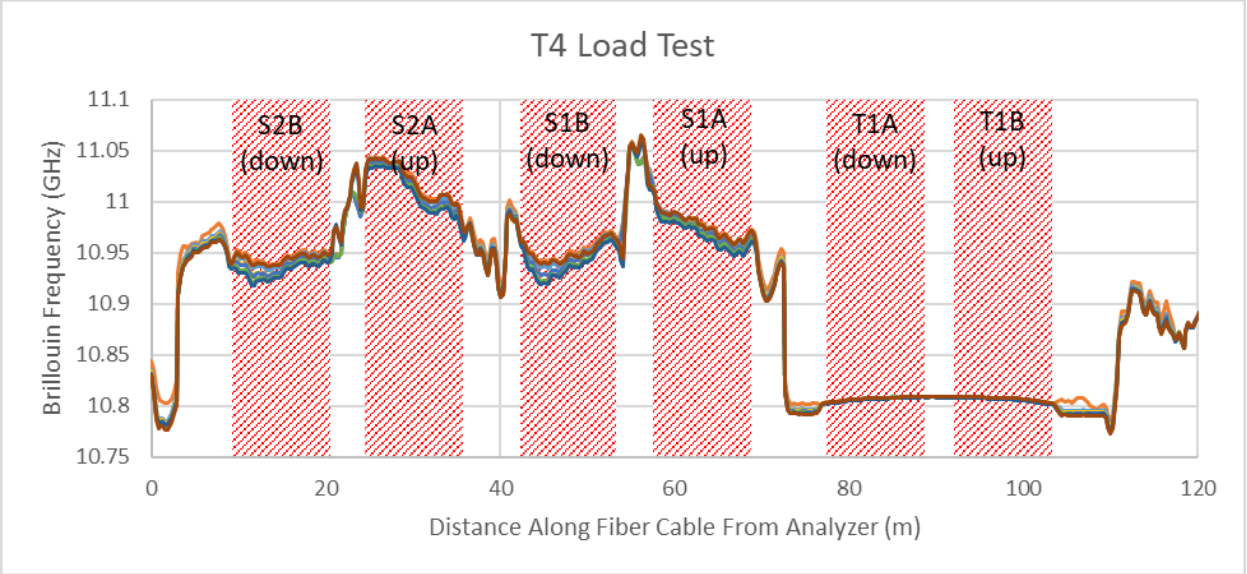

Figure 4-138: T4 load test, raw Brillouin frequency within pile T4

The development of strain over time at 7.5 feet below the top of casing in all four verticals, as well as the average strain, are shown in Figure 4-139. A difference in the strain across the pile can be observed from the spread in the strain data. HB2 and HB3 experienced the highest strain during the load test, while HB1 and HB4 on the opposite side experienced the lowest. The magnitudes of the strains observed on the coordinating pairs of bars were relatively close to each other, indicating that the axis of asymmetry was approximately between HB2/3 and HB1/4, passing between each of the adjacent bar pairs.

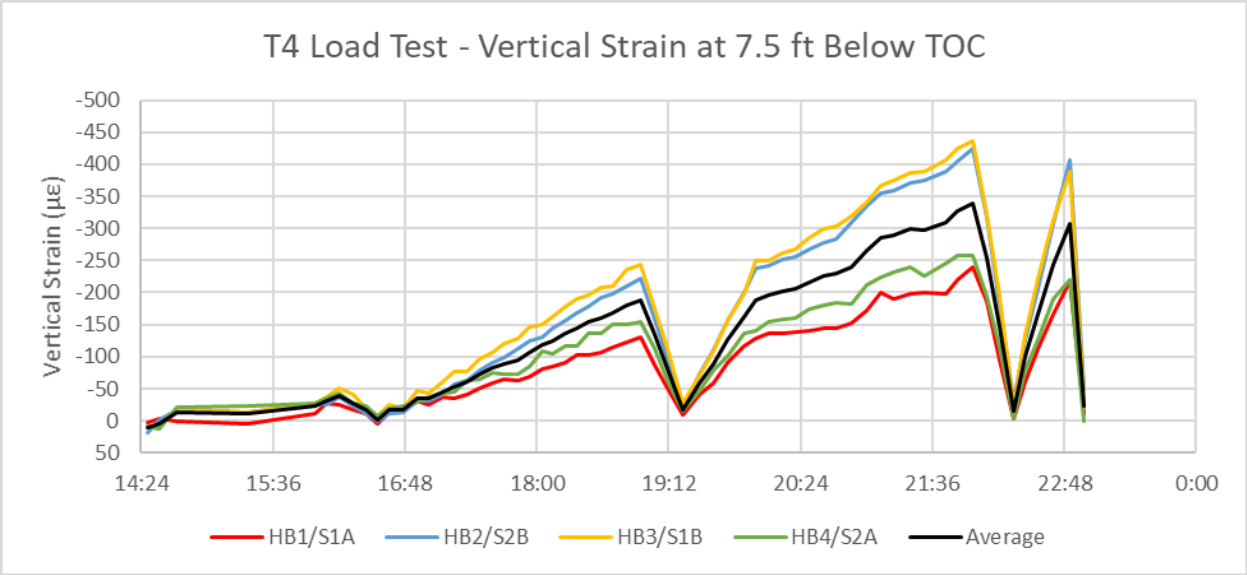

Figure 4-139: T3 vertical strain at 7.5 ft below top of casing over time

The development of strain within the pile over 6 loading increments (500 kips, 1050 kips, 1050 kips reload, 1500 kips, 1750 kips, and the final unload) are presented in *Figure 4-140* through *Figure 4-145*. As with the readings in T1 and T3, the presented load is approximate due to the deviation in the applied load from the "target" load and the variable load decay during the 5-minute fiber optic reading.

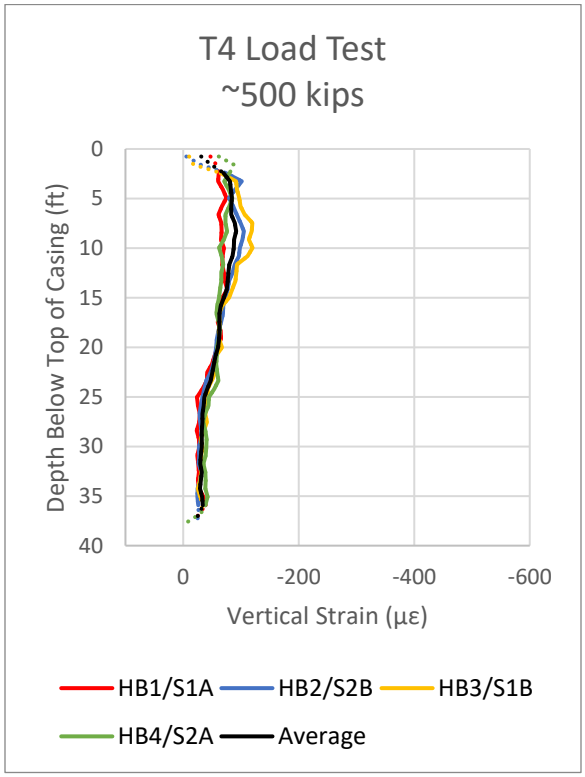

Figure 4-140: Vertical strain profile at ~500 kips load

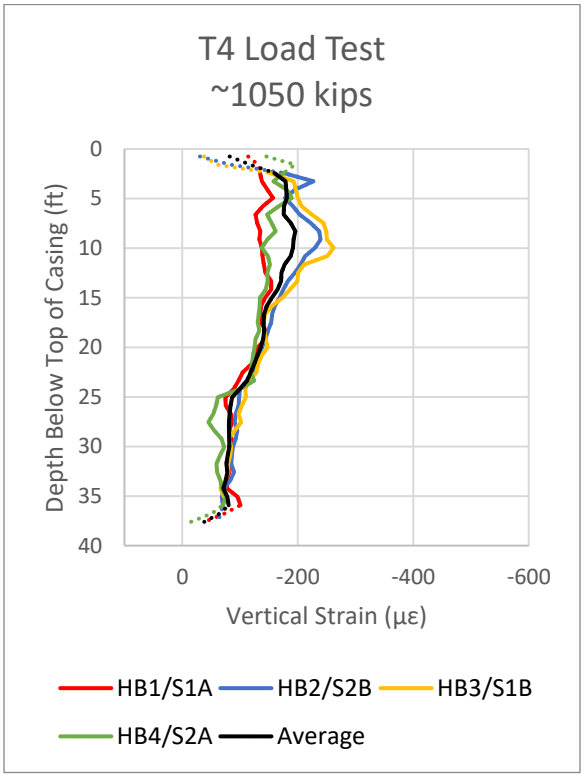

Figure 4-141: Vertical strain profile at ~1050 kips load

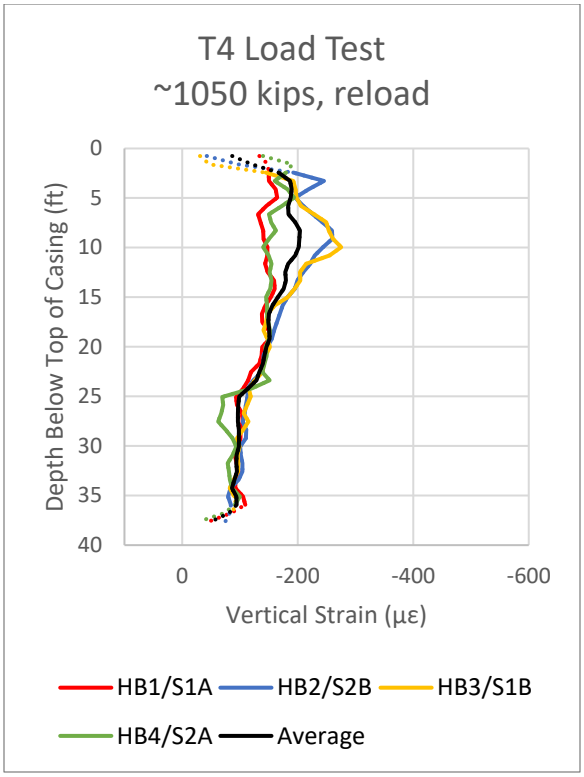

Figure 4-142: Vertical strain profile at ~1050 kips reload

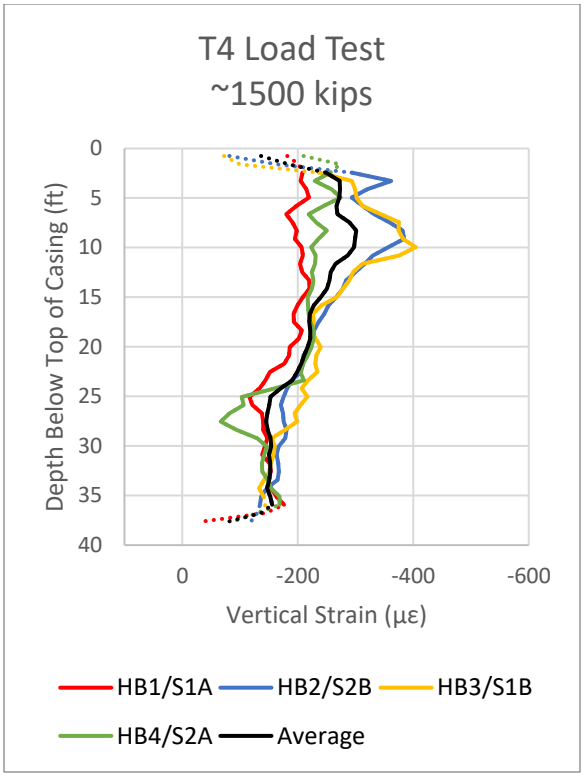

Figure 4-143: Vertical strain profile at ~1500 kips load

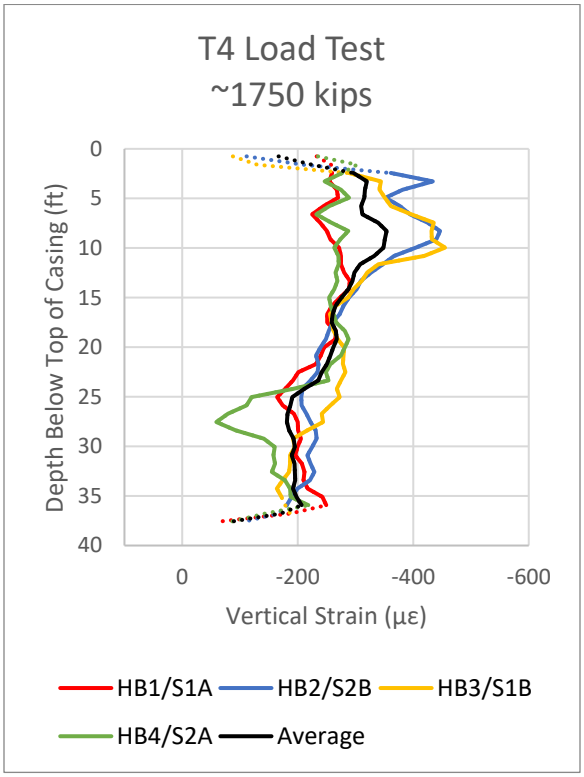

Figure 4-144: Vertical strain profile at ~1750 kips load

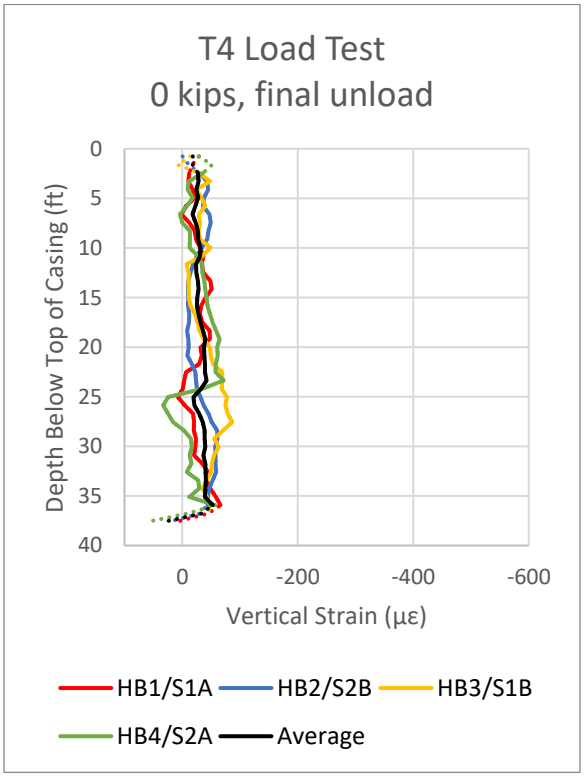

Figure 4-145: Vertical strain profile at 0 kips unload

At the 500-kip interval in *Figure 4-140*, a small separation in the strain between HB2/3 and HB1/4 can be observed in the top 15 feet of the pile. The separation grows in magnitude in the subsequent figures, peaking at the maximum load interval of 1750 kips in *Figure 4-144*. The shape and magnitude of the HB2 and HB3 strain curves are similar through all of the loading intervals with a positive concavity and a peak strain of 455 με on HB3 at a depth of 10 feet below top of casing. Likewise, the shape and magnitude of HB1 and HB4 are also similar through the maximum load, displaying a slight negative concavity above 15 feet below top of casing. A semi-defined negative peak is observed at 6.6 feet below top of casing with a magnitude of 232 με. Due to the lack of a well-defined peak on the HB1/4 pair, the symmetry is not as pronounced as that observed on test piles T1 and T2. It is therefore likely that, as with T3, there was less bending introduced into T4 during the load test. The average strain in *Figure 4-145* after removal of the load show a residual strain of approximately 30 με.

Summary

A summary of the fiber optic strain data from the load test is presented below.

- Non-uniform strains around the cross section of the pile were observed in all the tests. Based on the shape of the strain profiles, this is likely due to bending forces being introduced into the pile during the load test. In most cases, the strongest differential was confined to the top 20 feet of the pile.
- Comparing the average strain at the bottom of the "main" fiber optic profile in each pile (the final section of the solid line before spatial resolution from the base could affect the reading), the strain values were in the range of 190 – 277 με. The actual values are listed in Table 4-4.

Table 4-4: Load test final load and base strain

Pile	Grout System	Final Load	Final Base Avg. Compressive Strain
T1	None	~1750 kips	191 με
T2	RIM Cell	~1950 kips	239 με
T3	Open-type	~2027 kips	277 με
T4	Closed-type	~1750 kips	207 με

- Of the piles with a final reading at 0 kips, all the readings showed average residual strains with a value on the order of 30-50 με.

4.5 Discussion

Following the completion of the lab and field testing, the results were analyzed to evaluate the three research hypotheses.

Hypothesis 1: Installation of Strain Cables in Concrete without Pretension

The first hypothesis of the research project is that fiber optic strain cables in piles, when fully encapsulated in concrete, can be installed with slack removed but without additional pre-

tension with no detrimental effect on compressive strain measurements. The test for this is a comparison between the point-based vibrating wire strain gauges and the corresponding fiber optic strain measurements during the load testing. A negative test result would be the case that the strain measurements between the two systems constantly vary across the measured recordings. A positive test result would be the case that the strain measurements do not vary significantly across the measured recordings.

Six levels of vibrating wire strain gauges were included in each of the project test shafts, installed and read by the University of Missouri team. The quantity and plan location varied between the levels and did not directly correspond to the four verticals of distributed strain fiber optic cable. The levels, number of sensors, and average depth are presented in Table 4-5. Note that the average depth is an average between the four test shafts – within each given test shaft all strain gauges for each level were installed at the same depth.

Table 4-5: Test pile vibrating wire strain gauge levels

Level	Number of SGs	Average Depth, ft. BTOC
1	4	36.6
2	3	30.9
3	3	23.9
4	3	17.0
5	3	10.0
6	2	1.9

Due to the variable strain changes within the pile observed during grouting, the strain comparison between the two measurement systems was performed on the data generated during load testing. Since the SGs and fiber optic strain cables were not installed in the same plan location within the piles, a direct comparison between the data at specific gauge locations is not possible. Instead, a comparison between all WGs and all four distributed strain fiber optic verticals is presented at six representative load increments. The average strain at each reading level between the two systems is separately plotted for each load increment, which removes the variation between the readings due to the difference in plan location.

a) Test Pile T1, Control (no base grout)

The strain measurement results for the distributed fiber optic system and the SGs in pile T1 are presented in Figure 4-146 to Figure 7-12. Beginning in Figure 4-146, the spread of the individual SGs are approximately enveloped by the four fiber optic strain verticals. This trend continues in the other four load increments as well as the final unload reading presented in Figure 4-156. Turning to the plots of the measured strain average with depth, the two measurement sets show good agreement both in magnitude and the shape of the strain profile. Excluding readings at the bottom of the pile where the spatial resolution constraints of the fiber optic system

affected the readings (represented by the dashed lines at the bottom of the pile), the maximum difference between the two averages was on the order of 30 με.

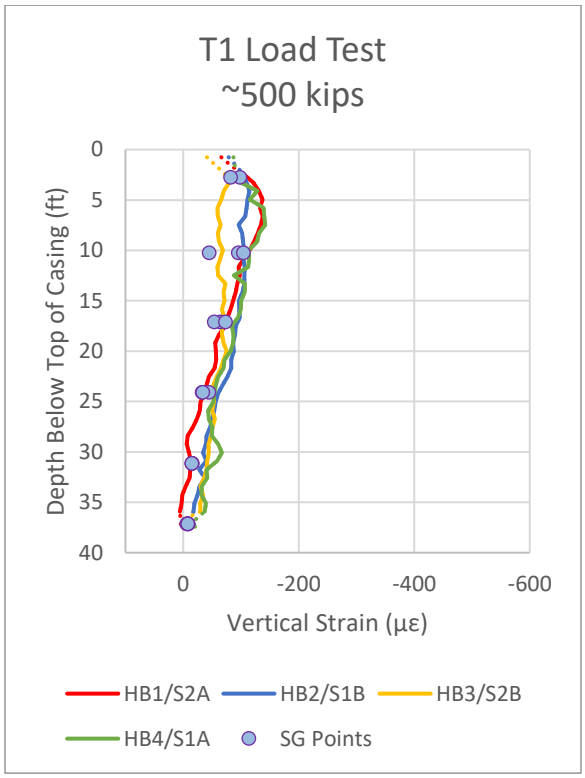

Figure 4-146: Vertical strain profile at ~500 kips load

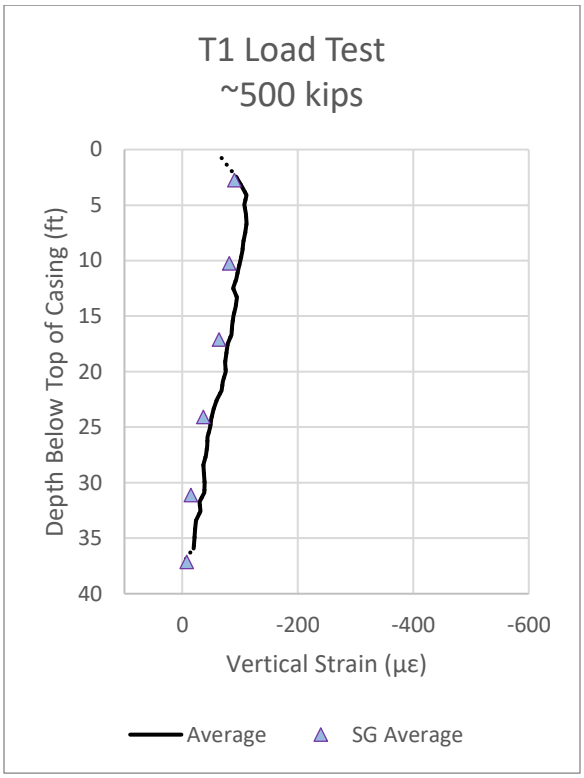

Figure 4-147: Average strain profile at ~500 kips load

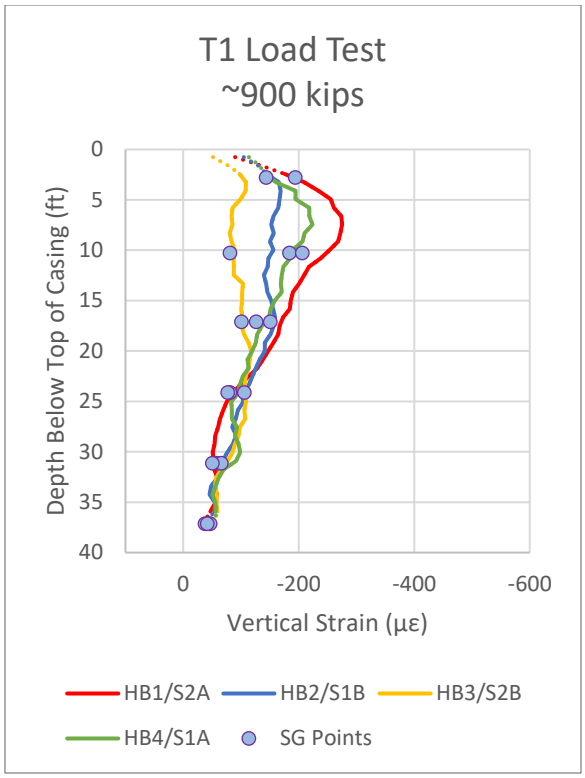

Figure 4-148: Vertical strain profile at ~900 kips load

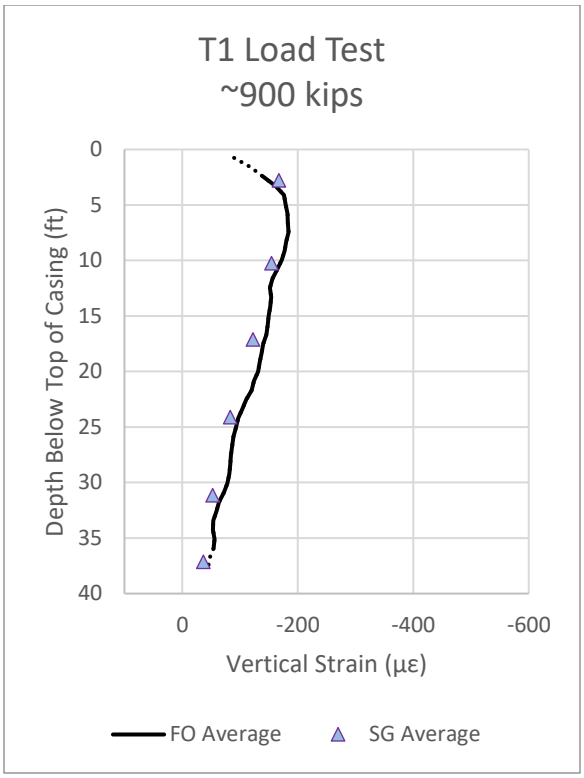

Figure 4-149: Average strain profile at ~900 kips load

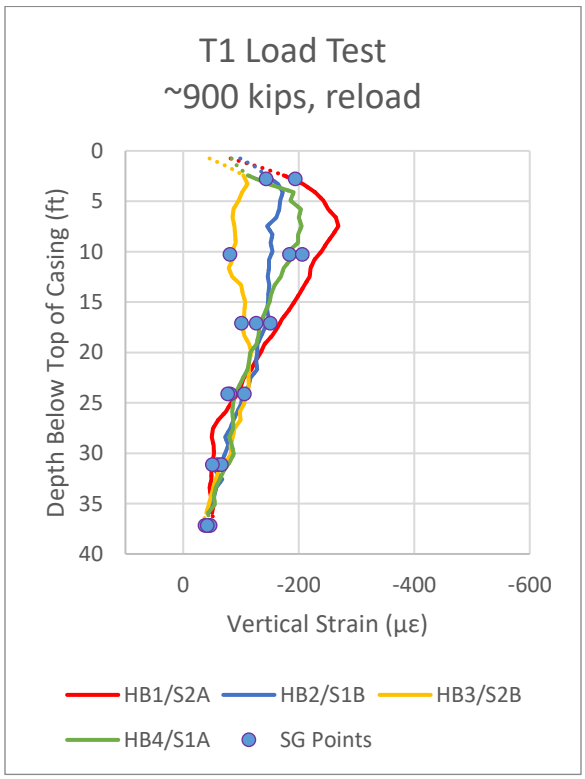

Figure 4-150: Vertical strain profile at ~900 kips reload

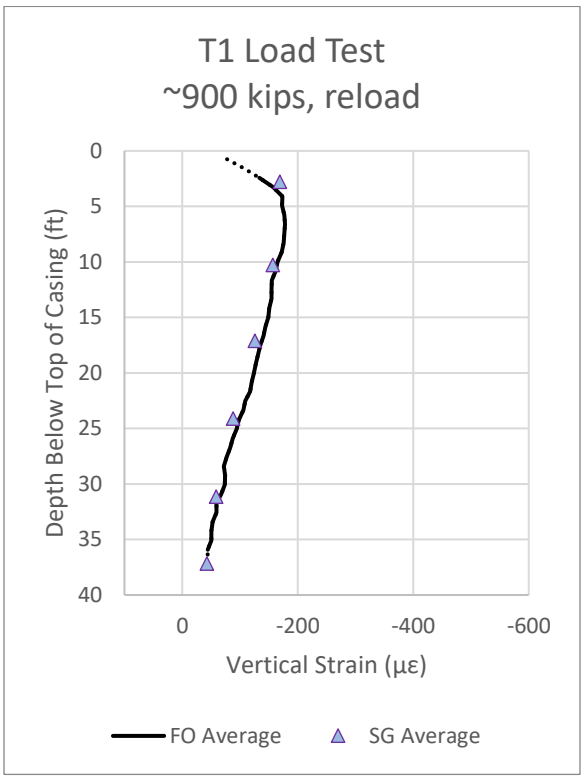

Figure 4-151: Average strain profile at ~900 kips reload

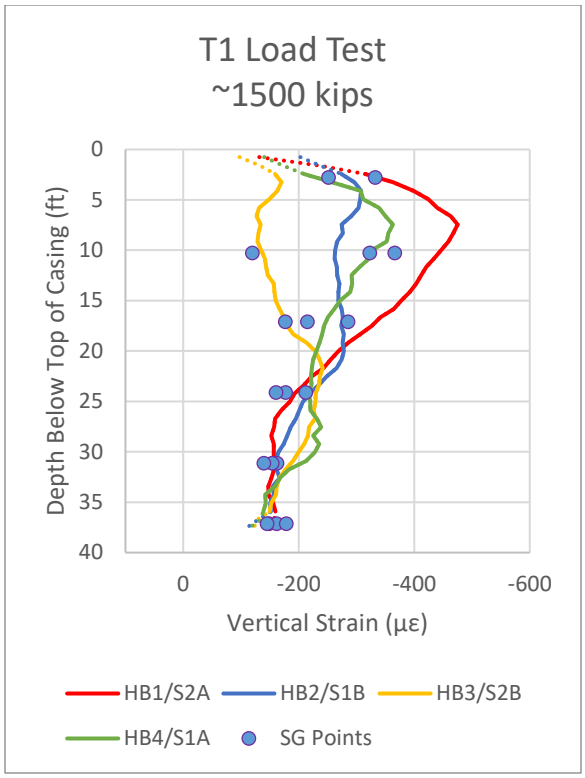

Figure 4-152: Vertical strain profile at ~1500 kips load

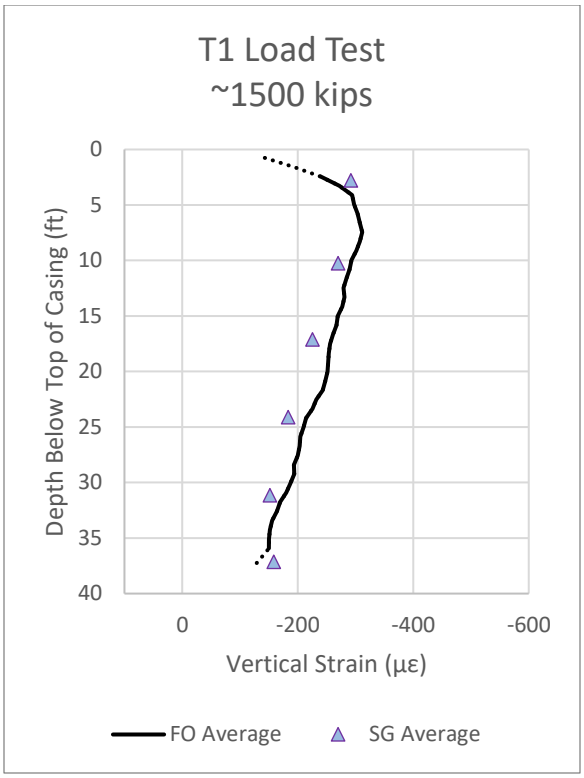

Figure 4-153: Average strain profile at ~1500 kips load

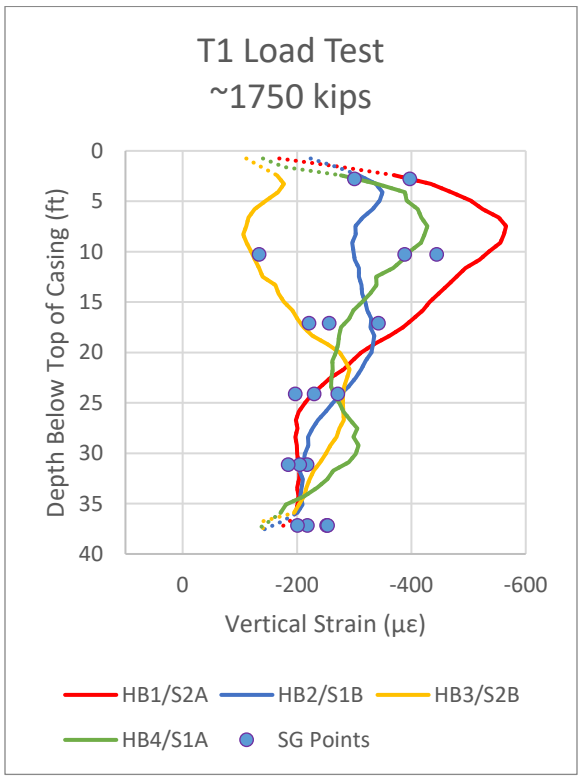

Figure 4-154: Vertical strain profile at ~1750 kips load

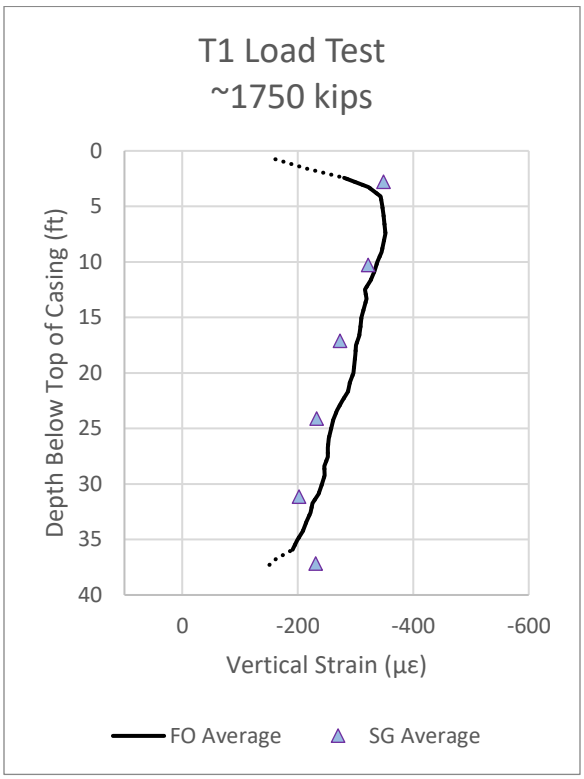

Figure 4-155: Average strain profile at ~1750 kips load

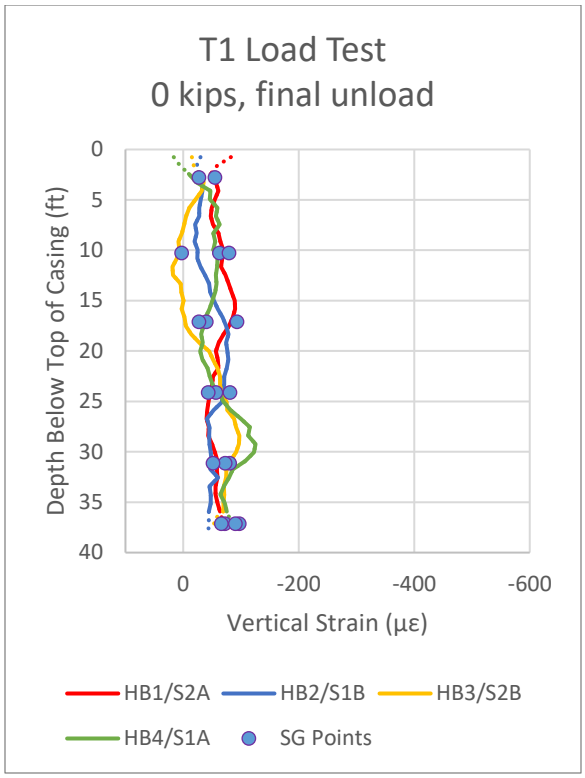

Figure 4-156: Vertical strain profile at 0 kips unload

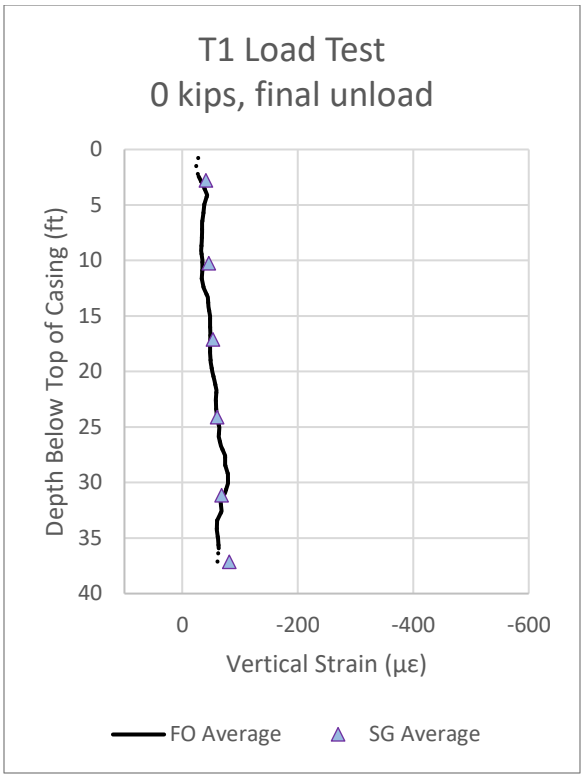

Figure 4-157: Average strain profile at 0 kips unload

b) Test Pile T2, RIM Cell

The strain measurement results for the distributed fiber optic system and the SGs in pile T2 are presented in Figure 4-158 to Figure 7-24. Similar to the results from pile T1, the individual SG readings at each level are approximately enveloped by the four strain gauge verticals. It is noted that the peak strain values measured by the SG are lower than the highest readings in the fiber optic strands, a trend most apparent in Figure 4-166 at the peak load increment of ~1950 kips. This difference is also observed in the plots of the strain averages, where the SG readings are up to approximately 75 με below the corresponding fiber optic average. One potential explanation for this difference is that the plan orientation of the strain gauges within the pile were such that a gauge was not located on the axis of peak strain within the pile, likely associated with bending within the top portion of the pile. By being shifted off this axis, the SG readings would potentially register lower strains at each elevation within the top portion of the pile. A second potential cause of the difference could be an overestimation of the strain within the fiber optic cable due to an error with the ALICIA fiber optic analyzer. However, since the SG and fiber optic readings agree closer in value at the bottom portion of the pile, it is not thought that the ALICIA analyzer is the cause of the observed strian difference.

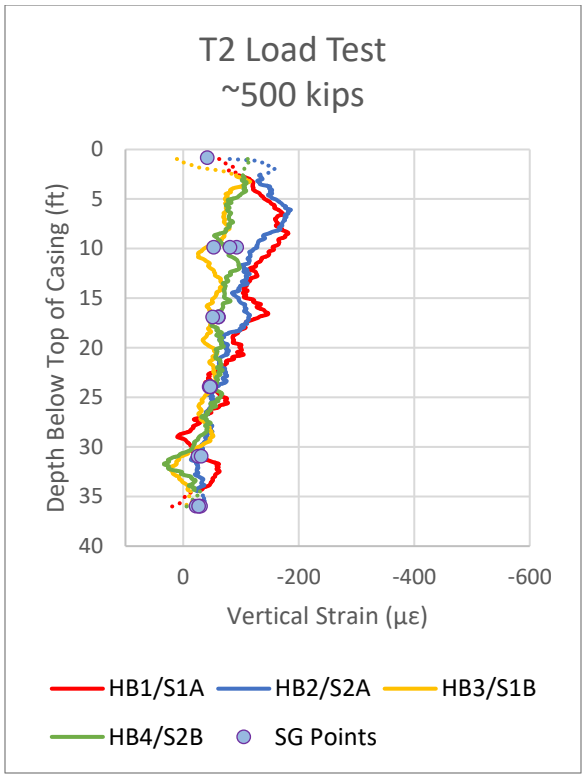

Figure 4-158: Vertical strain profile at ~500 kips load

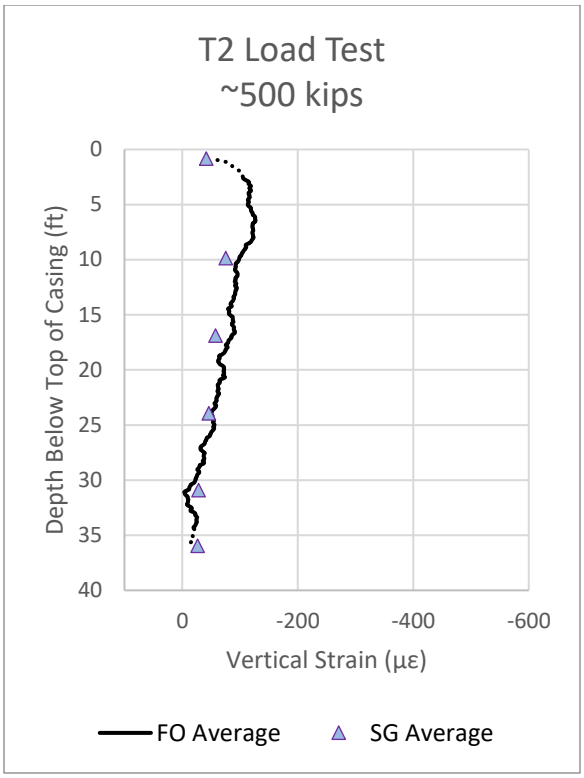

Figure 4-159: Average strain profile at ~500 kips load

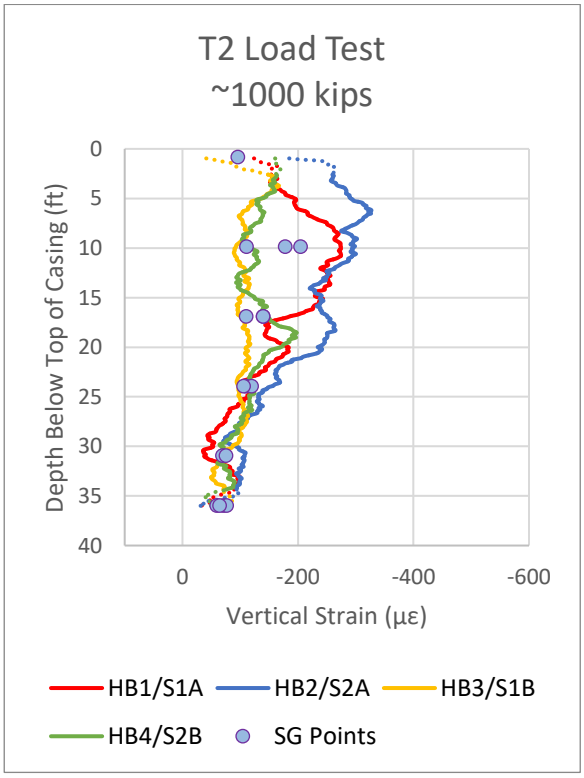

Figure 4-160: Vertical strain profile at ~1000 kips load

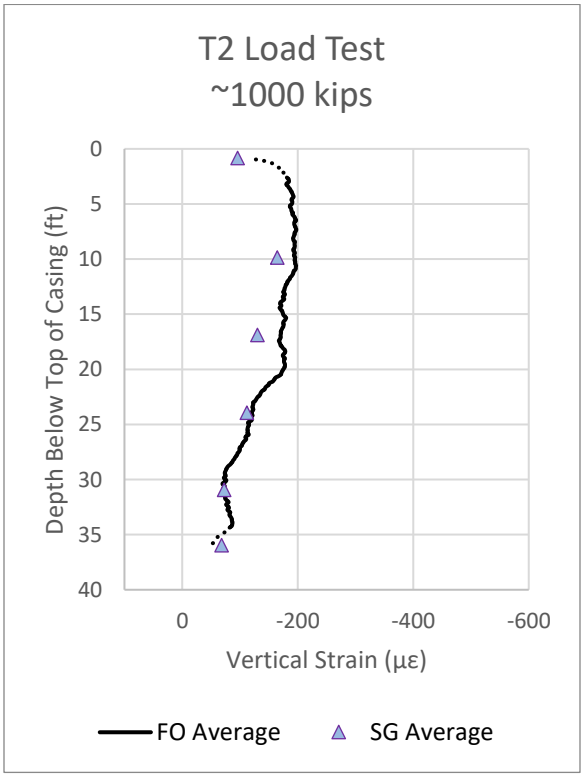

Figure 4-161: Average strain profile at ~1000 kips load

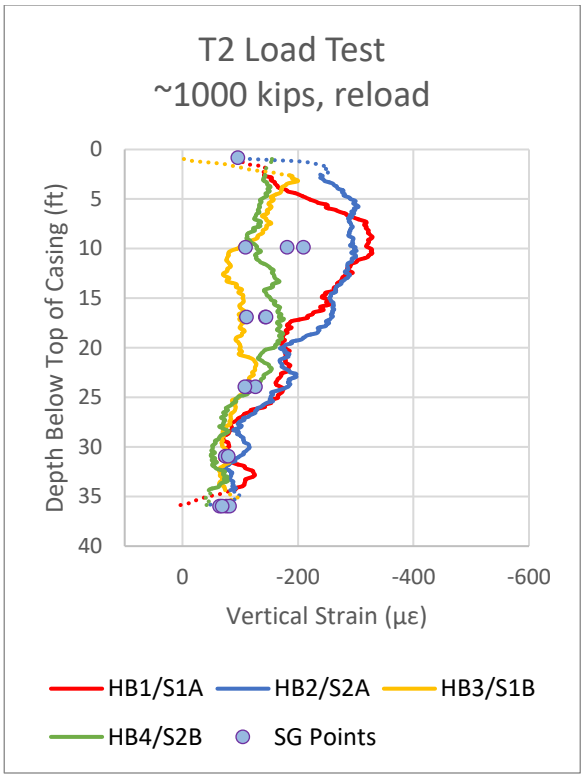

Figure 4-162: Vertical strain profile at ~1000 kips reload

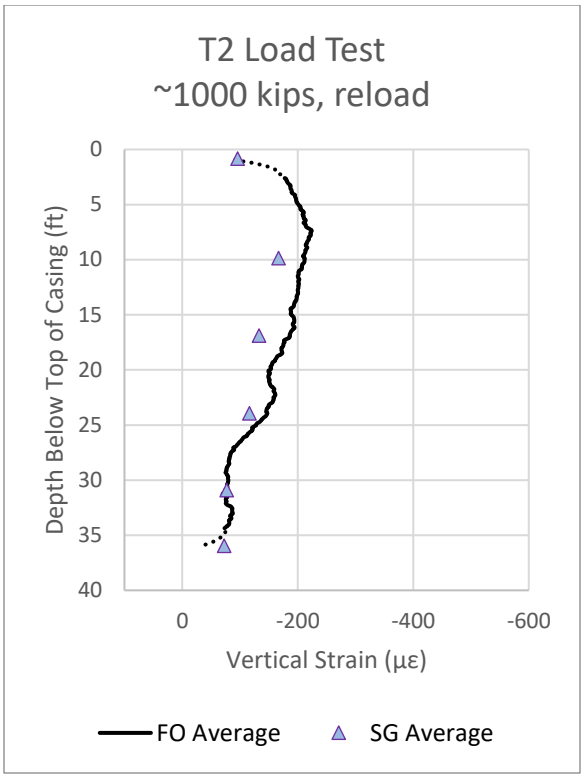

Figure 4-163: Average strain profile at ~1000 kips reload

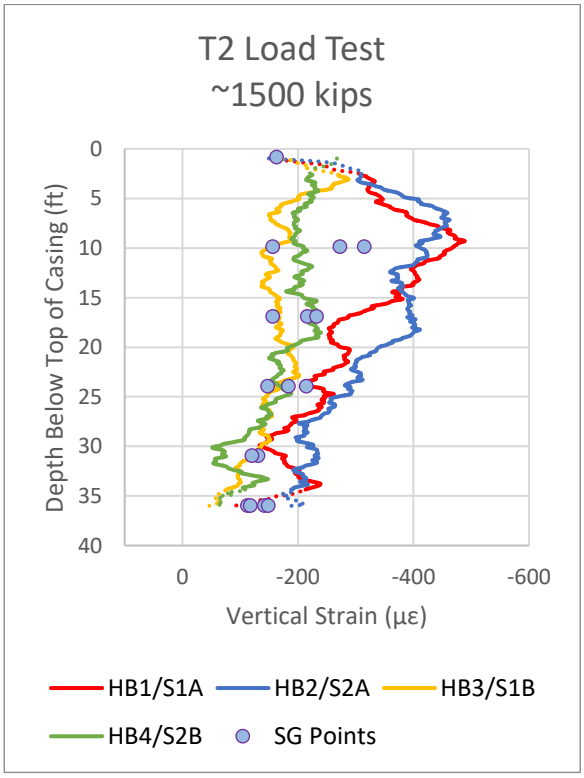

Figure 4-164: Vertical strain profile at ~1500 kips load

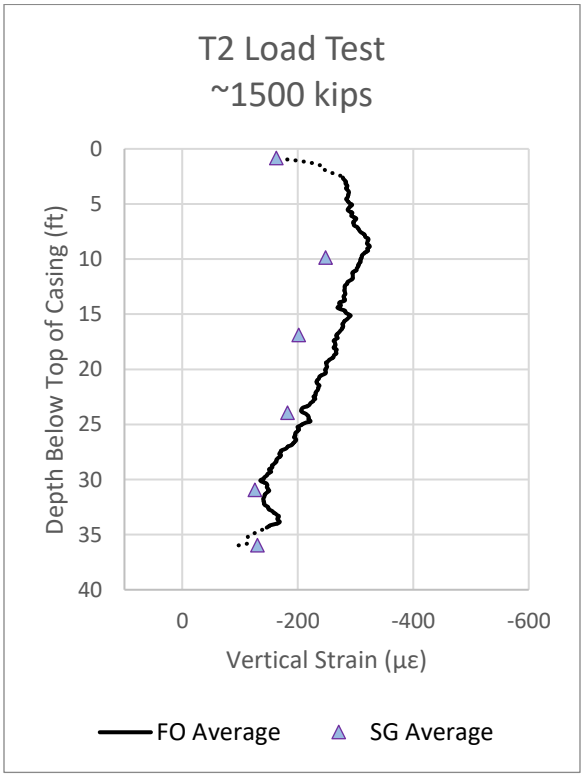

Figure 4-165: Average strain profile at ~1500 kips load

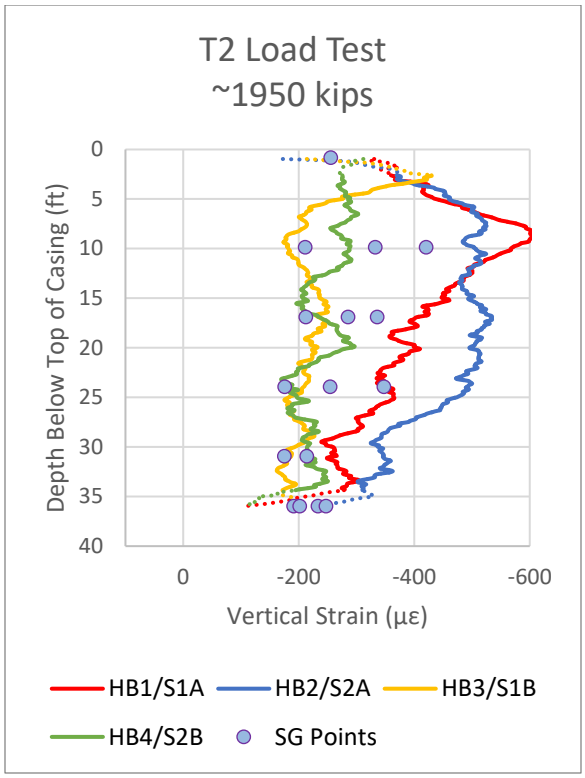

Figure 4-166: Vertical strain profile at ~1950 kips load

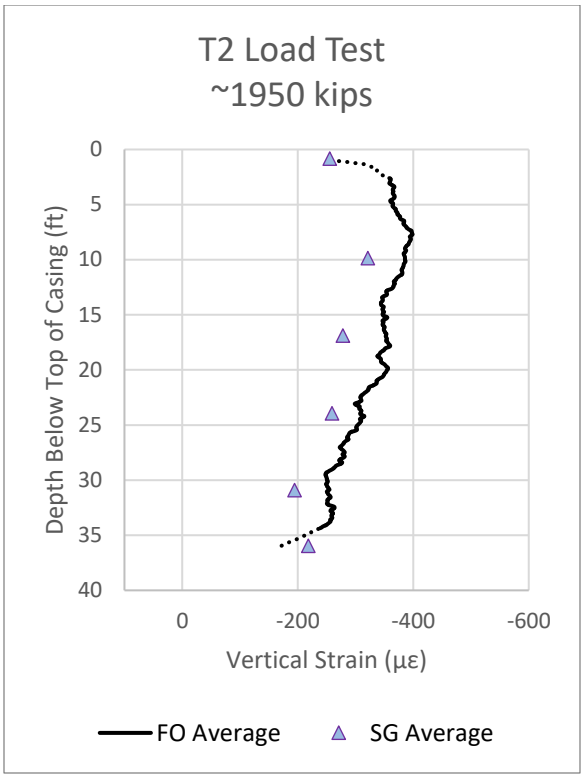

Figure 4-167: Average strain profile at ~1950 kips load

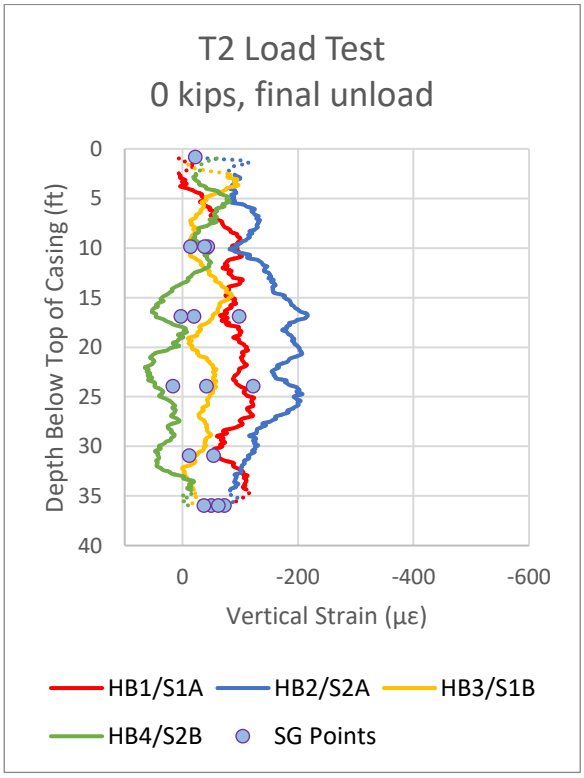

Figure 4-168: Vertical strain profile at 0 kips unload

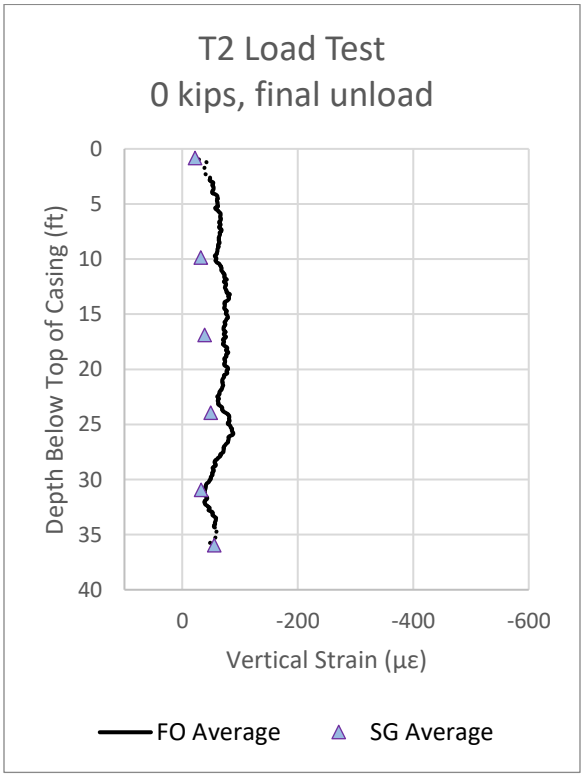

Figure 4-169: Average strain profile at 0 kips unload

c) Pile T3, Open-Type (tube-à-manchette)

The strain measurement results for the distributed fiber optic system and the SGs in pile T3 are presented in Figure 4-170 to Figure 7-36. Similar to the results from T1 and T2, the SG readings are approximately enveloped by the four fiber optic verticals. The range of strain magnitudes at each reading elevation between the two measurement systems are relatively similar, a trend most apparent at the peak load of ~2027 kips shown in Figure 4-178. Looking at the figures comparing the average strain with depth between the two systems, there is close agreement in both the magnitude and shape of the strain profile between the two systems. The maximum difference between the caluclated averages was approximately 20 με, observed in the final profile in Figure 4-181 at ~700 kips during the unload just prior to the fiber optic cable being severed.

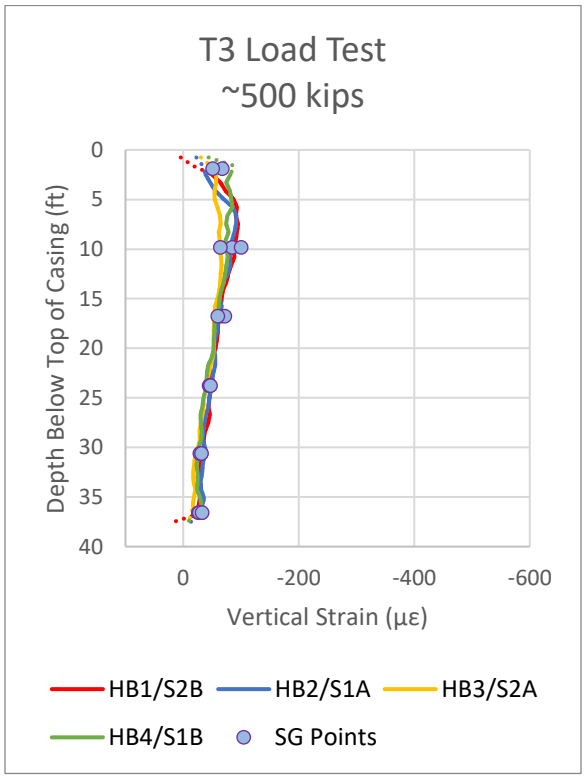

Figure 4-170: Vertical strain profile at ~500 kips load

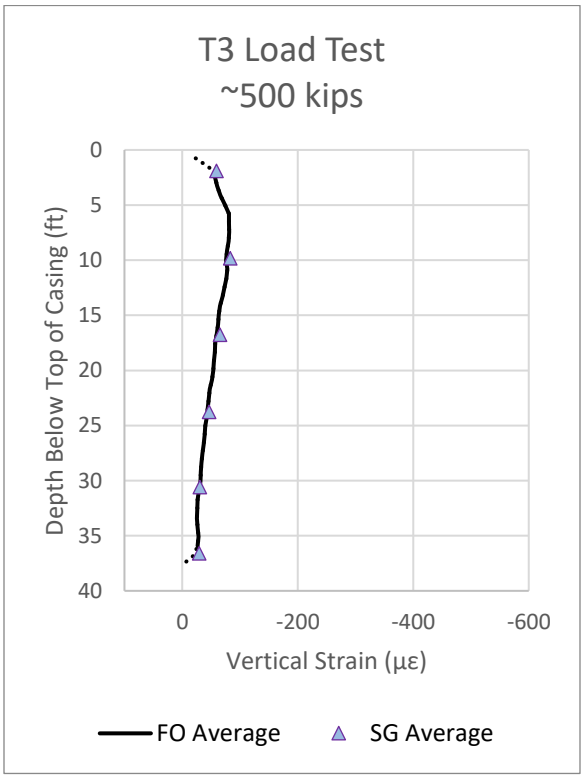

Figure 4-171: Average strain profile at ~500 kips load

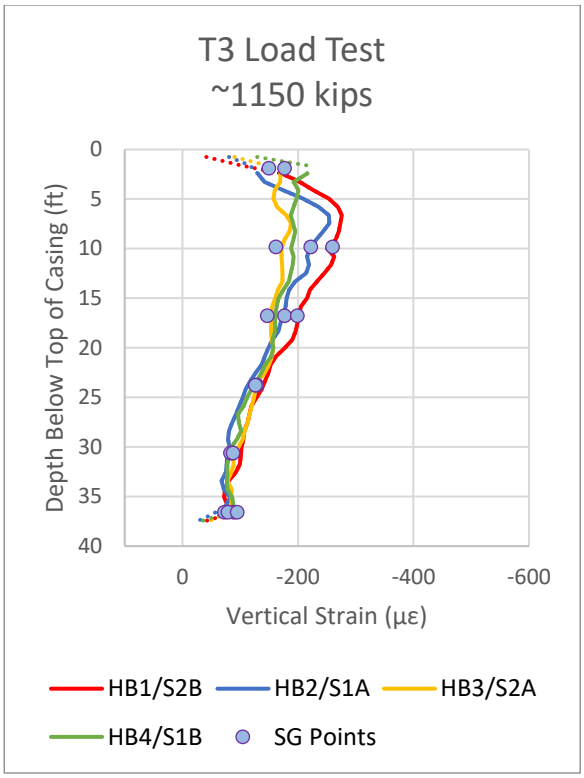

Figure 4-172: Vertical strain profile at ~1150 kips load

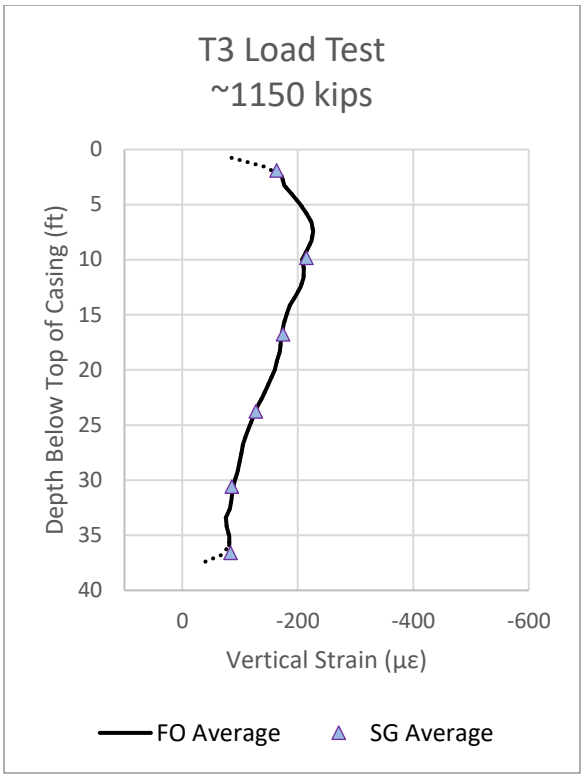

Figure 4-173: Average strain profile at ~1150 kips load

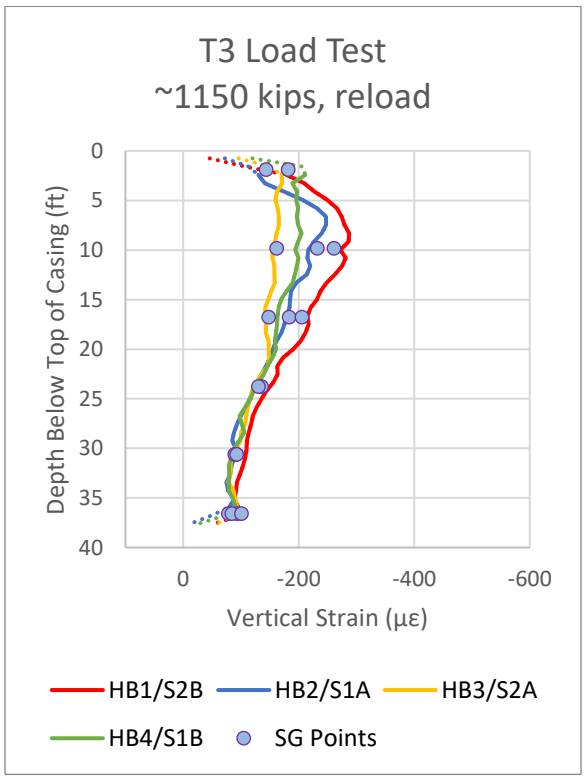

Figure 4-174: Vertical strain profile at ~1150 kips reload

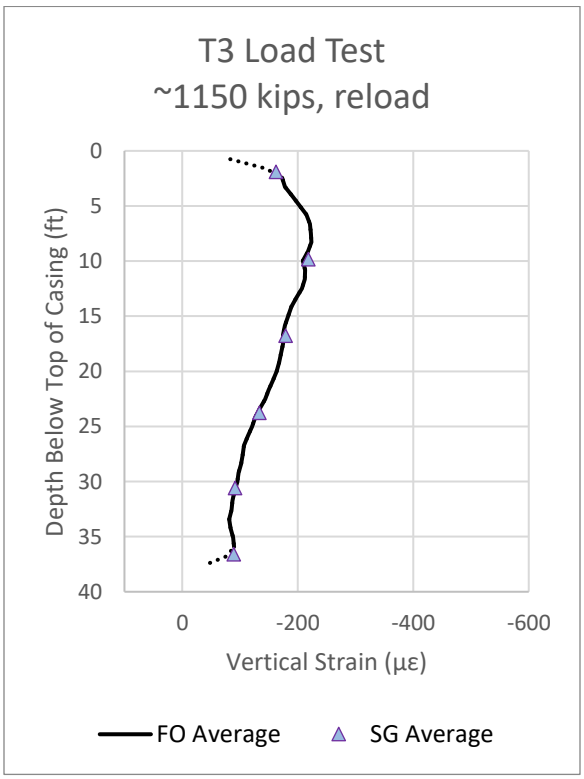

Figure 4-175: Average strain profile at ~1150 kips reload

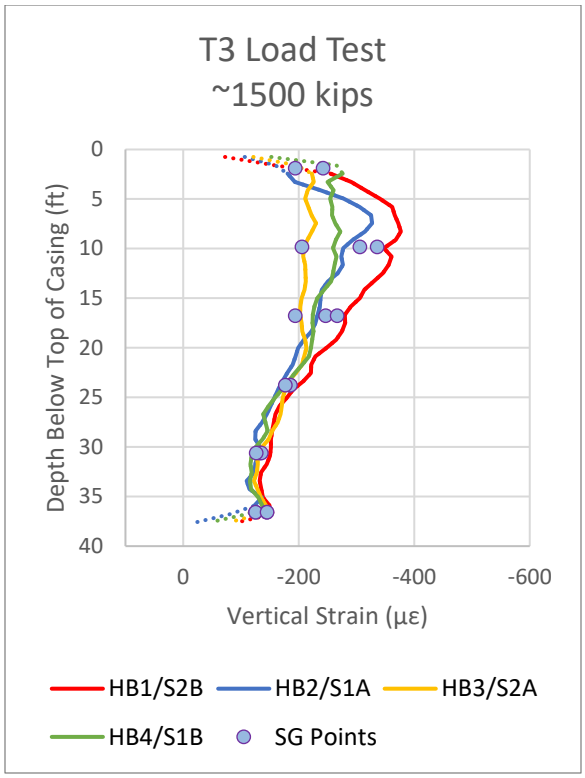

Figure 4-176: Vertical strain profile at ~1500 kips load

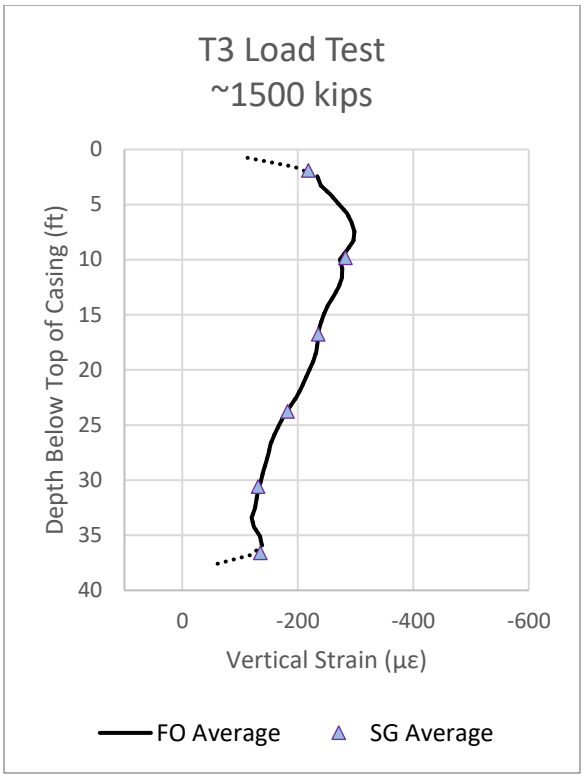

Figure 4-177: Average strain profile at ~1500 kips load

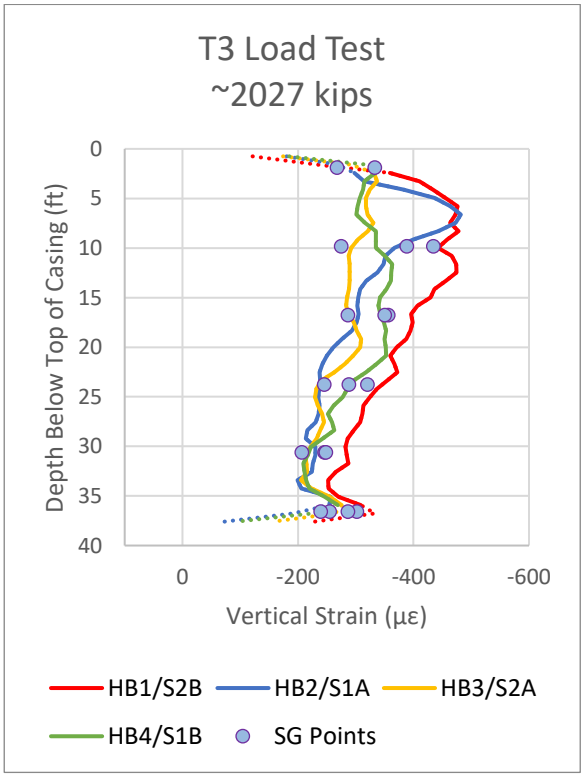

Figure 4-178: Vertical strain profile at ~2027 kips load

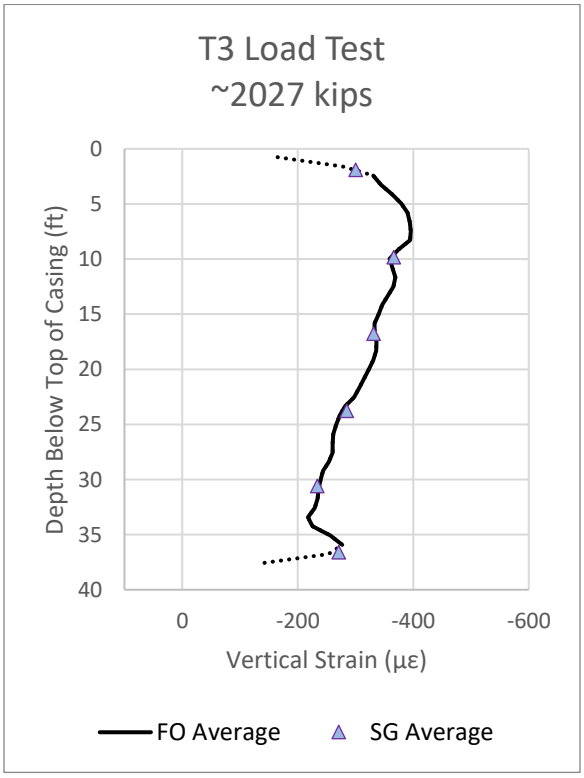

Figure 4-179: Average strain profile at ~2027 kips load

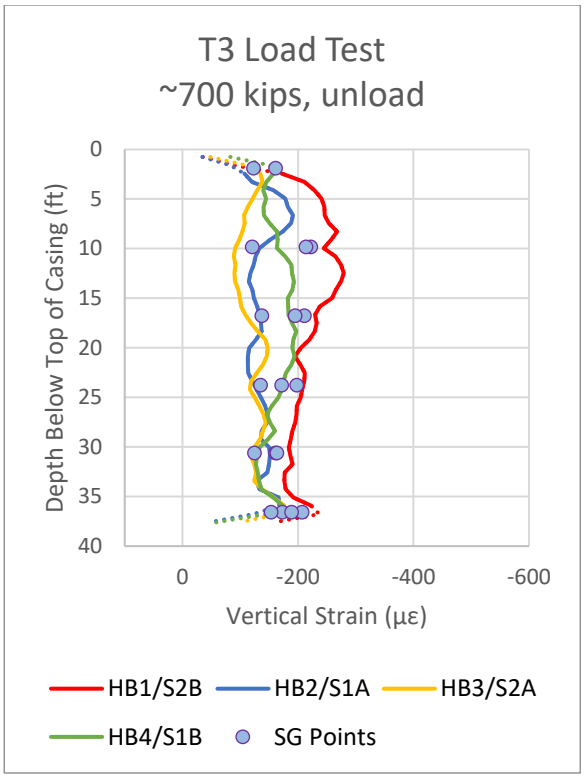

Figure 4-180: Vertical strain profile at 0 kips unload

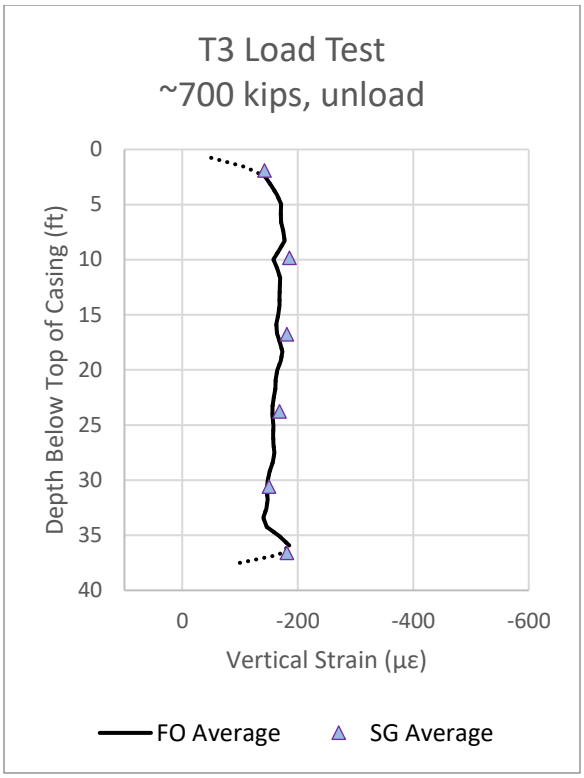

Figure 4-181: Average strain profile at 0 kips unload

d) Pile T4, Closed-Type (bladder)

The strain measurement results for the distributed fiber optic system and the SGs in pile T4 are presented in Figure 4-182 to Figure 7-48. As with the other test piles, the range of the individual SG readings are approximately enveloped by the fiber optic verticals. A small deviation is observed at the 10- and 17-foot levels, where the lowest SG magnitude is consistently lower than the corresponding lowest fiber optic reading. This slight shift, as well as the peak SG values at the same levels consistently being below the peak in the fiber optic data, may explain the sight difference observed at the same depths in the average strain profiles between the SG and

fiber optic data. A maximum difference in the two average strains of 46 με was observed at the peak load of ~1750 kips, shown in Figure 4-191.

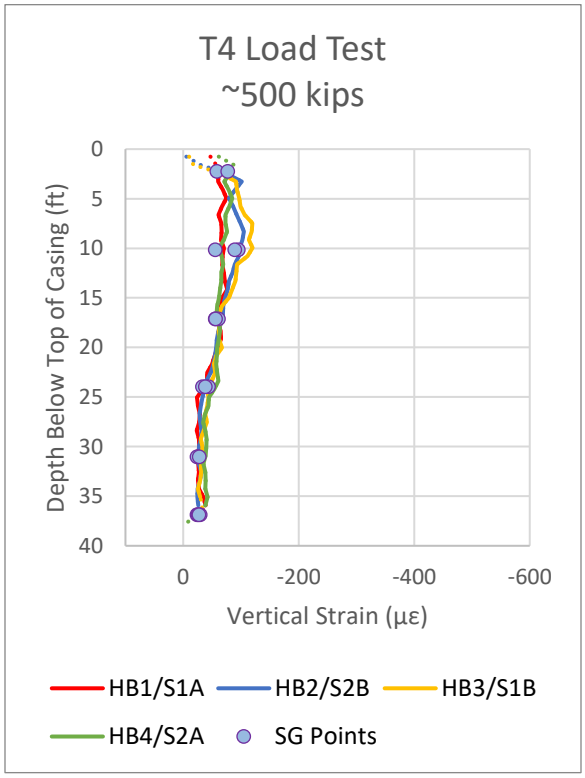

Figure 4-182: Vertical strain profile at ~500 kips load

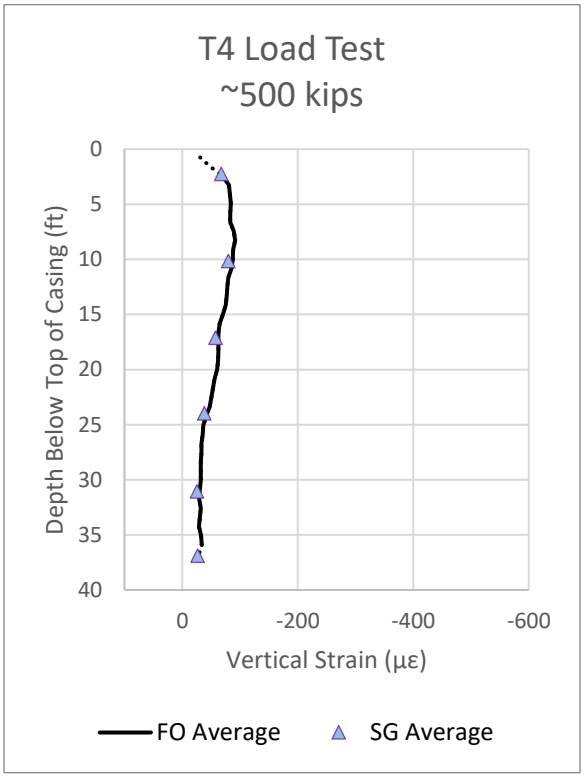

Figure 4-183: Average strain profile at ~500 kips load

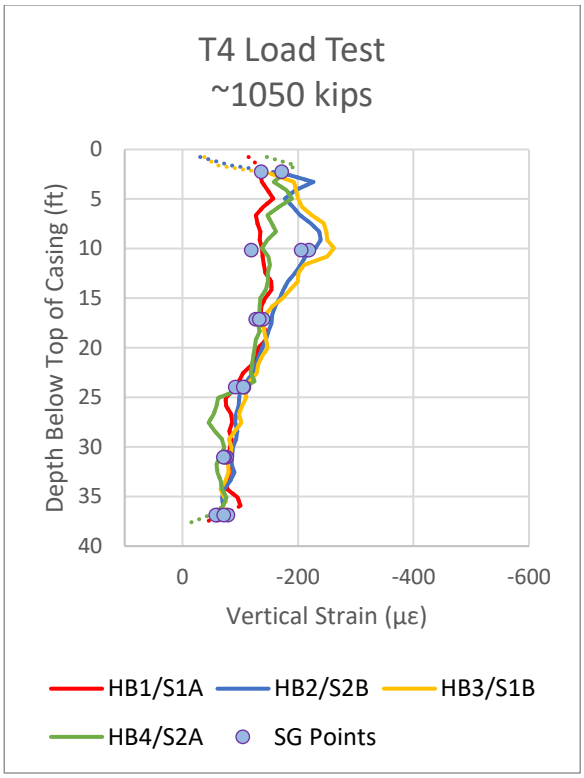

Figure 4-184: Vertical strain profile at ~1050 kips load

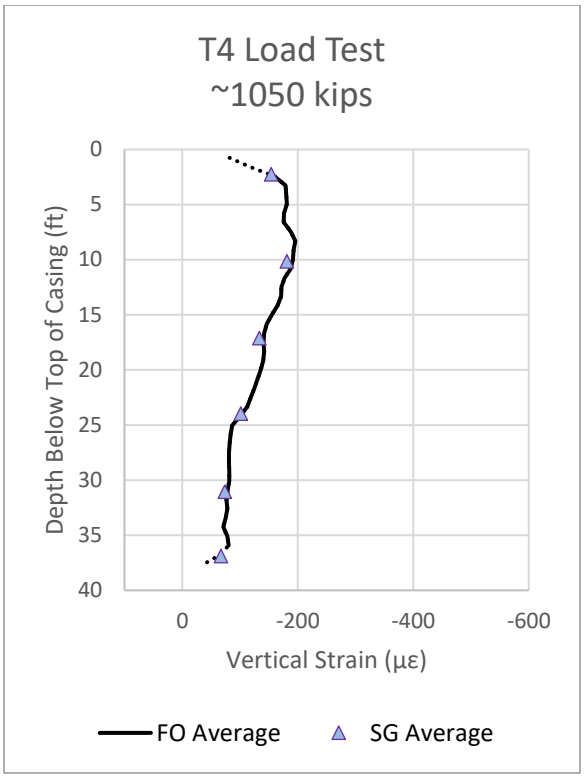

Figure 4-185: Average strain profile at ~1050 kips load

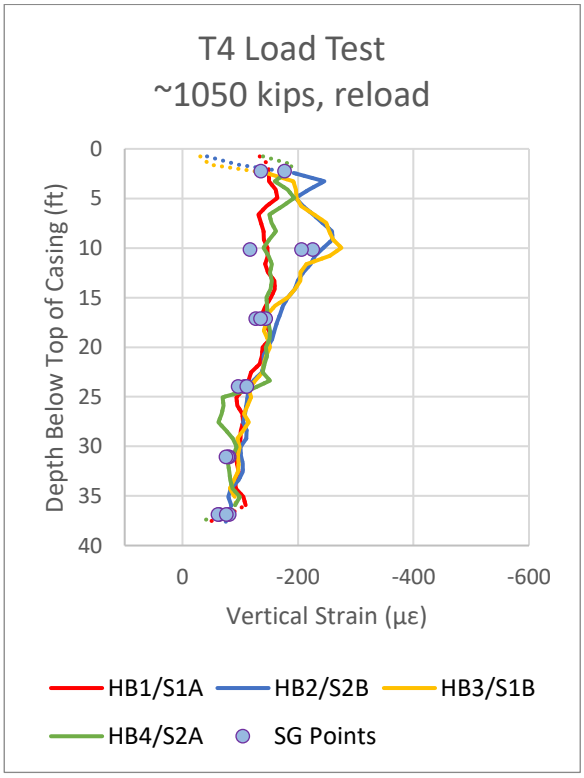

Figure 4-186: Vertical strain profile at ~1050 kips reload

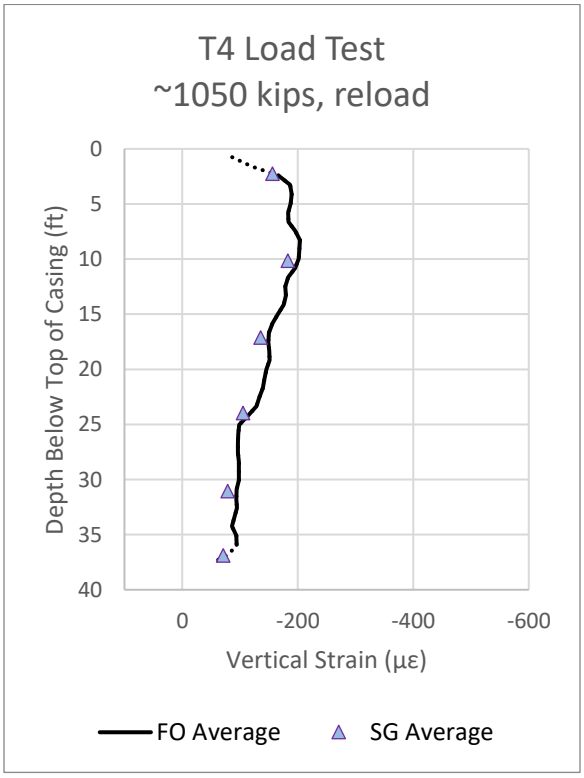

Figure 4-187: Average strain profile at ~1050 kips reload

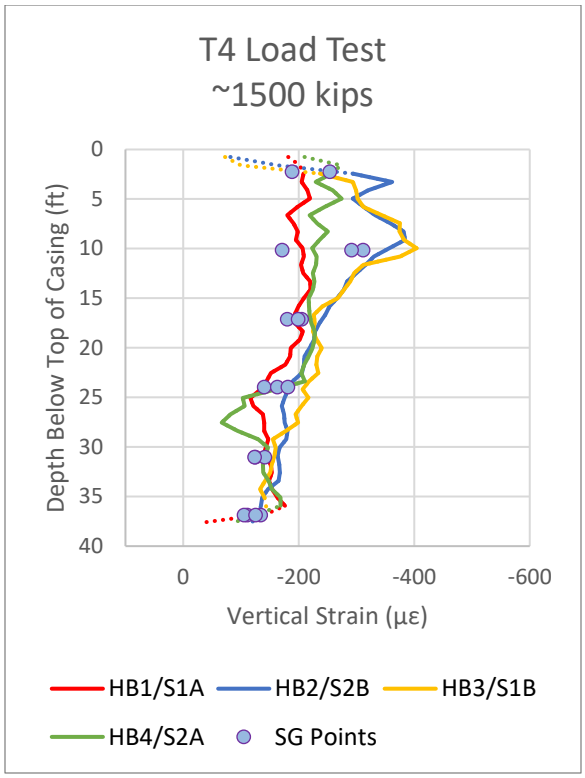

Figure 4-188: Vertical strain profile at ~1500 kips load

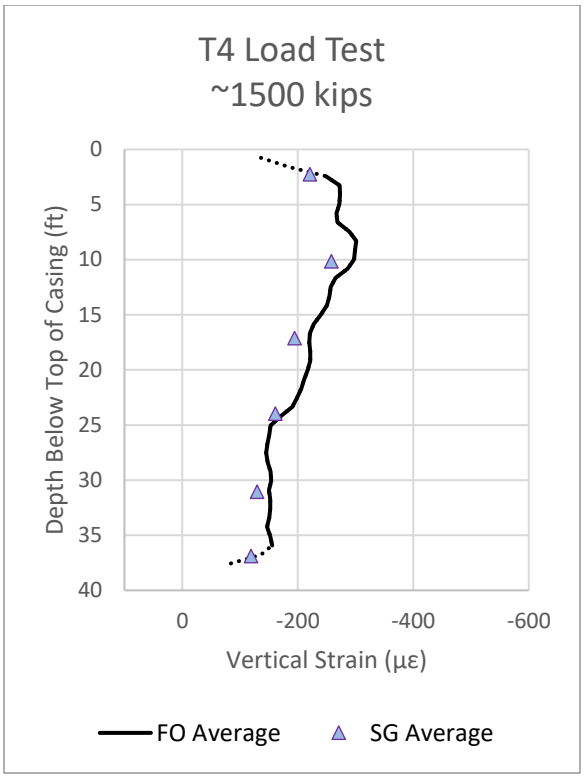

Figure 4-189: Average strain profile at ~1500 kips load

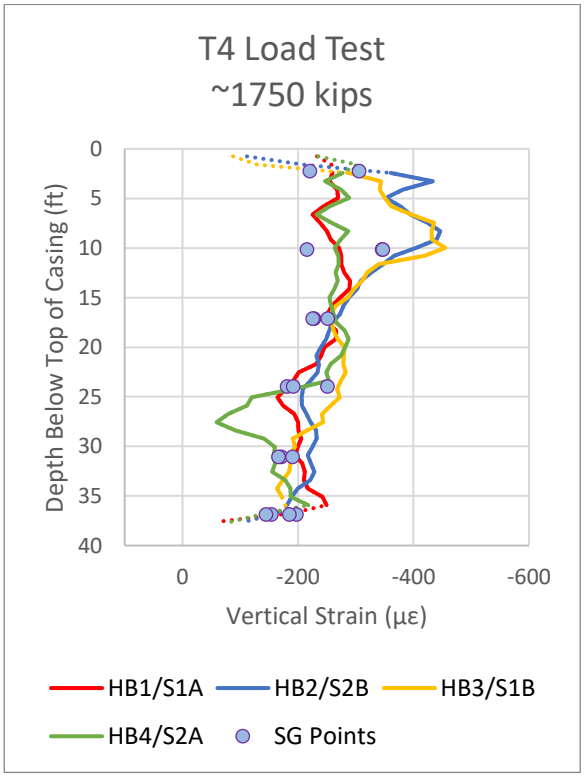

Figure 4-190: Vertical strain profile at ~1750 kips load

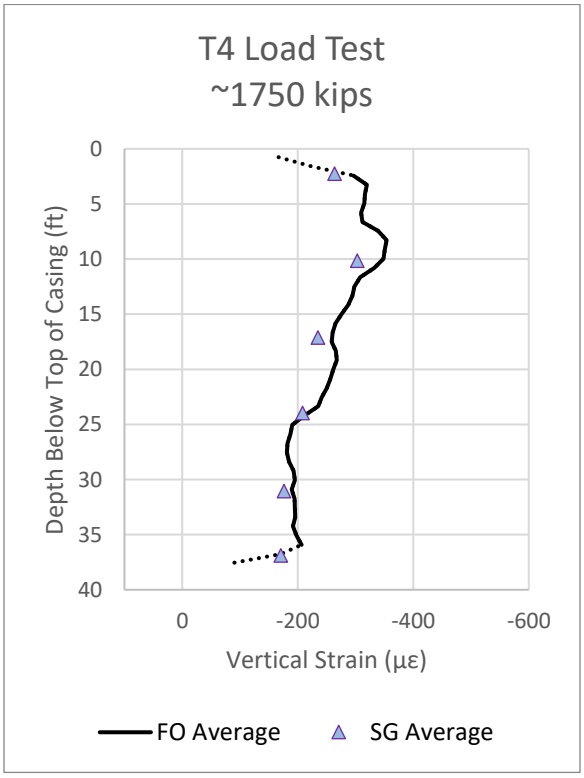

Figure 4-191: Average strain profile at ~1750 kips load

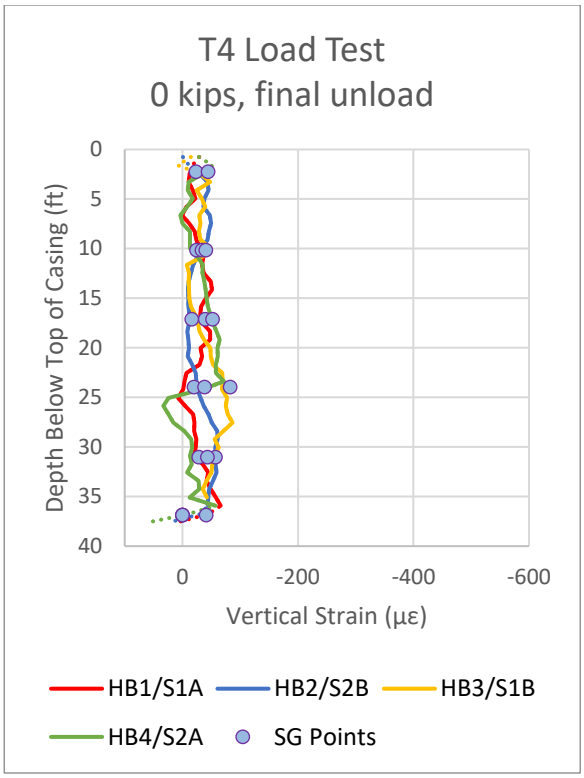

Figure 4-192: Vertical strain profile at 0 kips unload

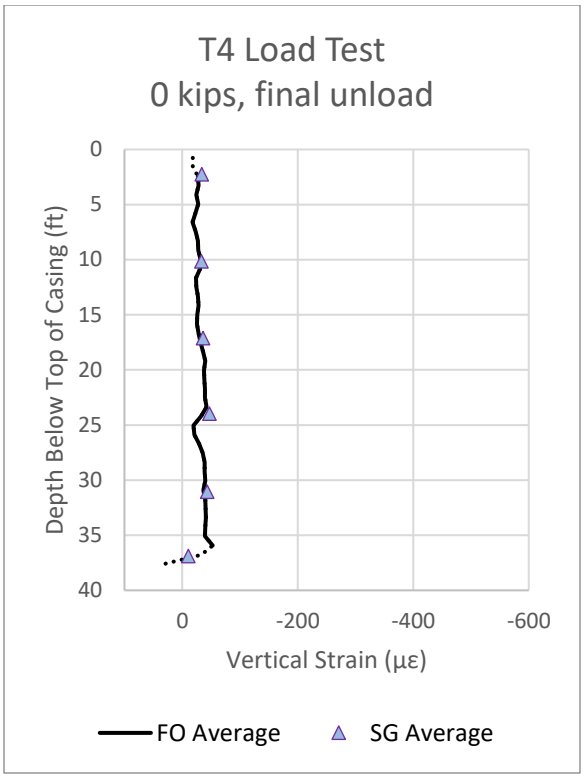

Figure 4-193: Average strain profile at 0 kips unload

Reviewing the strain comparison over the four test shaft load results, the strain measurements produced by the distributed fiber optic system were comparable to the conventional vibrating wire strain gauges. Differences in individual readings can be partially explained by the difference in placement within the pile at each elevation, an effect exacerbated by the non-uniform strain profiles associated with potential bending in the top portions of the piles. Nevertheless, the fiber optic strain profiles bracketed the individual strain gauge readings in the evaluated load intervals. The agreement between the two systems is even stronger when comparing the average profiles, which removes the effect of the non-overlapping installation locations of the vibrating wire strain gauges with the fiber optic verticals. The differences for the 18 evaluated strain profiles using the Omnisens commercial analyzer (T1, T2, T4) are plotted in a histogram in Figure 4-194.

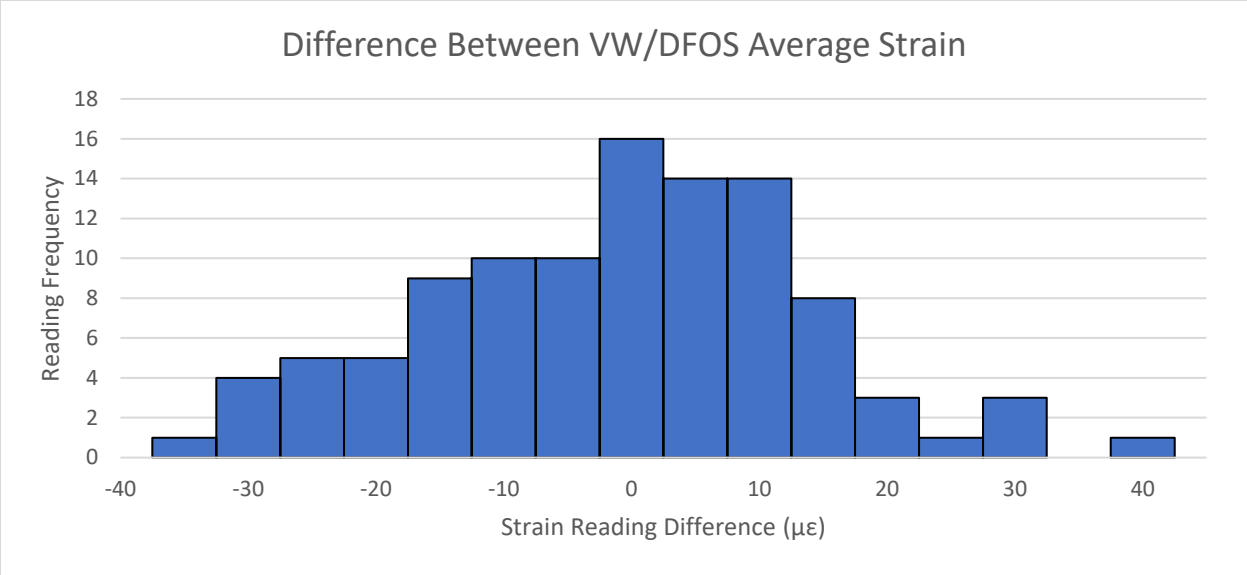

Figure 4-194: Strain reading differences in average profiles during load testing between Omnisens strain profiles and corresponding vibrating wire strain gauges

The mean difference between the strain readings at corresponding elevations between the two systems is 2 με with a standard deviation of 19 με. The near-zero mean difference between the two systems indicates that the strain measurements of the fiber optic system are equal to those of the conventional vibrating wires strain gauges. The observed standard deviation is within the published statistical distribution of the Omnisens analyzer of +/- 25 με in BOTDA mode. This indicates a positive test result for the original hypothesis – indicating that the strain measurements of fiber optic cables are valid when fully encapsulated in concrete, without the need for additional pretension during installation.

Hypothesis 2: DFOS Strain Profiles and Outlier Evaluation

The second hypothesis of the research project is that distributed fiber optic strain profiles allow for a more complete understanding of strain variation in the pile with depth, enabling accurate assessment of measurement validity. Installation of 3 or 4 strain verticals fibers also allows reconciliation of non-uniform strain across the pile and calculation of any bending forces observed. The test for this is an evaluation of a vibrating wire strain gauge measurement set that was identified as instrument error and was originally discarded. A negative test result would be if the fiber optic strain profile does not provide any additional information to evaluate the validity of the questionable reading. A positive test result would be if the fiber optic strain profile provides additional information to evaluate the validity of the questionable reading.

Non-uniform strains were observed across many of the observed piles during grouting and load testing. This variation was observed in both the vibrating wire strain gauge measurements as well as the DFOS strain profiles. As is the common approach, the discrete strain gauge measurements were averaged at each level and most of the analysis was based upon the average strain for each measurement elevation. While non-uniform loading of the pile is not

unexpected during post grouting and was observed in the open- and closed-type delivery systems, special care was taken during the pile preparation and seating during the load test process to ensure the applied load was uniform. This preparation included cutting the pile and casing level, as determined by survey, as well as placement of a sand bed and steel loading plate to equally distribute the load on the pile. A photo of the sand bed preparation is shown in Figure 4-195.

Figure 4-195: Sand bed preparation of test pile prior to load test

Due to the attention and effort in preparing and seating the loading jacks to be uniform and perpendicular to the pile face, the applied load was assumed to be aligned with the pile. This assumption is consistent with the standard approach of top-down pile load tests, with best practices dictating a similar level of care and preparation in aligning the applied load with the pile. Large strain variations across the pile are therefore not expected, and strain measurements are often evaluated for validity based on this implicit understanding.

During the initial processing of the vibrating wire strain gauge data from the load test, the researchers managing the conventional monitoring program identified a sensor in pile T1 that was suspected of providing inaccurate data due to a potential malfunction. The suspect sensor showed deviation from the other two sensors installed at that elevation, with the deviation increasing to the highest magnitude at the maximum load interval of 1750 kips. The strain gauge data and average are shown with the outlier included in Figure 4-196 and with the outlier removed in Figure 4-197.

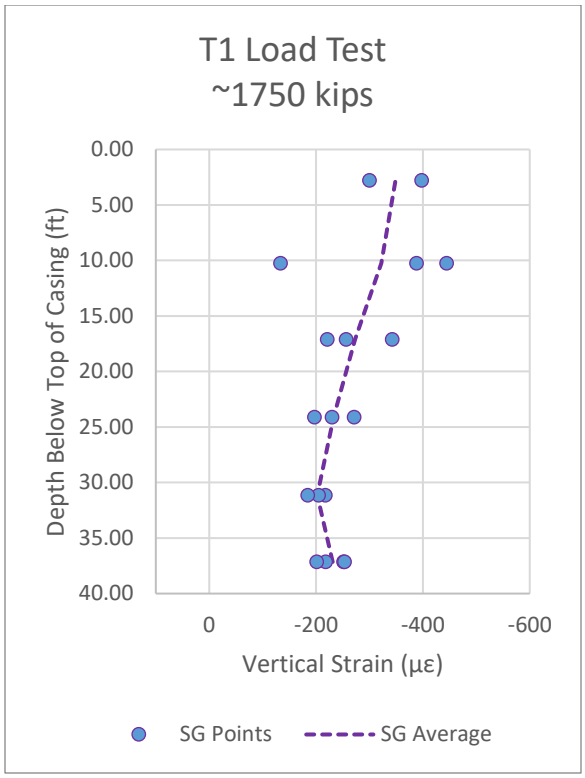

Figure 4-196: SG strain profile with outlier

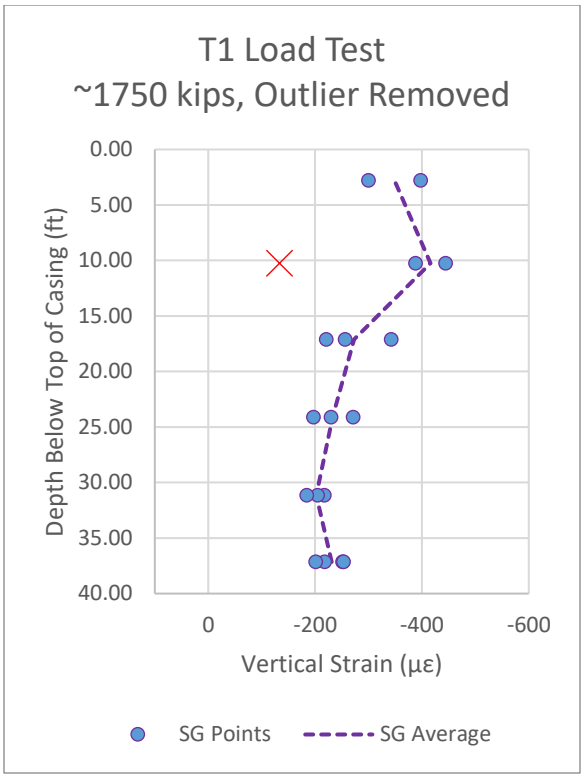

Figure 4-197: SG strain profile without outlier

As can be seen in Figure 4-196, a single sensor at approximately 10 feet below the top of casing is registering a strain of less than half the other two sensors at that level. On this basis, it was proposed that the sensor had failed, and that processing of the load testing strain measurements should proceed with that sensor being omitted from the data set. The result of this reprocessing is shown in Figure 4-197.

The fiber optic strain profiles for the same load interval are shown in Figure 4-198.

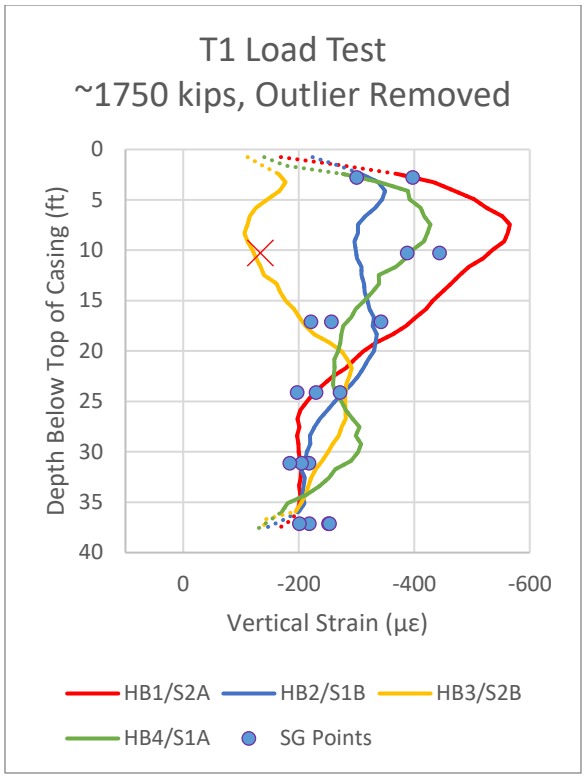

Figure 4-198: Potential strain gauge outlier and corresponding fiber optic strain profiles

Figure 4-198 shows that the potential outlier at 10 feet plots almost directly upon the HB3 fiber optic strain vertical profile. This confirmed the validity of the measurements of this sensor, as well as provided context to the overall strain behavior in the pile. The strain distribution in Figure 4-198 indicates a bending moment in the pile has been introduced during the top-down loading, with a central line approximately between HB2 and HB4.

The strain due to bending in the pile, $\varepsilon_{bending}$, has a maximum value of 230 με at 8.3 feet below the top of casing. Potential causes such as inclination of either the applied load or the installed pile were ruled unlikely causes due to the care in the seating of the load apparatus and verticality measurements of the pile taken during installation. An additional potential cause of the bending is eccentricity between the 42-inch-diameter cased upper portion of the pile and the smaller 36-inch-diameter bored section of pile below. A cross section of this is shown in Figure 4-199.

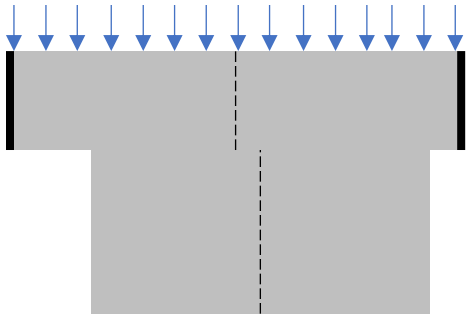

Figure 4-199: Diagram showing potential offset between cased and uncased pile sections in T1

Under the maximum load of 1750 kips, an offset of 2.6-inches between the cased and uncased portion of the pile would be enough to induce the bending strains observed. This is within the construction tolerances and practices observed on the site, where the center line of the uncased pile was controlled by survey, but the starter casing was roughly placed using an excavator and forklift prior to the start of drilling.

This case shows the value of the continuous strain profiles generated by the DFOS monitoring in evaluating potential outliers and understanding the real, non-idealized behavior of the pile during loading. It is within the standard practice of load test monitoring and analysis to evaluate and discard outlier or erroneous data based on an idealized expectation of the pile behavior under loading. In this case, the standard deviation of the strain gauge spread at all elevations at 1750 kips was 62.7 με. The outlier point is 188.3 με below the (inclusive) strain average at the 10-foot reading level, or 3.0 standard deviations. Standard statistical outlier detection methods based on intervals of standard deviation away from the mean would support the identification of this sensor as an outlier. The result of this would be overestimating the average strain at 10 feet by 30% - increasing from 321 με with the outlier included to 416 με with the outlier omitted. In the processing of the load test results, this would lead to an overestimation of the frictional soil capacity in the 10- to 17-foot strain interval, in addition to missing the real behavior of the pile under the eccentric load.

This analysis provides a positive result for the hypothesis that the continuous strain profiles provided by DFOS measurements allow for a more complete understanding of strain variation in the pile with depth, resulting in a more accurate assessment of measurement validity. Absent the fiber optic records, it is likely that the low strain reading at 10-feet would have been discarded as invalid during evaluation of the strain data. However, the distributed strain readings of the fiber optic system show that this strain readings is valid and should be included in any subsequent evaluation of the pile load test. A 2-vertical fiber optic strain monitoring design would not necessarily have allowed the outlier to be evaluated and the bending of the pile to be recognized and quantified. The inclusion of 4 fiber optic strain vertical cables resulted in a more accurate evaluation of the average strain within the pile at the outlier level, as well as showing the non-idealized bending behavior of the pile under the vertical loading of the load test.

Hypothesis 3: Correction of Variable Strain Effect on Fiber Optic Readings

The third hypothesis of the research project is that the architecture of the commercial fiber optic analyzer has a quantifiable effect on the processed strain output when the strain along the sensing cable is changing during the reading interval. The test for this is to analyze and quantify the difference between the uncorrected output from the analyzer with one with a temporal correction applied. A negative test result would be that the two data sets do not vary significantly. A positive test result would be that the corrected data set varies significantly from the uncorrected data set.

Based on the lab testing in Chapter 3 and the understanding that the load in the piles were not constant throughout the fiber optic reading intervals (apart from ALICIA) during base grouting and the load tests, the fiber optic strain profiles presented in this chapter represent a temporal sampling of the strains in the pile during the approximate five-minute reading. The reading architecture used in the commercial Omnisens analyzer “sweeps” the range of frequencies within the reading window, from lowest to highest. Where each frequency peak along the fiber falls within the scan determines the specific time within the reading that the strain at that point is registered.

The temporal effect is proportional to the magnitude of the strain variation during the reading. As such, the highest load increment during load testing was chosen for analysis. This corresponds to the peak load of 2027 kips applied during the load test of test shaft T3. Using the load cell data at the top of the pile, recorded every 5-6 seconds, the fiber optic strain readings can be approximately corrected to a single point in time and associated load. This process quantifies the effect of the analyzer architecture on the resulting strain profile. The approach requires adopting the assumption that the strains within the length of the pile are linearly dependent on the applied load in the analysis period. While this assumption is not strictly valid for all load cases, it forms an upper limit for the potential shift in strain resulting from the load decay during the hold period.

During each hold period during the load test of T3, a single fiber optic reading was taken, taking on average just under 5 minutes. During this time, the load applied to the pile would decay from its initial peak as the pressure in the actuators gradually reduced (the reduction is understood to be attributed partially to pressure losses within the system, as well as the vertical movement of the pile head away from the reaction frame under higher loads). In the peak load interval for T3, the fiber optic reading started at a maximum registered load of 2027.7 kips. During the 294.7 seconds to complete the fiber optic reading, the measured load dropped 7% to 1885.7 kips. The load decay curve, as well as the start and stop of the fiber optic reading, is shown in Figure 4-200.

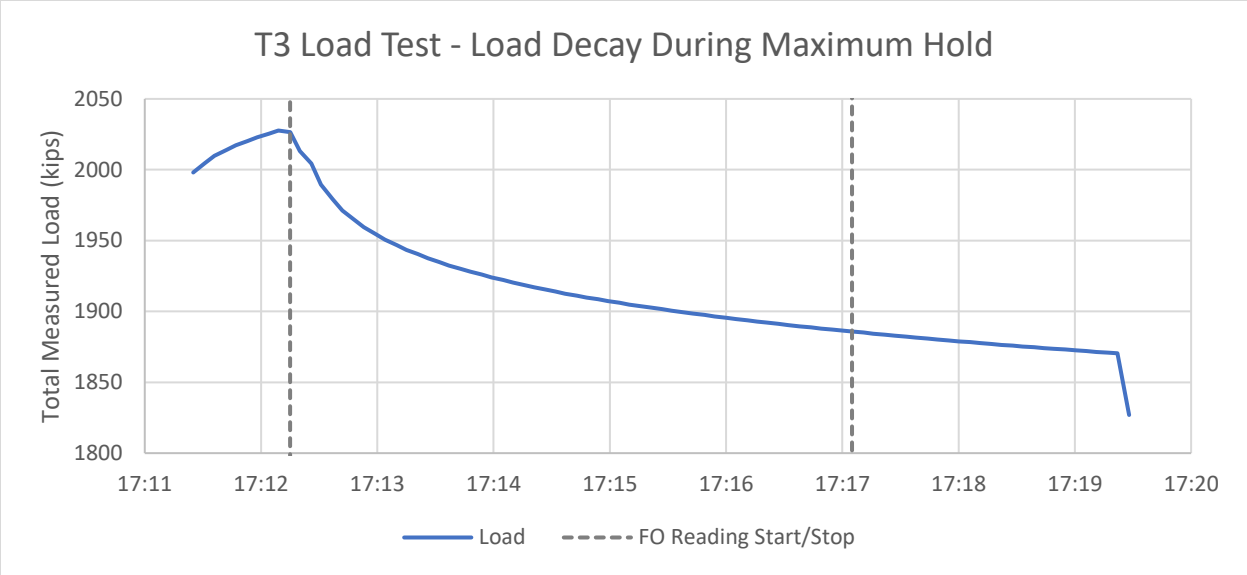

Figure 4-200: Load decay during peak interval in T3 load test

The start and stop of the fiber optic reading are shown in Figure 4-200. As can be seen, the reading started just following the peak load after the load test operator reported that they had stopped adding pressure to the actuators.

The raw frequency profile of the 2027 kip fiber optic reading is shown in Figure 4-201. The lower and upper scanning frequency bounds, set within the analyzer configuration, are shown in dashed black lines at 10.7 GHz and 11.1 GHz, respectively.

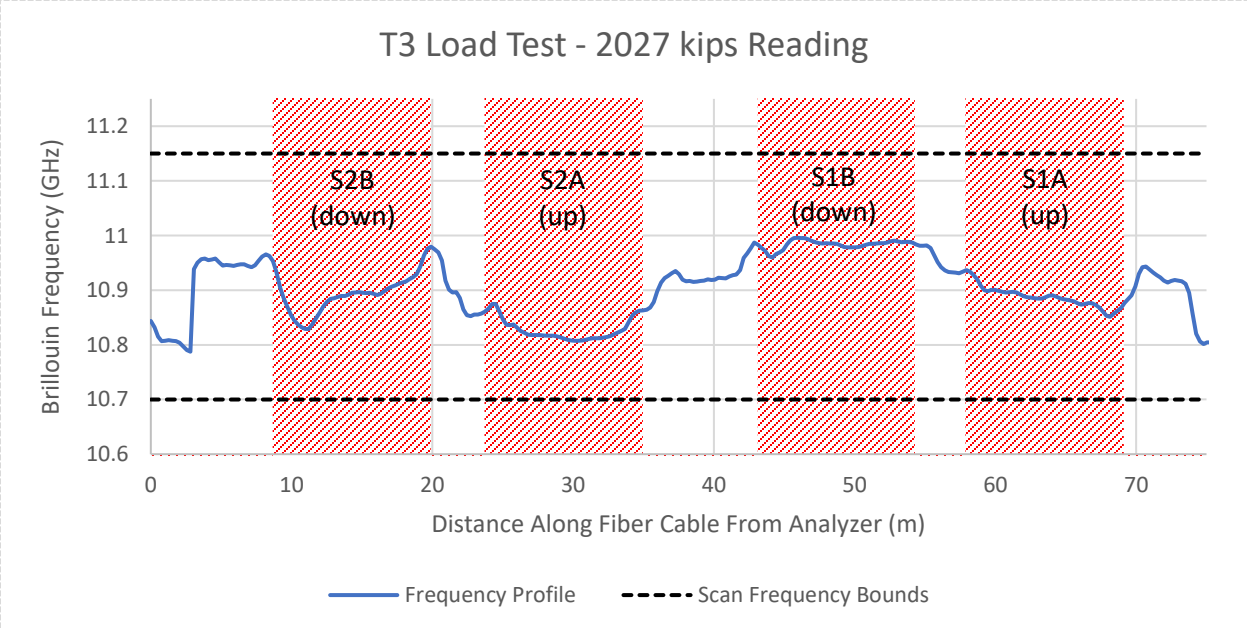

Figure 4-201: Raw frequency profile of 2027 kip fiber optic strain reading

Using the baseline readings taken prior to the start of the load test and the calibration factors for the strain cable, the frequency profile above can be processed into four individual strain profiles with depth. This was originally presented in Figure 4-134 and is reproduced as Figure 4-202.

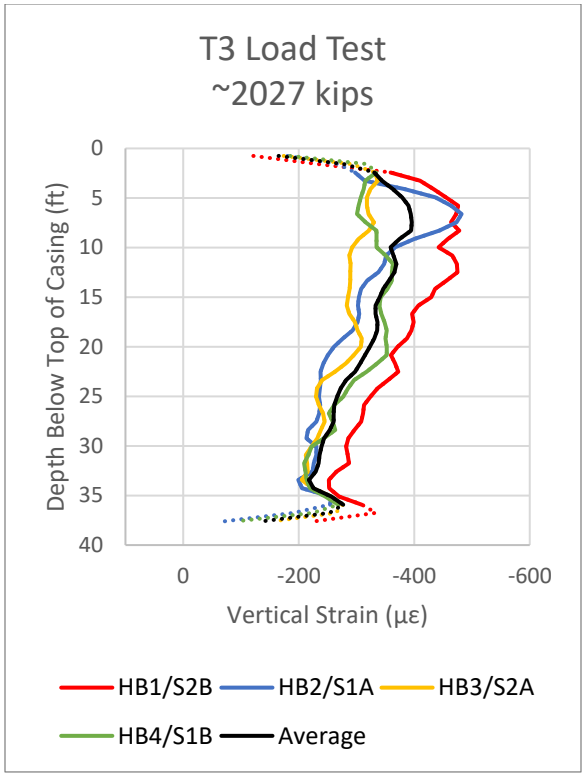

Figure 4-202: T3 load test vertical strain with depth at maximum applied load (uncorrected)

Within the configuration of the analyzer, a frequency step for the reading was set at 0.0005 GHz (0.5 MHz). Between the bottom and top frequency, this means that 901 individual frequency scans were taken during the reading. Dividing the recorded reading time of 294.699 seconds by the number of steps, 3.057 steps were completed each second, with a corresponding shift in frequency of 0.0015 GHz/second. Using this frequency rate, the approximate scan frequency that the analyzer was reading for each second of the total read time can be calculated. Inverting this approach and applying it to the raw frequency profile of the strain reading, the nearest second when each measurement point within the pile was interrogated during the total reading was estimated. The scan time of each strain measurement point within the pile is shown in Figure 4-203.

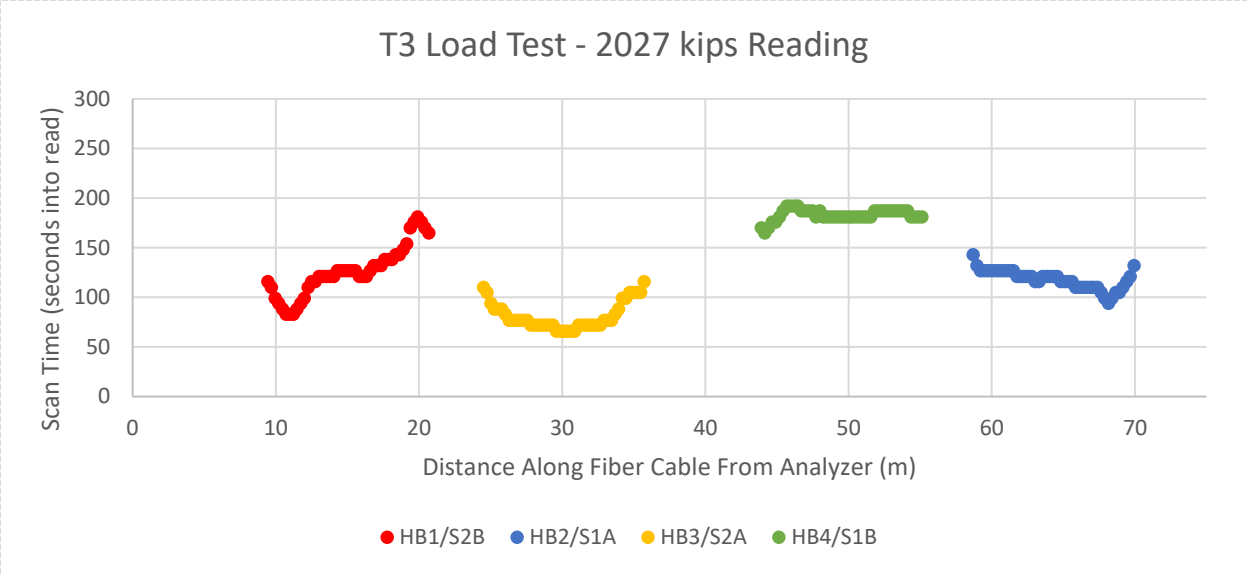

Figure 4-203: Scan time of each reading point within the 4 strain verticals

As shown in Figure 4-203, there was not only variation in the time when the individual measurements were taken during the total scan, both within and between the individual strain verticals; the first strain measurement did not take place until 66 seconds into the reading. Using the calculated time when each reading point was interrogated and synchronizing the start of the reading to the associated load measurement in the pile, the approximate load at the top the pile when each reading was taken is evaluated. This is presented in Figure 4-204.

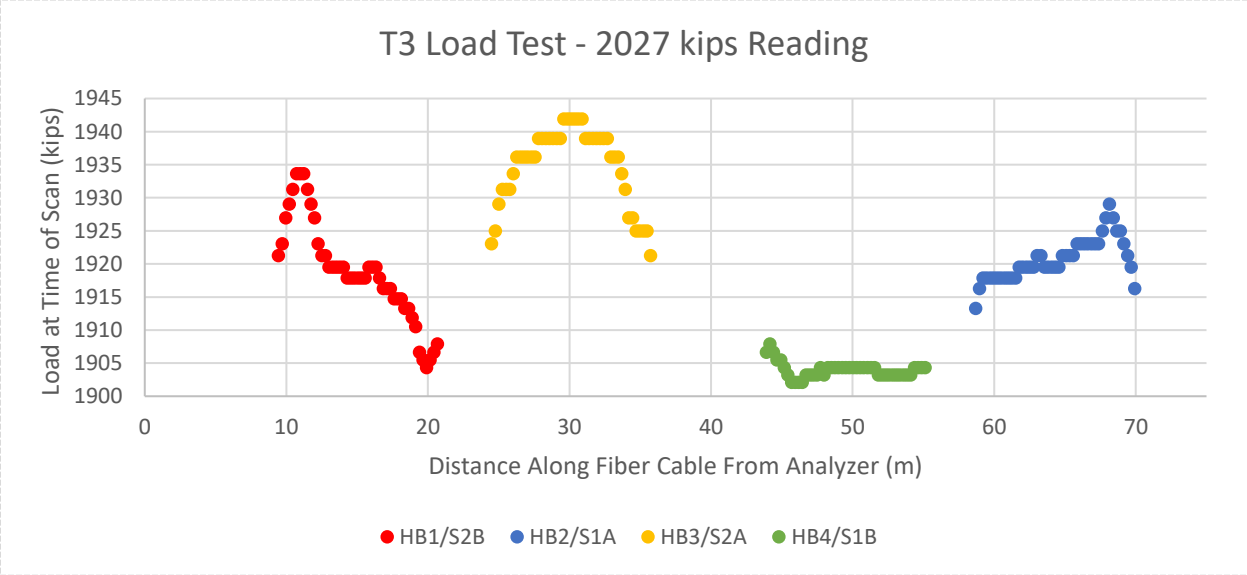

Figure 4-204: Measured load at top of pile for each reading point scan time

Once the measured load at the top of the pile has been determined for each measurement point within the fiber optic profile, the measured strain can be normalized (scaled up) by the corresponding percentage of the maximum load at each point. This provides an upper bound

approximation of what the instantaneous strain profile within the pile would have been at the start of the reading when the maximum load was applied. The applied normalization equation is presented below.

$$\varepsilon_{i,0} = \frac{\varepsilon_{i,t}\, P_0}{P_t}$$

where

$\varepsilon_{0,i}$ = the equivalent strain at point *i* at time 0 (max load)
$\varepsilon_{t,i}$ = the measured strain at point *i* at associated reading time *t*

P_0 = the measured applied load at the top of the pile at time 0 (max load)

P_t = the measured applied load at the top of the pile at time *t*

The original and normalized strain profiles for the four strain verticals and the average strain are presented in Figure 4-205 to Figure 7-58.

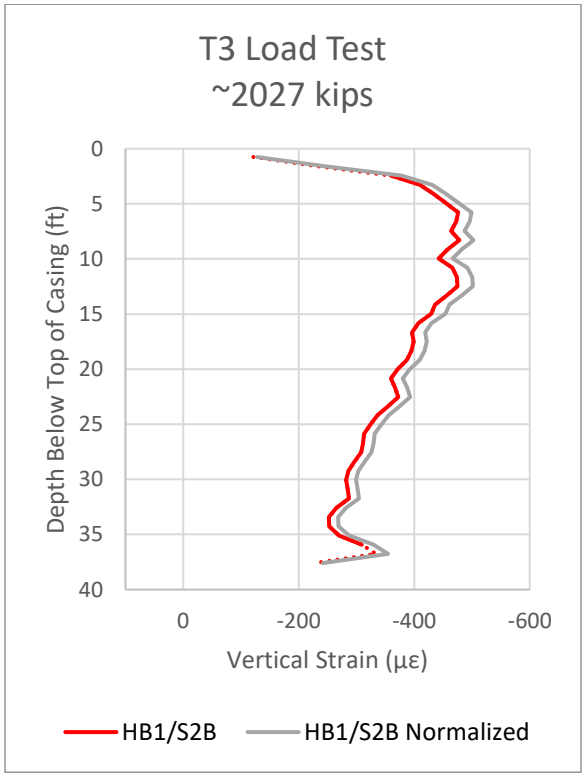

Figure 4-205: Normalized strain profile HB1

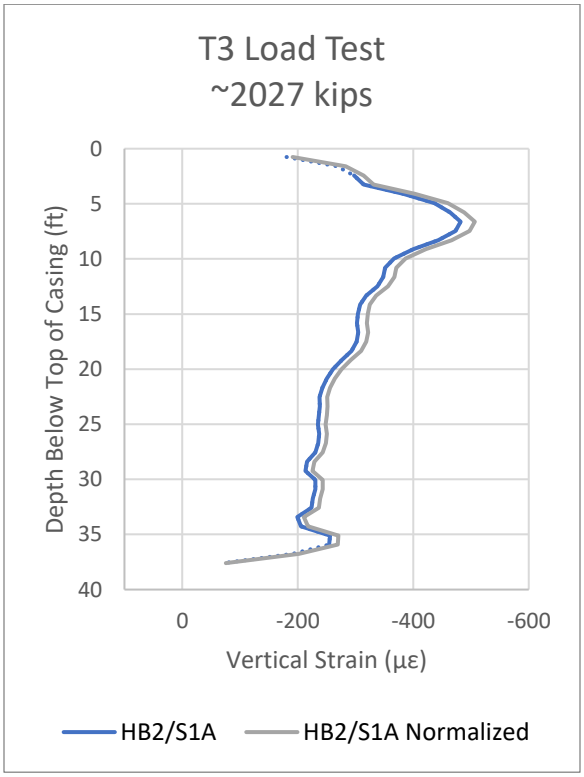

Figure 4-206: Normalized strain profile HB2

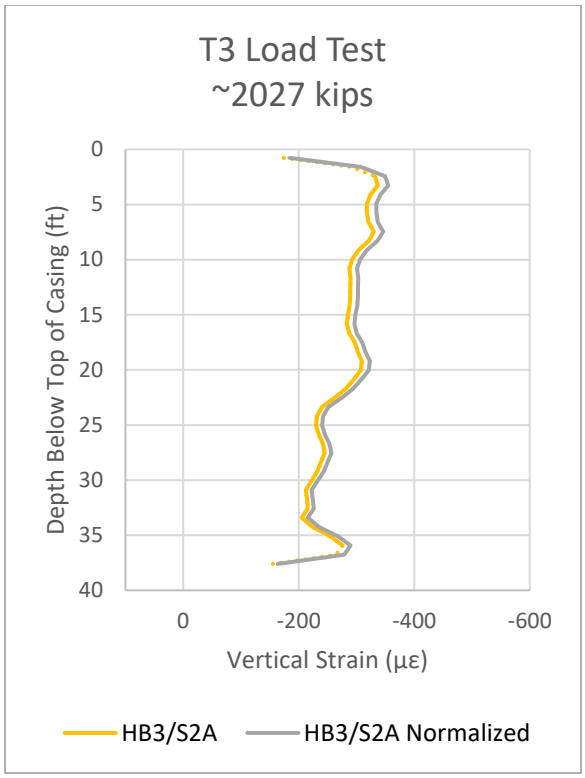

Figure 4-207: Normalized strain profile HB3

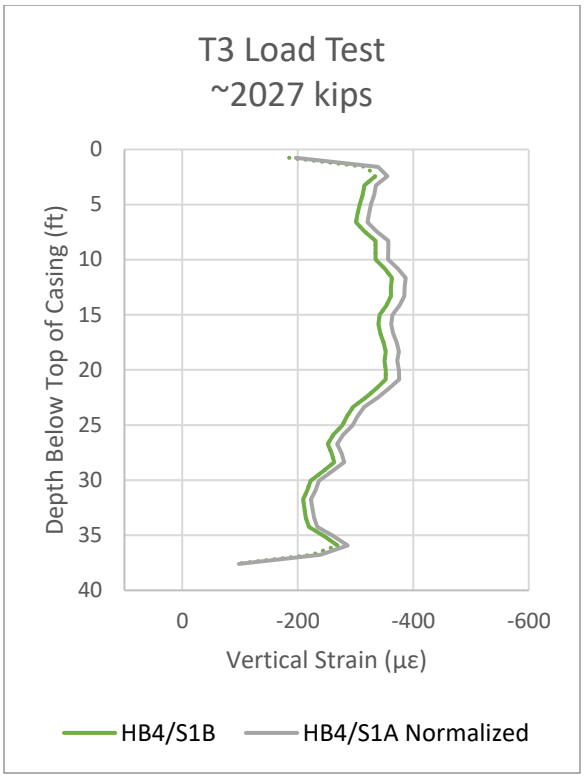

Figure 4-208: Normalized strain profile HB4

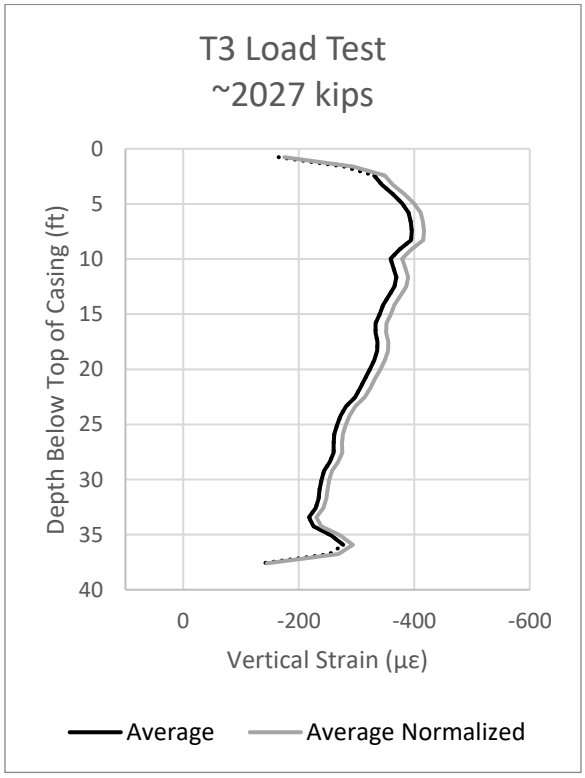

Figure 4-209: Average normalized strain profile

As can be seen in Figure 4-205 through Figure 4-209, the relative difference between the original and normalized strain profile is relatively small compared to the total magnitude of the measured strain. The maximum strain correction made in the normalization process across all four verticals had a magnitude of 26.7 με, with an average correction value of 17.0 με.

Based on the laboratory testing summarized in Chapter 3 and the above analysis and normalization, it is possible to correct for the effect of the temporal variation of strain along the fiber optic cable during the analyzer reading duration. Evaluating this effect and correction on the maximum load and decay observed within the load test data set for the project, the effect is relatively small with a magnitude just above the overall accuracy of the system of 15 με. This is a weakly positive test result of the hypothesis. While the scanning architecture of the commercial analyzer does result in a quantifiable shift in the data output during transient strain, the significance of this difference in the evaluated case is less than 5% of the total measurement. However, for future monitoring projects where the strain variation during readings is of a large enough magnitude that the effect on the strain profile is significant, the correction procedure above can be applied so long as a detailed record of the applied load is available, the fiber optic and load readings can be synchronized, and the change in load during the reading interval can be approximated as proportional to the strain change during the same time.

Summary

Based on the laboratory and testing results of this research, all three of the original hypotheses were able to be confirmed. The results for each hypothesis test are summarized below.

Hypothesis 1: Installation of Strain Cables in Concrete without Pretension

The distributed fiber optic strain results were compared to the point-based conventional strain measurements for all four pile load test records. A comparison between the corresponding measurements yielded a mean difference of 2 με with a standard deviation of 19 με between the systems. This indicates a positive test result for the original hypothesis, confirming that the strain measurements of the fiber optic cable are valid without the need for pretension of the cable during installation.

Hypothesis 2: DFOS Strain Profiles and Outlier Evaluation

The distributed fiber optic strain results from the load test of pile T1 were evaluated to assess the validity of the identification and omission of a potential outlier data point in the conventional strain gauge data set. A standard approach to outlier detection based on deviation from the mean would likely have resulted in the data point to be discarded, however the fiber optic strain data not only confirmed the point's validity, but it also provided important context to the data by showing the continuous strain profile above and below the suspected outlier. The 4 vertical fiber optic strain cable arrangement allowed for the identification and quantification of the non-idealized bending behavior in the pile during the vertical loading of the load test. These results indicate a positive result for the original hypothesis.

Hypothesis 3: Correction of Variable Strain Effect on Fiber Optic Readings

The record of changing load during the final load interval during the load test of pile T3 was used to quantify and correct the error introduced by the commercial fiber optic analyzer architecture. The non-uniform shift was calculated by calculating the reading time based on the scanning frequency and the associated load measured by the load cell during the hold period. This correction was applied to the fiber optic strain profiles, resulting in an approximate 5% increase in the calculated strain magnitude over the pile length. This result indicates a weakly positive result for the original hypothesis; confirming the effect and the ability to correct for impact of temporal strain, but also showing that the effect is of a relatively small magnitude in the evaluated case. However, the result highlights the importance of recognizing the effect of the analyzer architecture and applying a correction when the strain variation is large during the reading interval.

5. Distributed Fiber Optic Sensing for Vertical Soil Deformation

Distributed fiber optic sensing offers a range of benefits for the measurement of vertical soil deformation. Conventional surface monitoring through vertical surveying and subsurface monitoring using deep settlement points or borehole extensometers provide discrete point measurements of relative ground displacement vertically along the borehole column. However, for complicated stratigraphy and non-uniform loading, relying on a half-dozen or fewer measurement points along a borehole can still require significant interpolation between the measurement depths. DFOS can remove the need for interpolation by providing a continuous strain profile along the vertical installation, allowing for a complete view of the local and global strain development within the subsurface.

The conventional approach to measure subsurface vertical displacement is to install a vertical array of discrete measurement points within a geotechnical borehole. This is commonly achieved using either a fixed borehole extensometer, in which the measurement points are anchored at discrete depths within the borehole and movements are transferred to the surface using a wire or rigid rod, or a probe extensometer, which consists of a series of measuring points spread at various depths along a vertical access pipe. Fixed borehole extensometers rely on the anchors within the borehole to transfer vertical soil displacements to the ground surface by mechanical means, at which point they can be measured either manually or using an electronic displacement gauge. Multi-point borehole extensometers (MPBX) allow for several anchor points to be installed at different depths within a borehole, although space constraints at the measurement head often limit the number of anchors to eight or less. Probe extensometers allow for more measurement points to be installed along the vertical borehole, with the only constraint being that the operator must be able to accurately differentiate between the discrete reading points. However, probe extensometer measurements are generally less accurate and can become time consuming when manually read as the number of measurement points is increased.

The technology of DFOS allows a continuous strain profile to be measured along a vertical installation, removing the need to select a limited number of data points based on space and reading constraints in the borehole for conventional extensometers. Through the installation of a single strain cable, installed either single-ended or in a loop, a continuous profile of strain can be taken from the ground surface. This allows for the precise localization of the vertical position and magnitude of subsurface movements. Furthermore, the resulting data can be integrated to provide the relative displacement with depth.

This chapter presents the results of two field deployments of DFOS for subsurface vertical displacement measurement. The first project is comprised of an array of four borehole-installed fiber optic cables to monitor subsurface uplift on the landside of a levee on the Mississippi River. The second project is a trial installation of a fiber optic strain cable via a Cone Penetration Test (CPT) rig to monitor soil deformation during a surcharge loading program. The

background, installation, and monitoring results for each project are presented herein. The chapter is divided into the following sections:

5.1 Literature Review
5.2 Distributed Fiber Optic Monitoring of Levee Uplift
5.3 Distributed Fiber Optic Monitoring of Surcharge Loading Program
5.4 Discussion

5.1 Literature Review

As compared to applications in deep foundation monitoring, the use of Brillouin scattering DFOS for the measurement of vertical ground displacements is relatively undeveloped. The earliest borehole deployments of fiber optic sensing cables were used to measure relative displacement between discrete anchor points using interferometry or an Electronic Distance Meter (EDM) (Blum et al. 2008). These measurement systems functioned in a similar manner as a borehole extensometer; with a tensioned fiber stretched between a subsurface fixed anchor and a head at the ground surface. In this application, the rod of a conventional borehole extensometer was replaced with the tensioned fiber optic cable. However, as with a borehole extensometer, each installed fiber optic cable could only measure changes in length between the two fixed points and could not be used to measure or localize strains in between. For this reason, this early application is not considered a distributed fiber optic system.

The first published use of a Brillouin-based DFOS monitoring system for borehole strain was used for the localization of strains at the bottom of a landslide slip surface (Iten et al. 2009; Puzrin et al. 2010). The fiber optic cable was installed in an abandoned vertical inclinometer casing, itself installed within the footprint of an active landslide. After placement of the fiber optic cable, the inclinometer casing was backfilled with a bentonite-cement grout. There is no mention in the series of articles summarizing this project of whether any pretension was applied to the fiber optic cable during installation. The fiber optic cable was monitored for localized strain concentration using a BOTDA analyzer to localize the slip surface of the landslide mass. The study was focused on the determination of the location of the slip surface and not the accumulated vertical displacement along the installation. Indeed, since the fiber optic cable was installed within the previously installed inclinometer casing, vertical soil deformation around the installation could not reliably be transferred to the sensing fiber.

The first published use of fiber optic for distributed measurement of vertical soil deformations was in 2013 in the UK, when a cable was deployed in a geotechnical borehole to monitor ground heave during the demolition of a building (Bell et al. 2013). Little detail is given regarding the installation, and the resulting strains and interpreted vertical movements were so small as to fall within the accuracy limitations of the fiber optic analyzer. Nevertheless, this project represents the first attempt at measuring a continuous vertical strain profile in soil, as well as the integration of the strain data to generate a profile of vertical deformation. The monitoring results from this study are shown in Figure 5-1.

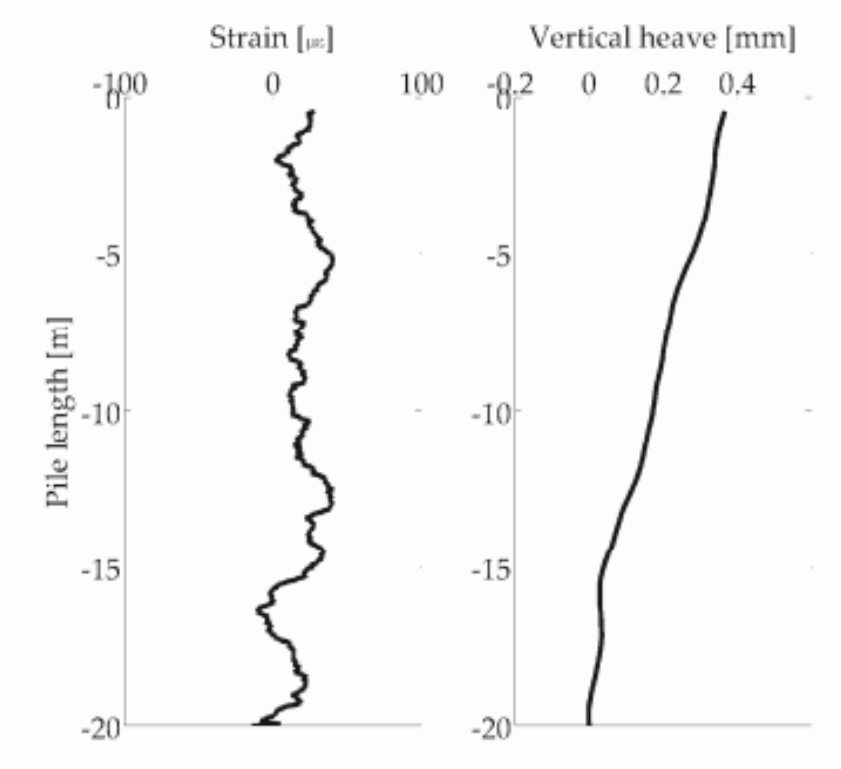

Figure 5-1: Borehole strain and calculated vertical heave from pile monitoring project (Bell et al. 2013)

In Figure 5-1, a trend in the slope of the vertical heave profile can be observed to divide the monitored depth above and below 15 meters. There is no discussion of this trend in the publication, however it demonstrates the value of a distributed system in localizing changes in the subsurface movements.

A borehole-based fiber optic sensing system was developed and commercialized by Marmota Engineering AG under the name BoreScan, based on the research of Dr. Michael Iten. The system is comprised of a strain sensing fiber optic cable, pretensioned against a sacrificial rod and attached to a weight at the bottom of the borehole. The installation is then backfilled with a cement-bentonite grout chosen to approximate the stiffness of the surrounding soil. This system was deployed in a published case study monitoring settlement impacts of a new building construction above an existing pipeline (Rabaiotti et al. 2015). Settlements with depth were monitored using vertical fiber optic installations and the results showed good agreement between predictions from numerical analysis and surface survey measurements. This case study also represented the first time that a fiber optic vertical installation was installed with a conventional extensometer for validation – unfortunately, the conventional extensometer failed midway through the monitoring duration. The settlement profiles measured by the two systems are shown in Figure 5-2.

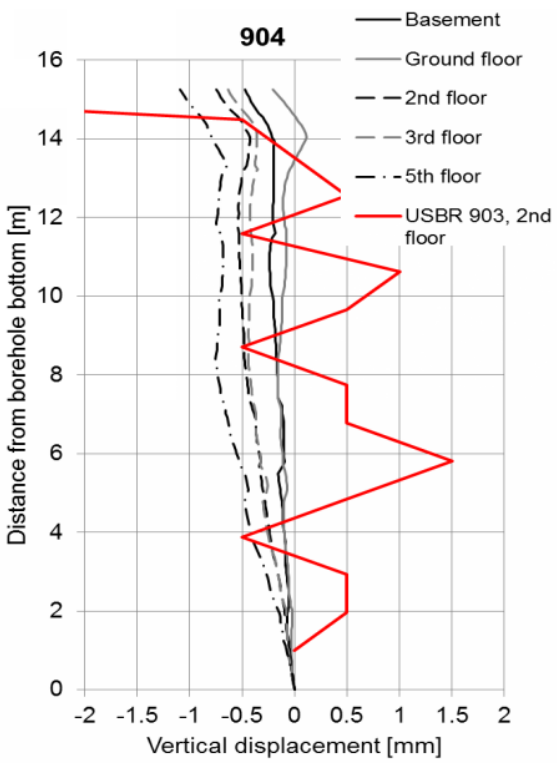

Figure 5-2: Fiber optic monitoring (dashed) and conventional extensometer monitoring (USBR) of ground deflections during building construction (Rabaiotti et al. 2015)

Marmota Engineering has continued to deploy the BoreScan fiber optic monitoring system across Europe, including for landslide slip surface identification and vertical soil displacement measurements (Marmota Engineering 2021). Unfortunately, no further publications have resulted from these deployments so it is not possible to assess any further advances or development that may have resulted.

Parallel research on borehole-deployed fiber optic cable has been successfully undertaken in China (Wu et al. 2015). In a field trial in Suzhou, three types of distributed fiber optic strain sensing cable were deployed in a 200-meter-deep borehole to monitor subsidence associated with groundwater extraction. The test was performed with three distributed fiber optic sensing cables, including the Nanzee metal-reinforced cable used in the projects of this report. The cables were installed in the borehole using a sacrificial guide hammer (weight) to drag the cables and apply pretension. The borehole was backfilled using a sand-gravel-bentonite mixture, chosen based on laboratory testing to maximize the strain transfer to the fiber optic cable and match the stiffness of the native soil, although the specific mix design is not included. The test showed that the fiber optic monitoring system was able to localize and quantify the vertical settlement within the subsurface, with the metal-reinforced cable showing the best strain performance while balancing survivability during installation.

State of Practice

The literature is relatively sparse in terms of detail regarding the installation and best practices for the use of distributed fiber optic strain monitoring for vertical soil deformation. The following best practices represent the common traits among the most recent literature publications.

- Brillouin-based fiber optic sensing is used for strain monitoring, most often single-ended BOTDR.
- Strain fibers are installed vertically in a conventionally drilled borehole.
- A weight is used to guide the strain fiber to the bottom of the borehole and apply a pretension during installation.
- Backfill is performed following installation of the fiber optic cable, using a grout mixture containing bentonite and unspecified quantities of water, cement, and sand or gravel.
- Complimentary temperature cables are often not installed, and the ground temperature field is treated as constant below a shallow zone at the ground surface where air temperatures affect the ground temperature. Readings in the shallow zone are often discarded.
- Strain readings are integrated from the bottom-up to calculate displacement profiles.

Literature Gaps and Proposed Research

Reviewing the published literature covering the use of distributed fiber optic sensing for monitoring of vertical soil deformation, several gaps were identified which provide areas of focus for future research to advance the field.

- Analysis of localized strains: One of the primary benefits of using DFOS for the measurement of vertical soil deformations is the identification and quantification of localized strain concentration. This benefit, often impossible with discrete-point extensometers, allows for a more detailed analysis of the contribution of discrete soil layers and transitions to the observed displacements. Such a detailed approach is not present in the literature.
- Temperature compensation: Where the top of the monitoring vertical was not protected from temperature changes at the ground surface, thermal effects were observed to effect the strain readings several meters into the ground. For installations where fiber optic strain data is being integrated to calculate cumulative ground deformations, it is necessary to measure the temperature fluctuations along the strain fiber and correct for the thermal strain in the data.
- Quantification of pretension and associated limitations on measurement range: In all the previous research summarized above, the strain fiber optic cable was installed in a vertical geotechnical borehole and was pretensioned using a weight at the bottom, occasionally in combination with a rigid rod. This pretension is critical for measuring settlement within the soil column, as the loss of tension would potentially result in the decoupling of the fiber optic cable with the movements of the soil as the fiber went

slack. While pull-out tests on the fiber optic cables have been performed, no lab or field trials have been located investigating the effect of soil strains exceeding the applied cable pretension.
- Installation of strain cable via CPT: The installation of fiber optic strain sensing cable is limited by the time-consuming drilling and sampling of the initial geotechnical borehole. Development of a direct-push installation method would result in a faster and less expensive installation option for DFOS soil deformation monitoring.

Based on the identified gaps, the following hypotheses can be formulated for additional research:

- Hypothesis 1: Distributed fiber optic strain sensing offers a distinct advantage over conventional monitoring for the identification and quantification of localized strain and deformation behavior in the subsurface.
- Hypothesis 2: Temperature compensation is necessary for strain installations where surface temperature fluctuations affect the strain cable, and the data is intended to be integrated to calculate cumulative surface deformation.

The above hypotheses have been used to directly inform the research objectives of the two subsurface strain monitoring projects, presented in the following sections.

5.2 Distributed Fiber Optic Monitoring of Levee Uplift

A key hazard in the operation and maintenance of any levee system is the formation of sand boils. If left unchecked, sand boils can result in significant underground erosion and lead to potential failure of the levee. The most common way for sand boils to be identified in the field is by direct observation; either during routine inspection along the levee length or, as is often the case, incidental discovery by a passerby. The mechanism through which sand boils form as the confined water pressure under the aquitard blanket exceeds the weight of the blanket itself has been hypothesized to also result in local vertical uplift at the bottom surface of the aquitard. Current methods to remotely monitor the development of landside pressures have centered around the deployment of piezometers in the water bearing layer. The goal of this research project is to explore the feasibility of using DFOS technology to measure the development of vertical strain within the subsurface on the landside of a levee and correlate the local and global movements to fluctuations of local river level, water pressure, and the associated sand boil hazard.

A field installation to assess the feasibility of DFOS for measuring subsurface deformations on the landside of a levee was commissioned by the U.S. Army Corps of Engineers (USACE). The UC Berkeley research team developed and installed an array of four vertical fiber optic sensing strings at a previously remediated sand boil site along the Mississippi River levee in Black Hawk, Louisiana. The previous remediation is comprised of a series of relief wells parallel to the levee which have been observed to flow during flood stage at this section of the river. This continued underseepage formed an ideal test bed to prove the effectiveness of the fiber optic sensing

approach to measure subsurface vertical deflections, as well as directly measure the hypothesized uplift at the bottom surface of the clay blanket. The local river level fluctuations directly affect the subsurface water pressure under the levee, which in turn causes uplift of the clay blanket.

Project Overview

The Black Hawk levee project site is approximately 30 river miles south of Natchez, MS. The levee sits on the west bank of the main stem of the Mississippi River. The levee is part of the Mississippi River and Tributary Project. At the project site, the average crest elevation is 78 feet NGVD and with a width of 20 feet and a landside V:H slope of 1:4.5. The levee was constructed in stages from a small agricultural levee in the 1800s to its current configuration in the 1940s. During the 1940s levee enlargement, a borrow pit was excavated near the landside toe to build the embankment. The State Route 15 highway is located on the landside slope at an elevation of 70 feet (USACE 2018).

The geology of the area is typical of the lower Mississippi River. The foundation material of the levee is a 60- to 65-foot-thick blanket consisting of natural levee, crevasse splay, and backwater swamp deposits. The blanket deposits are typically fat clay but can contain silt or sand lenses from crevasse splay deposited during historical breaches of the natural levee. Underlying the blanket is a 150-foot-thick substratum deposit of sand and gravels. The substratum starts with fine grain sand (SP) and grades to gravel with depth. A thick layer of undifferentiated tertiary clays underlays the substratum sands and gravels. The water table beneath the levee is influenced by the river level and rises and falls with the stages of the river.

In 2017, a large sand boil was discovered in the landside borrow pit at the site. A site investigation and analysis were commissioned, however a forecast highwater event in March 2018 was determined to pose a significant threat to the levee because of the likely reactivation of the sand boil and the associated risk of progressive failure. An emergency remediation was installed comprised of 68,000 tons of river deposited sand over the boils, capped with 4,000 tons of limestone. Following the emergency remediation, a series of relief wells were designed and installed between the levee toe and the levee-side-edge of the borrow pit.

The fiber optic monitoring array for the Black Hawk levee was designed to maximize the monitoring coverage of the behavior beneath the landside of the levee. The array was installed in a square pattern between the river and the previously remediated sand boil. A satellite view of the test site is shown in Figure 5-3.

Figure 5-3: Satellite view of the Black Hawk test site

The installation plan is comprised of four boreholes on the land side of the levee between the river and the previously remediated sand boil. The four boreholes are oriented in an approximately square pattern, with one side parallel to the levee and the second side perpendicular. One of the perpendicular sides is approximately in line with the previously remediated sand boil, with the second separated by a distance to the northwest of approximately 150 feet. On the parallel sides, two of the boreholes (BH1 and BH4) were proposed to be installed along the levee slope, while the two downslope boreholes (BH2 and BH3) were proposed to be installed past the toe on the native foundation soil. This orientation allows for the comparison of two complimentary cross sections during the project monitoring – one comparing results between the boreholes in line with the sand boil and those to the side, as well as the boreholes installed within the slope of the levee and those located beyond the toe.

Vertical Fiber Optic Cable Installation via Drilled Borehole

The installation methodology developed for the project was a system of two complimentary fiber optic sensing cables – one temperature and one strain – installed in each borehole. The borehole diameter was chosen as 8 inches to allow adequate space for the planned instrumentation and sacrificial tremie pipe, while not being so oversized as to run the risk of attenuating the vertical deflections of the soil as they manifest around the grout column.

The boreholes were installed in two separate phases – Phase I in August 2021 consisting of Boreholes 1 and 2; and Phase II in October 2021 consisting of Boreholes 3 and 4. Two separate trenches were dug to connect the boreholes installed in each phase back to the Tricon container. The trench was approximately 2 feet deep, with the fiber optic cables laid at the bottom in the native soil. After the cable installation was complete, the removed native soil was used for backfill. A close-up map of the installation array is shown in Figure 5-4.

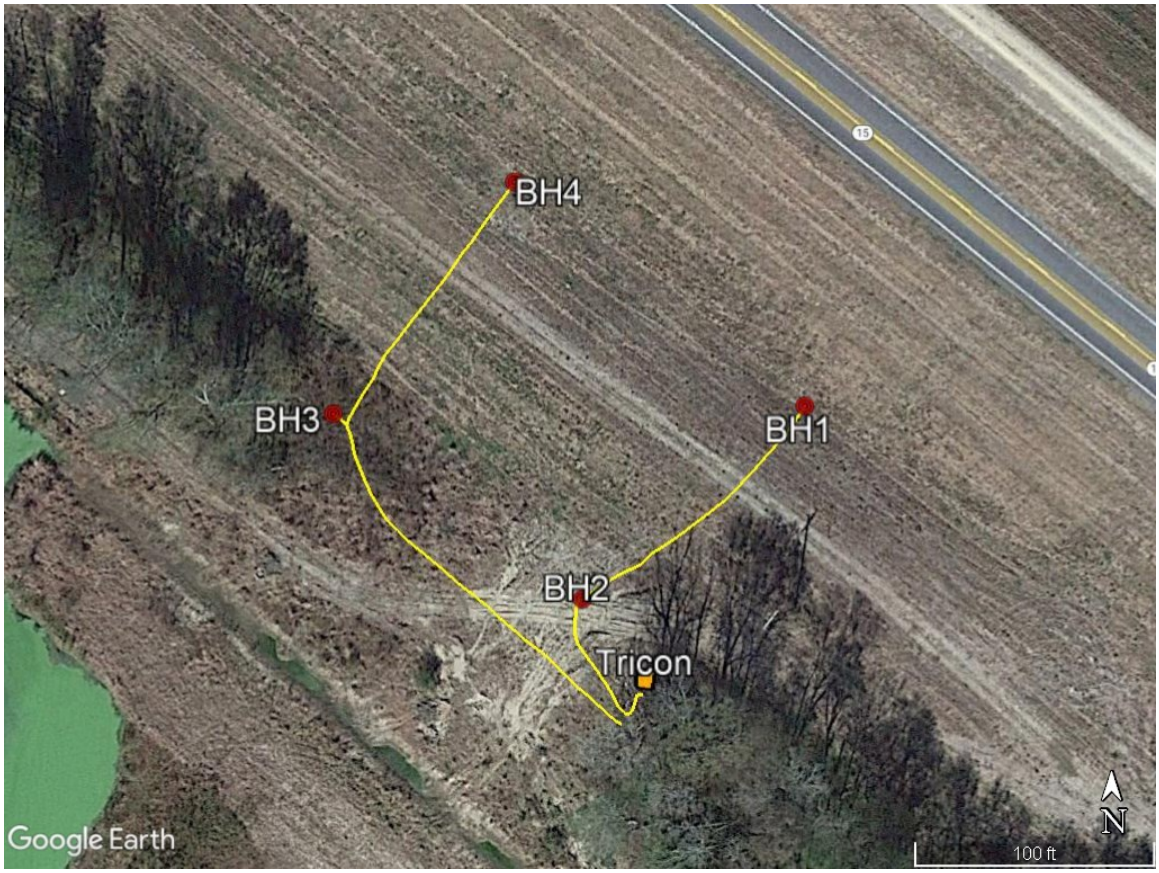

Figure 5-4: DFOS borehole array and trench layout

The boreholes were drilled using a mud rotary drilling rig with an 8-inch diameter. The target depth for each of the boreholes was 100-feet from the existing grade at each borehole location, with the intention of extending through the fat clay (CH) layer into the underlying sand (SP). The installation date, total depth, and clay-sand contact depth for each borehole are presented in Table 5-1.

Table 5-1: Borehole installation dates and key depths

Designation	Install Date	Clay/Sand Contact	Final Depth
BH1	August 17-18, 2021	67-68 feet	103 feet
BH2	August 18, 2021	46 feet	95 feet
BH3	October 26-27, 2021	49.5-55.5 feet	103 feet
BH4	October 25-26, 2021	62.5-64 feet	103 feet

The distributed strain and temperature sensing cable configuration for each borehole comprised a single temperature cable going down the borehole and a corresponding single strain cable returning up the borehole (Note: The directions of “up” and “down” are arbitrary since each installation consists of a complete U). A splice between the temperature and strain cables was installed just above the bottom of each borehole, joining the optical fiber core of the two cables together so that they formed a continuous U. The splice was housed in a PVC tube with waterproof and tension-resistant glands at either end to hold the fiber.

One of the most critical performance requirements of the borehole fiber optic installation was to safely protect the fiber optic cable at the turnaround point at the bottom of the borehole. While the fiber optic interrogation system used for the project allows for a single-ended reading, the decision was made early in the design process to network both the strain and temperature cables in each borehole together, as well as all four boreholes. This resulted in all the sensing fibers to be oriented in series in a single, unbroken loop, allowing for simultaneous reading of all the DSS/DTS sensing fibers across the project.

The fiber optic turnaround detail was installed on the bottom section of the tremie pipe, prior to installation in the borehole. The intention of this detail was to:

a) Control the radius of curvature of the fiber optic cable as it transitioned from one vertical to the second
b) Protect the fiber optic cable from damage or kinking during installation into the borehole
c) Provide a fixed reaction on the strain cable against which to pretension the cable following installation in the borehole
d) Prevent tension from being applied to the downhole splice

The turnaround detail consisted of a PVC T-joint attached to the bottom of the tremie pipe via a coupling. This allowed for grout to flow unimpeded out of the tip of the tremie pipe while also providing a fixed radius so that the fiber optic cable could be attached to complete the 180° turn. A thinner strain cable was used for the turnaround since it can accommodate a lower radius of curvature than the comparatively stiffer temperature cable. A photo of the turnaround detail is shown in Figure 5-5.

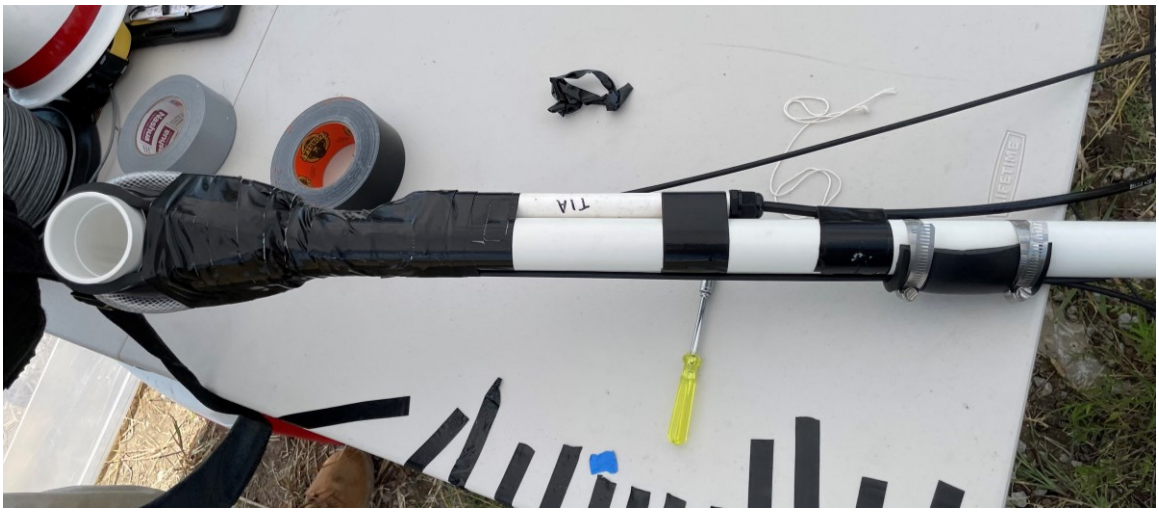

Figure 5-5: Fiber optic cable turnaround detail

Following completion of the drilling of the borehole, the drill rod was extracted in preparation for installation of the tremie pipe and grouting of the borehole. The bottom section of the tremie, complete with the pre-prepared end detail, was installed first within the borehole, followed by the additional threaded tremie pipe sections. Special care was taken not to rotate the tremie pipe during installation into the borehole to prevent twisting of the fiber optic cables around the tremie pipe, potentially resulting in a spiral configuration of the fibers.

Additional instrumentation beyond the strain and temperature fiber optic cables was installed in each borehole. These included dedicated fiber optic cable loops for DAS readings, as well as multiple vibrating wire piezometers. Care was taken in the installation of these additional instruments to avoid any potential conflict or effect on the readings from one system to the others.

Once the entire length of the tremie pipe was installed into the borehole, the borehole was filled with an instrumentation-specific grout mix. The mix was chosen based on guidance from Mikkelson (2002), based on an instrumentation cement-bentonite grout for medium to hard soils. The mix design was chosen to optimize the performance for the four measurement systems in each borehole, maximizing the strain compatibility for vertical movements, the temperature conductivity across the grout, the acoustic transmissivity within the grout, and the horizontal hydraulic conductivity to the piezometers. The mix design is reproduced in Table 5-2.

Table 5-2: Cement-bentonite grout for Medium to Hard soils, reproduced from Mikkelsen 2002

Material	Weight	Ratio by Weight
Water	30 gallons	2.5
Portland Cement	94 lbs. (1 sack)	1
Bentonite	25 lbs. (as required)	0.3
Notes	*The 28-day compressive strength of this mix is about 50 psi, similar to very stiff to hard clay. The modulus is about 10,000 psi.*	

Following completion of the grouting of the borehole, the drill rig was removed from atop the borehole to allow access to the cables at the ground surface. All the cables were gently pulled, taught to straighten the cables, and remove any slack in the borehole. The cables, except for the strain cable, were taped to the stick-up of the tremie pipe.

The intended purpose of the fiber optic strain cable was to measure vertical ground deflections, with movements both in uplift as well as settlement. While any uplift would result in an increase in the tension in the embedded strain cable, settlements of a large magnitude could result in the cable going slack within the grout column and no longer reporting accurate strain measurements. To prevent this case, a calibrated pretension was applied to the strain cable in each borehole to maintain the cable in tension during potential settlement that develops during the monitoring period. This approach had been used on previous vertical fiber optic soil deployments, with the additional step taken on this project of measuring the imposed pretension force on the cable. A metal mesh cable grip was used to grasp the strain cable to apply the calibrated tension firmly. A photo of the metal grip installed on the cable is shown in Figure 5-6. A grip design, which is attached using a removable metal bar, was chosen as to allow the grip to be attached at an intermediate point along the cable, rather than being threaded from one end of the cable as in a closed-grip design.

Figure 5-6: Mesh cable clamp used to apply measured pretension to strain cable (photo credit: Hubbel Inc.)

The pretension force was applied to the strain cable by pulling up on the mesh clamp attached to the cable. Once the target tension force of 50 pounds was achieved, two metal pipe clamps were tightened around the tremie pipe and strain cable to lock the tension force within the cable during the curing of the grout column. These clamps were then removed once the grout had reached a sufficient cure strength to grasp the strain cable. The applied tension was measured using a digital force gauge called the Force One FDIX, manufactured by Wagner Instruments. The force gauge had a load hook that was attached to the loop on the cable clamp grasping the strain cable. During the Phase I installation, the tension was applied by hand by pulling upwards on the force gauge while a second researcher tightened a pair of clamps to hold the tension during curing. A photo of the force gauge and the tightening clamps is shown in Figure 5-7.

Figure 5-7: Handheld pretension of strain cable during Phase I installation

It was found during the Phase I installation that it was difficult to maintain a constant force by hand. During the second installation, a ratchet strap attached to the top of the tremie pipe was used to apply a constant force to the strain cable prior to locking off. A photo of this modified setup is presented in Figure 5-8.

Figure 5-8: Ratchet-controlled pretension setup for strain cable during Phase II installation

Each borehole location was completed using a rectangular traffic-rated vault box to house and protect the excess cable and ground-level splice connections for the duration of the project. Entry slots for the cable to enter and exit each box from the connecting trenches were cut into the side skirts, and the box was buried flush with the surrounding ground. The cable at each borehole was neatly coiled together to allow access for potential future modifications to the system, such as splicing in additional cable or bypassing a borehole network in the event of damage to the downhole section. A photo of the enclosure configuration is shown in Figure 5-9.

Figure 5-9: Enclosure vault used to protect the cable at the top of each borehole array

Once the grout had cured, the clamps holding the applied pretension on the strain cables were removed. The tremie pipe stick-up was trimmed below the lip of the enclosure to allow the lid to be installed. This final step concluded the installation procedure for each of the borehole fiber optic arrays.

After completing the Phase I installation and removing the tension clamps at the top of the two boreholes, the two borehole arrays were networked and the end closest to BH2 was connected to the fiber optic analyzer in the Tricon container. Following the completion of the third and fourth boreholes, the Phase I and Phase II loops were spliced together to create a continuous loop of the temperature and strain cables of all four borehole arrays. The order of the borehole interrogation from the fiber optic analyzer in the Tricon container is BH2 → BH1 → BH3 → BH4. A schematic diagram showing the networked orientation of the four boreholes is shown in Figure 5-10.

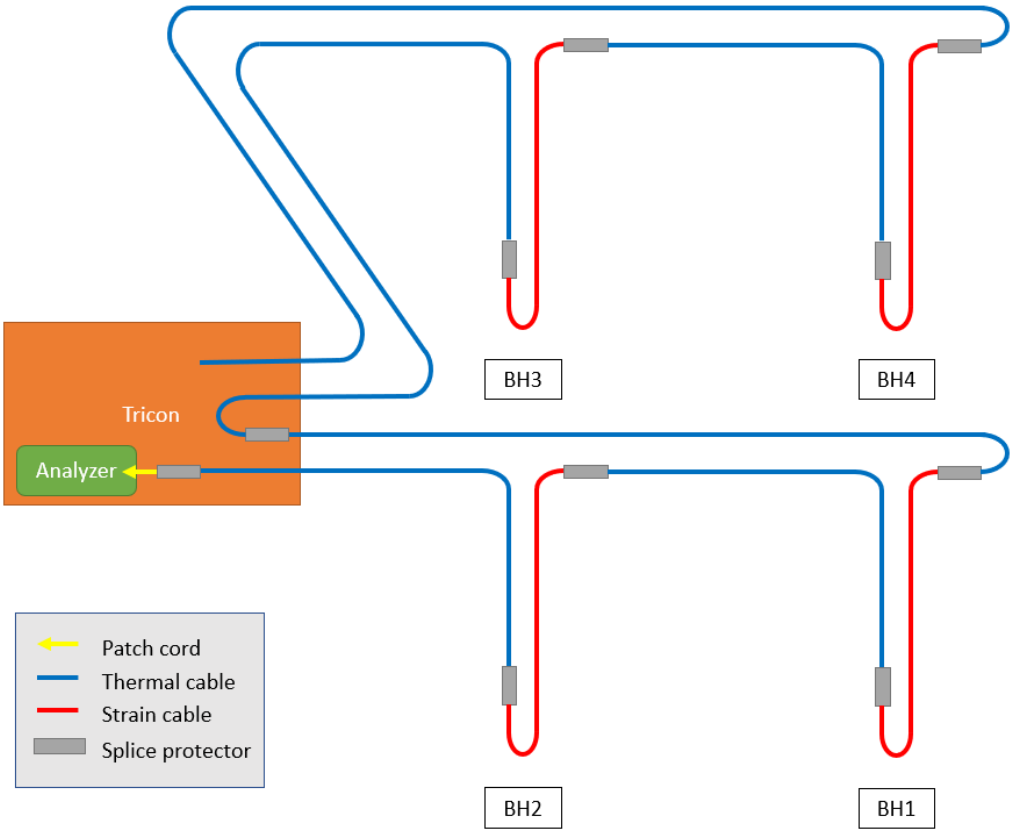

Figure 5-10: Schematic diagram of DTS/DSS cable loop routing

Fiber Optic Monitoring Results

The DSTS fiber optic analyzer was installed within the Tricon container, along with the other complementary monitoring systems at the test site. The Tricon is connected to utility power and connected to the internet using a cellular uplink. The analyzer and control server power connections are routed through an uninterrupted power supply (UPS) to protect the system in the event of a power surge or failure. The system is programmed such that, in the event of a power failure lasting longer than the battery backup of the UPS, the system will restart and continue logging once the power comes back online. The initial data collection was scheduled at 5-minute intervals, later reduced to 15-minute intervals before finally being set at 6-hour intervals for the long-term monitoring. The data is saved on the control server and automatically backed up off-site using a file sharing system.

The number of readings over time is shown in Figure 5-11. This highlights the 3 changes in reading frequency (changes in the slope of the number of readings), as well as the gaps in monitoring when power failures at the site caused the system to go offline (horizontal sections in the graph).

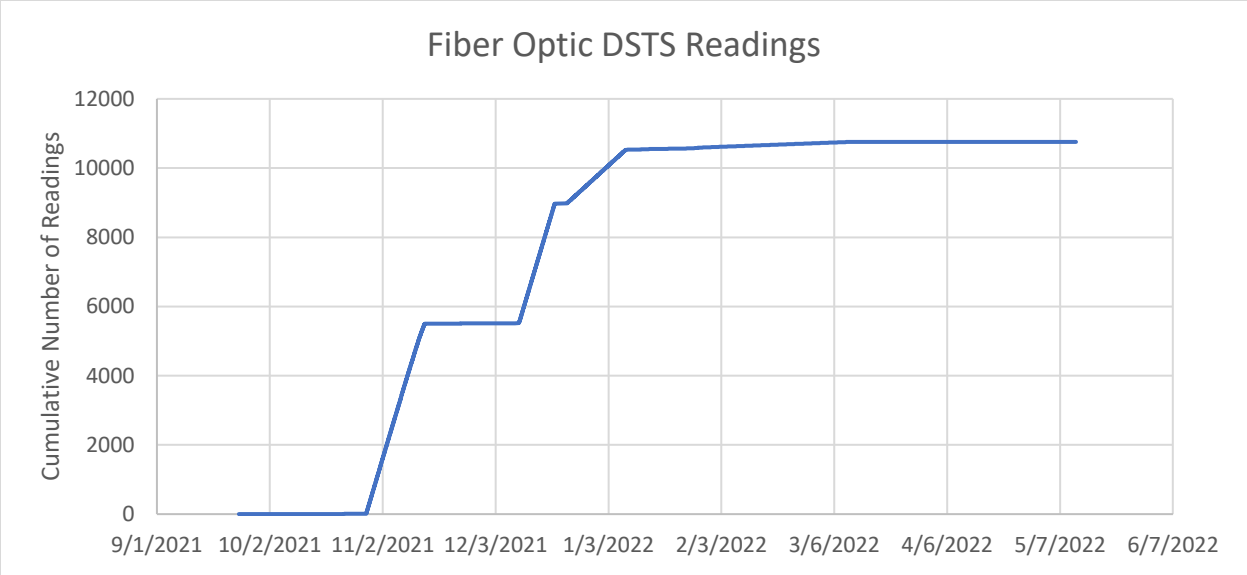

Figure 5-11: Fiber optic analyzer reading accumulation

Prior to interpreting the fiber optic data, an initial baseline must be chosen for the installation since both the thermal and strain processing of the fiber optic data relies on relative changes in frequency along the fiber optic cable. An initial set of readings for the two Phase I boreholes was taken on September 23, 2021, following the removal of the tension clamps and the reconnection of the analyzer to the network during a subsequent trip to the site. The second round of readings was taken on November 3, 2021, following the removal of the tension clamps on BH3 and BH4. The results of the Phase I and Phase II initial readings are shown in Figure 5-12.

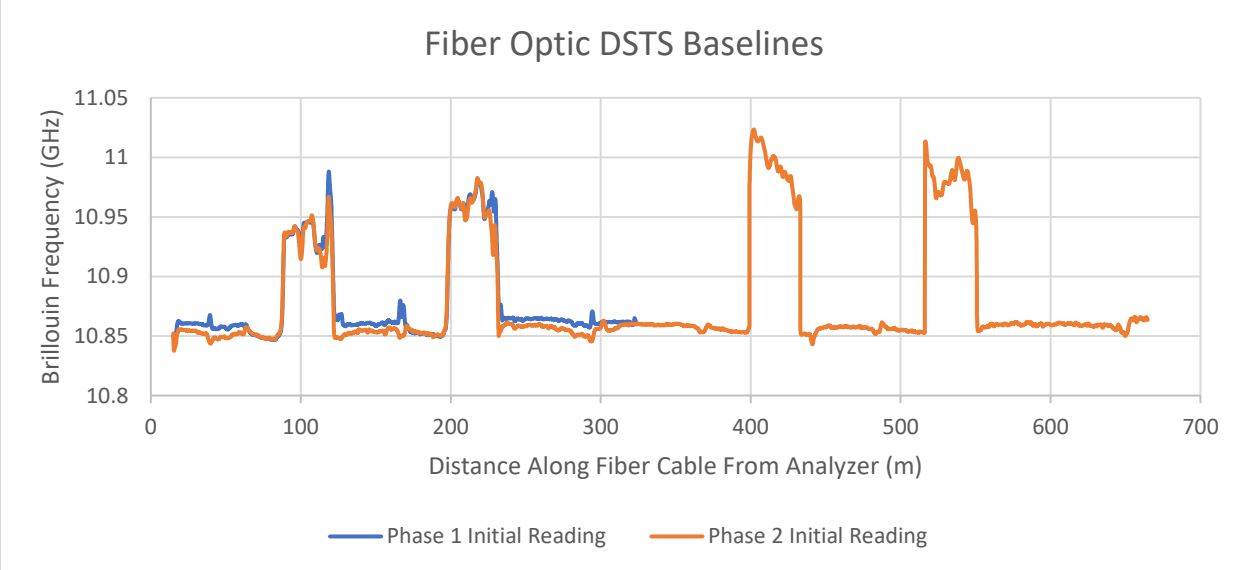

Figure 5-12: DFOS strain and temperature baseline Brillouin peak frequency profiles

In Figure 5-12, the higher frequency sections of the frequency graph (~10.92 – 11.03 GHz) are the sections of strain cable, while the lower frequency sections (~10.85 – 10.86 GHz) are the sections of thermal cable. The later, November 3 readings were chosen as the primary baseline for the project. While an earlier baseline could be used for the Phase I boreholes, it was decided that a unified baseline across the project would be best for ease of comparison between the data sets.

Also shown in Figure 5-12, the post-processed output of the DFOS analyzer is peak Brillouin frequency versus distance along the fiber optic cable measured from the analyzer. The final step in preparing the data for strain and temperature processing is assigning physical locations in the field to distances along the fiber optic cable, a process called indexing. This is performed by carefully notetaking the lengths of fiber optic cable installed in each segment of the field installation and comparing the transition distances between cable types that are observable within the frequency output. The indexed distances are presented in Table 5-3.

Table 5-3: Fiber optic DSTS array index locations

Borehole	Segment	Start (m)	Stop (m)	Direction in Borehole
BH1	temperature (T1)	166.3	197.3	down
	strain (S1)	199.1	230.1	up
BH2	temperature (T2)	58.9	87.4	down
	strain (S2)	89.0	117.5	up
BH3	temperature (T3)	367.6	398.6	down
	strain (S3)	400.4	431.4	up
BH4	temperature (T4)	484.6	515.6	down
	strain (S4)	517.4	548.4	up

In looking at the initial temperature data for the four boreholes, the temperature was observed to be affected by daily surface fluctuations to a depth of approximately 20 feet below ground surface, with the changes becoming more pronounced as the surface temperatures cooled from the average temperatures in early November when the baseline was taken. The temperature profiles with depth over five reading periods are presented in Figure 5-13 through 7-5.

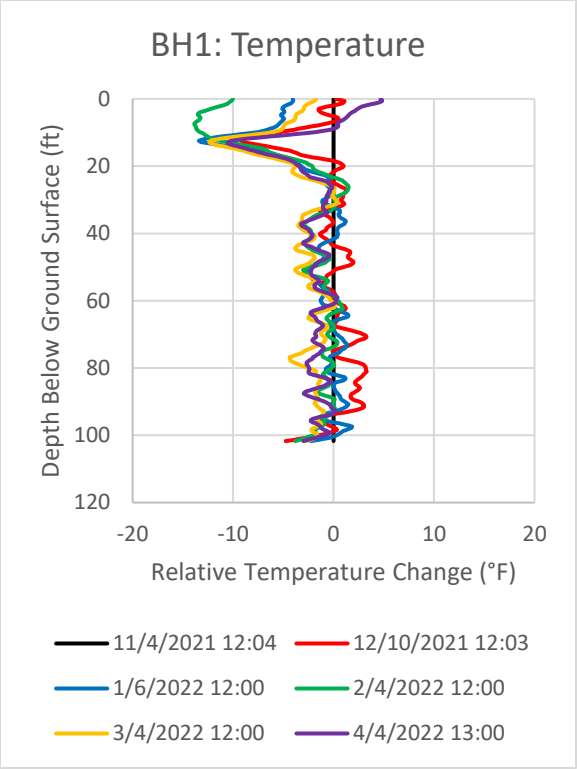

Figure 5-13: BH1 temperature profiles

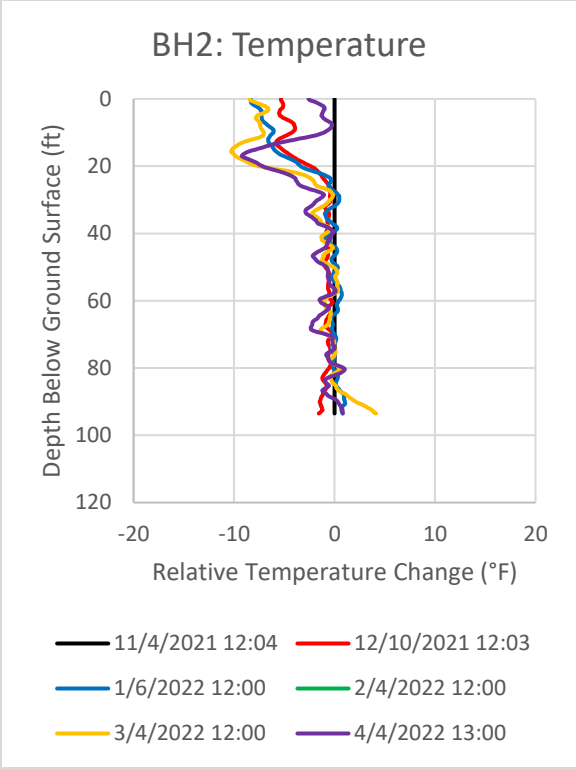

Figure 5-14: BH2 temperature profiles

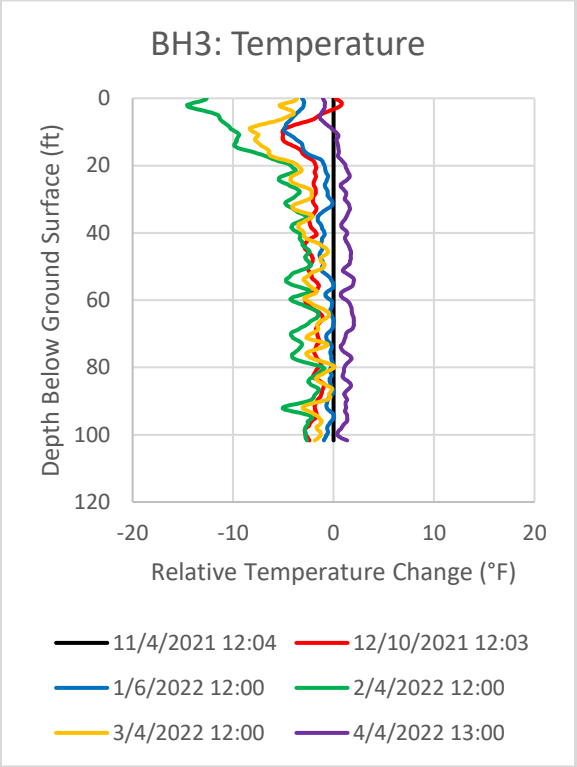

Figure 5-15: BH3 temperature profiles

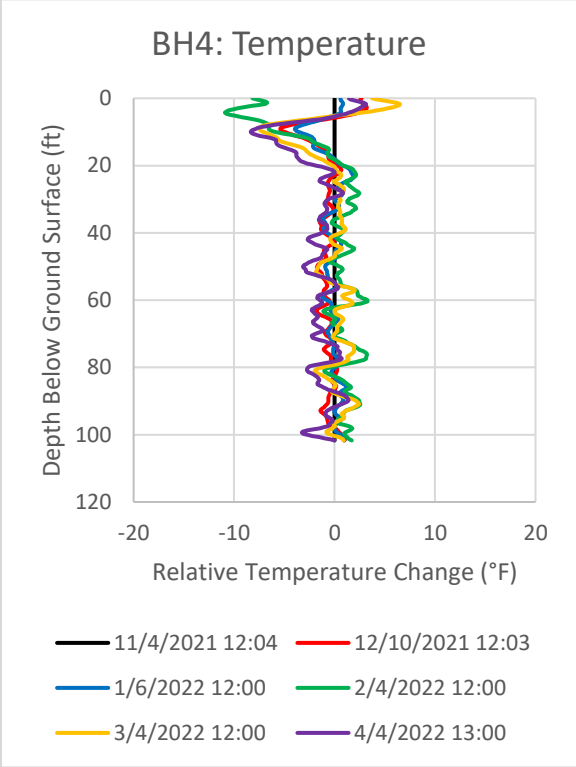

Figure 5-16: BH4 temperature profiles

The temperature profiles in all 4 boreholes show variation over the six readings in the top 20 feet of the profile, indicating that the temperature over this depth is fluctuating with time. However, only the profile for BH2 shown in Figure BH2 displays the conventional linear temperature influence of surface temperature, starting at the largest deviation at the surface and linearly varying until it reaches the stable temperature of the ground below the influence zone. The other 3 boreholes show a peak temperature decrease at approximately 10-feet below the ground surface, after which the temperature increases slightly towards the ground surface. There were no stratigraphic transitions noted in the boring logs at these depths. The cause of this deviation is unknown; however, it is possible that this transition correlates to the groundwater table on the dry side of the levee which is assumed to be 10-20 feet below ground surface.

The effect of the temperature changes in the top 20 feet of the boreholes is also evident in the strain cable readings, necessitating the use of thermal measurements to compensate for the effects of temperature changes on the strain cable. This is performed by calculating the differential temperature rise or lower on the thermal cable, converting this to the relative frequency change using the strain cable thermal coefficient, and then correcting for the portion of the measured strain that was caused by thermal changes. The thermal compensation is most pronounced in the top 20 feet where the temperature changes were the highest in magnitude – the compensation applied in the lower portions of the borehole where the temperature was more stable were minimal by comparison. The compensated strain profiles for the 4 boreholes are presented in Figure 5-17 through 7-9.

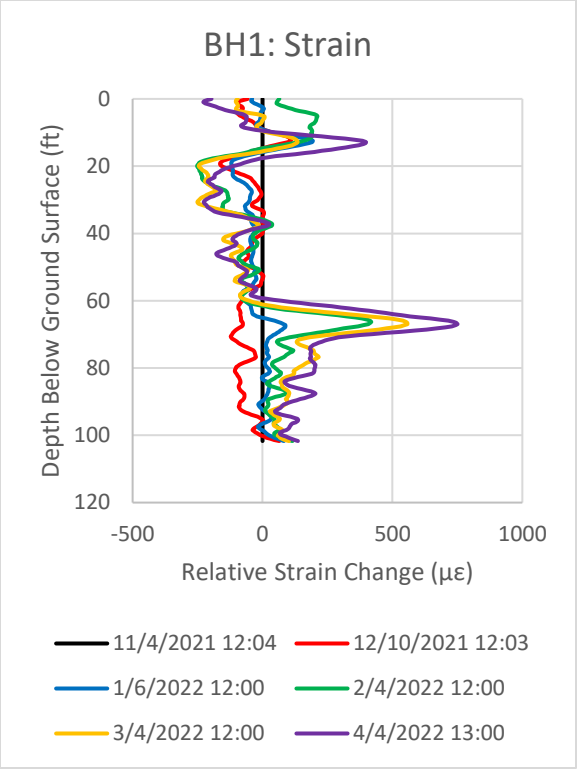

Figure 5-17: BH1 strain profiles

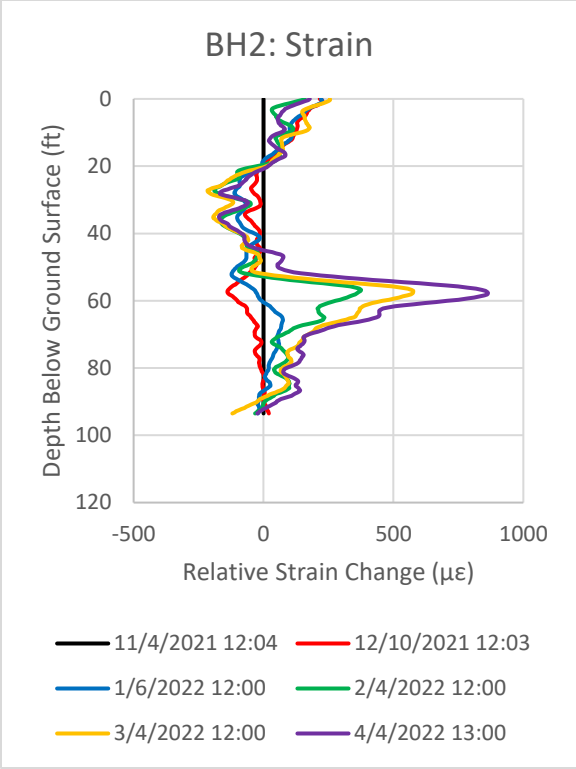

Figure 5-18: BH2 strain profiles

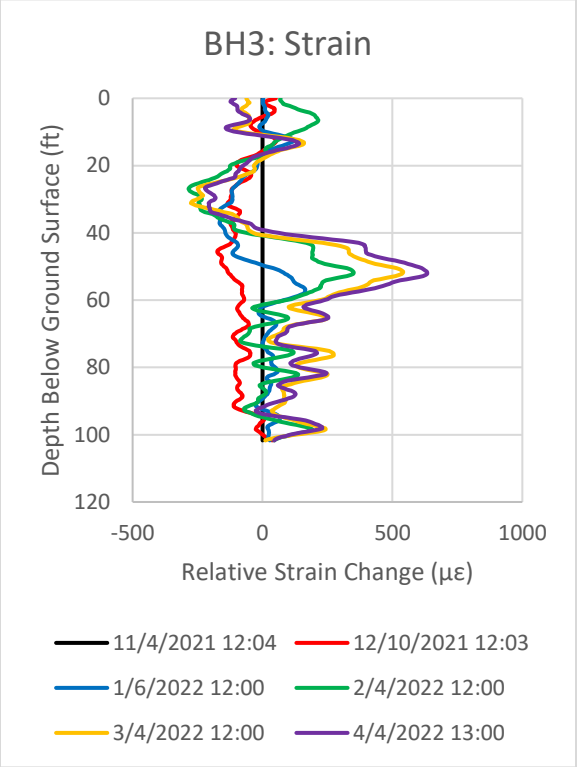

Figure 5-19: BH3 strain profiles

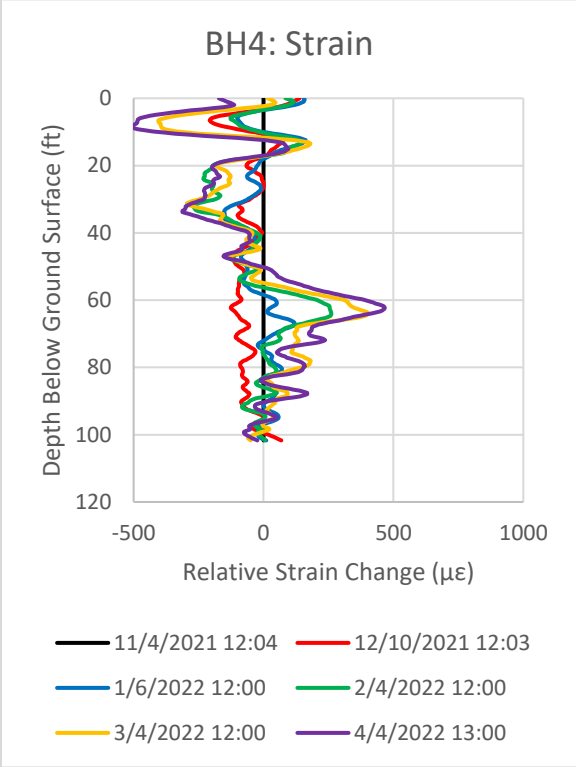

Figure 5-20: BH4 strain profiles

The most pronounced trend across all four boreholes is a peak of tension strain observed at depth in the reading of January 19, 2022. The depth of the peaks closely lines up with the logged stratigraphic transition from clay to sand in boreholes BH1 (67'), BH3 (52'), and BH4 (62'). The tensile peak in BH2 (57') was approximately 11 feet below the recorded transition depth of 46 feet in the boring log. Looking at the rest of the profiles, a similar variation in the strain measurements as the trends observed in the temperature profiles is observed in the top 20 feet. This supports the potential for a localized stratigraphic variation in this area that is affecting the temperature and strain readings. In the remainder of the profile depths, outside the top 20 feet and the tensile peak at the clay/sand transition, the variation within the strain profiles is approximately +/- 50 με over the monitoring period with a slight trend towards compression within the clay.

Looking more closely at the tension variations at depth, the strain development over time at the peak depths can be plotted for the four boreholes. The resulting plot is shown in Figure 5-21. The variation in strain at the peak depth follows the same trend and approximate magnitude across the four boreholes.

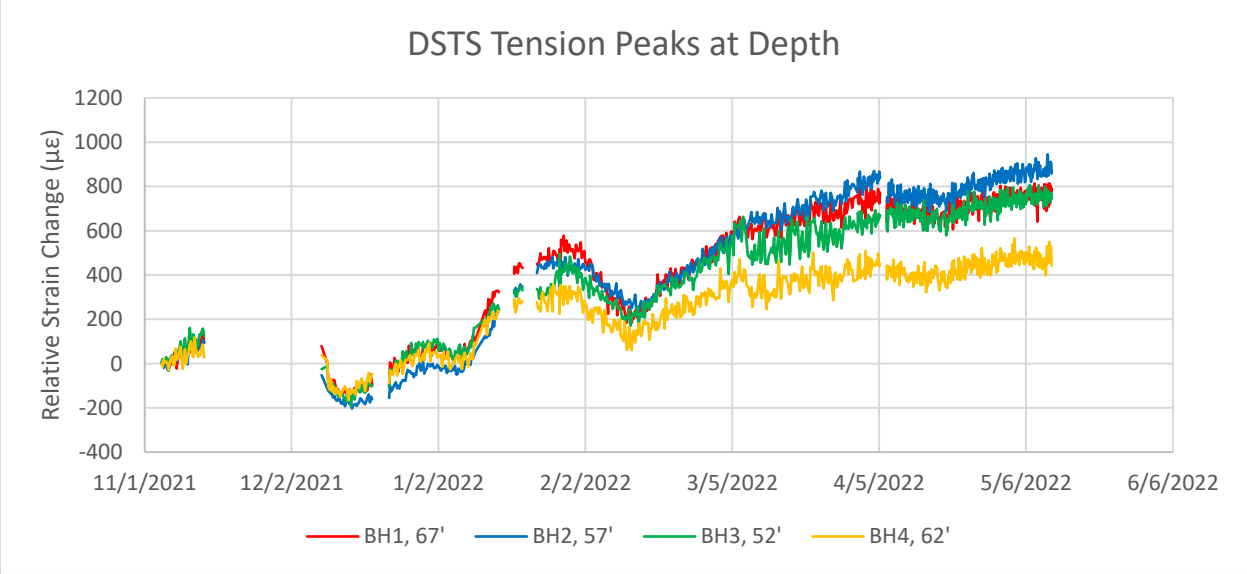

Figure 5-21: DSTS tension peaks at depth over time

Further insight can be gained by comparing the average peak strain at depth to the river level measurements at the nearby Natchez monitoring station. The result is shown in Figure 7-11. Looking at the comparison between the average peak strain at depth and the nearby river level gauge, there appears to be a correlation between the two, albeit with a variable time lag between changes in the river level and the corresponding rise in tensile strain.

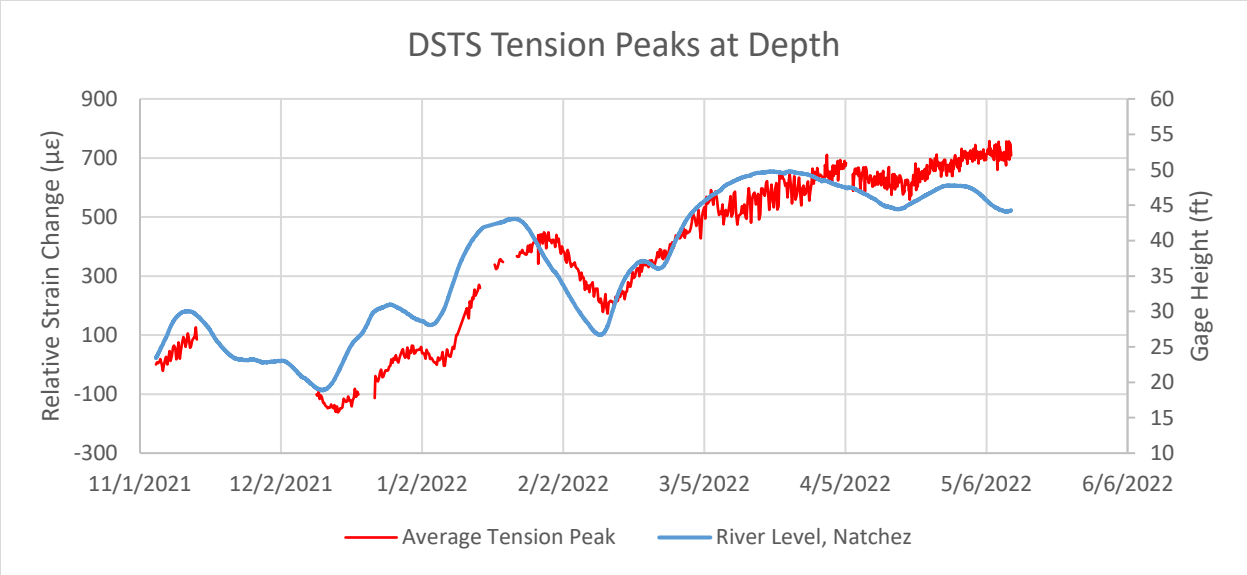

Figure 5-22: Average at-depth peak strain and peak river level at Natchez, MS station over time

The strain profile measurements can be integrated to evaluate the vertical displacement profile of the soil with depth. This process consists of multiplying the individual strain measurements by the gauge length of 0.1 m and summing the resulting displacements from the bottom of each borehole to the ground surface. The profile is vertical settlement relative to the bottom of the borehole. The resulting profiles are presented in Figure 5-23 through 7-15. The displacement profiles for the four boreholes show similar trends. Small settlement values developed early in the monitoring period, reaching a maximum settlement of less than 0.1 inch was measured in early December before the trend reversed into January. The maximum uplift value was measured at depths corresponding to the tension peaks observed in the strain data, with the vertical movements attenuating slightly within the clay before reaching the ground surface.

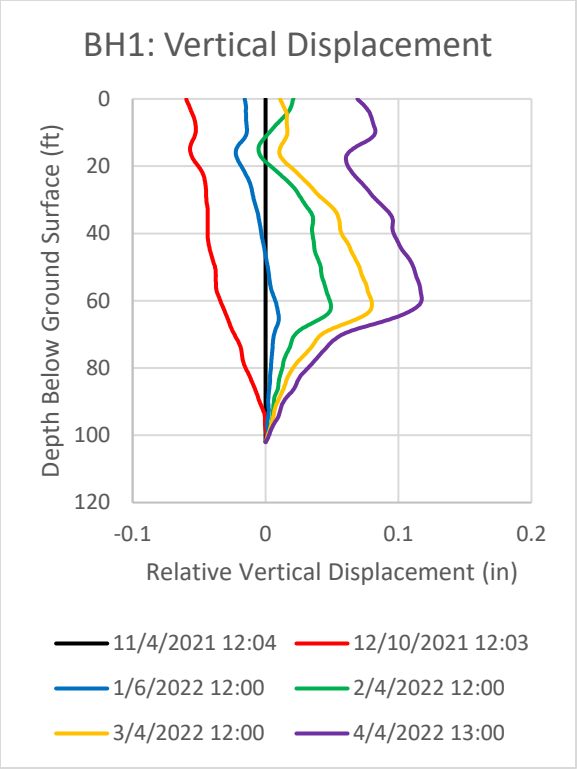

Figure 5-23: BH1 displacement Profile

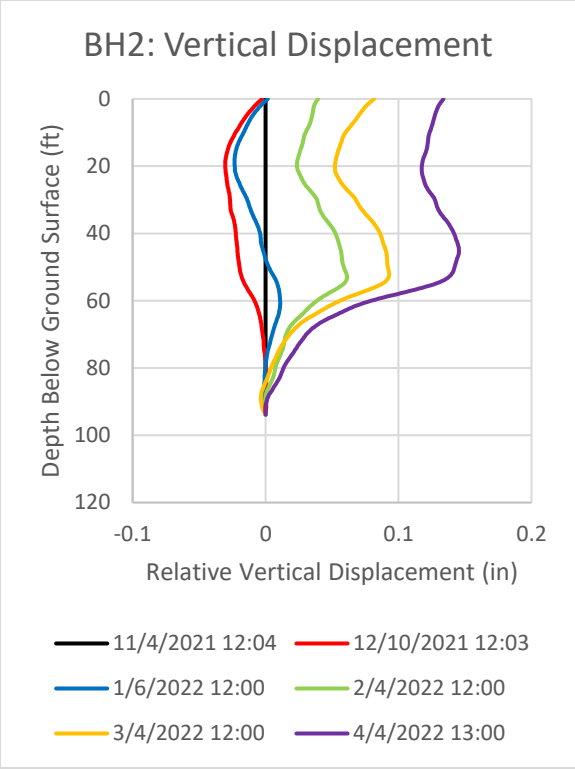

Figure 5-24: BH2 displacement profile

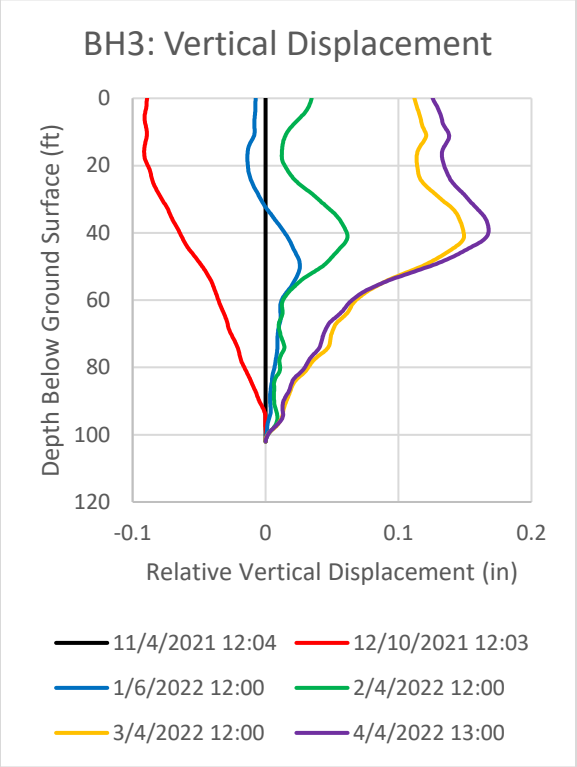

Figure 5-25: BH3 displacement profile

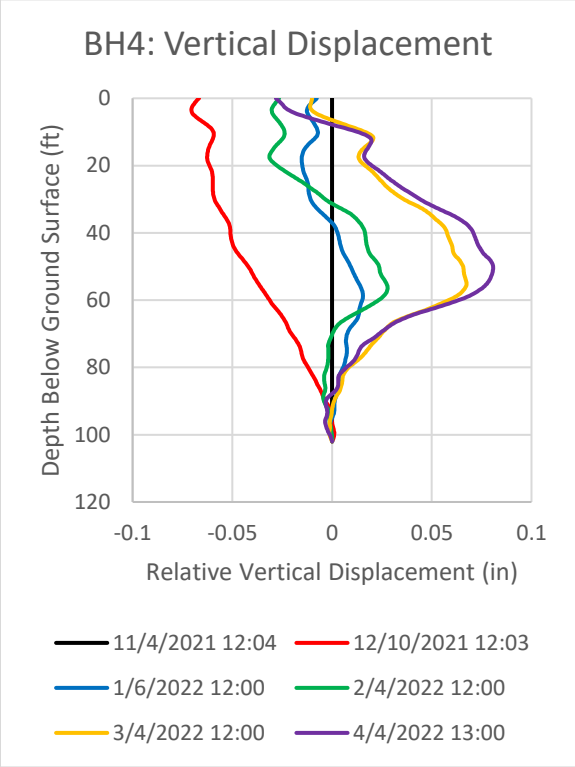

Figure 5-26: BH4 displacement profile

The values at the ground surface in the preceding figures represent the calculated surface displacement at the borehole locations. The surface displacement for the individual boreholes over time is plotted in Figure 5-27.

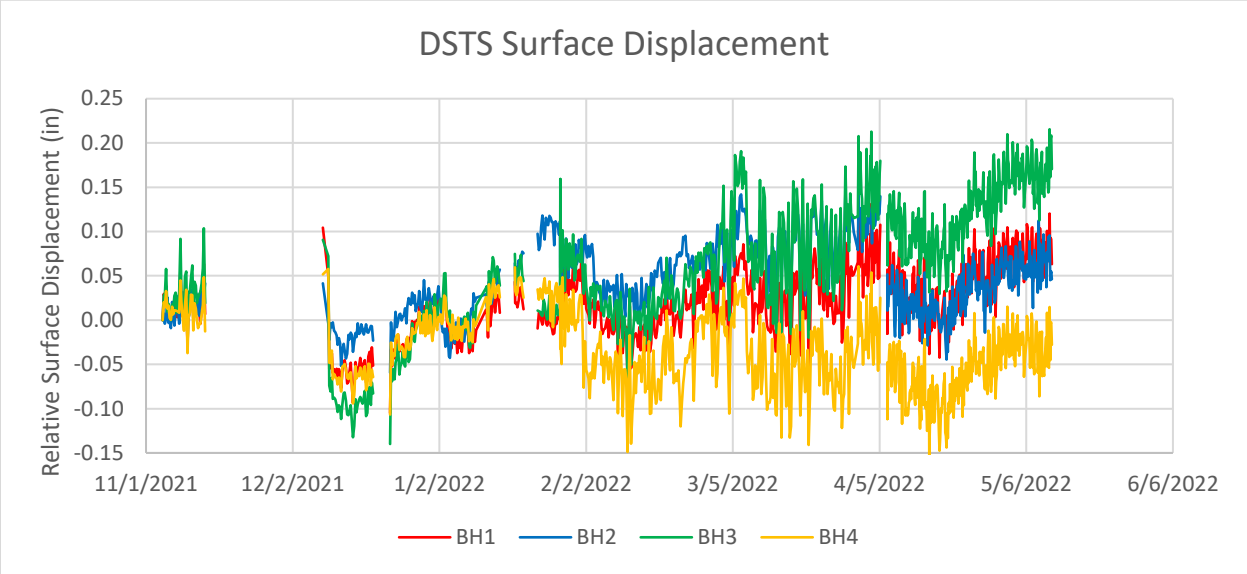

Figure 5-27: Calculated surface displacement for the individual fiber optic boreholes over time

The noise level in the data in Figure 5-27 is much higher than the corresponding plots of the peak tension strains presented in Figure 5-21. This is due to the compounding of the reading errors during integration over the fiber optic sensing length. The cumulative error at the surface that results from the integration of the individual strain points the average depth of 100 feet is approximately +/- 0.025 inches. This is approximately an order of magnitude higher than the error expected from the commercial Omnisens analyzer but is still well below the measurement threshold of conventional surface settlement techniques and is considered acceptable for this application.

The magnitude of the calculated surface displacements between the boreholes is similar except for in BH4. Looking at the displacement profiles with depth in Figure 5-23 through Figure 5-26, the peak displacements at the bottom of the clay blanket are attenuated more strongly to the ground surface in BH4 than the other three boreholes, particularly in the 0–30-foot depth interval. This indicates that there is a difference in stratigraphy at BH4, potentially consisting of a higher clay content in the transition from the foundation material into the levee.

The surface displacements follow a similar trend as the river level fluctuations at the nearby Natchez station. The average surface displacement and the river level over time are shown in

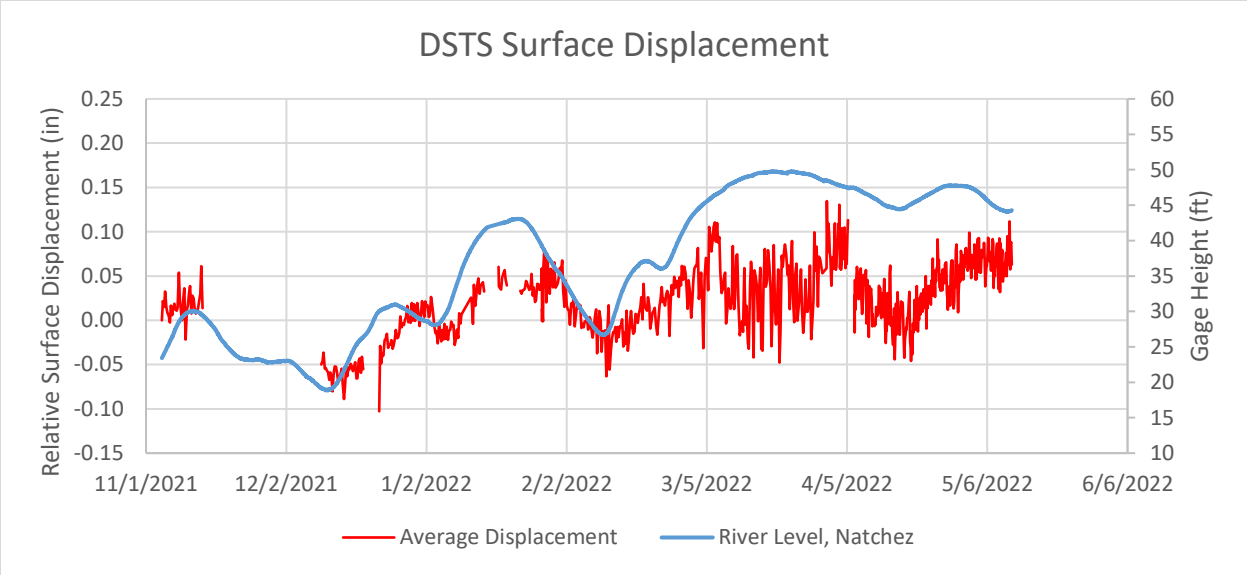

Figure 5-28: Average surface displacement and peak river level at Natchez, MS station over time

As can be seen in Figure 5-28, the fluctuations in the river level follow the same trend as the average surface displacements calculated from the fiber optic strain profiles. Changes in both the average displacement and the tension peaks lag the river level fluctuations by approximately 4 days. The correlation coefficient, r, between the average displacement and the river level is 0.66, indicating a positive correlation between the two data sets. The correlation increases to 0.95 if comparing the magnitude of the individual peak tension strains shown in Figure 5-17 through Figure 5-18 with the river level as this data is more closely correlated with the river level and associated uplift pressures. The relationship between the individual peak strain at depth with the associated river level, lagged 4 days, is shown in

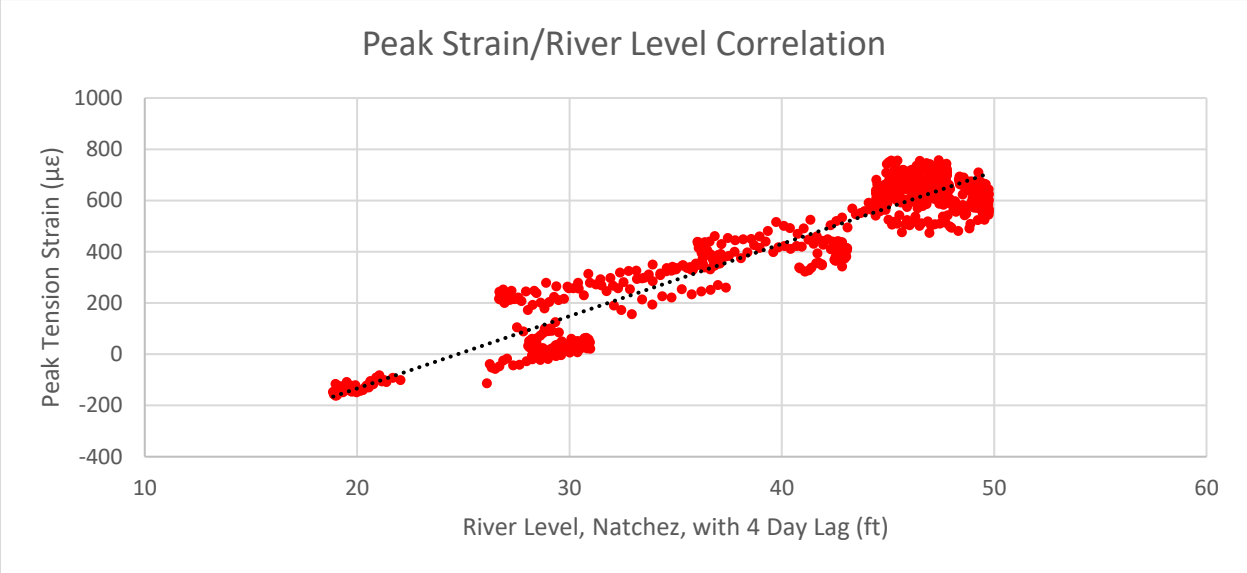

Figure 5-29: Correlation plot between the peak subsurface tension strain magnitude and the river level with a 4-day lag

The trend observed in Figure 5-29 indicates that the uplift observed both at depth at the bottom of the clay blanket and the associated movements at the ground surface can be attributed to the increase and decrease in the groundwater pressure in the sand layer below the levee, driven by the river level. The magnitude of the surface displacement is relatively small, under 0.15 inches, and is below the accuracy threshold of the leveling survey set up at the site to track the elevation change of the ground surface at the borehole arrays.

Summary

This field research has shown the viability of distributed fiber optic sensing (DFOS) as a measurement tool for quantifying and localizing the subsurface uplift beneath a levee associated with fluctuations in the retained river levels. It has also provided direct measurement of the uplift of the aquitard blanket, a behavior which has, to the best of the research team's knowledge, not been directly measured previously. This could serve as a local measurement for the formation of sand boils, which, it is hypothesized, would cause the measured strain peaks and surface deflection to decouple from the associated river level as the hydraulic pressure is released to the ground surface. This technique could be potentially expanded to remote sensing, with high resolution vertical scans being used to capture the uplift and potential collapse associated with a sand boil formation. Monitoring at the Black Hawk site is planned to continue into 2023 to further explore this use case. Further analysis and discussion of the data from this project as it relates to the research hypotheses is presented in Section 5.4.

5.3 Distributed Fiber Optic Monitoring of Surcharge Loading Program

The limited literature state of practice for the use of DFOS for the monitoring of vertical soil deformation has been to install the sensing cable in a conventional geotechnical borehole with a pretension applied to the cable. The second research project utilizing DFOS for vertical soil deformation monitoring was undertaken to explore the installation of the fiber optic sensing cable using a direct-push approach with a CPT rig and assess the performance of the fiber optic installation during large deformations. This novel installation method offers the ability to decrease installation time and cost while also creating an overlapping soil profile from the instrumented CPT push to compare and correlate the subsequent strain measurements. The project chosen for the field test is a surcharge program designed to reduce settlement of a soft clay deposit during construction and operation of future facilities on the site. As a result, a large amount of settlement was anticipated during a relatively short period of time, offering the opportunity to observe the performance of the fiber optic installation through and beyond its strain limit.

Project Overview

The research site chosen for the deployment of the fiber optic monitoring system is located on Treasure Island in the San Francisco Bay, California. The island was artificially constructed in the late 1930s on a shallow shoal north of the adjacent Yerba Buena Island. The island is comprised of sand fill dredged from the nearby bay, placed over the existing shoal and soft clay underlying

the bay to raise the elevation above sea level. The original use of the island was to host the Golden Gate International Exposition, after which it was converted to military use by the US Navy until the base was closed in the late 1990s. A major redevelopment project is currently underway to build a range of new mixed-use housing and supporting infrastructure. In support of this planned development, several geotechnical site improvement projects have been recommended to address a range of potential hazards. One of the geotechnical improvement projects is a surcharge loading program to reduce the impacts of consolidation settlements associated with loading of the soft Young Bay Mud deposits on future construction. The thickness of the Young Bay Mud varies dramatically across the island, with an approximate thickness of 25 feet at the monitoring location. Several stages of surcharge loading were planned for the location, with an initial lift of 8 feet and an associated calculated settlement of up to 12 inches. A summary of the stratigraphic units encountered at the project site is presented in Table 5-4.

Table 5-4: Stratigraphy of the project site

Stratigraphic Unit	Depth Below Original Grade, ft.	Description
Fill	0 – 39	Fills, hydraulically placed beneath sea level, silty sand with silt and clay lenses
Young Bay Mud	39 – 64	Soft to medium-stiff, high to low plasticity clay
Old Bay Clay	> 64 m	Older clay unit, very stiff to hard

The monitoring of the surcharge program was performed using two complimentary methods. A grid of settlement plates was installed at the top of the original ground surface across the surcharge area with a series of riser pipes through the fill, terminating in survey prisms read automatically by a network of robotic total stations surrounding the site. This created a record of the cumulative vertical displacement of the ground surface during the surcharge program. To track the progress of the fill placement, an Unmanned Aerial Vehicle (UAV) was periodically flown over the surcharge area to take photos which were used to calculate the fill height across the site. This created a record of the elevation of the top of the fill surface with time, capturing the combined effect of new fill placement as well as the ongoing ground settlement.

To complement the monitoring program, a vertical fiber optic strain cable was proposed to be installed directly beneath one of the settlement plates within the surcharge area. The site was deemed to be a good field test of the proposed installation method by CPT due to the low chance of refusal before the competent stiff clay underlying the more compressible Young Bay Mud, as well as the relatively short timeline over which a large magnitude of settlement was expected to occur. This would provide a test of the installation method, the fiber optic monitoring itself, as well as the anticipated decoupling as large strains developed within the

consolidating clay. A diagram of the stratigraphy and the installed instrumentation is shown in Figure 5-30.

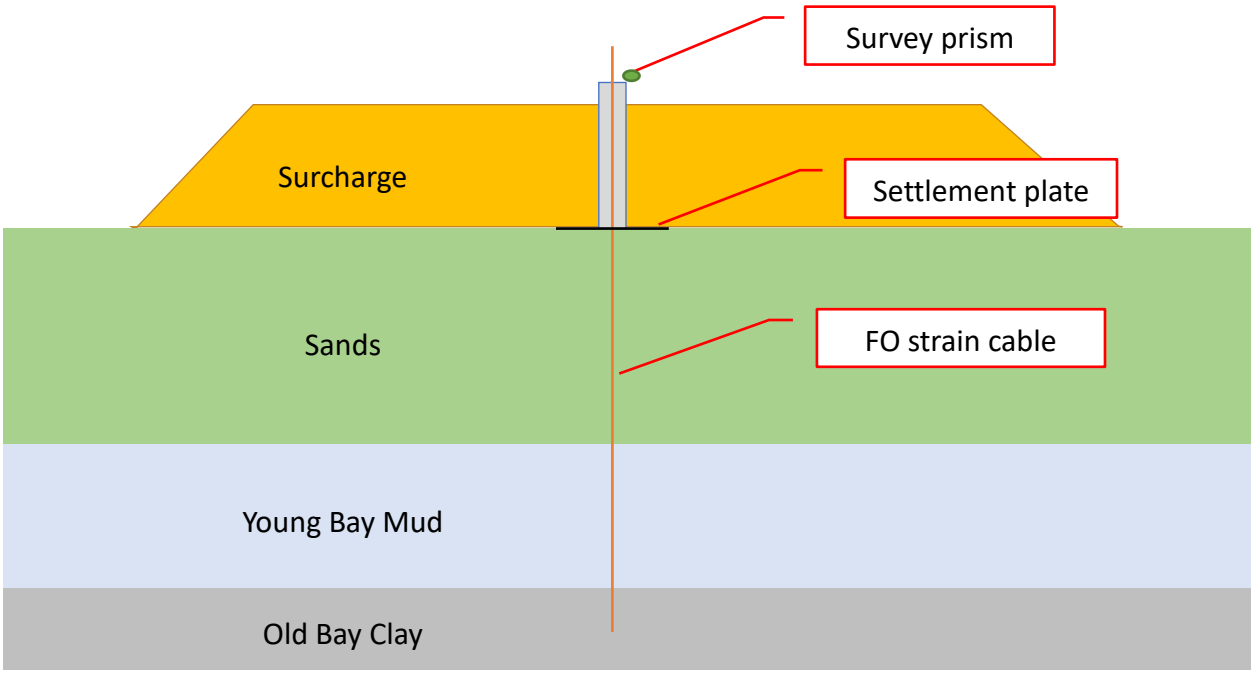

Figure 5-30: Schematic diagram of the CPT fiber optic installation

Vertical Fiber Optic Cable Installation via CPT

One of the main goals of the field trial was to develop and test a method of installing the fiber optic cable via CPT, rather than the previously adopted deployments in conventional geotechnical boreholes. This new method would offer the benefit of significantly reducing the time and cost associated with installation of a fiber optic extensometer, especially when compared to the more involved installation and assembly of a conventional multi-point borehole extensometer. The installation was prepared by first advancing an instrumented CPT, creating both a complete CPT record of the precise location of the fiber optic installation, as well as serving as a pilot hole for the fiber optic cable. Once the instrumented CPT had reached the termination depth, set as a minimum of 9.8 feet (4 times the spatial resolution of the fiber optic analyzer) beyond the bottom of the Young Bay Mud, the cone was extracted from the ground, leaving the hole open. The fiber optic installation had been prepared beforehand by attaching a length of armored strain cable to the center of a sacrificial “dummy” CPT cone, machined out of a block of aluminum. A photo of the prepared fiber optic assembly is shown in Figure 5-31

Figure 5-31: Prepared fiber optic cable and dummy CPT tip

To begin the installation, the fiber optic cable was threaded through several hollow CPT rods and the excess cable was pulled out, so the dummy cone was seated against the first rod and taped in place to remain secure before the push began. A photo of the dummy cone in place prior to installation is shown in Figure 5-32.

Figure 5-32: Dummy cone taped in place at the bottom of the first CPT rod

The dummy cone and trailing fiber optic cable was then pushed into the previously opened hole, with the fiber optic cable threaded through the rods as installation progressed. Once the dummy cone reached the bottom of the previously pushed hole, the cone was pushed an additional 2 feet into undisturbed soil to increase the fixity of the tip. A cement-bentonite grout was then poured into the rods as they were extracted, chosen based on the mix for "Grout for Soft Soils" published by Mickelson (2002) to avoid the grout column from being stiffer than the Young Bay Mud. Following full extraction of the rods and topping off the grout, the strain cable was pretensioned to approximately 2000 με and fixed via clamp to maintain the tension during grout curing. A photo of the completed installation and tension frame is shown in Figure 5-33.

Figure 5-33: Completed fiber optic installation and tension frame, immediately following installation

Since the CPT attachment detail could only accommodate a single fiber optic cable, no temperature cable was installed at the site. While a complimentary temperature cable would allow for thermal compensation of the strain measurements to be performed, previous research and local experience indicated that the expected temperature fluctuations at depth would be negligible. The presence of the surcharge fill pad over the original ground surface would also reduce the influence of diurnal and seasonal surface temperature changes on the shallow fiber optic readings. Further discussion of the necessity of thermal compensation for DFOS soil monitoring is presented in Section 5.4.

Fiber Optic Monitoring Results

Monitoring of the fiber optic installation was performed using a commercial analyzer operating in the BOTDR mode. The analyzer was configured using a spatial resolution of 0.75 m with a readout spacing of 0.25 m. The manufacturer reports a measurement repeatability of +/- 20 με (1 standard deviation) at comparable reading settings. A series of 3 initial baseline readings were taken 2 days after the installation, following removal of the tension frame. A photo of the standpipe riser and the fiber optic analyzer is shown in Figure 5-34.

Figure 5-34: Standpipe riser, fiber optic cable, survey reflector, and fiber optic analyzer

The processing of subsequent readings was performed by calculating the change in Brillouin frequency along the fiber and converting the delta into mechanical strain using a fixed constant for the fiber optic cable. Readings were performed on an approximately weekly basis, eventually reducing to bi-weekly and then monthly as the monitored settlement rate decreased with time. Three readings were taken during each field visit, with the readings compared with each other to detect any problems with the cable or analyzer and then averaged before converting into change in strain.

The primary data processing was focused on creating profiles of differential strain versus depth within the installation. By plotting this over time, it was possible to observe how the vertical strain was developing within the subsurface because of the surcharge load. A selected series of these plots are presented in Figure 5-35, separated by approximately a month apart.

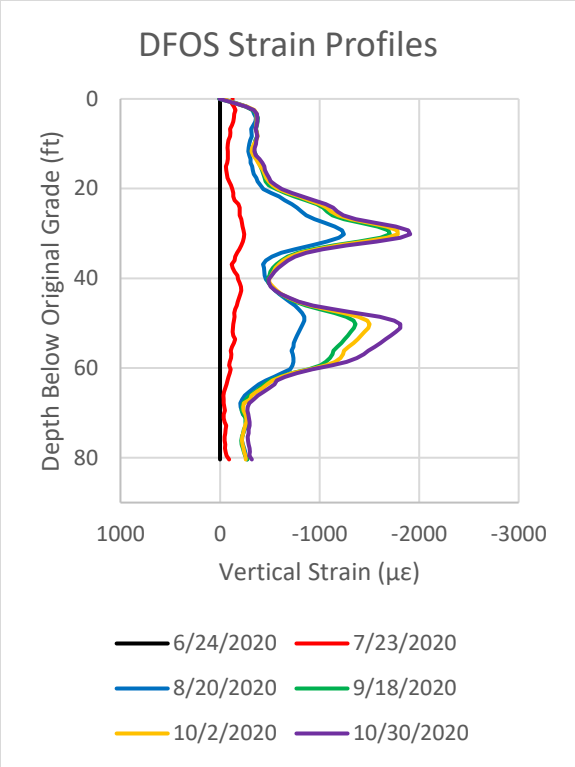

Figure 5-35: Treasure Island DFOS strain profiles

The baseline, taken on June 24, was prior to the placement of any of the surcharge on the site. By the reading on July 23, roughly 20 inches of fill had been placed. By the reading on August 20, the full 8.2 feet of the first stage of surcharge had been placed, with the fill height remaining constant until January of the following year. After the completion of the initial surcharge, two areas of concentrated strain became evident in the strain profiles. The deeper of the two, located at a depth of approximately 45 to 65 feet, corresponded to the bottom 20 feet of the Young Bay Mud deposit. The upper 5 feet of the Young Bay Mud display less strain than the mid- to lower- portions, suggesting that this area is slightly overconsolidated as compared to the deeper sections of the clay layer. Figure 5-36 shows the CPT results for the instrumented push prior to the fiber optic cable installation.

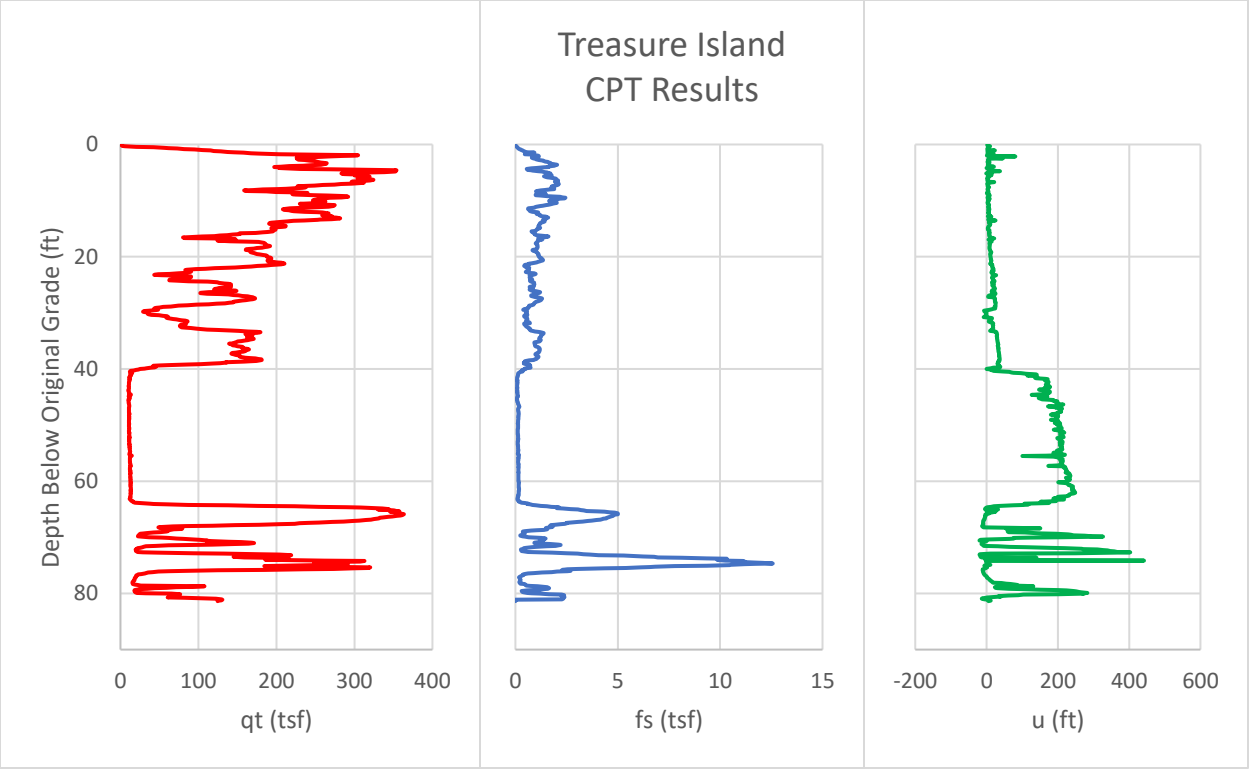

Figure 5-36: Treasure Island CPT results

Comparing the strain profiles in Figure 5-35 to the CPT results in Figure 5-36, the lower strain concentration corresponds closely to the low tip and sleeve resistances of the Young Bay Mud. However, the inferred change in overconsolidation ratio at the top of the clay layer is not clearly reflected in the CPT data. A second, shallower strain peak is observed at approximately 29.5 feet below the original grade. This upper layer is within the fills overlaying the deeper Young Bay Mud and is noted to potentially contain clay lenses. Although this unit was not identified as the target of the surcharge program, it is contributing to the overall settlement at the monitoring site. The peak in strain corresponds to a dip in tip resistance at the same elevation, indicating that a soft soil layer is driving the local strain concentration at this depth. It is not known if this layer is continuous over the site or if it is a local lens specific to this area.

The peak strain in the two primary compressible layers at 30 feet and 50 feet is plotted in Figure 5-37.

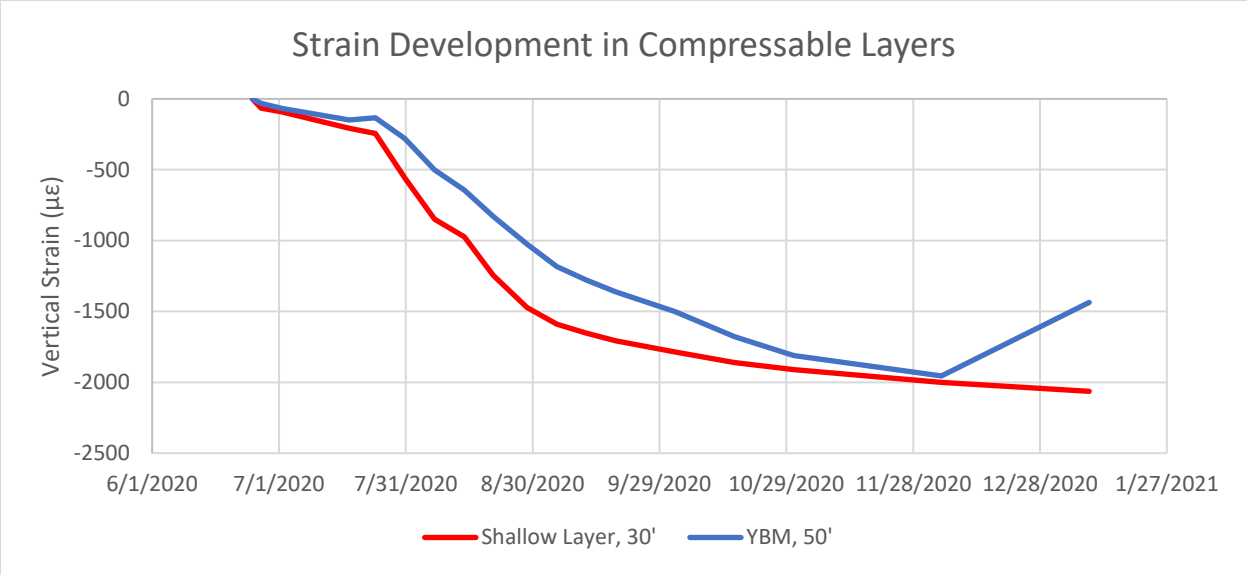

Figure 5-37: Peak strain development with time in the two primary compressible layers

The strain development in both layers is relatively steady under the initial 20 inches of surcharge through July 23, 2020. After placement of the full 8.2 feet of surcharge in late July, both layers display a significant increase in the rate of strain accumulation for 1-2 months, at which point the strain begins to slow. The shallow layer has a higher initial strain accumulation rate and reaches a slower linear section earlier than the Young Bay Mud. The Young Bay Mud has a more gradual decrease in the strain slope until the measured strain decreases in the final reading. This is indicative of a change in the strain transfer between the fiber optic cable and the surround soil and is discussed in further detail later in this section.

Due to the continuous nature of the fiber optic strain measurements, the strain profiles can be integrated to create a profile of settlement with depth. The settlement profiles for the selected dates of the previously shown strain profiles is shown in Figure 5-38.

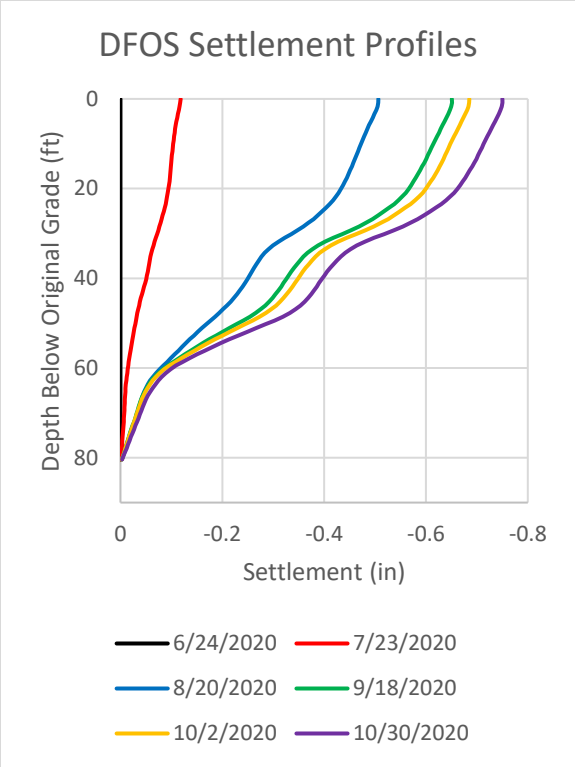

Figure 5-38: Treasure Island DFOS settlement profiles

As is expected, the steepest settlement gradients occur in the depths corresponding to the shallow and Young Bay Mud strain peaks. The values at the top of the settlement profiles represent the calculated settlement at the original grade, corresponding to the location of the settlement plate. The settlement plate was connected to a series of steel rods extending vertically through the fill to the top of the standpipe, where a survey prism was attached. The calculated surface settlement from the fiber optic records is plotted with the survey data from the prism attached to the settlement plate as read by the robotic total station in Figure 5-39.

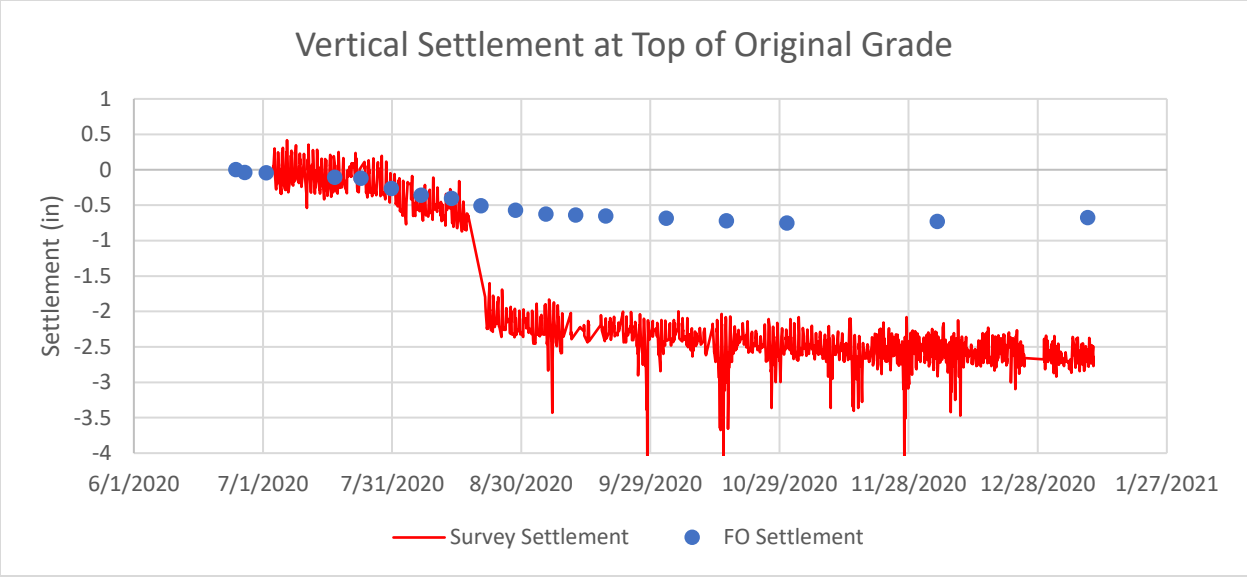

Figure 5-39: Settlement versus time as measured by the survey settlement plate and the integrated DFOS strain readings

A jump in the survey data of 1.6 inches was observed in the survey data in mid-August. Upon review of the field reports, it was determined that this jump corresponded in time to the addition of the next riser section on the settlement plate. The 1.6-inch discrepancy was due to a difference in the riser height and the input correction factor in the survey processing. As such, this jump is an error in the survey and does not represent movement in the field. A correction was applied to the survey data to remove the jump and the results are plotted in Figure 5-40

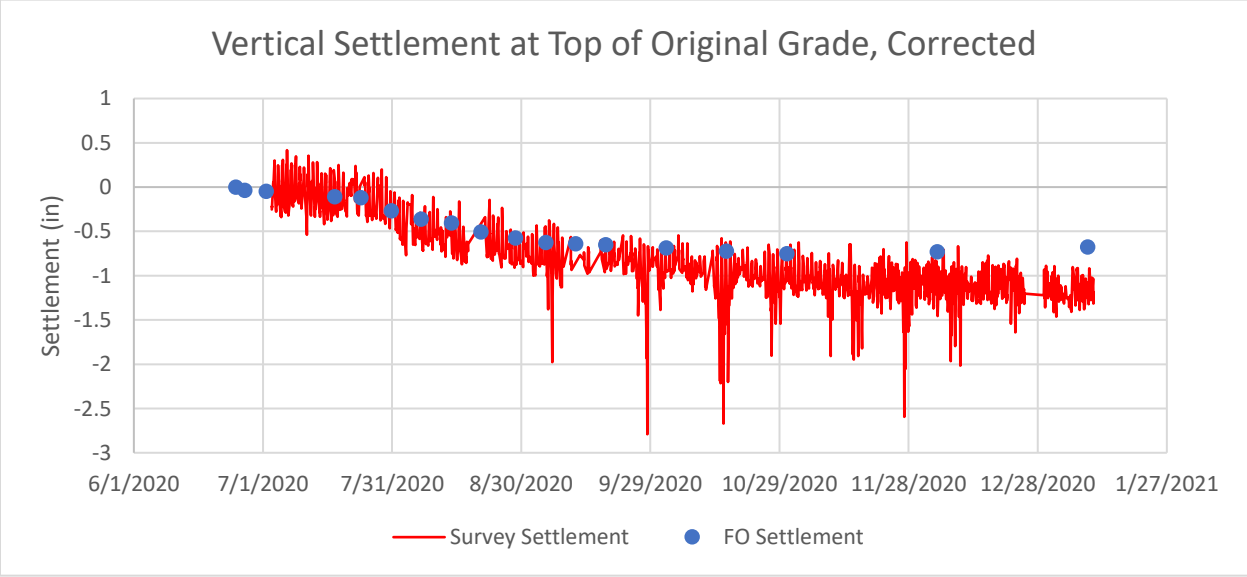

Figure 5-40: Settlement versus time, survey settlement corrected for erroneous jump

In Figure 5-40, the survey settlement and the calculated fiber optic settlement show good agreement for the first several months of monitoring, despite some noise in the survey data. Since each fiber optic point represents an integrated single reading, it is not possible to visually

observe the error of each reading. Instead, we can mathematically calculate the cumulative error of the calculated fiber optic settlement. The manufacturer-reported measurement error is approximately normally distributed with a 20 με standard deviation for each readout point. Expanding this range to 3 standard deviations (+/- 60 με) and propagating the error through the 97 readings from the base of the installation to the ground surface, we calculate an associated cumulative potential error of +/- 0.006 inches with a confidence of 99.7% for the calculated fiber optic surface settlement data.

Towards the end of the settlement plots in Figure 5-40, an increasing gap between the two data sets can be observed in the beginning of November and January. Plotting the strain profiles for the last four fiber optic readings in Figure 3, we note that the strains in the Young Bay Mud have begun decreasing after reaching a peak value of just below 2000 με.

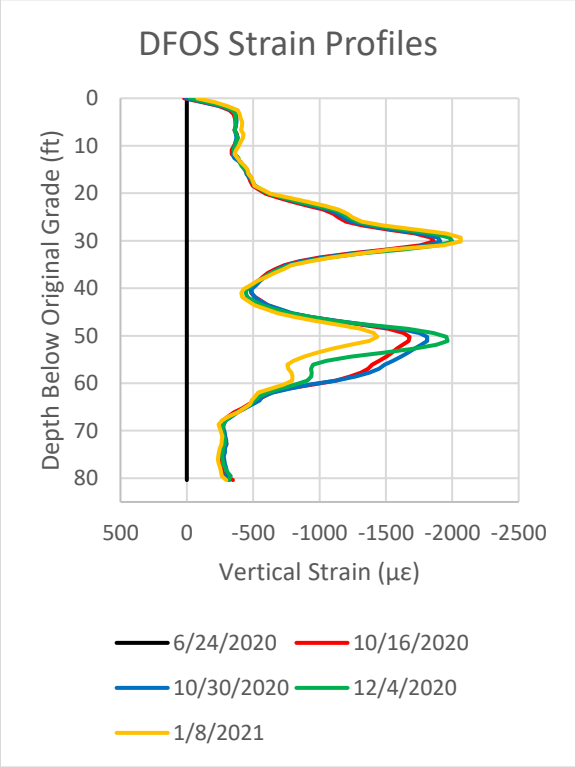

Figure 5-41: Decoupling of the fiber optic cable in the final DFOS strain profiles

The fiber optic strain decreasing in the Young Bay Mud despite continuing settlement measured by the survey marker indicates that the fiber optic strain cable had begun to decouple from the surrounding soil movements. During the installation, a pretension of approximately 2000 με was applied to the fiber optic strain cable during the grout curing. Once the soil had reached a similar strain level through the ongoing settlement, the cable lost all the applied pretension within the grout column. The result of this is that further settlement in the Young Bay Mud cannot be measured by the fiber optic strain cable, nor can the integrated surface settlement be accurately calculated from the data. The signature in the data – a peak corresponding to the

applied pretension, followed by a subsequent drop in strain – can be used to identify decoupling in future installations.

Summary

This research project has confirmed the practicality of installing fiber optic sensing cables via direct-push using a CPT rig. The techniques developed can be used for any fiber optic sensing cable, with the only variable being selection of a suitable grout consistency for the physical property to be measured (e.g., strain compatibility, vibration transference, etc.). The benefits of the expediency and lower cost of installation via CPT over conventional borehole offers the ability to install more monitoring points within a project or allow monitoring to be quickly deployed where it would otherwise be economically infeasible. Following this project, several other field deployments of fiber optic sensing cable using CPT have been performed following the installation techniques and practices developed herein.

The monitoring results of the DFOS strain measurements showed interesting behavior, both in the settlement concentration during surcharge loading as well as the fiber optic cable decoupling after reaching the pretension value. Concentrated strain was observed in both the Young Bay Mud deposit, which was the target of the surcharge loading program and was expected, as well as a shallower clay lens where settlement had not been predicted or analyzed. The quantification of the settlements of the Young Bay Mud, as well as the detection and quantification of the shallower compressible strata, offer a significant insight into the soil performance during loading beyond the 1-point survey data from the settlement plate. Based on these results, we can conclude that the use of CPT to install a fiber optic settlement monitoring system further builds upon the benefits that fiber optic strain monitoring offers. The complimentary data sets of the CPT profile, combined with the continuous fiber optic strain profile, can allow localization of strain to be correlated with the soil resistances of the CPT. While decoupling of the fiber optic strain cable was observed at higher strains, good agreement was shown by the system for strains below 2000 με with the cumulative surface settlement of the survey data. This strain limit is within the range of several common settlement monitoring tasks, when expected settlements are relatively limited in magnitude or concentration. For projects where larger strains are anticipated, changes to the sacrificial CPT tip can be made to potentially provide additional fixity at the base, allowing for a larger pretension to be applied during installation and expanding the application range of this technique. The use of distributed fiber optic sensing for monitoring of soil movements, and specifically the expedient installation via CPT, provides a valuable addition to the instrumentation choices that engineers and stakeholder have at their disposal to develop and maintain an understanding of subsurface movements.

5.4 Discussion

Based on the results of the levee and surcharge fiber optic monitoring, the results were analyzed to evaluate the three research hypotheses.

Hypothesis 1: DFOS for Identification and Quantification of Local Subsurface Strain

The first hypothesis of this research application is that DFOS can be used to identify and quantify highly localized strains that would be difficult or unlikely to be captured using conventional borehole extensometers. This hypothesis is explored by analyzing the localized movements on the two research projects.

Localized Strain – Levee Uplift Monitoring

One condition where localized strain was detected using DFOS was the uplift at the base of the blanket in the Black Hawk levee. The borehole drilling for the fiber optic arrays did not include sampling, making the identification of the transition from clay to the underlying sand imprecise at best. Selection of extensometer anchor elevations based on this imprecise borehole logging would be unlikely to be placed at the exact depth of the maximum uplift strain, missing the peak magnitude of the uplift behavior. This issue is magnified when looking at the fiber optic strain profiles, where the depth of the peak uplift strain varies by 15 feet over the four fiber optic arrays. For this reason, measurement by DFOS holds a definite advantage for the identification of the localized uplift strain. However, the quantification of the strain cannot be directly verified by other measurements on the site. No other subsurface displacement instrumentation was installed, and the calculated vertical displacements at the surface were below the accuracy limitation of conventional leveling survey performed at the site. For this reason, the quantification validation must be performed by a comparison of the measured strains and displacements with those predicted through analysis.

The approach chosen for the calculation of the levee seepage behavior is based on the blanket theory developed by the USACE in response to flooding on the Mississippi River in the early 20th century. The theory resulted in the publication of a series of closed-form solutions to calculate uplift pressure caused by levee underseepage based on the levee geometry and the permeabilities of the blanket and foundation materials, first published in 1956 and most recently summarized in Appendix B of EM 1110-2-1013 (USACE 2000). The solution deemed most appropriate for the levee conditions at the Black Hawk site are captured in Case 7c, comprised of a semi-pervious top stratum both river- and landside with a finite distance to an open seepage exit. In the analysis case, the seepage exit is treated as the line of previously installed relief wells. A diagram showing this case is presented in Figure 5-42.

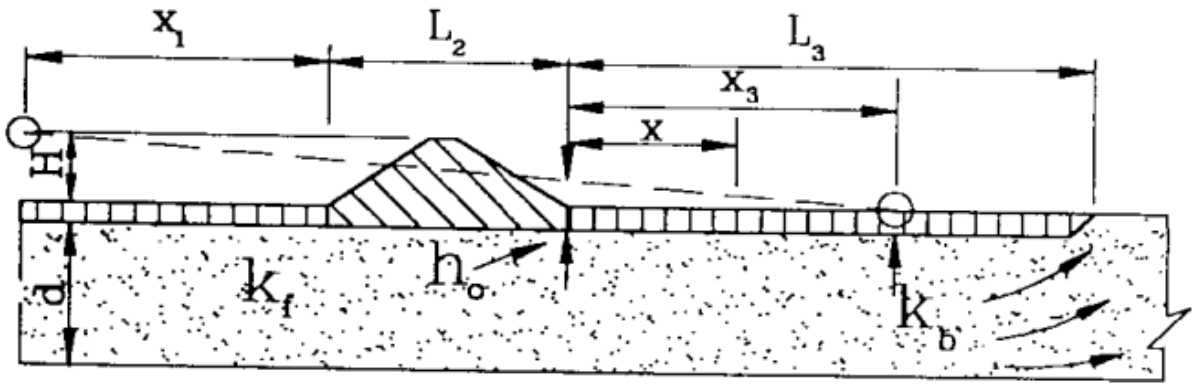

Figure 5-42: Case 7c seepage analysis of levees (USACE 2000)

A river level elevation of 64 feet, measured on February 22, 2022, was used in the analysis. This represents a minor crest in the river level, 11 feet below the design maximum river height, and is at or slightly below the calculated activation river level for the relief wells. The remaining parameters used for the analysis are presented in Table 5-5.

Table 5-5: Blanket pressure calculation parameters

H	river flow line height	26 feet
x_1	distance from effective seepage entry to riverside levee toe	1100 feet
L_2	base width of levee and toe	550 feet
L_3	distance from landslide levee toe to effective seepage exit (relief wells)	200 feet
d	thickness of pervious substratum	96 feet
z_{bl}	thickness of landside blanket	62 feet
k_f	horizontal permeability of pervious substratum	$1225*10^{-4}$ cm/s
k_{bl}	vertical permeability of landside top stratum	$0.15*10^{-4}$ cm/s

The governing equations from the USACE design guide are as follows.

$$h_0 = \frac{Hx_3}{x_1 + L_2 + x_3}$$

$$x_3 = \frac{\tan h(cL_3)}{c}$$

$$c = \sqrt{\frac{k_{bl}}{k_f z_{bl} d}}$$

Adjusting for the change in elevation from the levee toe to the installation depth of the fiber optic arrays, we calculate an expected water pressure at the base of the blanket of 28 psi.

Piezometers installed in the fiber optic borehole arrays within 5 feet of the base of the blanket registered average pressures of 26 psi on the February 22 crest, within 2 psi of the expected value. The piezometer readings nearest the base of the blanket for BH1 and BH2 are shown in Figure 5-43, as well as the corresponding peak strain magnitude.

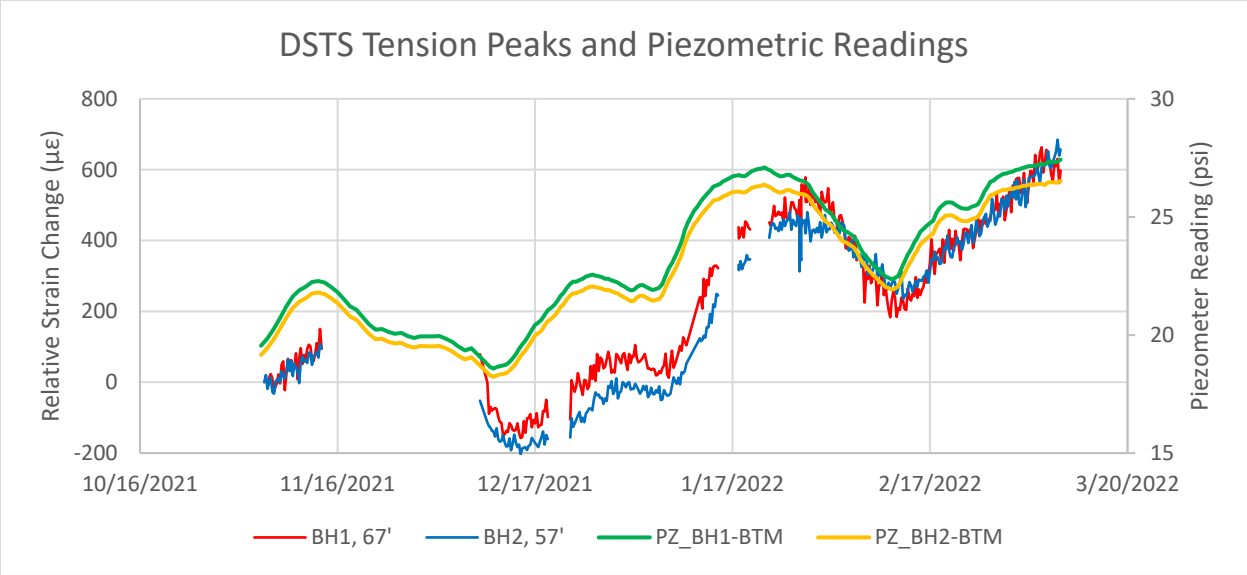

Figure 5-43: Strain peaks and piezometric readings at the bottom of the blanket in BH1 and BH2

As can be seen, the strain measurements peak approximately 4-5 days following the peak in the piezometer data, displaying the same lag as the river level results in Figure 5-22 and Figure 5-28. This indicates that the semipervious blanket is continuous beneath the river channel, causing a delay in the fluctuations of the river and the associated change in water pressure on the landside.

Using the measured water pressure from the piezometers, we can estimate the associated uplift strain at the bottom of the blanket. To achieve this, we must revisit the original underpinnings of the USCE Blanket Theory. In the original publication in 1956, it was hypothesized that sand boils would form when the hydrostatic uplift pressure in the pervious stratum exceeded the submerged total weight of the top stratum (USACE 1956). This concept of the critical uplift criteria is the underpinning of the Blanket Theory and the design of several of the remedial control measures. Following on this concept, we can calculate an estimate of the localized uplift strain at the bottom of the blanket layer by applying the measured uplift pressure against the resting weight of the overlying blanket and predicting the associated strain.

A CPT was performed within the footprint of the fiber optic borehole array in early 2018 to inform the planned sand boil remediation. The CPT, numbered BHK-35.18C, measured 62 feet of soft clay underlain by a transition zone of silty sand to a clean sand substratum. The CPT profile was not included in the original design report appendix (USACE 2018a), but it was

included as a plate in the associated solicitation bid package for the remediation works (USACE 2018b). A capture of the CPT results is presented in Figure 5-44.

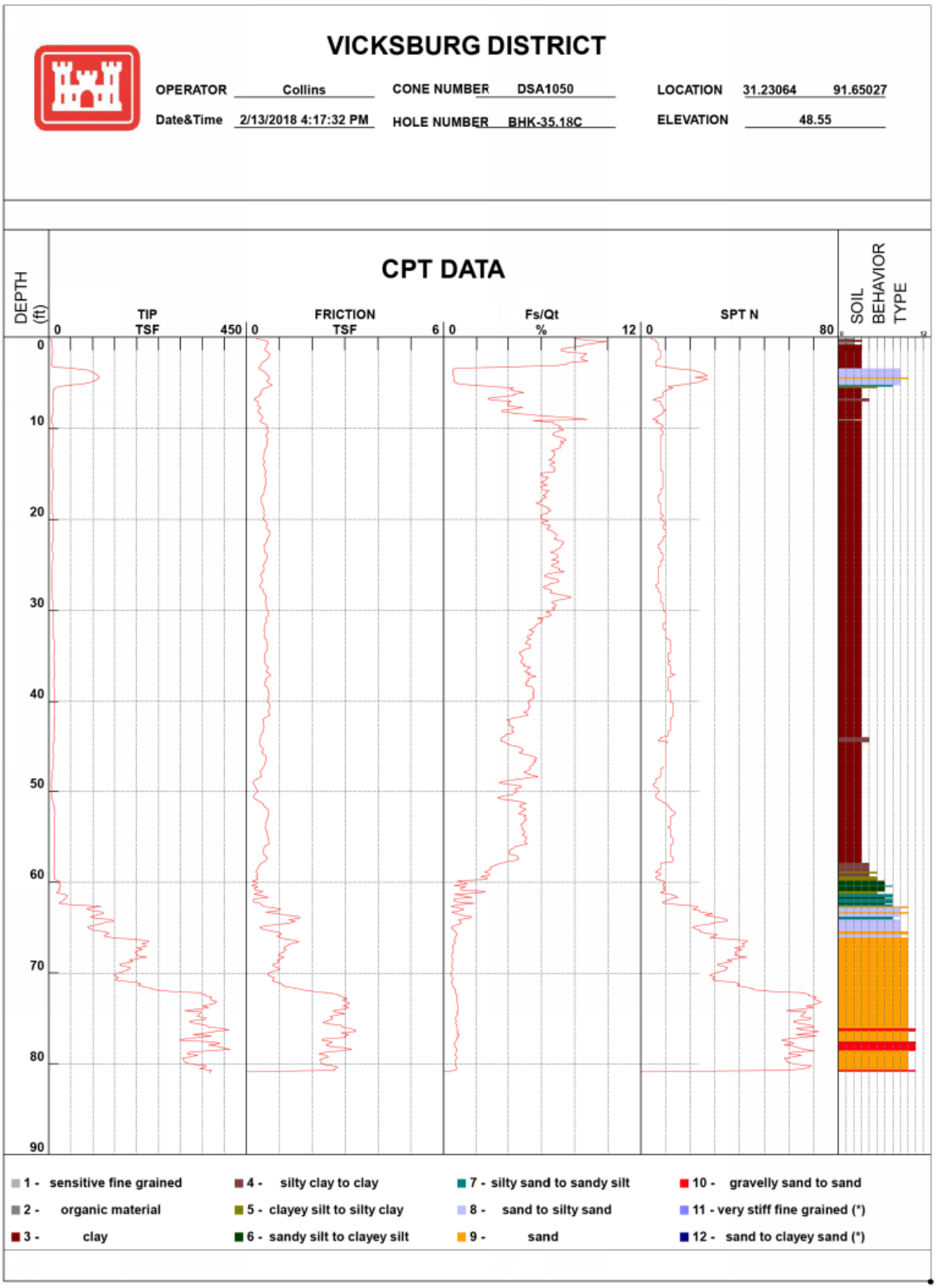

Figure 5-44: CPT BHK-35.18C profile (USACE 2018b)

The tip and sleeve friction profiles were digitized using an image recognition tool, and the associated data at the bottom of the clay blanket was extracted. The Young's modulus, E', of the silty clay just below the bottom of the blanket was calculated using the equation proposed by Robertson for uncemented silica-based soils of Halocene or Pleistocene age, presented below (Robertson 2009).

$$E' = 0.015\left[10^{(0.55I_c+1.68)}\right](q_t - \sigma_{v0})$$

From the above relationship, we calculate a Young's modulus of $2.0 \cdot 10^6$ psf. With a measured excess porewater pressure of 1120 psf over hydrostatic, we calculate an associated local strain of 520 με. The measured peak strains following the late January river crest for BH1 and BH2 were 530 and 480 με, respectively. The calculated relationship can be extrapolated and applied to the entire piezometric record in the BH1 and BH2 boreholes. Since the measured strains are relative to the initial baseline, the referenced pressures have also been baselined to the initial November 4, 2021 reading, as well as shifted by 4 days to reflect the observed time lag. The results of this analysis are shown in Figure 5-45.

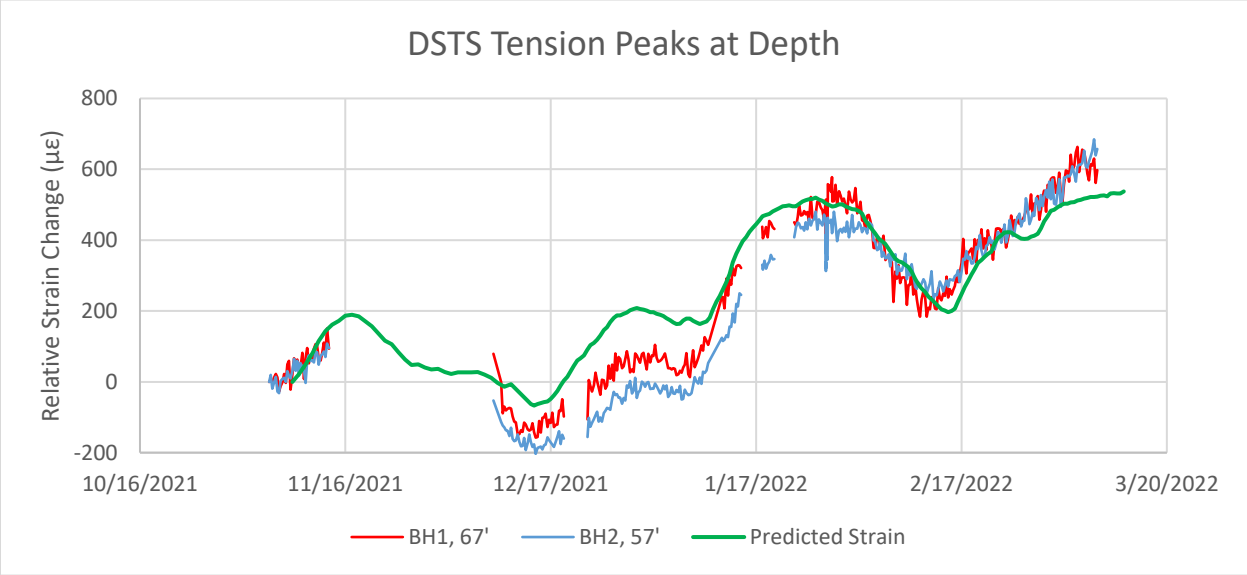

Figure 5-45: Measured and predicted peak uplift strain in BH1-BH2 cross section

The predicted and measured strain magnitudes show relatively good agreement. One notable exception is the period between early December 2021 and early January 2022, when the measured strains are approximately 100-200 με lower than the predicted values. This dip corresponds to the lowest measured elevation of the river, as well as strain values below the initial baseline. Further monitoring is needed to ascertain if this is a limitation of the fiber coupling in this strain regime or a non-linear dropoff between the uplift pressure and the associated uplift strain.

The uplift strains measured and calculated at the levee are highly localized and are not able to be reliably measured or detected by conventional measurement techniques. The likelihood of

accurately placing a borehole extensometer at the precise location where the peak strains were observed is remote, and without multiple anchors in close proximity it would be impossible to determine if the true peak had been measured. Furthermore, the small relative displacements in reference to the ground surface (on the order of 0.01 inches) are within the +/- 0.1% full-scale accuracy limitations of many extensometer heads, depending on the overall range chosen. This represents a positive test result and confirms the original hypothesis that DFOS can be used to identify and quantify highly localized strains, such as the uplift at the bottom of a levee blanket. The subsequent analysis of the predicted uplift water pressure and the associated strains provides an indirect validation of the fiber optic measurements, given that they could not be directly validated using conventional instrumentation or ground survey. This furthermore is the first published direct measurement of the uplift of the clay blanket, providing support for the long-hypothesized uplift pressures which inform much of the U.S. Army Corps of Engineers' design basis for levee seepage.

Localized Strain – Surcharge Loading

Localized strain was also detected using DFOS during the surcharge loading monitoring on Treasure Island. Two areas of strain concentration were detected in the measurement profiles – one concentrated in the Young Bay Mud and a second in a previously unidentified shallow deposit, likely a clay lens. While the displacements of the Young Bay Mud could likely be measured using a conventional extensometer at the top and bottom of the clay layer, the shallow lens was not identified in the geotechnical investigation and is unlikely to have been identified for an anchor location. While the relative impact of the shallower clay lens is small when compared to the settlements in the Young Bay Mud, it could have an impact in another project built on a similar profile.

The integrated vertical displacements measured by the DFOS strain array were able to be validated using the survey monitoring measurements of the settlement plate. As was discussed in Section 5.3, the two displacement measures showed good agreement prior to the decoupling of the fiber optic cable in November 2020. The fiber optic records allow us to quantify the relative contributions of the two deforming layers and compare the results

On the last reading prior to decoupling on October 30, 2020, a calculated surface settlement of 0.75 inches was detected by the fiber optic monitoring system. The readings from the survey system ranged from 0.80 to 1.1 inches, reflecting the high noise in the data but still in general agreement with the overall magnitude of settlement calculated using the DFOS data. The strain and settlement profile for the October 30 reading is shown in Figure 5-46 and Strain profile of 10/30 reading Figure 5-47: Settlement profile of 10/30 reading, respectively.Figure 5-46:Strain profile of 10/30 reading Figure 5-47: Settlement profile of 10/30 reading

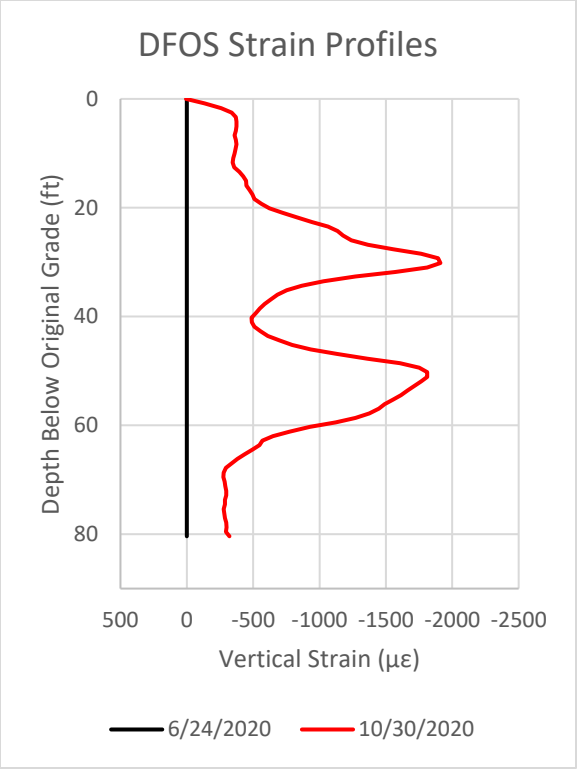

Figure 5-46:Strain profile of 10/30 reading

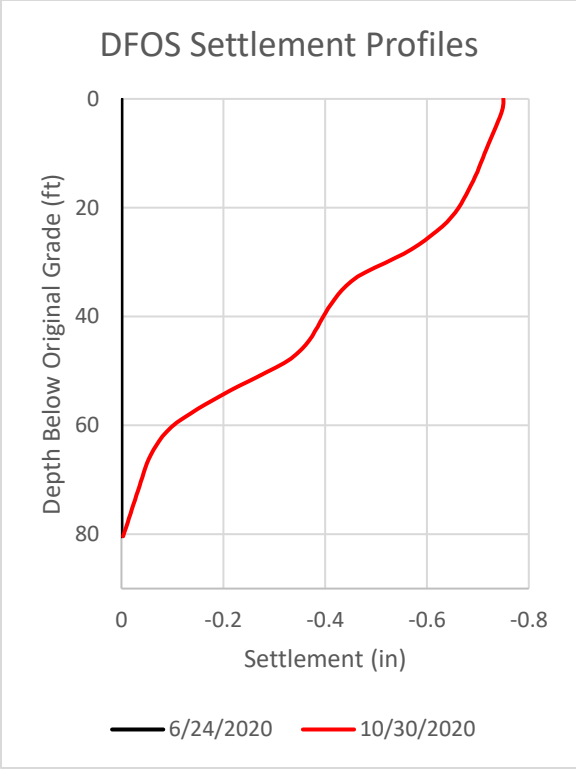

Figure 5-47: Settlement profile of 10/30 reading

Looking at the settlement profile, it is possible to isolate the relative portion of the 0.75 inches of surface settlement attributed to the Young Bay Mud and the shallower deposit. In the October 30 reading, the Young Bay Mud contributed 0.34 inches of settlement (45% of the total), while the shallow deposit contributed 0.27 inches of settlement (36% of the total). The magnitude of settlement of each of the two layers were relatively similar; however, the displacements of the shallower deposit were not anticipated in the initial loading design. The consolidation behavior of the two layers is shown in Figure 5-48. The shallow layer has a higher starting strain, having compressed under the initial 20 inches of fill. The period covered by the chart is the time and period during which the full 8.2 feet of surcharge of the full lift was in place. The Young Bay Mud accumulates strain at a similar rate initially as the shallower layer, however it accelerates to a faster rate as the Young Bay Mud enters virgin compression.

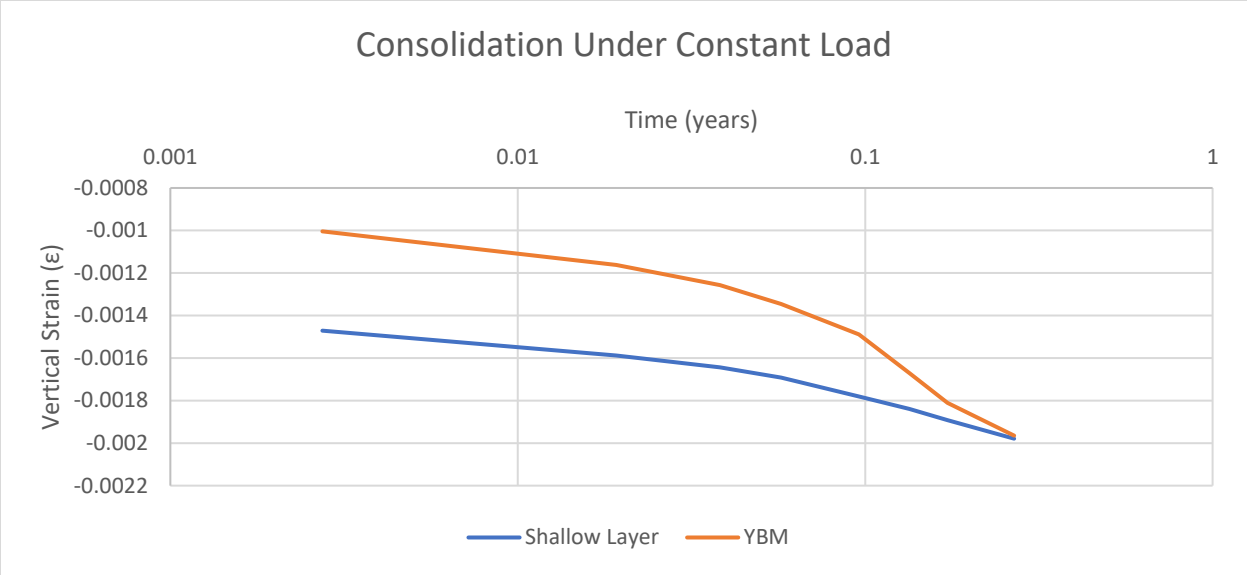

Figure 5-48: Time rate of strain plot for the consolidation of the shallow layer and the Young Bay Mud under constant load

The timing of the additional stages of surcharge is based on the calculation of the degree of consolidation that the Young Bay Mud (the target of the surcharge program) has reached. Subsequent stages are only placed once the Bay Mud has reached the target degree of consolidation. If all the observed surface settlement measured by the settlement plate is attributed to the Young Bay Mud, the project engineer would incorrectly calculate that the Young Bay Mud has reached a higher degree of consolidation than is true when determining the placement of the next surcharge stage. If the limited factor is strength of the Young Bay Mud, as is often the case in surcharge programs, this could potentially result in a soil failure if the load is applied too early. While the design and calculation of the surcharge program was not made available by the project engineers, we can calculate the degree of consolidation likely reached by the Young Bay Mud as of the October 30 reading. Two consolidation tests using constant rate of strain were performed on samples from the Young Bay Mud (ENGEO et al. 2019). The compression index, C_c, calculated from the test results for the applicable axial stress interval were 0.126 and 0.156. Using this information, as well as the height of the Young Bay Mud and the initial and final effective stress, we can calculate a total expected consolidation settlement S_c of 0.9 to 1.5 inches under the initial 8.2-foot lift. Comparing this to the measured settlement of 0.34 inches, the settlement was approximately 23 to 38% S_c. Although the precise spacing and geometry of the wick drains on the site are not known, an assumed triangular geometry with 8-foot-spacing would result in a predicted degree of consolidation of 42% after 3 months. This shows agreement between the calculated and predicted consolidation values, although it is not known what the acceptance criteria for this surcharge stage was prescribed as.

Summary

The localized strain in the levee uplift monitoring and the surcharge loading program were captured and quantified by the DFOS strain monitoring installations. It is improbable if not impossible that the localized strain at the blanket boundary at the levee site, or the thin compressible layer at the surcharge site, would be captured using a conventional extensometer measurement system. This represents a positive test result for the hypothesis that distributed fiber optic strain sensing offers a significant advantage over conventional monitoring for the detection and measurement of localized subsurface vertical strain. The subsequent calculations and analysis in each of the loading cases further validate the measurements and demonstrate the value that the continuous strain and displacement readings can offer.

Hypothesis 2: Temperature Compensation for Vertical Soil Monitoring

The second hypothesis of the research project is the necessity of temperature compensation for the DFOS strain measurements in installations where surface temperature changes will affect the strain cable. The published state of practice is to treat the ground temperature as constant, thereby removing the need for thermal measurement or compensation. The test for this hypothesis is to analyze the extent of temperature fluctuations in a subsurface DFOS installation and quantify the effect on the strain and displacement output. A negative test would be that the temperature does not fluctuate significantly within the strain fiber, or that the fluctuations are not significant enough to have a material effect on the strain and displacement profiles. A positive test result would be that the surface temperature fluctuations do have a significant effect on the strain readings and that compensation is necessary to ensure accuracy of the data.

The need for thermal compensation for Brillouin-based strain sensing is well documented in the literature and may be considered the standard of practice (Kechavarzi et al. 2016). However, surface or subsurface temperature measurements have not been incorporated in the published research trials using DFOS for vertical soil monitoring. In cases where this is addressed, the authors propose that the temperature of the subsurface may be treated as stable during the monitoring duration and thermal compensation is therefore not required. While this is generally true at depth, diurnal and seasonal temperature variations at the ground surface can cause changes in the temperature of the soil extending into the ground. The magnitude and depth of the temperature effect depends on several factors, including the thermal conductivity of the soil and the relative differential between the surface temperature and the steady soil temperature. The effect of temperature changes in the subsurface can alter the interpreted strain readings and have an even greater impact on the integration of strain into displacement. While the strain readings in the top portion of a DFOS strain installation may be discarded in recognition of this impact, this makes calculation of the displacements at the ground surface impossible as the strain contribution of the discarded depth would be ignored.

At the Black Hawk levee site, complementary strain and temperature cables were installed in all four monitoring boreholes. Diurnal and seasonal temperature changes were observed in all of

the records, with temperature variations of over 10° Fahrenheit and effects extending up to 20 feet below the ground surface. The measured temperature variation over time for BH1 in 10-foot increments is plotted in Figure 5-49.

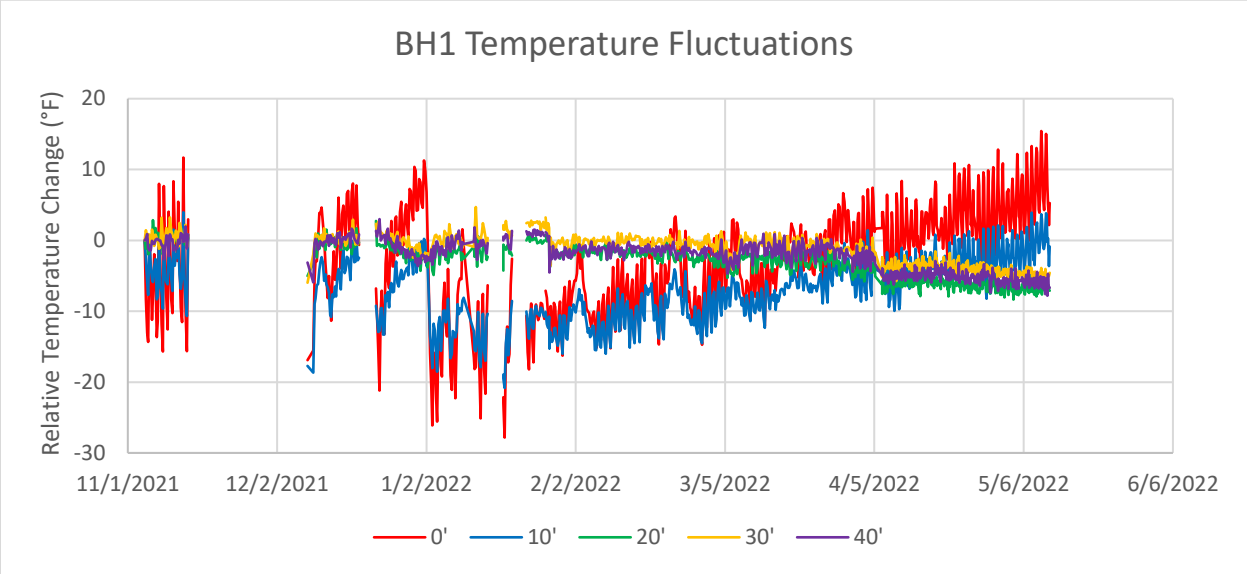

Figure 5-49: BH1 DFOS temperature fluctuations over time

The dominant feature of the temperature data is the high degree of variation in the 0- and 10-foot depth measurements. The average daily fluctuations are over 10 degrees at the ground surface and 5 degrees at a depth of 10 feet. The readings from 20, 30, and 40 feet below grade are relatively stable by comparison, however they show a gradual 5 degree decrease between March and May. This plot shows that the surface temperature fluctuations have a real and quantifiable impact on the fiber optic cables for 10-20 feet below the ground surface, as well as a seasonal change in temperature across the borehole in the relatively stable deeper zones.

With the temperature fluctuations that were measured, it is possible to isolate the relative impact that they have on the strain readings at the corresponding depths. The temperature correction factor, combing the thermal coefficients of both the Belden thermal cable and the Nanzee strain cable, was calculated to be 19.7 με/°F. The relative strain effect of the temperature fluctuations is plotted in Figure 5-50.

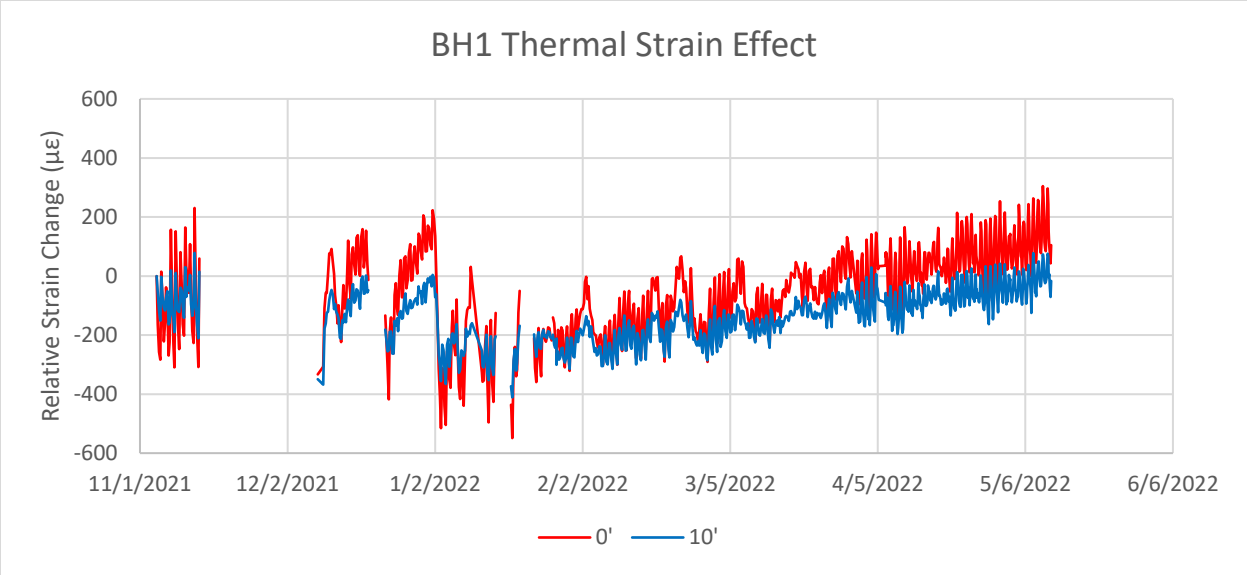

Figure 5-50: BH1 equivalent strain effect of measured thermal fluctuations

The thermal effect on the strain readings fluctuation between +/- 400 με. This is an order of magnitude greater than the strain resolution of the fiber optic analyzer and is in the same range as the processed strain readings' magnitude. Due to the significance of the thermal effect, It is necessary to apply temperature compensation on the strain readings within the top portion of the fiber optic borehole records. Temperature compensation is applied during the frequency processing of the fiber optic data and is applied across the entire strain record by depth with the corresponding temperature reading.

The impact of the temperature fluctuations on the strain sensing cable is magnified when integrating the strain data into displacement. The equivalent surface strain delta calculated by isolating the thermal effect is shown in Figure 5-51

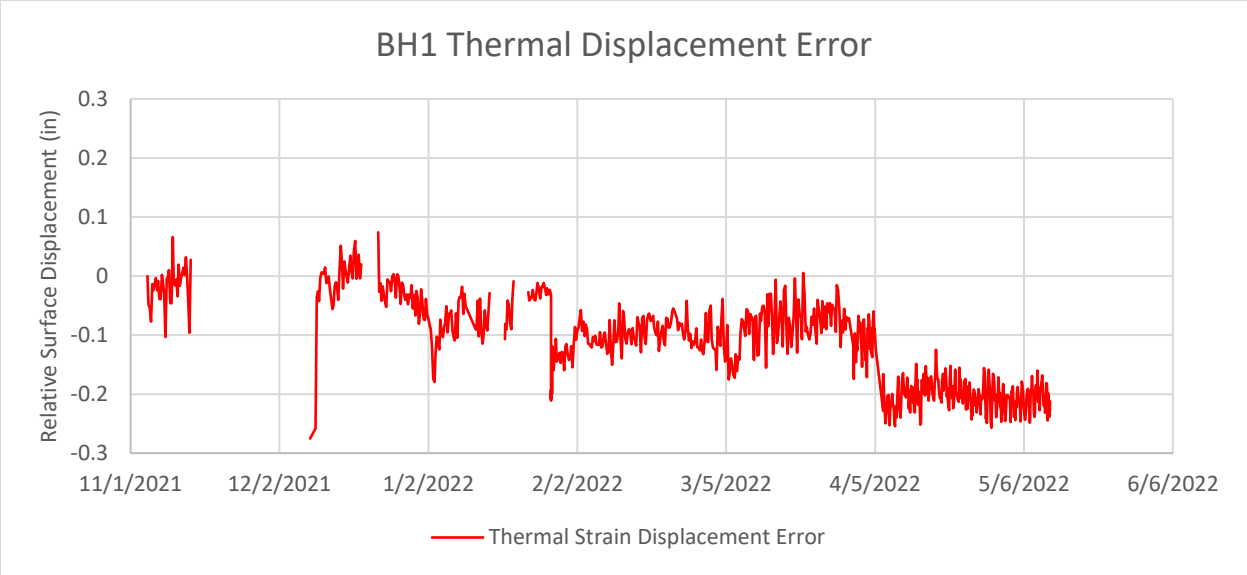

Figure 5-51: BH1 thermal strain displacement error

The combined effect of the temperature fluctuations recorded in BH1 reaches a maximum effect of over 0.2 inches on the calculated relative surface displacement. This error is double the magnitude of the maximum corrected surface displacement of 0.1 inches in BH1.

As has been demonstrated, the impact of temperature fluctuations along the vertical fiber optic strain cable has a significant effect on the Brillouin strain measurements of the installation. The vertical extent and magnitude of these changes are well above the threshold for requiring compensation in the strain record, often reaching magnitudes several times the error of the analyzer, into the 100s of με. This represents a positive test result for the original hypothesis, and we can recommend that a thermal cable be incorporated into vertical strain measurement installations to perform thermal compensation of the measured data. While there are caveats and practices that can be adopted to partially mitigate the temperature effects, such as projects where the baseline and monitoring are close enough within time that the temperature fluctuations are not significant or ongoing, the default should be to measure the temperature and make an informed determination later if the observed impact is large enough to warrant thermal compensation.

As was mentioned in Section 5.3 on the use of fiber optic monitoring for the surcharge loading program, no thermal fiber optic cable was installed on the project, nor was temperature compensation performed on the strain dataset. The justification for this was that the measurement section of the fiber optic strain cable, terminating at the top of the original grade, would be capped with approximately 8-feet of surcharge soil. This cap of soil was presumed to effectively isolate the top of the measurement portion of the cable from temperature changes at the surface. Since no direct temperature measurements were taken using a complementary thermal fiber optic cable, another method must be employed to evaluate the potential temperature impact on the measurement interval. At the top of the original grade, an extra 120

feet of strain cable was left to allow enough slack to thread through the vertical standpipes and reach a remote reading site off the surcharge pad if vehicular access to the standpipe was cut off. This extra cable was left loosely coiled between and during readings and was not subjected to any external mechanical strain. The measured frequency fluctuations in this section of cable, therefore, were due to temperature fluctuations in the cable between reading intervals. The Brillouin frequency over time of the loose cable and the reading at the top of the original grade is shown in Figure 5-52.Figure 5-1

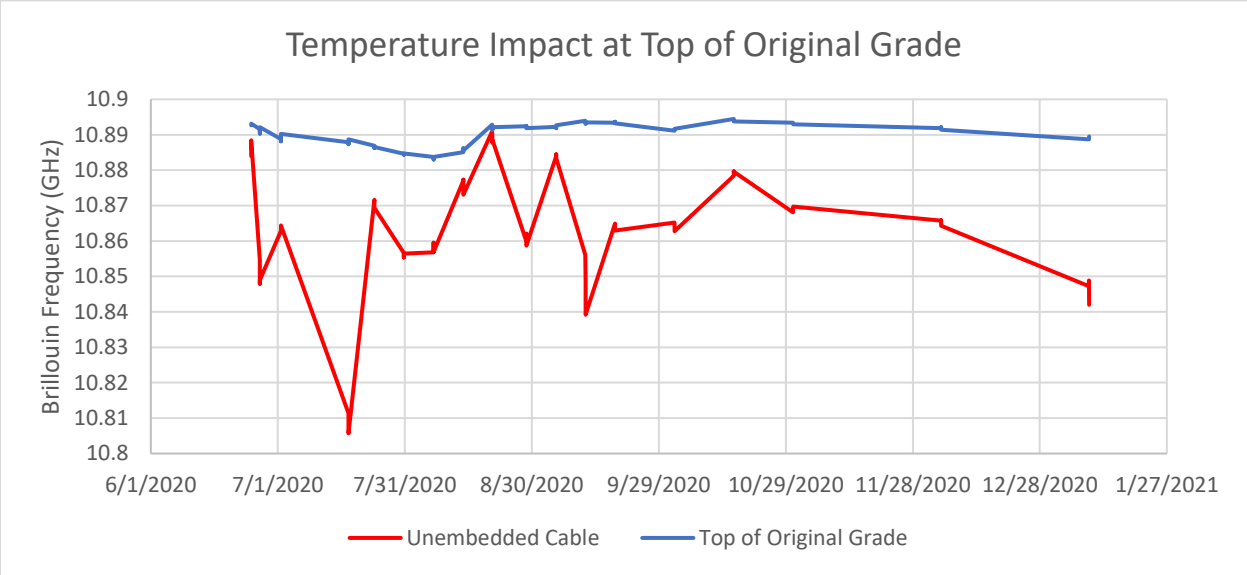

Figure 5-52: Brillouin frequency over time of loose, unembedded cable and the top of the measurement interval

From a visual inspection, the frequency fluctuations of the unembedded cable and the embedded cable do not closely correlate. This indicates that the temperature changes affecting the unembedded cable were not having a significant impact on the measurement portion of the installation. Despite the lack of impact in this case, for future long-term vertical soil monitoring installations it is recommended to install a separate, complementary thermal fiber optic cable to allow for quantification and correction of the potential temperature effect on the strain measurements.

6. Conclusion and Recommended Future Work

This dissertation presented a series of research projects into the deployment and improvement of distributed fiber optic sensing for geotechnical applications. The work included laboratory experiments to characterize the sensing performance of the fibers and optical analyzers used in the research, as well as three field trials with detailed analysis of the measurement and geomaterial performance. Several novel findings were enabled using DFOS, including measurement of bending in a controlled top-down pile load test, quantification of uplift strain on the landside of a levee, and localization of compressive strain during a surcharge loading program. Based on the research, the following best practices are recommended.

6.1 Best Practices for Fiber Optic Monitoring of Strain in Deep Foundations

DFOS has been shown to offer an improved method for monitoring temperature and strain in deep foundations. While research into this field has been ongoing for over two decades, several improvements have been explored in this research and validated as offering distinct benefits over the current standard of practice and conventional instrumentation alternatives. The results are summarized below.

Instrumentation Design and Installation

- A minimum of three fiber optic strain verticals should be deployed around the reinforcement cage of instrumented large-diameter deep foundations, with four being preferable for BOTDA where looped cable routing is required. This approach is consistent with best practices in structural health monitoring of surface assets but has not been adopted for deep foundations. The benefit of a 3- or 4-vertical deployment is to allow identification of non-uniform strain behavior and reconcile bending direction and magnitude, as shown in Section 4.5, Hypothesis 2. This represents an improvement over the current state of practice of single or 2 vertical fiber optic cables installations.
- At least one thermal fiber optic cable should be deployed in each monitored deep foundation to allow measurement of temperature changes during the monitoring period. While thermal compensation may not be deemed necessary if the temperature remains stable during testing, the absence of measurements precludes verification of this assumption and correction if necessary. In cases where construction activity may change the temperature within the pile, such as during grout injection, a thermal fiber optic cable should be paired with each strain cable for 1:1 thermal compensation measurement. This was shown in Sections 4.3 and 4.4.
- Strain fiber optic cables which are fully encapsulated in structural concrete during construction do not require pretensioning during installation to accurately measure compressive strain in the pile. The confinement of the concrete and the comparative small stiffness of the fiber optic cable provide strain compatibility through large compressive strains. This improvement over the current state of practice simplifies installation and reduces the chance of breakage on site during cage placement and concreting. This was shown in Section 4.5, Hypothesis 1.

- Validation data sets may be necessary for applications where DFOS is being deployed for the first time. However, DFOS for temperature and strain measurements have proven to provide comparable measurements to conventional instrumentation and may be considered mature enough to be deployed alone. In critical projects, fiber optic loops may be prudent to deploy to provide redundancy in the event of damage or breakage of the fiber optic cables during installation. This approach was taken in Section 4.2.

Measurements During Loading

- Careful attention should be paid to the reading duration of the fiber optic analyzer and the load fluctuations within the pile during the reading. When possible, the load within the pile should be held constant during the reading interval. For load testing with an analyzer with a long (several minutes) reading duration, this would require a test control system which is load controlled rather than pressure, volume, or displacement controlled. Alternatively, new research and commercial analyzers with reading times at or under one second can be used when loads cannot be held constant for several minutes. In cases where the load is not held constant during the reading interval, careful measurement of the load should be taken, and the reading architecture of the analyzer should be considered in processing and presenting the data. When possible, the effect of transient strain on the measurement output should be quantified and/or corrected. The effect was confirmed during laboratory testing in Section 3.4 and the correction was applied to field data in Section 4.5, Hypothesis 3. This effect has not been previously written about or quantified in the literature.
- Standard commercial fiber optic analyzers are not appropriate for applications with rapidly changing loading within the pile, such as those encountered during base grouting. Research or commercial analyzers with fast reading intervals, less than 0.1 seconds, should be adopted in these cases and tested to confirm their ability to capture rapid strain changes. This was observed in the data presented in Section 4.3. This consideration is not currently included in the state of practice.

Data Processing and Analysis

- Strain measurements should be evaluated in the full context of the pile behavior during loading before identifying or discarding suspected erroneous data. The non-idealized behavior of deep foundations during loading can be captured using DFOS monitoring best practices and it is to the benefit of the engineer to evaluate the data as such. Averaging data with depth, while the standard practice, should be done only first exploring non-uniformities in the strain distribution and identifying the explanation and potential impact of this behavior. This approach was presented in Section 4.5, Hypothesis 2. This represents an improvement over the current state of practice.

6.2 Best Practices for Distributed Fiber Optic Sensing for Vertical Soil Deformation

DFOS offers a range of benefits over conventional point-based monitoring of vertical subsurface displacement. This research has identified several novel applications for the technology as well as improvements in the installation and processing of the subsequent data.

Instrumentation Design and Installation

- Fiber optic cables can be installed within conventional geotechnical boreholes, or as piloted in this research, direct push via CPT. The soil should be logged and characterized whenever possible to correlate later measurements to observed changes in the stratigraphy. This approach formed the basis of the work in Chapter 5. The installation of fiber optic cable via CPT was a new development of this research.
- It is necessary to pretension fiber optic strain cables in soil installations to accurately measure compression of the soil. The effective pretension acts as an upper limit of the localized strain that can be captured by the monitoring fiber. When possible, the pretension should be controlled and measured during the field installation, both by measuring the load using a tension meter as well as taking fiber optic strain readings of the sensing fiber to confirm uniform strain along the monitoring section. The pretension must be maintained during the curing of the cement grout and should be measured again during the baselining of the installation. This approach was taken in the work presented in Sections 5.2 and 5.3.
- The fiber optic cable should be grouted into place using a suitable geotechnical grout mixture. Care should be taken to not select too strong of a grout which could compromise the strain transfer between the soil and the fiber optic cable. Best practices for grouting of conventional geotechnical instrumentation should be applied, and the grout strength should be chosen to approximately match the soil unit where the most important deformations are anticipated. This approach was taken in the work presented in Sections 5.2 and 5.3. The application of geotechnical instrumentation grout to fiber optic installations has not been previously published and may be an improvement over the current state of practice, although the grout selection is not often specifically discussed in the literature.
- The fiber optic strain cable should be installed to a termination depth below the area of anticipated movement. It is recommended that the fiber be firmly anchored at least 10 feet or 3 meters into stable ground. This approach was taken in the work presented in Sections 5.2 and 5.3.
- Thermal fiber optic cable should be deployed in strain installations to allow for temperature measurement and thermal compensation. This is particularly necessary for installations where the strain data is intended to be integrated to calculate surface deformation. Temperature fluctuations can occur both at the ground surface as well as at depth which can have a significant effect on the calculated strain and displacement within the installation. This was discussed in Section 5.4, Hypothesis 2. This represents an improvement over the current state of practice, where strain cables are installed

without temperature correction and the ground temperature is treated as constant during analysis.

Measurements During Monitoring

- For projects where readings are being taken intermittently (the analyzer is not connected and monitoring continuously at a set interval), a minimum of three measurements should be taken at each reading. The three measurements should be compared with each other to confirm that the analyzer is functioning within its expected repeatability, and the measurements should be compared with the previous reading to confirm that the data is valid and is within an expected range. This step enables the user to diagnose potential issues with connection or the analyzer in the field, rather than after returning to the office. This practice was applied in the intermittent readings in Section 5.3.
- Jumps or shifts in the data should be interrogated promptly and noted within the data reporting. Error correction should be performed only after identifying, and if possible, resolving the cause. This approach has been applied in the work in Sections 5.2 and 5.3.
- Survey elevation should be established at the top of the fiber optic installation at the baseline so that the calculated surface displacement can be validated during the monitoring program if needed. This has been applied in Sections 5.2 and 5.3.

Data Processing and Analysis

- Localized areas of strain concentration should be evaluated and compared to exploration and stratigraphic data in the area. These measurements likely represent real data and provide insight into the soil behavior that is not otherwise possible without the use of DFOS. This was the case in the measurements presented in Sections 5.2 and 5.3, as well as discussed in detail in Section 5.4, Hypothesis 1. The localization of levee uplift at the clay blanket and the localized strain during surcharge loading are new findings and have not been previously documented in the literature.
- If local strains approach the pretension value, be watchful for signs of potential decoupling. The signature of decoupling (in compression) is a decrease in compression in continuing readings, despite a lack of substantive change (i.e., unloading) on the site. The decoupling can be further verified by comparing the integrated displacements with the survey elevation measurements at the top of the installation. This was discussed in Section 5.3. The effect and data signature of decoupling of the fiber optic cable from the soil is a new finding and has not been previously published in the literature.

6.3 Recommendations for Future Work

Based on the findings and limitations of this work, the following areas have been identified as benefiting from future research.

DFOS for Post Grouting of Deep Foundations

The results of this study indicate that the suitability of DFOS for the monitoring of foundation strains during post grouting depends on the reading time of the analyzer. The grout injection process is highly erratic, and the loads imparted at the base of the pile are even more so. While the benefits of strain measurement during grouting has been established as an important QA/QC tool, DFOS only becomes a viable solution if the reading time can be reduced to 1 second or less. This removes the temporal variability introduced by the analyzer architecture and can more accurately capture the strain distribution in the pile, both in depth and plan section. It is recommended that DFOS using an analyzer with a fast read time be deployed for a future post grouted foundation test, and the results be analyzed for further insights into the grout delivery performance.

DFOS as a Detection Tool for Sand Boil Development

This research represents the first time that uplift strains at the base of the blanket layer on the landside of a levee have been directly measured and correlated with changes in the river level and excess water pressure. The triggering event for sand boil formation, according to the USACE blanket theory, is when the excess water pressure exceeds the weight of the blanket and a fracture forms in the blanket, allowing a sand boil to form and reach the surface. It is hypothesized that this sand boil formation would result in a rapid loss in pressure, coinciding with a partial collapse of the uplift strain at the bottom of the blanket. This has yet to be directly verified and, if confirmed, could act as a remote sensing technique for the formation of new sand boils. While this technique would require a fiber optic cable to be deployed at the sand boil location, multiple vertical fiber optic arrays could be quickly installed using CPT and networked together to a single analyzer.

Increasing Anchor Force in CPT Installed Strain Cables

As has been previously discussed, the compressive strain that is able to be measured by a fiber optic cable installed in soil is limited by the pretension that is applied to the cable during installation. The pretension is limited by the anchorage force of the sacrificial CPT tip. An increase in the resistance of the tip to pull out could be achieved through either increased length of the tip resulting in increased friction or the addition of anchoring fins which would resist upward movement. This would allow a greater pretension to be applied, increasing the upper strain limit of the installation.

Bibliography

de Battista N, Kechavarzi C. 2021. Monitoring of Piles and Diaphragm Walls with Distributed Fibre Optic Sensors. In: Piling 2020: Proceedings of the Piling 2020 Conference. ICE Publishing. p. 497–502.

de Battista N, Kechavarzi C, Soga K. 2016. Distributed fiber optic sensors for monitoring reinforced concrete piles using Brillouin scattering. In: Sixth European Workshop on Optical Fibre Sensors. Vol. 9916. SPIE.

Bell A, Soga K, Ouyang Y, Yan J, Wang F. 2013. The role of fibre optic instrumentation in the re-use of deep foundations. In: Proceedings of the 18th International Conference on Soil Mechanics and Geotechnical Engineering. Paris, France. https://www.issmge.org/publications/online-library.

Bennett PJ, Klar A, Vorster TEB, Choy CK, Mohamad H, Soga K, Mair RJ, Tester PD, Fernie R. 2006. Distributed optical fibre strain sensing in piles. In: Reuse of Foundations for Urban Sites: Proceedings of International Conference. Watford, UK. p. 105–114. https://www.researchgate.net/publication/265684641.

Bersan S, Bergamo O, Palmieri L, Schenato L, Simonini P. 2018. Distributed strain measurements in a CFA pile using high spatial resolution fibre optic sensors. Eng Struct. 160:554–565. doi:10.1016/j.engstruct.2018.01.046.

Blum JA, Nooner SL, Zumberge MA. 2008. Recording earth strain with optical fibers. IEEE Sens J. 8(7):1152–1160. doi:10.1109/JSEN.2008.926882.

Bruce DA. 1986. Enhancing the performance of large diameter piles by grouting. Ground Engineering.

Day TJ, Boeckmann AZ, Loehr JE. 2015. Separating Contributions from Pre-Mobilization and Ground Improvement for Post-Grouted Drilled Shafts. In: IFCEE 2015. Reston, VA: American Society of Civil Engineers. p. 951–960. http://ascelibrary.org/doi/10.1061/9780784479087.086.

DFI, Large MEB. 2016. Workshop on Quality Assurance For Post-Grouted Drilled Shafts (FHWA-HIF-16-015). Oakland.

ENGEO, Papadopulos S, Espinosa P, Stuecheli P, Tootle JJ. 2019. Geotechnical Exploration. Wastewater Treatment Plant - Site Development. Treasure Island, San Francisco, California.

FHWA, Loehr JE, Marinucci A, Duffy PH, Gomez J, Robinson H, Day T, Boeckmann A, Cadden A. 2017. Evaluation and Guidance Development for Post-Grouted Drilled Shafts for Highways (FHWA-HIF-17-024). https://www.fhwa.dot.gov/engineering/geotech/pubs/hif17024.pdf.

Iten M, Schmid A, Hauswirth D, Puzrin AM. 2009. Defining and monitoring of landslide boundaries using fiber optic systems. In: International Symposium on Prediction and Simulation Methods for Geohazard Mitigation. Kyoto, Japan.

Kechavarzi C, Soga K, de Battista N, Pelecanos L, Elshafie MZEB, Mair RJ. 2016. Distributed Fibre Optic Strain Sensing for Monitoring Civil Infrastructure. de Battista N, Elshafie MZEB, Pelecanos L, Kechavarzi C, Mair RJ, Soga K, editors. ICE Publishing. https://www.icevirtuallibrary.com/doi/abs/10.1680/dfossmci.60555.

Klar A, Bennett PJ, Soga K, Mair RJ, Tester P, Fernie R, St John HD, Torp-Petersors G. 2006. Distributed strain measurement for pile foundations. In: Institution of Civil Engineers: Geotechnical Engineering. Vol. 159. p. 135–144.

Lizzi F. 1981. The design of large diameter cast-in-situ bored piles using a “pilot” pile and congruence equations. Ground Engineering.:24–33.

Marmota Engineering. 2021. Project References: BoreScan. [accessed 2021 Dec 12]. https://www.marmota.com/projects.php?keywords=BoreScan.

Mikkelsen PE. 2002 Dec. Cement-Bentonite Grout Backfill for Borehole Instruments. Geotechnical Instrumentation News.:38–42.

Mohamad H, Soga K, Pellew A, Bennett PJ. 2011. Performance Monitoring of a Secant-Piled Wall Using Distributed Fiber Optic Strain Sensing. Journal of Geotechnical and Geoenvironmental Engineering. 137(12):1236–1243. doi:10.1061/(asce)gt.1943-5606.0000543.

Mullins G. 2016. Construction QA/QC Methods for Postgrouting Drilled Shafts. Journal of Performance of Constructed Facilities. 30(4). doi:10.1061/(asce)cf.1943-5509.0000827.

Ohno H, Naruse H, Kurashima T, Nobiki A, Uchiyama Y, Kusakabe Y. 2002. Application of Brillouin scattering-based distributed optical fiber strain sensor to actual concrete piles. IEICE Transactions on Electronics. E85C(4):945–951.

Ouyang Y, Broadbent K, Bell A, Pelecanos L, Soga K. 2015. The use of fibre optic instrumentation to monitor the O-Cell load test on a single working pile in London. In: XVI ECSMGE Geotechnical Engineering for Infrastructure and Development. p. 643–648. https://www.researchgate.net/publication/304628304.

Ouyang Y, Soga K, Leung YF. 2011. Numerical Back-analysis of Energy Pile Test at Lambeth College, London. In: Geo-Frontiers. ASCE.

Pelecanos L, Soga K. 2018. Development of load-transfer curves for axially-loaded piles using fibre-optic strain data, finite element analysis and optimisation. In: 9th European Conference on Numerical Methods in Geotechnical Engineering (IX NUMGE). Porto, Portugal. https://www.researchgate.net/publication/326368823.

Pelecanos L., Soga K, Chunge MPM, Ouyang Y, Kwan V, Kechavarzi C, Nicholson D. 2017. Distributed fibre-optic monitoring of an Osterberg-cell pile test in London. Géotechnique Letters. 7(2):152–160. doi:10.1680/jgele.16.00081.

Pelecanos Loizos, Soga K, Elshafie M, de Battista N, Kechavarzi C, Chang YG, Ouyang Y, Seo H-J. 2017. Distributed Fiber Optic Sensing of Axially Loaded Bored Piles. Journal of Geotechnical and Geoenvironmental Engineering. 144(3). doi:10.1061/(ASCE)GT.1943-5606.0001843.

Puzrin AM, Iten M, Hauswirth D. 2010 Dec. Advanced Geotechnical Applications of Distributed Fiber-Optic Sensing. Geotechnical Instrumentation News.:29–32.

Rabaiotti C, Iten M, Fischli F. 2015. Implementation of fibre-optic vertical extensometers for safety monitoring. In: FMGM 2015: Proceedings of the Ninth Symposium on Field Measurements in Geomechanics. Perth: Australian Centre for Geomechanics. p. 631–644.

Robertson PK. 2009. Interpretation of cone penetration tests - a unified approach. Canadian Geotechnical Journal. 46(11):1337–1355. doi:10.1139/T09-065.

Ruiz ME, Pando MA. 2009. Load Transfer Mechanisms of Tip Post-Grouted Drilled Shafts in Sand. In: Contemporary Topics in Deep Foundations. Reston, VA: American Society of Civil Engineers. p. 23–30. http://ascelibrary.org/doi/10.1061/41021%28335%293.

Silwinski ZJ, Fleming WGK. 1984. The integrity and performance of bored piles. In: Piling and Ground Treatment. Institution of Civil Engineers. p. 211–223.

Soga K, Kwan V, Pelecanos L, Rui Y, Schwamb T, Seo H, Wilcock M. 2015. The Role of Distributed Sensing in Understanding the Engineering Performance of Geotechnical Structures. In: XVI European Conference on Soil Mechanics and Geotechnical Engineering. Edinburgh, UK.

Soga K, Luo L. 2018. Distributed fiber optics sensors for civil engineering infrastructure sensing. Journal of Structural Integrity and Maintenance. 3(1):1–21. doi:10.1080/24705314.2018.1426138.

U.S. Army Corps of Engineers (USACE). 1956. Investigation of underseepage and its control, lower Mississippi River levees. Technical Memorandum No. 3-424. Vicksburg, MS.

U.S. Army Corps of Engineers (USACE). 2000. Design and construction of levees: Engineering Manual EM 1110-2-1913. Washington, DC. http://www.usace.army.miVinetlusace-docs/.

U.S. Army Corps of Engineers (USACE). 2018a. Geotechnical Report: West Bank Mississippi River Levees in Louisiana, Blackhawk Relief Wells Item 328-R. Vicksburg, MS.

U.S. Army Corps of Engineers (USACE). 2018b. MRL Item 328-R Seepage Remediation. Solicitation No W912EE-19-R-0006.

Vulliet L, Inaudi D, Wyser A, Vurpillot S, Pflug L. 1995. Development of interferometric fiber optic extensometers to monitor geostructures. In: Field Measurements in Geomechanics 4th International Symposium. Bergamo.

Winters D. 2014. Selected Topics in Foundation Design, Quality Assurance, and Remediation. [Tampa]: University of South Florida. https://scholarcommons.usf.edu/etd.

Wu J, Jiang H, Su J, Shi B, Jiang Y, Gu K. 2015. Application of distributed fiber optic sensing technique in land subsidence monitoring. J Civ Struct Health Monit. 5(5):587–597. doi:10.1007/s13349-015-0133-8.